DEVELOPMENT OF MULTIVALVE-BASED BIOPRINTING TECHNOLOGY

Alan Faulkner-Jones

Submitted for the degree of Doctor of Philosophy

Heriot-Watt University

Institute of Biological Chemistry, Biophysics and Bioengineering, School of Engineering and Physical Sciences

April 2015

ABSTRACT

Pluripotent stem cells (PSCs) are the most favourable sources of cells for tissue engineering applications due to their unique potency and self-renewal characteristics however they are quite fragile and can be directed to differentiate erroneously by the application of external forces. A novel multi-nozzle valve-based bioprinting platform was developed that was able to position droplets of bio-ink – such as cells in suspension – with high spatial accuracy and low impact. Volumes as low as 2 nL were successfully dispensed. Several different versions of the machine were created before the final machine was made integrating improvements and solutions to problems encountered during development. A complete evaluation of cell compatibility was carried out in order to quantify the response of cells to the bioprinting process. In the first ever study of this kind, the viability and pluripotency of human embryonic and induced pluripotent stem cells was investigated post-printing and were found to be almost completely unaffected by the bioprinting process. Many cells require a 3D culture environment in order to maintain their in vivo functions. A hybrid bioprinted-hanging-droplet technique was used to create uniform spheroid aggregates of programmable sizes from PSCs which could be used to direct PSC differentiation or as building blocks for tissue generation. Hydrogels can also be used to recreate the 3D in vivo cellular environment using the bioprinter. Alginate and hybrid polypeptide-DNA hydrogels were used, the latter for the first time with a bioprinting platform. Complex 3D structures could be created in a layer-by-layer approach with programmable heterogeneous properties throughout. Cells were added to the hydrogel precursor solution and used to bioprint 3D structures. The cells were found to be functional and highly viable while being encapsulated throughout the 3D structure of the bioprinted hydrogel which will allow the future creation of more accurate human tissue models. PSCs were successfully directed to differentiate into hepatocyte-like cells. It was shown that the bioprinting process did not interrupt or alter the pre-programmed differentiation of the cells which means that these cells can be patterned in 3D using the bioprinter while differentiating, greatly speeding up the creation of mini-liver tissue. Hepatic stellates and HUVECs were co-cultured with the hepatocyte-like cells in various ratios in an attempt to improve their hepatic function. However, no clear improvement in cytochrome P450 activity was observed indicating that further optimisation is required in this area.

DEDICATION

Dedicated to the memory of my grandfathers, John David Bennett and Dennis Faulkner, who were both engineers and I hope would have enjoyed reading about my research.

ACKNOWLEDGEMENTS

I would like to express my deep and sincere thanks to the many people who have assisted me during the course of this research; this thesis simply could not be here without their help.

Foremost thanks to my supervisor, Dr. Will Shu, for his many years of guidance, support, help and encouragement. He has been invaluable in keeping me motivated in the face of negative reviewer comments and perhaps more importantly he took a chance with me venturing outside his specialty which has been an excellent learning experience for us both.

Special thanks to the School of Engineering and Physical Sciences (EPS) support staff: Rebecca Crawford who has so often booked my travel, sometimes at extremely short notice; Richard Kinsella and the other technicians in the Mechanical Engineering workshop for their advice and fabrication of key components of the bioprinters; and Cameron Smith in stores who has always endeavoured to get me the best prices and the speediest deliveries on my orders.

I am extremely grateful to the Scottish Universities Physics Alliance (SUPA) for the prize studentship which funded this project. Also thanks to Roslin Cellab for supporting the biological cell experiments; in particular Jason King and John Gardner for their helpful comments, advice and suggestions also Cath Fyfe for using the bioprinter to perform experiments. I am grateful too for the members of Prof. Dongsheng Liu's research group at Tsinghua University for sharing their hydrogel expertise.

Special appreciation is due to my colleagues, many of whom I have come to regard as close friends and to my parents, I am extremely grateful for their support and encouragement throughout my life.

Finally, and most importantly, I must thank my wife for all her continuing love and understanding. She was always there to help me maintain perspective and get a decent amount of sleep when I would write code late into the evenings.

ACADEMIC REGISTRY
Research Thesis Submission

Name:	Alan Faulkner-Jones		
School/PGI:	School of Engineering and Physical Sciences		
Version: *(i.e. First, Resubmission, Final)*	Final	Degree Sought (Award **and** Subject area)	PhD Mechanical Engineering

Declaration

In accordance with the appropriate regulations I hereby submit my thesis and I declare that:

1) the thesis embodies the results of my own work and has been composed by myself
2) where appropriate, I have made acknowledgement of the work of others and have made reference to work carried out in collaboration with other persons
3) the thesis is the correct version of the thesis for submission and is the same version as any electronic versions submitted*.
4) my thesis for the award referred to, deposited in the Heriot-Watt University Library, should be made available for loan or photocopying and be available via the Institutional Repository, subject to such conditions as the Librarian may require.
5) I understand that as a student of the University I am required to abide by the Regulations of the University and to conform to its discipline.

* *Please note that it is the responsibility of the candidate to ensure that the correct version of the thesis is submitted.*

Signature of Candidate*:*		Date:	

Submission

Submitted By *(name in capitals):*	
Signature of Individual Submitting:	
Date Submitted:	

For Completion in the Student Service Centre (SSC)

Received in the SSC by *(name in capitals):*			
Method of Submission *(Handed in to SSC; posted through internal/external mail):*			
E-thesis Submitted (***mandatory for final theses***)			
Signature:		Date:	

TABLE OF CONTENTS

LIST OF TABLES

LIST OF FIGURES

NOMENCLATURE

M_W	Molecular Weight
2D	Two-Dimensional
3D	Three-Dimensional
XYZ	Three-dimensional datum axes
CNC	Computer Numerical Control [machine]
FWHM	Full Width at Half Maximum
OD	Outer Diameter
DC	Direct Current
CAD	Computer-Aided Design
CAM	Computer-Aided Manufacture
MAPLE DW	Matrix-Assisted Pulsed Laser Evaporation
BioLP	Biological Laser Processing
LIFT	Laser-induced Forward Transfer
AFA-LIFT	Absorbing Film-Assisted Laser-Induced Forward Transfer
LG DW	Laser-Guided Direct Writing
CIJ	Continuous Inkjet
DOD	Drop-on-Demand Inkjet
SEA-JET	Static-Electricity Actuated Inkjet
SIJ	Superfine Inkjet
EHDJ	Electrohydrodynamic Jet
µCP	Micro-Contact Printing
FACS	Fluorescence-Activated Cell Sorting
ELISA	Enzyme-Linked Immunosorbant Assay
FFF	Fused Filament Fabrication
FDM	Fused Deposition Modelling
CLSM	Confocal Laser-Scanning Microscope
TIRF	Total Internal Reflection Fluorescence microscope
KO	Knockout
RT	Room Temperature
UV	Ultraviolet
IR	Infrared

pH	Potential of Hydrogen - negative 10-base log (power) of the positive hydrogen ion concentration; measure of acidity
DNA	Deoxyribonucleic Acid
HSP	Heat Shock Protein
ICG	Indocyanine Green [dye]
CYP	Cytochrome P450 [enzyme]
EDTA	Ethylenediaminetetraacetic Acid
PBS	Phosphate-Buffered Saline
DAPI	4',6-diamidino-2-phenylindole – A commonly used nuclear and chromosome counterstain
MG	Matrigel™
GFR-MG	Growth Factor-Removed Matrigel™
DMEM	Dulbecco's Modified Eagle Medium
SFM	Serum-Free Media
DMSO	Dimethyl Sulphoxide
FBS	Foetal Bovine Serum
FDA	Fluorescein Diacetate
hbFGF	Human basic Fibroblast Growth Factor
HGF	Hepatocyte Growth Factor
AFP	Alpha-Fetoprotein
HNF4α	Human Nuclear Factor 4α
ZO-1	Zona Occludens 1 [protein]
CHO	Chinese Hamster Ovary [cell]
SMC	Smooth Muscle Cell
HUVEC	Human Umbilical Vein Endothelial Cell
HUVSMC	Human Umbilical Vein Smooth Muscle Cell
HSF	Human Skin Fibroblast [cell]
ESC, ES	Embryonic Stem Cell
PSC	Pluripotent Stem Cell
iPSC	Induced Pluripotent Stem Cell
hESC, hES	Human Embryonic Stem Cell
hPSC, hiPS	Human Pluripotent Stem Cell
hMSC	Human Mesenchymal Stem Cell
HEPG2	Human Hepatoma cell line G2

HEK, HEK293, 293	Human Embryonic Kidney cell line 293
HLC	Hepatocyte-Like Cell
NIH-3T3, 3T3	Mouse fibroblast cell line
AtT-20	Mouse pituitary epithelial-like cell line
mESC	Mouse Embryonic Stem Cell
EB	Embryoid Body
ECM	Extracellular Matrix
HA	Hyaluronic Acid
Ct	Chitosan
PVA, PVOH, PVA1	Polyvinyl Alcohol
PEG	Polyethylene Glycol
PEO	Polyethylene Oxide
POE	Polyoxyethylene
PLLA	Poly($_{L}$-lactic) Acid
PDMS	Polydimethylsiloxane
PCL	Polycaprolactone
ABS	Acrylonitrile Butadiene Styrene
PLA	Polylactic Acid
HDPE	High Density Polyethylene
DXF	Drawing Exchange Format
STL	Standard Tessellation Language
PC	Personal Computer
MS	Microsoft
USB	Universal Serial Bus
EoF	End of File
GUI	Graphical User Interface
PSU	Power Supply Unit
RAMPS	RepRap Arduino Mega Pololu Shield
LCD	Liquid Crystal Display
EEPROM	Electrically Erasable Program Memory

LIST OF PUBLICATIONS BY THE CANDIDATE

Faulkner-Jones A, Fyfe C, Gardner J, King J, de Souza P, Courtney A and Shu W, (2014). "3D bioprinting of human pluripotent stem cells and their directed differentiation into hepatocytes for the creation of mini-livers," *Biofabrication* (In preparation).

Li C, **Faulkner-Jones A**, Dun AR, Jin J, Chen P, Xing Y, Yang Z, Li Z, Shu W, Liu D and Duncan RR, (2015). "Rapid Formation of a Supramolecular Polypeptide–DNA Hydrogel for In Situ Three-Dimensional Multilayer Bioprinting," *Angewandte Chemie International Edition* (Early View). DOI: 10.1002/anie.201411383.

Faulkner-Jones A, Greenhough S, King JA, Gardner J, Courtney A and Shu W, (2013). "Development of a valve-based cell printer for the formation of human embryonic stem cell spheroid aggregates," *Biofabrication* **5** 015013. DOI: 10.1088/1758-5082/5/1/015013.

Faulkner A and Shu W, (2012). "Biological cell printing technologies," *Nanotechnology Perceptions* **8**(1), pp.35-57.

Chapter 1 – Introduction

1.1 Background

> "Every contrivance of man, every tool, every instrument, every utensil, every article designed for use, of each and every kind, evolved from a very simple beginning."
>
> Robert Collier

Biological cell printing is a relatively new technology in the fields of Bioengineering and Regenerative Medicine. It can be defined as the use of computer-aided transfer processes for the quick and reliable patterning and assembling living and non-living materials with a prescribed two- or three-dimensional organisation in order to produce bio-engineered structures for various applications including regenerative medicine, pharmacokinetic and cell biology studies [1].

1.1.1 Timeline

Printing technology has come a long way from its origins, when information was recorded on clay tablets in Mesopotamia [2]. By the 15th century, printing had become prevalent in Europe due to the widespread availability of paper which spurred advances from simple woodblock printing to the much quicker and more durable moveable type printing press [3]. Up until this point printing technology had been purely mechanical in nature, but in the 18th century a new process – lithography – was invented [4]. Lithography utilises hydrophobic chemicals to repel the ink solution from the negative areas of the image, creating the first method for printing with a completely smooth surface [5].

Developments in the late 20th century in modern, computer-based printing techniques developed the photocopier and laser and inkjet printers. The photocopier was invented by an American office worker named Chester Carlson; it operates on the principle of static electricity, attracting toner to the drum before transferring it to the paper [6]. Laser printers were a direct descendent of photocopier Xerography technology, but rather than using natural light to determine the patterns of toner on the photosensitive drum, a scanning laser beam is used to neutralise the charge on the drum [7]. Inkjet printing technology is divided into Continuous Inkjet and Drop-on-Demand, the latter being further divided into thermal and piezoelectric types. The basic premise of the

inkjet techniques is to apply an electrical signal to a heating pad or piezoelectric material, triggering the production of a single drop of ink (in the case of Drop-on-Demand) or a stream of droplets (in Continuous Inkjet) [8].

Printing technology has advanced; it is no longer limited to the mass production of the written word. Just before the turn of the millennium, a paper was published which laid the foundations of a completely new field using the techniques of printing to pattern biological materials [9]. The authors of this paper used a modified Optical Tweezers technique to gently nudge cells in the required direction, but even at this early point it was clear that the authors grasped the power of this novel technology: *"the ability to organize cells spatially into well-defined 3D arrays that closely mimic the native tissue architecture can potentially help in the fabrication of engineered tissue"* [9,10].

Only a few years later this exciting new field had emerged, now widely referred to as Biofabrication, with experiments being conducted worldwide [10–12]. Until very recently the majority of the research being undertaken was focused on "proof-of-principle" of several different printing techniques, including those based on laser pulses, inkjets and other, more novel, approaches. So much has already been achieved, but how could this field be developed further?

1.1.2 Motivation

Due to the different ways that biological cell printing technology can be set up, it can be applied to many diverse applications.

Prescription drugs are extremely widespread in society today, but the amount of time and money that is expended on the development of new drugs is not well known. New drug development can take from 10 to 20 years, with an estimated average of about 9 to 12 years [13,14]. In addition, only around 16% of the drugs that begin preclinical testing are approved for human use [15]. This low success rate can be partly attributed to the different responses that animals and humans have to the drugs being tested; some drugs may be dropped that would have worked on humans because they didn't have the desired effect on animals. A possible solution to this might be the creation of micro-tissue-laden chips called "organ-on-a-chip" [16], which produce the same physiological reaction that the entire organ would, but on a much smaller scale. This would result in a

shorter period of clinical testing, more effective drugs and an end to animal testing and vivisection.

The disparity between the number of patients on waiting lists for organ transplants and the number of transplants that are performed each year has continued to grow over the last decade; in the US in 2009 there were 105,567 waiting list candidates but only 28,459 transplant procedures took place [17]. A possible solution to this might be the creation of whole organs using a biological cell printer.

However, construction of thick tissues via cell printing such as the heart, kidney, lung and liver is not currently possible due to the inability to include the intricate vascular system required to ensure that every cell in the tissue are no further than ~1 mm away from a source of nutrients and oxygen within the engineered tissue mass [18,19]. Therefore, tissues created using cell printing have been limited to thin tissues such as skin. For instance, the current research focus of the Wake Forest Institute for regenerative medicine is printing skin over open wounds with simple inkjet valves attached to an XYZ plotter [20,21].

1.2 Aims and Objectives

The overall aim of this thesis is to develop a novel mechanical device that can quickly and reliably position viable biological cells and other liquid materials into pre-determined three-dimensional patterns – a cell printer. Cells must be viable and morphologically identical post-printing. Manual cell patterning methods are inefficient, costly, critically dependent on skilled operators and developed by trial and error with little process optimisation. Cell printing techniques automates this task, greatly improving the reliability of the results through increasing the repeatability of experiments and greatly sped up experiments. These techniques also open the door for the bottom-up generation of 3D tissues.

Aside from the development of the cell printer platform, this work has the following research objectives:

- To validate that the printer can dispense repeatable and programmable numbers of cells into pre-determined patterns.

- To investigate the response of cells, including fragile cells such as stem cells, to the printing process, including an analysis of the effect of altering the parameters of the printer.

- To further develop the printing platform to allow portability and for multiple cell types and biomaterials to be printed together.

- To design and carry out experimental work to explore possible applications for this technology.

1.3 Structure of the Thesis

Each chapter of this thesis will describe a different part of the research:

- Chapter 1 presents the background of this thesis and details the aims and objectives of the research.

- Chapter 2 summarises the fundamentals of biological cell printing technologies, including detailed descriptions of each technique, as well as cellular response, comparisons and conclusions. A background in human stem cell biology is provided, in particular the generation of liver cells from human stem cells. Three-dimensional culturing techniques are also reviewed, including spheroid aggregates and the use of hydrogels.

- Chapter 3 describes the methodology and experimental details for the projects in the following chapters. This will include aspects of design, calibration, and initial testing phases.

- Chapter 4 presents the experimental work on the creation and development of the biological cell printing platform. This includes aspects of the design, construction and software development.

- Chapter 5 evaluates the response of cells, including fragile human stem cells, to the bioprinting process. The function and viability of human embryonic stem cells and human induced pluripotent stem cells were examined to ensure they were unaffected by the bioprinting process.

- Chapter 6 describes the first example of the generation of spheroid aggregates from human embryonic stem cells together with an analysis of the dimensions of the aggregates compared to the initial number of seeded cells.

- Chapter 7 covers the experiments with the aim of creating 3D liver micro-tissues. This includes the bioprinting of alginate hydrogels, an analysis of the effect of different concentration ratios and the creation of complex 3D structures. Also presented in this chapter are descriptions of the protocol for directing the differentiation of human pluripotent stem cells into hepatocytes and the analysis of these cells functionality and an investigation into the effect of supporting cells on these generated hepatocyte-like cells.

- Chapter 8 contains the three-dimensional bioprinting of smart DNA related hydrogels. This will include analysis of results after experiments in cell viability, hydrogel component biocompatibility and bioprinting and analysis of complex 3D structures.

- Chapter 9 concludes this thesis and provides recommendations for future work in this area.

1.4 References

[1] Guillemot F, Mironov V, and Nakamura M, (2010). "Bioprinting is coming of age: report from the International Conference on Bioprinting and Biofabrication in Bordeaux (3B'09)," *Biofabrication*, **2**(1), p. 010201.

[2] Matthews R, (2005). "Chapter 12: The Rise of Civilisation in Southwest Asia," *The Human Past*, C. Scarre, ed., Thames & Hudson, pp. 432–471.

[3] Meggs PB, (1998). *A History of Graphic Design*, John Wiley & Sons.

[4] Senefelder A, (1911). *The invention of lithography*, The Fuchs & Lang Manufacturing Company.

[5] Carter R, Day B, and Meggs P, (2002). *Typographic Design: Form and Communication*, John Wiley & Sons.

[6] Stoyles P, and Pentland P, (2006). *The A to Z of Inventions and Inventors: M to P*, Black Rabbit Books.

[7] Wenander PE, and Lundquist CE, (1976). "Laser printing method and system" Patent Number 3,965,476, June 1976.

[8] Romano FJ, (2000). *Digital Printing: Mastering ON-Demand and Variable Data Printing for Profit*, Windsor Professional Information.

[9] Odde DJ, and Renn MJ, (1999). "Laser-guided direct writing for applications in biotechnology," *Trends in biotechnology*, **17**(10), pp. 385–389.

[10] Ringeisen BR, (2009). "43: The Evolution of Cell Printing," *Fundamentals of tissue engineering and regenerative medicine*, Springer, Berlin, pp. 613–631.

[11] Hopp B, Smausz T, Antal Z, Kresz N, Bor Z, and Chrisey D, (2004). "Absorbing film assisted laser induced forward transfer of fungi (Trichoderma conidia)," *Journal of applied physics*, **96**(6), pp. 3478–3481.

[12] Tasoglu S, and Demirci U, (2013). "Bioprinting for stem cell research," *Trends in Biotechnology*, **31**(1), pp. 10–19.

[13] Dickson M, and Gagnon JP, (2009). "The Cost of New Drug Discovery and Development," *Discovery Medicine*, **4**(22), pp. 172–179.

[14] Kaitin K, (2010). "Deconstructing the Drug Development Process: The New Face of Innovation," *Clin Pharmacol Ther*, **87**(3), pp. 356–361.

[15] Paul SM, Mytelka DS, Dunwiddie CT, Persinger CC, Munos BH, Lindborg SR, and Schacht AL, (2010). "How to improve R&D productivity: the pharmaceutical industry's grand challenge," *Nature Reviews Drug Discovery*, **9**, pp. 203–214.

[16] Huh D, Matthews BD, Mammoto A, Montoya-Zavala M, Hsin HY, and Ingber DE, (2010). "Reconstituting Organ-Level Lung Functions on a Chip," *Science*, **328**(5986), pp. 1662–1668.

[17] (2011). "organdonor.gov | The Need Is Real: Data," *U.S. Government Information on Organ and Tissue Donation and Transplantation* [Online]. Available: http://organdonor.gov/about/data.html. [Accessed: 02-Apr-2014].

[18] Baptista PM, Siddiqui MM, Lozier G, Rodriguez SR, Atala A, and Soker S, (2011). "The use of whole organ decellularization for the generation of a vascularized liver organoid," *Hepatology*, **53**(2), pp. 604–617.

[19] Atala A, (2011). "Tissue engineering of human bladder," *British Medical Bulletin*, **97**(1), pp. 81–104.

[20] Binder KW, Zhao W, Park GY, Xu T, Dice D, Atala A, and Yoo JJ, (2010). "In situ bioprinting of the skin for burns [Poster]," Advanced Technology Applications for Combat Casualty Care (ATACCC), Florida, USA.

[21] Binder KW, Zhao W, Aboushwareb T, Dice D, Atala A, and Yoo JJ, (2010). "In situ bioprinting of the skin for burns," *Journal of the American College of Surgeons*, **211**(3), p. S76.

Chapter 2 – Literature Review

2.1 Introduction

This multi-disciplinary thesis draws from several different topics, and research areas, from biological cell printing to biocompatible hydrogels to stem cell biology. These topics are reviewed in this chapter. Section 2.2 describes a number of different approaches for printing viable biological cells into programmed patterns, including traditional and modern techniques. The methods of each technique are described and their advantages and limitations listed. Section 2.3 provides a background to human stem cell biology, and in particular the methods used to direct the differentiation of human stem cells to specific lineages. Section 2.4 presents some of the different hydrogels used for three-dimensional cell encapsulation. Finally, Section 2.5 relates specific conclusions and insights drawn from the literature review.

2.2 Biological Cell Printing

2.2.1 Optical Tweezers

Optical Tweezers, a well-known technique for the manipulation of nanometre and micrometre-sized particles suspended in a solution, was pioneered in 1970 by Arthur Ashkin at Bell labs [1]. Optical tweezers are now well-established tools in the physical and life sciences. Forces up to 200 pN can be applied to particles with extremely small dimensions; even particles as small as 5 nm, such as cells, can be manipulated [2,3]. Cell throughput rates can be extremely high and have been measured in the region of $\sim 1 \times 10^6$ cells/s [2].

A typical optical tweezers setup is shown in Figure 2.1. A laser beam is tightly focused by sending it through a microscope objective; small dielectric spherical particles (such as biological cells) can be trapped and manipulated at the narrowest point of the focused laser beam, known as the beam waist. Two forces act on the cell(s) located at or sufficiently close to the beam waist; the scattering force produced by the photons striking the cell along their propagation direction, and the force produced by a gradient of field intensity [3]. The magnitude of these forces exerted on the cell depends on the cell size and laser wavelength. These forces act together to bring cells which are out of the trap to the centre of the trap. Almost all cell types can be harmlessly trapped by selecting a wavelength of laser that is not absorbed by the cells [4].

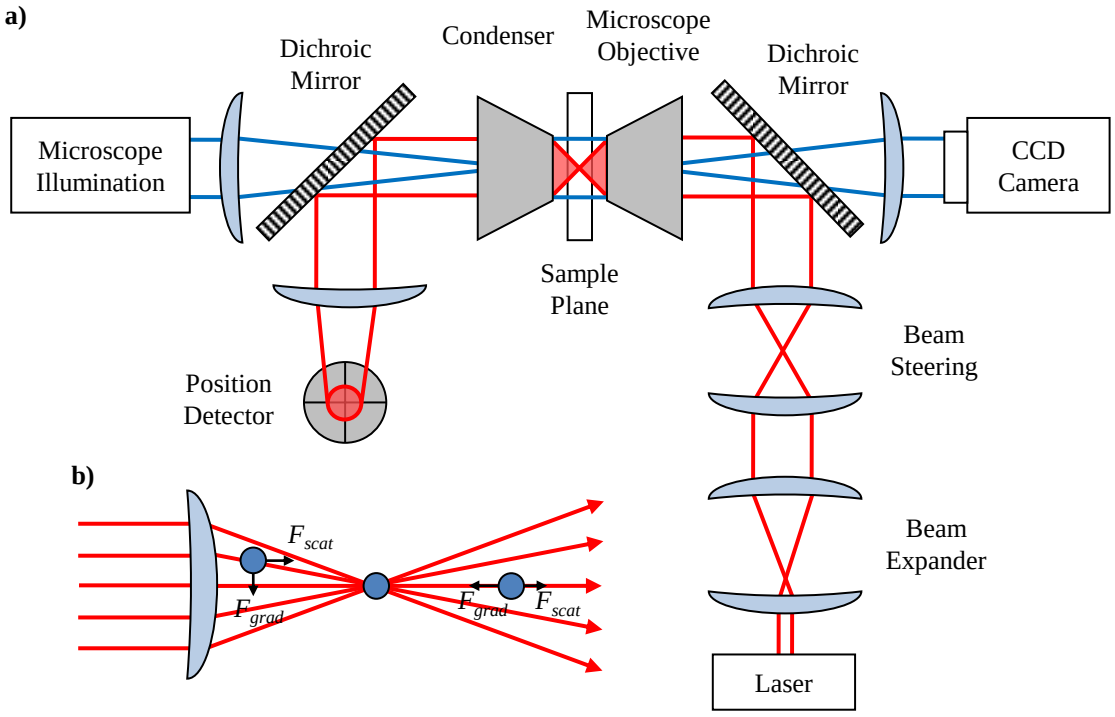

Figure 2.1 *– Simplified schematic of an optical tweezers system: a) typical experimental setup; b) working principles of optical tweezers*

Optical tweezers has several advantages compared to other techniques. As this technique is non-contact, cells can be moved from one reservoir to another in a few seconds without any extra-cellular media being dragged along with them. This means that there is no contamination if different types of cells are used and studies can be conducted in real-time [4].

It was originally thought that the optical tweezers technique was purely non-invasive in nature; however, studies by Liu et al. showed that cells can be heated sufficiently to affect their physiological state [5].

Unfortunately this technique is only suitable for transporting cells on a single plane and the small size of the volume that can be trapped limits the number of cells that can be manipulated at once [6]. Therefore, despite its advantages over other techniques, Optical Tweezers do not meet the demands of cell printing.

2.2.2 Laser-Based Direct-Write Techniques

Laser-based additive writing was originally used to create mesoscopic electronic components such as conductors, capacitors and resistors with a high spatial accuracy of

~1-3 μm [7]. Thanks to this high accuracy laser-based direct-write techniques became extremely attractive to the fields of biomedicine and bioengineering.

There are several variations on the standard laser-based direct-write technique; the most prolific techniques for cellular applications are *matrix-assisted pulsed laser evaporation direct writing* (MAPLE DW) [8,9], *biological laser processing* (BioLP) [8,10,11], *laser-induced forward transfer* (LIFT) [8,12–14], *absorbing film-assisted laser-induced forward transfer* (AFA-LIFT) [8,15], and *laser-guided direct writing* (LG DW) [8].

With the exception of LG DW, these techniques operate in distinctly similar ways [8] (Figure 2.2). Each of these techniques utilise a laser transparent ribbon, usually glass or quartz, the underside of which is coated with cells that are uniformly suspended within a thin layer of cell culture medium mixed with glycerol (or similar) to a cell concentration of around 1×10^8 cells/mL to a thickness of between approximately 10-100 μm [9,10]. A receiving substrate is coated with 50-200 μm of cell culture medium to maintain cellular viability [10,11], mounted on a computer-controlled motorised stage and positioned beneath the ribbon facing the cell-coated side. In order to transfer the cells from the ribbon to the substrate, a pulsed laser beam is fired at the transparent ribbon. The energy of the laser passes through the ribbon and causes the rapid volatilization of the cellular support layer creating the necessary force to allow the cells to drop the small distance (30-1000 μm [13]) between the ribbon and the receiving substrate. The amount of biomaterial that is transferred, including cells and suspension, can be expressed as a function of the focused laser spot size, the thickness of the biomaterial layer on the target, and the laser fluence [9,13].

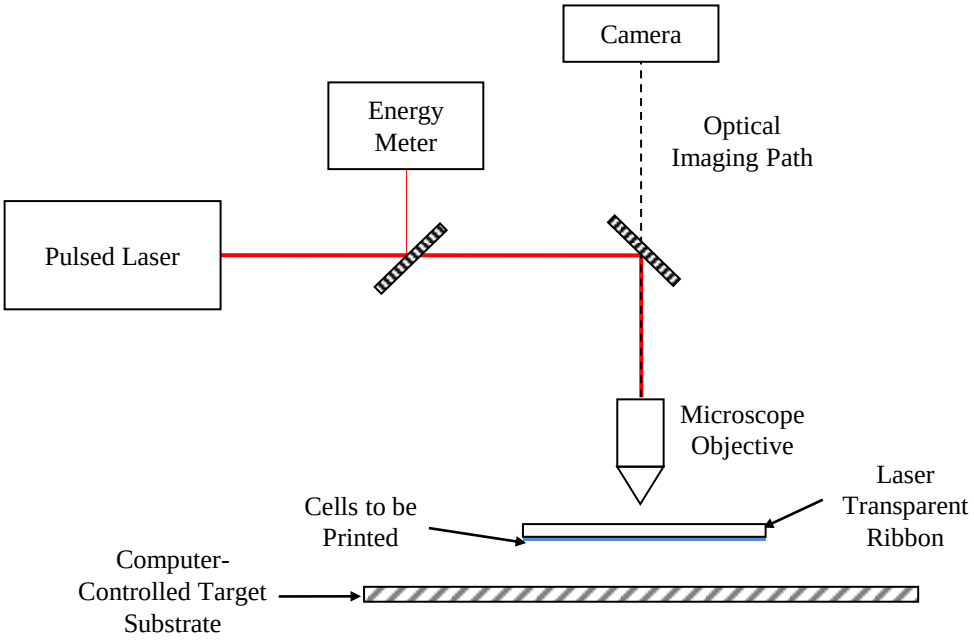

***Figure 2.2** – Simplified schematic of a LIFT, AFA-LIFT, BioLP or MAPLE DW system used for cell printing (adapted from [8]).*

Laser-induced forward transfer (LIFT) [8,12,13,16] utilises a high-powered pulsed laser. Guillotin et al. used a Nd:YAG crystal laser (Navigator 1, Newport Spectra Physics) with 1064 nm wavelength, 30 ns pulse duration, 5 kHz repetition rate and 7 W mean power [12]. In addition to the higher powered laser, LIFT adds a thin (~50-60 nm [12,13]) coating of a laser-absorbing biocompatible material such as titanium, titanium oxide, gold or silver [8] to the laser transparent ribbon in order to protect the cells from the laser pulses.

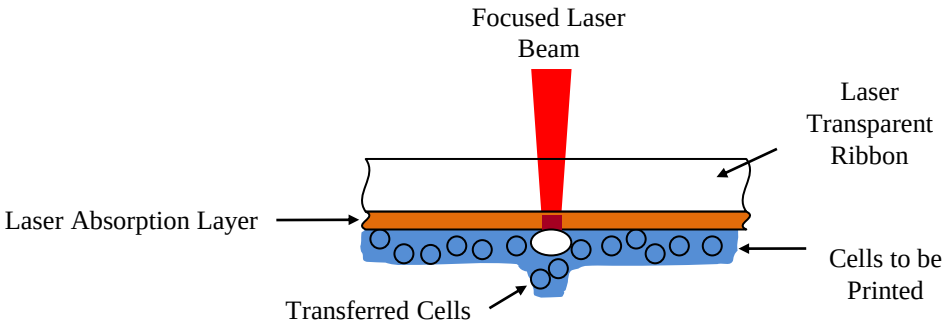

***Figure 2.3** – Simplified schematic of a LIFT ribbon arrangement (adapted from [8]).*

Absorbing film assisted laser induced forward transfer (AFA-LIFT) [8,15] uses the same technique as LIFT, but rather than a thin layer of laser-absorbing material, a thicker (~100 nm [8]) sacrificial layer of metal is used to interact with the laser. Hopp

et al. used a KrF Excimer laser with 248 nm wavelength, 30 ns pulse duration, laser fluences varied between 35-2600 mJ/cm^2 and a 50 nm thick layer of silver [15].

Matrix assisted pulsed laser evaporation direct write (MAPLE DW) [8,9,11] is a slightly different technique compared to the previous two, the major difference being that MAPLE DW utilises a low-powered pulsed laser operating in, or near, the UV range of the spectrum. Barron et al. used an ArF Excimer laser (Lambda Physik LPX-300i) with 193 nm wavelength, 20 ns pulse duration, laser energies between 15 and 30 μJ/pulse and laser fluences between approximately 157–315 μJ/cm^2 [9]. The other difference that sets this method apart is that instead of thin laser absorption or sacrificial layers, the underside of the laser transparent ribbon is coated in an aqueous based biological support layer, typically composed of a laser absorbing biopolymer and cell attachment layer. The UV light from the laser is absorbed by the water, causing vaporisation of some of the liquid at the interface in the biological support layer and resulting in the ejection of the material below [11].

Biological laser printing (BioLP) [8,11,14] is the most recent adaptation of the classic laser-based techniques. The technique is similar to LIFT and MAPLE DW, but utilises a laser absorbing interlayer rather than the biological matrix support used in MAPLE DW [10,11]. This absorption layer is typically composed of titanium or a titanium oxide coating approximately 75–85 nm thick [10]; like the layers used in the other techniques, it prevents the laser from interacting with the biomaterial but also improves the reproducibility of transfer by normalising the laser interaction [11]. An example of a laser system used for BioLP would be the one used by Barron in [10,11] which was a quadrupled Nd:YAG (Continuum Mini-Lite) with 266 nm wavelength, 5 ns FWHM, 1–15 Hz repetition rate and laser fluences approximately 191–382 mJ/cm^2.

Table 2.1 *– A comparison of the different laser-based techniques in this review.*

	Laser	Laser fluence/ energy	Spot size (μm)	Drop size	Cell viability (%)	Bio-ink viscosity range (mPa·s)	Advantages/ *limitations*	References
LIFT	Nd:YAG λ = 1064 nm	65-260 nJ	10	12 fL	~98	>100	Extremely small droplets possible	[6,12,13,17]
AFA-LIFT	KrF Excimer λ = 248 nm	355 mJ/cm^2	~10	Not reported	75	Not reported		[15]
MAPLE DW	ArF Excimer λ = 193 nm	157-315 μJ/cm^2	80-100	90 pL	100	>40	*Laser radiation transferred to cells*	[8,9,18–20]
BioLP	ArF Excimer λ = 248 nm	33 mJ/cm^2	30-120	30 pL	>95	2-431	<1% laser radiation transferred to cells	[10,21,22]

Substantial amounts of stress can be applied to cells during the printing process, especially at higher velocity transfer speeds possible with laser direct-write techniques. The expression of heat shock proteins (HSP) are a good marker of stress endured during the printing process as they are known to be expressed by cells undergoing thermal and mechanical stresses [23,24]. Barron et al. conducted an experiment to show the amount of HSP expressed by BioLP deposited cells with a positive and negative control, the results indicated that only minimal amounts of HSP60/70 were expressed [21].

Various types of cells have been used to test this technique including human osteosarcoma cells (MG-63 ATCC CRL-1427), Chinese hamster ovary (CHO) cells, rat cardiac cells (ATCC CRL-1764, Rat-2) cells encapsulated in picolitre droplets at rates varying from 1-5,000 droplets per second (higher rates are possible but these are more usual). Cell viabilities were demonstrated to be high.

Laser-based cell printing techniques have proven their ability to print cells into precise pre-programmed patterns. An example of this control would be Guillotin et al. with their Olympics logo printed using the LIFT technique [12] (Figure 2.4).

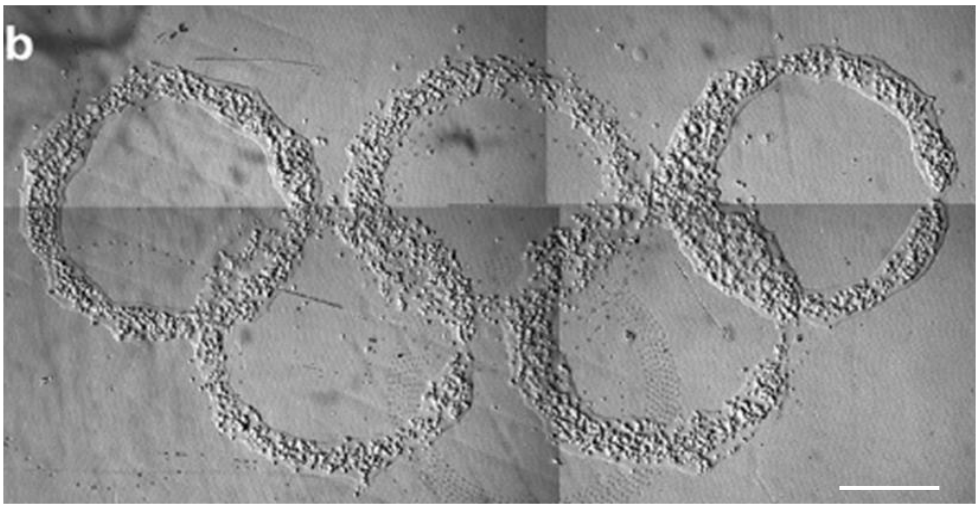

Figure 2.4 *– Cells printed in the form of the Olympics logo (scale bar 500 µm) [12]*

Nahmias et al. created a 3D cellular structure on a collagen-coated surface by depositing three alternating layers of hepatocytes and hydrogels on top of each other using laser guided 3D cell writing [25]. Cell viability and proliferation was well-maintained post-deposition [26].

***Figure 2.5** - Three cells (indicated by arrows) deposited on top of each other. Image taken perpendicular to the axis of deposition (scale bar 50 µm) [25]*

Laser-based direct-write techniques have several advantages over other techniques. As these techniques use an orifice-free transfer process, it is unaffected by biomaterial adhesion and therefore adapts easily to variations in the viscosity of the biological material [11]. Other advantages include an extremely fast material transfer (9×10^{-8} mL/s) [9,11,24], and contamination is avoided because there is no direct contact between the laser, ribbon and substrate [11]. Spatial accuracy is better than 5 µm [9,11], and live/dead assays reveal a near 100% cell viability with this technique [8,9,11].

Current techniques can transfer various numbers of cells, either single or multiple; between 0 and 8 cells can be dispensed per droplet [9], so laser-based techniques have great potential to be used to create micro-cellular features such as micro-vasculature networks.

As laser-based direct-write techniques were not originally developed for biological material transfer, there are a number of disadvantages. These include expensive instrumentation, varying transfer rate due to inhomogeneous biological layer [27], possible genetic damage due to UV/IR laser energy exposure [5,21], poor reproducibility in certain techniques, limited deposition rates depending on the laser repetition rate [11] and possible damage to cells due to mechanical shear forces during the jet formation and impact on the substrate [22]. An added weakness of the MAPLE DW technique is its requirement of laser absorbing matrix materials [15].

2.2.3 Inkjet Printing

Inkjet printing was, until recently, used almost exclusively to print documents in 2D. With a few slight modifications, however, this technology can be used to print bio-ink solutions containing live cells. Inkjet technology was first adapted for use with biological materials by Wilson & Boland in 2003 [28]; their printer was converted from an off-the-shelf ink-jet printer. Due to their low cost and high throughput, inkjet printing has become an extremely popular cell printing technique [8,28–31].

Inkjet printing techniques can be differentiated from some similar techniques by their use of the surface tension of the bio-ink itself as a valve [32]. There are many different types of inkjet printing techniques, but they can generally be sorted into two main groups: continuous (CIJ) and drop-on-demand (DOD). Continuous inkjet technology is unsuitable for bioprinting applications due to the lower accuracy and increased sources of potential contamination of the bio-ink [33,34]; therefore, only DOD inkjet techniques are described here.

Droplets are ejected from a nozzle by applying a pulse of pressure to the fluid bio-ink solutions in the supply tube upstream of the nozzle. There are several methods of creating this pressure pulse: thermal bubble, piezoelectric, and electrostatic. Both thermal and piezoelectric types have been modified for use as cell printers [28,35].

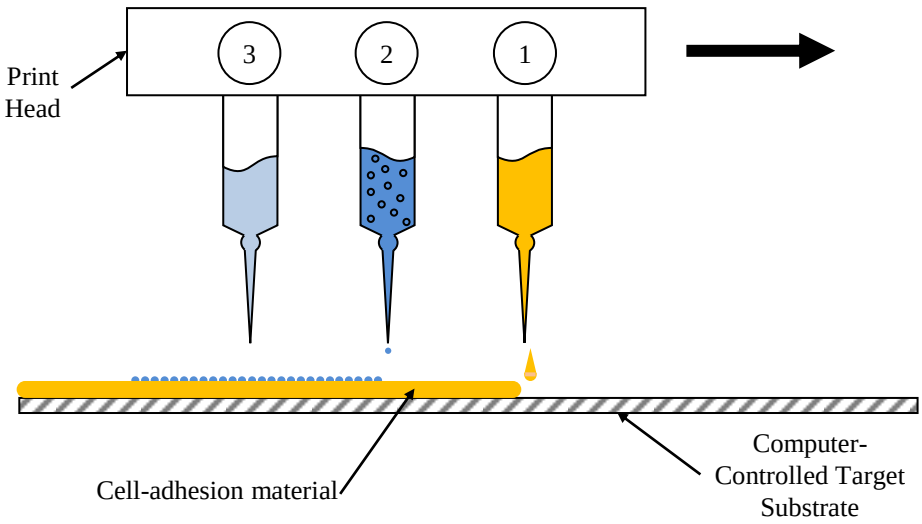

Figure 2.6 *– Simplified schematic of an inkjet system used for cell printing (adapted from [36])*

Piezoelectric materials are crystalline materials which deform when subjected to an electric potential. There are two common types of piezoelectric material: bimorphs

(which bend like a drum head) and rods (which elongate). A section of this material (either in a rod or bimorph configuration) is attached to the outer wall of the bio-ink channel upstream of the nozzle and configured to squeeze the channel. This creates a pressure pulse which results in a droplet being ejected from the nozzle. The electrical pulses which energise the piezoelectric materials are typically in the microsecond range [37–39].

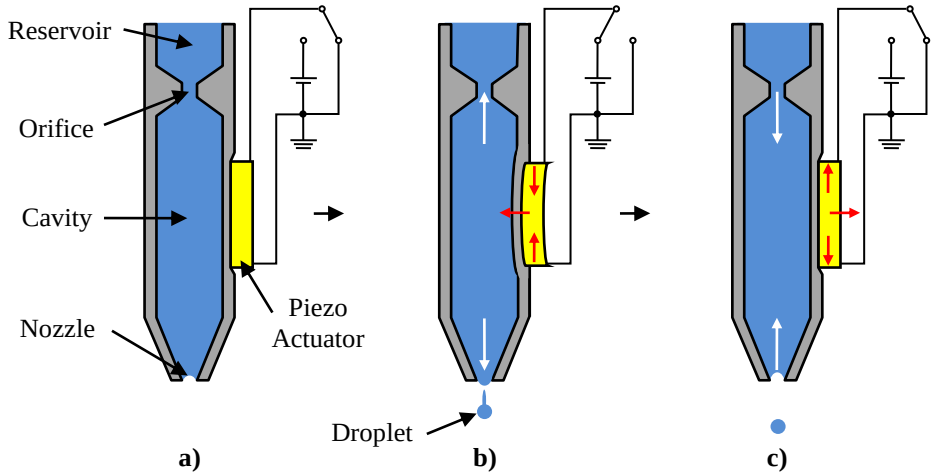

Figure 2.7 *– The process of droplet ejection in a push pull piezoelectric inkjet system: a) initial state; b) DC voltage applied across the piezoelectric material and a droplet is ejected (push); c) DC voltage is removed (pull) (adapted from [40])*

Thermal bubble inkjet operates in much the same way as piezoelectric-based printers but, instead of piezoelectric material, the pressure pulse is created by a heater. The heater is composed of a thin film resistive metallic layer, typically less than 1 µm thick and around 15 µm across each side, attached to the inner wall of the bio-ink channel just upstream of the nozzle. By passing an electrical pulse of sufficient amplitude through the heater the temperature of the heater rises to a point high enough to boil the bio-ink. The bio-ink within a fraction of a micrometre of the heater vaporises, forming a bubble which expands. This expansion of the bubble creates a pressure pulse that results in a droplet being ejected from the nozzle. The bubble cools and collapses after a few microseconds and the surface tension of the bio-ink meniscus at the nozzle pulls more bio-ink down from the reservoir to refill the bio-ink channel. The electrical pulses which energise the resistive materials are typically in the microsecond range [37,38].

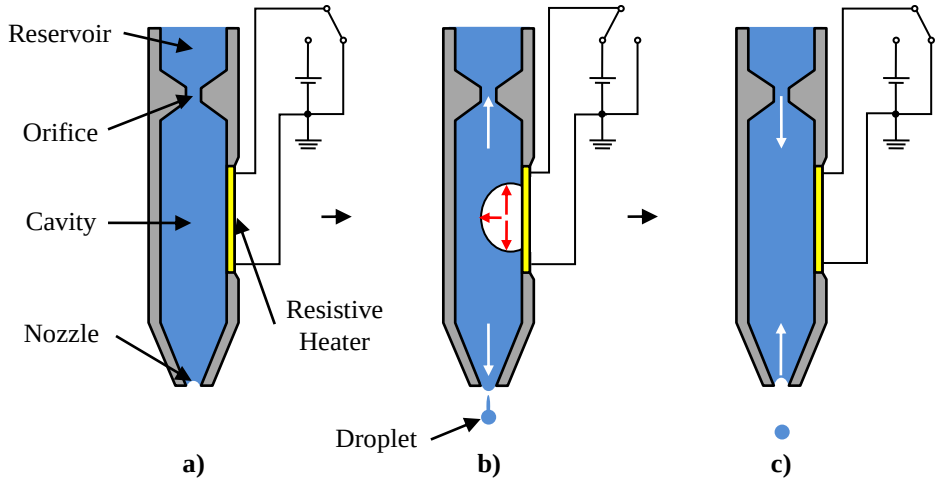

Figure 2.8 *– The process of droplet ejection in a thermal bubble inkjet system: a) initial state; b) DC voltage applied across the piezoelectric material and a droplet is ejected (push); c) DC voltage is removed (pull)*

SEA-JET (Static-Electricity Actuated InkJET) printing was developed by the Seiko Epson Corporation in 1998 [41]. It was created to address the cavitation problems associated with piezo and the large power requirements of thermal inkjet printing. The mechanism of the electrostatic actuator is comprised of a silicon pressure plate and an electrode which are positioned in parallel between two glass plates. The cavity above the pressure plate is filled with bio-ink from the reservoir.

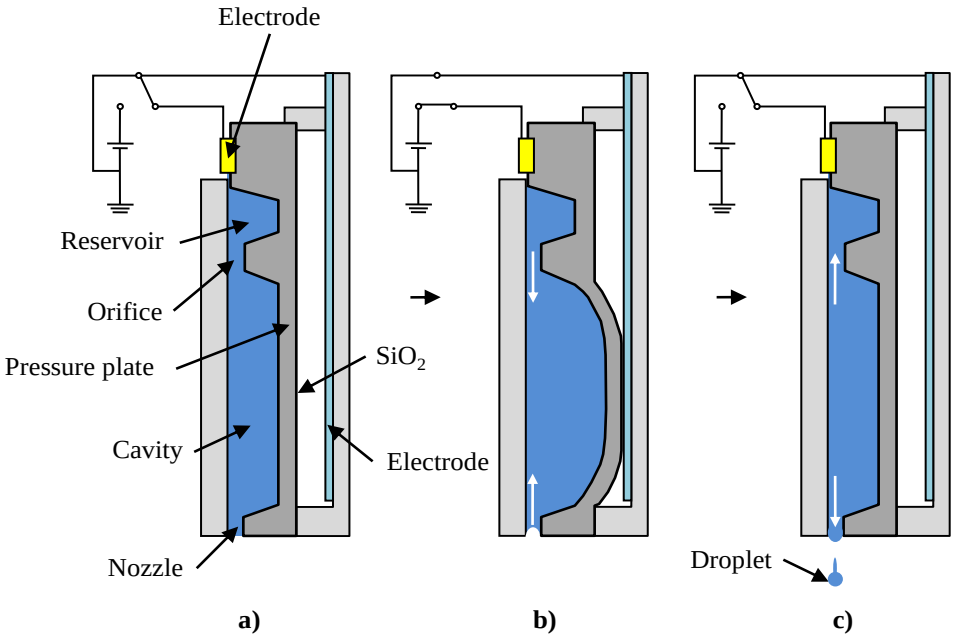

Figure 2.9 *– The process of ink ejection in an electrostatically actuated inkjet system: a) initial state; b) DC voltage applied between the pressure plate and the electrode (pull); c) DC voltage is removed and a droplet is ejected (push) (Adapted from [41]).*

An interesting new technique for inkjet printing called *Superfine Inkjet Printing* has recently been developed by Japan's National Institute of Advanced Industrial Science and Technology (AIST). Superfine Inkjet (SIJ) Printing dispenses droplets of sub-femtoliter volume which is 1/1000 of the volume of current inkjet devices on the market [42,43] (Figure 2.10).

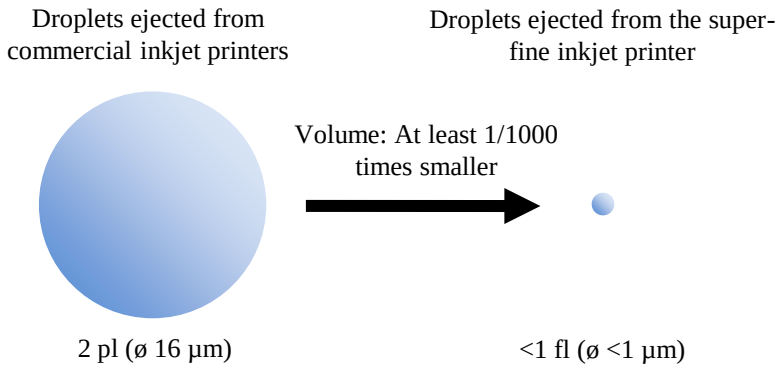

Figure 2.10 *– Comparison of standard and SIJ droplet sizes (Adapted from [43]).*

However, due to the novel nature of this technology, the majority of the technical information about the technique is protected, but based on the little information available, it is clear that this technique would not be suitable for printing viable cells as the size of each droplet is smaller than a single mammalian cell. It could be possible to use SIJ to deposit other biomaterials such as growth factors with extremely high control over the volume dispensed at set locations.

Table 2.2 *– A comparison of the different inkjet-based techniques in this review.*

	Spot size or resolution (µm)	Drop size	Cell viability (%)	Bio-ink viscosity range (mPa·s)	Advantages/ *limitations*	References
Piezoelectric	10	1-100 pL	75-80	1-20	*Vibrations can damage cells*	[34,44,45]
Thermal	85	130 pL	89	1-5	Ubiquitous *Higher power*	[34,45]
Electrostatic	30	1-100 pL	Not reported	Not reported	Lower power	[46,47]

Cells can undergo substantial shear forces during the printing process, especially with the narrow nozzle internal diameters used in inkjet techniques. Thermal inkjet also applies thermal energy so is more likely to damage the cells during printing. Cui et al. conducted an in-depth experiment to investigate the viability and apoptosis of printed

cells; they discovered that transient pores were developed in the cell membranes during printing which yielded a 30% transfection efficiency with co-printed plasmid-DNA [48].

Various types of cells have been used to test this technique including Chinese hamster ovary (CHO) cells, smooth muscle cells (SMC) encapsulated in picolitre droplets at rates varying from 1-10,000 droplets per second. Cell viabilities were demonstrated to be over 80% across various cell types.

Nakamura et al. (2008) used a custom built electrostatic inkjet 3D bioprinter to successfully fabricate a miniaturised tube with an external diameter of 100 µm and an inner lumen measuring approximately 25 µm in diameter from alginate hydrogel [46].

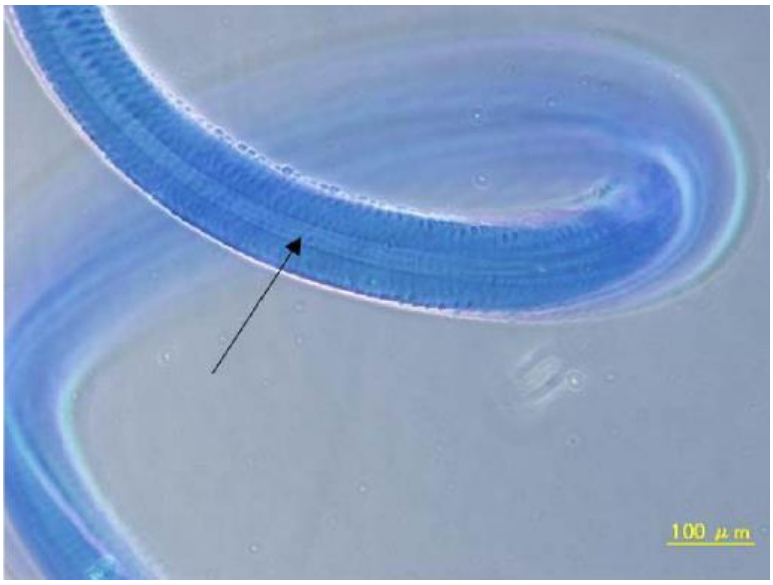

Figure 2.11 *– Detail view of the miniaturised tube with 50 µm radius; arrow indicates inner lumen [46]*

Inkjet-based techniques have several advantages over other techniques. Chief among them is the lower cost and simplicity of the technique facilitated by modifying off-the-shelf inkjet printers. Other strong points in its favour are the ability to using several different types of cells by simply adding more nozzles [35,49], and the high-throughput nature of the mechanism [28].

Inkjet-based techniques also have a number of disadvantages, the biggest of which is due to the technique being driven by the size of the nozzle: droplet diameters are approximately double the internal diameter of the nozzle used (which leads to larger droplet sizes compared to some of the other techniques). Nozzle clogging from cell

sedimentation and aggregation is also a problem if high cell concentrations (>5 x 10^6 cells/mL) are used [31]; however, adding a calcium ion (Ca2+) chelating agent to the bio-ink, such as EDTA (ethylenediaminetetraacetic acid), could help prevent nozzle failure and increase the bio-ink cell concentration by reducing cell aggregation [27,37]; however EDTA may be toxic to cells [50]. Other problems include a spatial accuracy of only ~50 µm (which is sufficient for cell printing but a higher spatial accuracy would be desirable), shear stress applied to the material being printed, and possible contamination [11,35,49,51].

Piezoelectric-based printers have increased power requirements (12-100 W) and higher vibration frequencies (30 kHz) due to the use of high viscosity bio-ink, which is enough to break and damage cell membranes [35].

Thermal-based printers suffer from possible heating effects as temperatures can reach 300°C or higher in some techniques which can cause many cells to die during printing [24,35,49].

2.2.4 Valve-Based Printing

Valve-based printing techniques are extremely similar to inkjet techniques. They comprise a static pressure reservoir, a small diameter nozzle, a voltage-controlled valve, and a two-dimensional translation mechanism (the print head) to which the other components are mounted (Figure 2.12). The reservoir is loaded with cells that are uniformly suspended within cell culture medium. The cells are delivered to the substrate by activating the voltage-controlled valve [52,53]. The amount of biomaterial, including cells and suspension, that is transferred can be expressed as a function of the nozzle diameter, the size of the cells, the inlet pressure and the amount of time the valve is open [54].

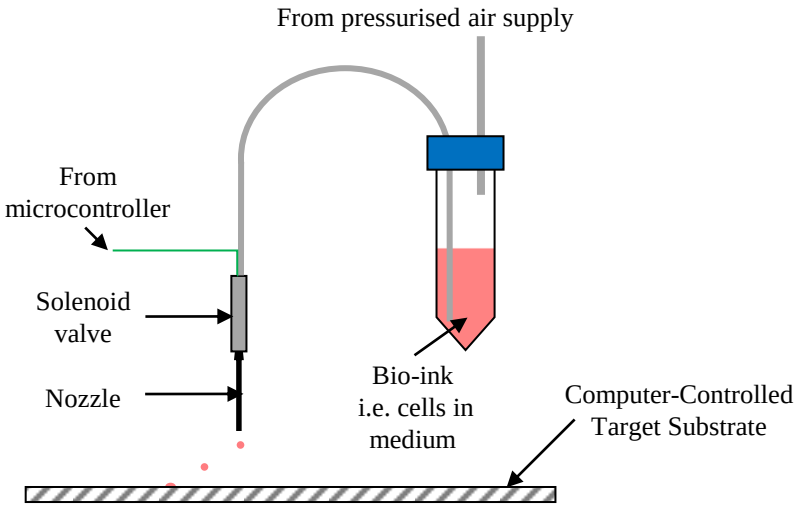

Figure 2.12 *– Schematic drawing of the valve-based cell dispensing system.*

Various types of cells have been used to test this technique, including NIH-3T3 mouse fibroblasts, AML-12 hepatocytes, HL-1 cardiomyocytes, mouse embryonic stem cells, fibroblasts and human Raji cells encapsulated in nanolitre droplets at rates varying from 1 to 20,000 droplets per minute. Cell viabilities were demonstrated to be over 90% across various cell types [53,54].

Weiss et al. (2012) developed a multi-head micro-solenoid valve-based bioprinter to fabricate heterogeneous structures with a bottom-up concentration gradient. Multiple growth factors were printed with spatial precision in a functionally graded manner into rat calvarial defect *in-situ* [26,55].

Valve-based techniques are one of the newest additions to this field and have repeatedly demonstrated extremely high final cell viability [56,57]; this can partly be attributed to the comparatively low shear stress created in this technique. Another useful advantage is that cell numbers in the dispensed droplets are more uniform than in other techniques [56]. Other advantages include the high-throughput nature of the technique (even with a single nozzle 1000 droplets could be dispensed in under a second [53]); as with inkjet printing it is easily expandable and cheap.

Just like inkjet techniques, valve-based techniques also have nozzles and therefore nozzle-based problems, such as clogging and the link between droplet diameters and nozzle diameters. However, nozzles used in valve-based systems are larger than those used in inkjet printers [37], so these problems are encountered far less often.

2.2.5 Bio-Extrusion Methods

Unlike the other techniques reviewed here, which typically deposit discrete droplets of low viscosity bio-inks in two-dimensional patterns, bio-extrusion deposits continuous streams of medium to high viscosity bio-inks.

Bio-extrusion (also called bioplotting) is defined as the process of extruding bio-inks of medium viscosity through a syringe. Bio-ink is extruded in continuous streams from a nozzle by applying a force to the bio-ink in the syringe, upstream of that nozzle. By drawing the tip of the nozzle along the substrate, 2D shapes can be created [58] and 3D structures can be formed by simply adding more layers to the top of the previous layer. This technique is usually applied to the creation of 3D scaffolds into which cells are seeded before culture, but it is also possible to deposit cells at the same time as the matrix material [59]. The basic mechanism of all bio-extrusion techniques is the same, but there are some differences introduced by various research groups. There are two main techniques used to apply the force to the bio-ink: motor-driven and pressure-driven systems. Some techniques also utilise temperature modifying components to increase the "printability" of bio-inks or to improve the properties of the printed structures or simply speed-up the curing time of certain gels.

Cohen et al. have constructed a custom solid freeform fabrication robotic platform that uses a motor to drive the deposition system [60]. The deposition system is a linear actuator-driven syringe with interchangeable nozzles in the form of syringe tips. The body of a disposable syringe serves as the bio-ink reservoir and as such can be easily exchanged to change the bio-ink during experiments. Bio-ink is dispensed in continuous cylindrical filaments by driving the linear actuator; by altering the speed of the linear actuator, more or less material is deposited. Coupled with the travelling speed of the deposition system (when driven using an XYZ positioning system such as a CNC machine) and the diameter of the nozzle attached to the syringe, the width of the extruded filament can be controlled.

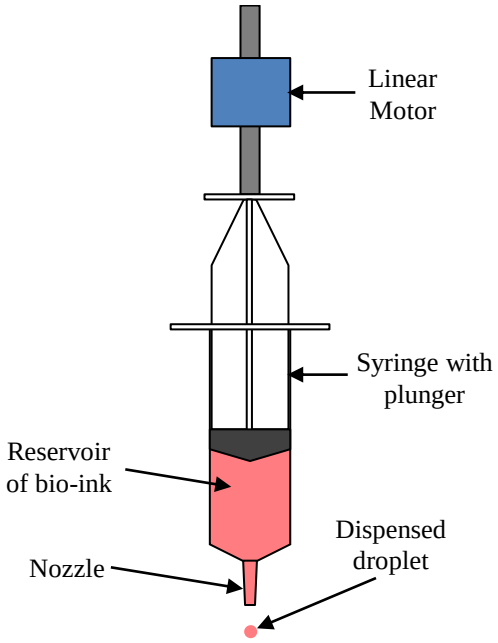

Figure 2.13 *– Simplified schematic of a bio-extrusion system.*

Pressure-driven systems operate in much the same way as motor-driven systems but instead of mechanically driving the bio-ink with a linear motor, the driving force is provided by positive low and constant pressure [58]. Bio-ink is dispensed in continuous cylindrical filaments by applying pressure to the inlet of the syringe. By precisely modulating the inlet pressure, more or less material is deposited.

Often solutions deposited using this technique requires the bio-ink to be stored and extruded at certain temperatures so they include cartridge heaters to keep the bio-ink at certain temperatures. For example, high viscosity materials would usually be unprintable, but they can be extruded if they are first heated to a higher temperature. Also, gelatin is a solution at physiological temperature (37 °C), but can reversibly form a gel when cooled (<29 °C). This is due to a conformational change from coil to helix that leads to chain association and eventually the formation of a three-dimensional network [59].

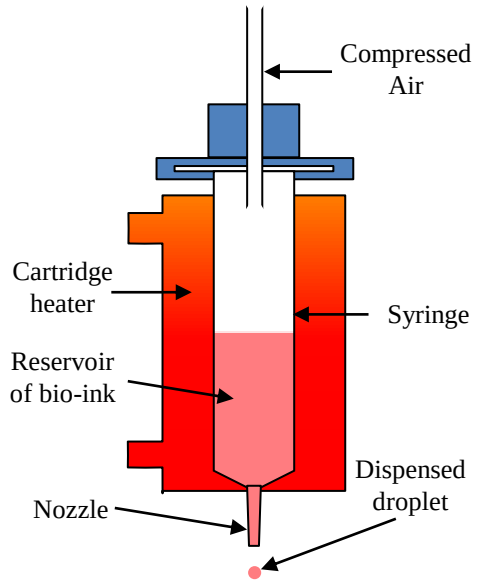

Figure 2.14 *– Simplified schematic of a bio-plotting system*

Two commercial machines are available that utilise bio-extrusion techniques for bioprinting: the EnvisionTEC 3D-Bioplotter® from Germany [61]; and Organovo's NovoGen MMX bioprinter from the USA [62].

Yan et al. (2005) used this technique to create a 3D structure composed of hepatocytes suspended in a gelatin/alginate hydrogel; cells remained viable and performed biological functions for more than 12 days [63].

Norotte et al. (2009) created small diameter vascular tubes (OD ranging from 0.9 to 2.5 mm) from cellular aggregate cylinders of human umbilical vein smooth muscle cells (HUVSMCs) and human skin fibroblasts (HSFs) to create multicellular constructs [64].

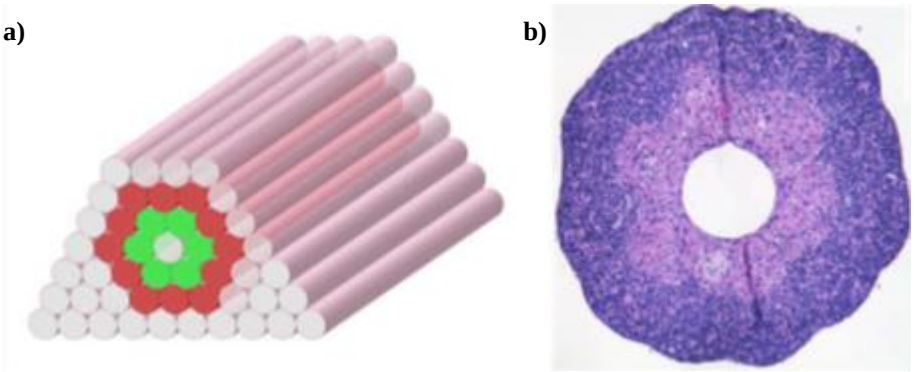

Figure 2.15 *– A double-layered vascular wall constructed from HUVSMC (green) and HSF (red) multicellular cylinders were assembled according to a specific pattern shown in a); b) results of histological examination of the structure in a) after 3 days of fusion [64]*

Bio-extrusion techniques have several advantages including the capability to create structures with highly accurate and structurally rigid 3D geometries which can be fabricated in a controlled manner. Complex 3D geometries are also possible due to the ability to deposit extra materials as a support matrix or scaffold. Furthermore, the ability to deposit cell-laden hydrogels potentially facilitates homogeneous distribution or positioning of cells, and therefore the capability to seed cells of specific cell types at discrete sections within the 3D structure [59,65].

There are also several limitations of the technique due to the use of high-viscosity biomaterials and nozzles in the technique; shear stress will be applied to cells as they pass through the nozzle and clogging is a potential issue [26]. This can be limited by optimising the applied force and nozzle diameter to the biomaterial currently in use [66]. Sufficiently high viscosity is essential for the bio-ink to overcome the surface tension-driven deposition which imposes a lower limit on bio-ink viscosity, highly fluid bio-inks with viscosities less than 100 mPa·s tend to leak out of the nozzle because the flow is controlled by surface tension effects [58,67].

A disadvantage of using pressure for bio-ink deposition is the extra limit on bio-ink viscosity; solutions with a viscosity greater than 700 mPa·s require much higher pressures to deposit, which may damage the tip and be a danger to the user [58,67].

2.2.6 Electrohydrodynamic Jet Printing

Electrohydrodynamic Jet Printing (or EHDJ), otherwise known as Bio-electrospraying or e-jet printing, was first demonstrated in the 1980s by John Fenn at Yale University [68]. Cell electrospinning (also considered a modified form of EHDJ) and electrospraying work on similar principles and are both described in this section. Rather than using thermal or laser energy to produce droplets, Electrohydrodynamic jet printing operates by applying an electric field between two charged electrodes which draws a jet of bio-ink which can form either discrete droplets or continuous fibres. [69].

A typical Electrohydrodynamic Jet Printing setup is composed of a syringe pump attached to a ~500 μm nozzle which is kept at a positive potential (0.5-0.9 KV/mm) with respect to the ground electrode above the receiving substrate positioned approximately 15 mm below the nozzle orifice [70,71]. The reservoir of the syringe is loaded with cells that are uniformly suspended to a concentration of between 1×10^{6}-

2×10^6 cells/mL [71]. In order to transfer the bio-ink between the nozzle and the substrate, a potential difference is applied between the nozzle and the ground electrode placed centrally below it; this external electric field accelerates the charged bio-ink exiting the nozzle towards the ground electrode. A cone of bio-ink forms at the nozzle orifice and a jet forms at the apex; either continuous fibres or discrete droplets are formed depending on the properties of the bio-ink. Flow rate, applied voltage and instrument setup determine the diameter and geometry of the generated fibres [72].

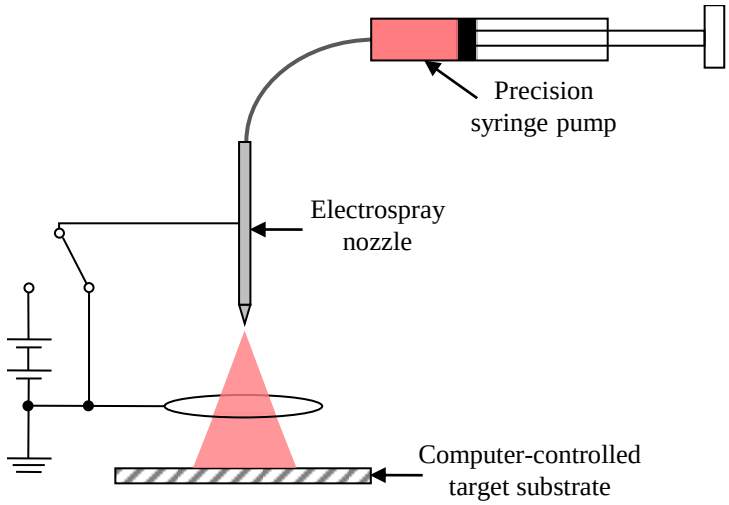

Figure 2.16 *– Simplified schematic of an Electrohydrodynamic Jet system used for cell printing (adapted from [71])*

Several cell types have been used, including Jurkat cells and mouse neuronal cells [70,71]. Each investigation showed that the process of Electrohydrodynamic Jet Printing does not in any way damage the cells. Cells that were examined post printing exhibited growth comparable to that of the control cells.

In this form, this technique has no control over the direction of bio-ink fibre generation during jetting, but has the ability to handle standard materials in large quantities for forming scaffolds in short periods of time. A modified version of the technique has been developed which increases the stability of the jet while retaining the high speeds of deposition by incorporating a co-axial nozzle [73,74].

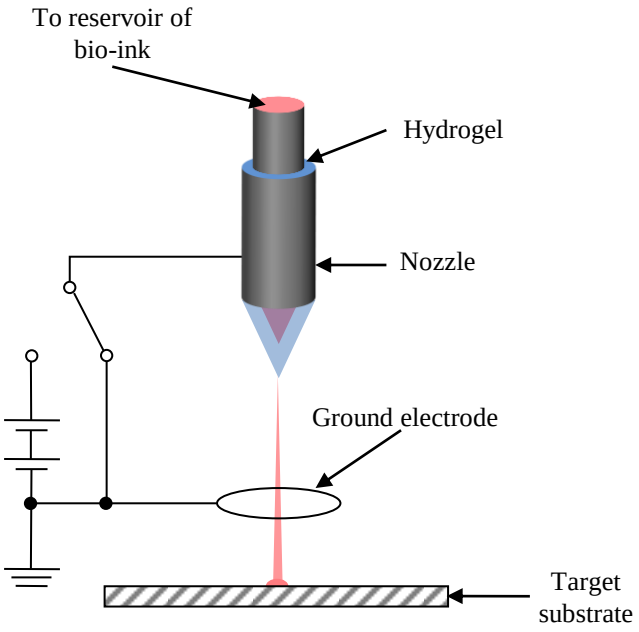

Figure 2.17 *– Schematic of a modified Electrohydrodynamic Jet system used for cell printing*

Bartolovic et al performed a study to determine if the cell electrospinning process affected the differentiation potential of mouse hematopoietic stem cells using a functional *in vitro* assay and an *in vivo* mouse model to investigate possible side effects. No negative effects were discovered [75].

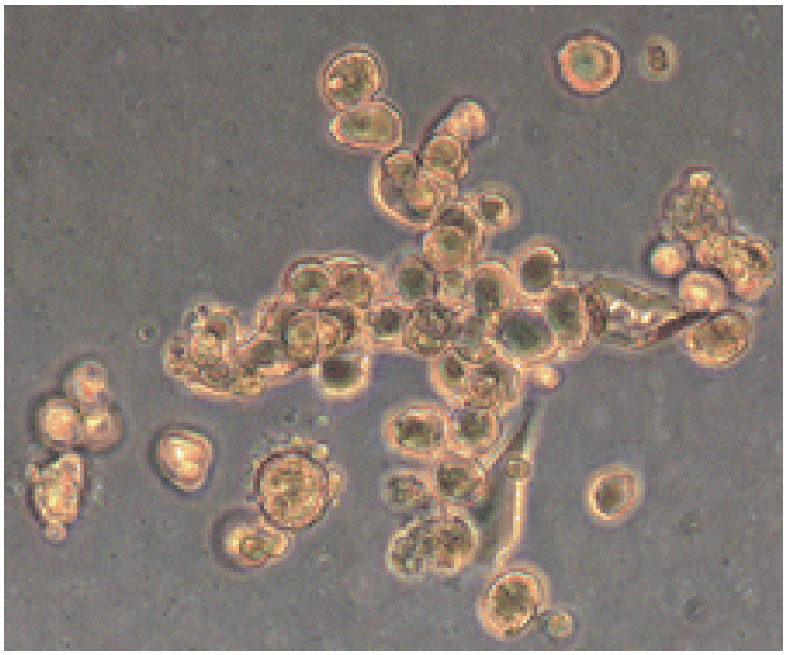

Figure 2.18 *– A representative micrograph of the heterogeneous cell population derived from hematopoietic progenitor cells of CD-1 mouse BM [75]*

A slightly different technique is Pyroelectric Jet printing, also known as pyro-Electrohydrodynamic Jet printing, instead of electrodes, liquid is dispensed by temperature varying the temperature of polar dielectric crystals [76]. A typical pyroelectric jet setup is shown in Figure 2.19. A heat source (usually a laser or a hot soldering iron tip) is applied to a sheet of pyroelectric material (such as lithium niobate). As the pyroelectric material heats up, local electric potentials are created that initiate the electrohydrodynamic effect in the fluid on the surface of the glass. This leads to the ejection of small droplets of fluid that are printed onto an intervening substrate with nanoscale resolution [77].

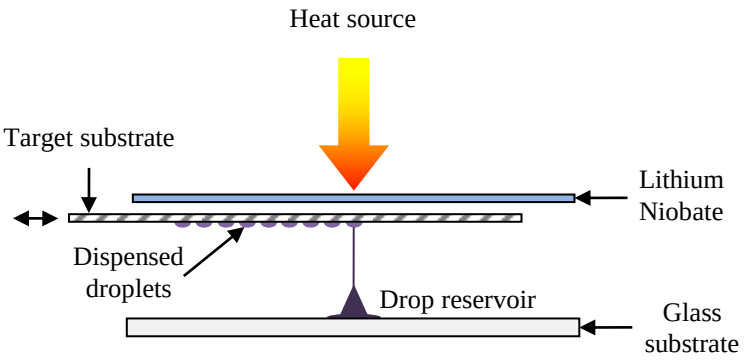

Figure 2.19 *– Simplified schematic of a pyroelectric jet system*

Problems may arise with this technique due to the effect of heating on the printed droplets: the evaporation rate of the fluid could be increased, and if cells are suspended within the fluid, they could be affected as well.

Electrohydrodynamic Jet Printing presents a new advantage that none of the other techniques have yet to achieve: both a continuous stream and discrete droplets of cell solution is possible which may be used to form cells into polymer threads that can be used as scaffolds [78]. Other strong points in its favour are: the 100% cell viability, the size of the droplets is independent of the nozzle size; extremely high concentrations of cells (>10^7 cells/mL) are possible; and the ability to use bio-inks with high viscosities (>10,000 mPa·s) [68–72,79]. Pyroelectric jet printing has the advantage of not having nozzles, thus avoiding the problems that so many of the other techniques can suffer from such as clogging. Since the pyro-electrohydrodynamic effect is triggered by a heat source, electrodes need not be used, making the system more flexible and easier to set up than EHDJ. Furthermore, attolitre droplets have been demonstrated with this technique [76,77,80].

However the use of heat and the small volume of the droplets in pyroelectric jet printing make it unsuitable for cell patterning.

Unfortunately to date there has been no papers published demonstrating that Electrohydrodynamic Jet Printing can be used to pattern cells in a controlled and reproducible manner. Another disadvantage is that the wide range of droplet sizes – between tens of microns and millimetres in diameter – during the same experiment [70,71]. Regrettably this means that this approach, in its current form, is unsuitable for high-resolution cell printing, as position and droplet size reproducibility are an absolute requirement for the majority of cell printing applications.

2.2.7 Acoustics

The first experiments using acoustic energy to transfer liquids was carried out by Alfred Lee Loomis in 1927; he observed that by immersing a high-power acoustic generator in an oil bath, a mound would appear on the surface that would *"[erupt] oil droplets like a miniature volcano*" [81,82].

Although there are variations in the techniques, they generally operate on the same principle: an acoustic generator is placed below (or above, depending on the desired direction for dispensation) the fluid to be dispensed and sends acoustic waves propagating through the fluid which focus at the interface between the fluid and the air creating a swell at the focal point which grow until they are large enough to pinch off and become droplets [82,83].

The first version of this technique utilised a single focused transducer located below a micro plate with multiple fluid-filled wells. The transducer moves from well to well and can trigger the ejection of droplets by sending acoustic waves that travel through the fluid to form a focal point, set using an acoustic lens, located just below the surface of the fluid [82,84,85]. This technique lacks the ability to simultaneously dispense multiple droplets unless multiple transducers are used which would increase the already relatively high power requirements [85].

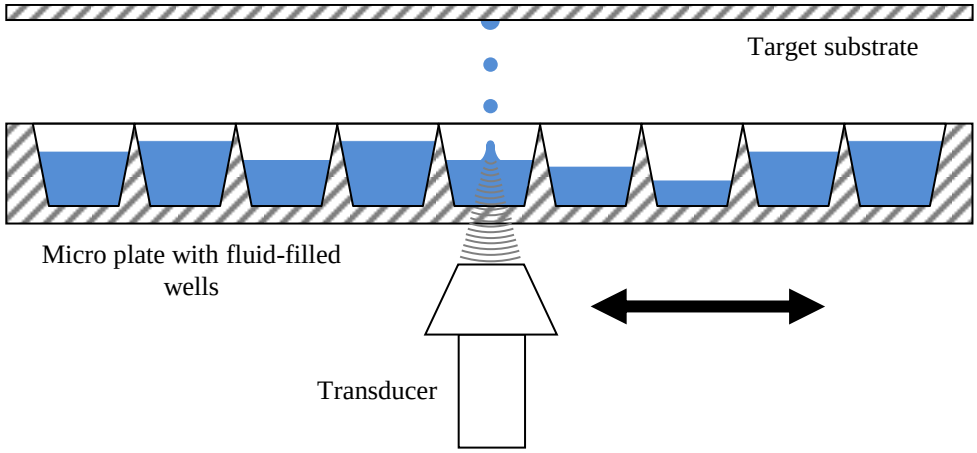

Figure 2.20 *– Simplified schematic of a classic transducer-based acoustic system (adapted from [82]).*

A newer version created by Utkan Demirci at Harvard-MIT Health Sciences and Technology and Harvard Medical School employs acoustically focused 2D micro-machined micro-droplet ejector arrays. Instead of using an acoustic lens to create the focal point, the focal point in this technique is formed by the constructive interference of surface acoustic waves which leak into the fluid medium. The substrate uniformity and fabrication ease ensures repeatability and the stable operation of the ejector array. The addition of microfluidic channels constantly refill the fluid, keeping the level constant and allowing the array to be orientated in any direction without affecting the printing process [85,86].

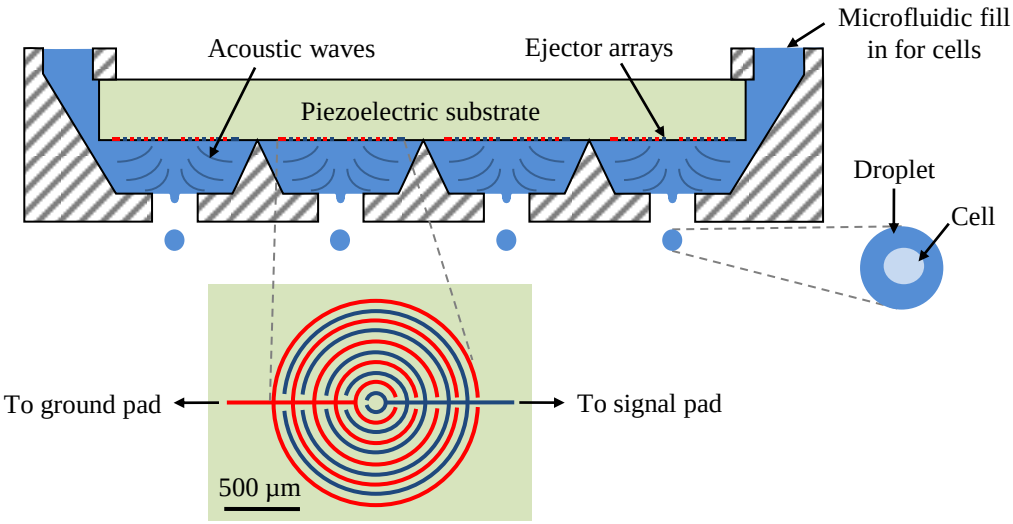

Figure 2.21 *– Simplified schematic of an interdigitated transducer-based Acoustic system (adapted from [85,86]).*

Various types of cells have been used to test this technique including AML-12 hepatocytes, HL-1 cardiomyocytes, mouse embryonic stem cells, fibroblasts and human

Raji cells encapsulated in acoustic picolitre droplets at rates varying from 1-100,000 droplets per second [87]. Cell viabilities were demonstrated to be over 89.8% across various cell types, even at high-throughput rates [85].

Acoustic techniques boast many advantages over other techniques: the droplets are ejected from an open pool without requiring a nozzle, thus avoiding the problems associated with them (such as clogging, heating and high pressures), and enabling the encapsulation and ejection single cells (or a few cells e.g. 1-3 cells per droplet was demonstrated by Demirci & Montesano [85]) with uniform ejection directionality, high consistency, and post-ejection viability (>89.8%). Small volume transfers in the picolitre and nanolitre range at low ejection velocities have been demonstrated which reduces the chance of cross-contamination due to splashing [82–86].

A slight problem with this technique is that heat is generated by the interdigitated transducers when they trigger a droplet dispense which raises the temperature in the fluid reservoir and could increase the evaporation rate, affecting the properties of the fluid, and droplet sizes. Fortunately the amount of heat generated is extremely small ($<5\times10^{-5}$ °C) and has plenty of time to dissipate before the next dispense is triggered even at 10 kHz it only takes ~90 μs to dissipate. This temperature rise could become an issue if the ejector array was much larger, or if it were operated at a continuous mode of ejection at higher frequencies for a long time [86].

2.2.8 Other Techniques

Apart from the techniques covered in the previous sections, a number of more traditional, but still widely used, cell printing techniques exist. A selection of these techniques are summarised in this section, including Micro-contact printing, Microarray spotting, and Photolithography.

Micro-contact printing (or μCP) uses a stamp created by photolithography to pattern cells onto the substrate – just like potato prints. First, a layer of photoresist is applied to a layer of silicon which is patterned by a photo-mask and UV light. Then a stamp is created by pouring PDMS over the patterned surface and curing it at high temperatures. Finally, the stamp is coated with cells in solution and brought into contact with the substrate, transferring the cells to the substrate in the pre-set pattern [8,88,89].

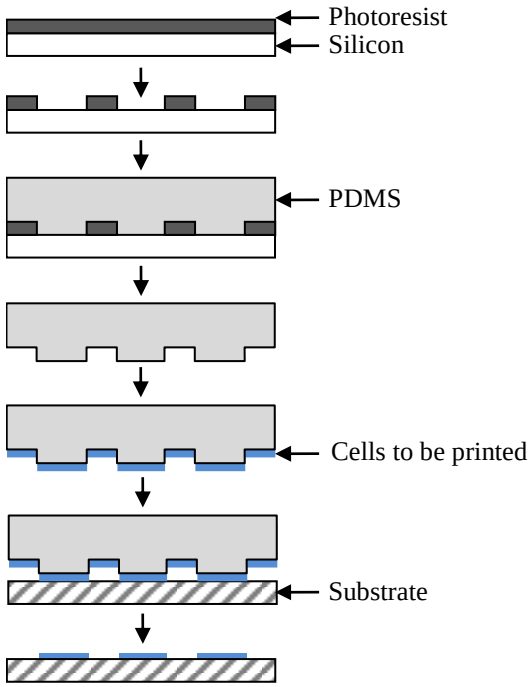

Figure 2.22 *– Schematic of the Micro-contact printing procedure (adapted from [90]).*

Micro-contact printing is a simple technique that can quickly pattern cells with a single stamp that can be reused to create the same pattern several times. However, a new stamp would be required for each new pattern and stamps can suffer from deformation and swelling/shrinking [8,88–90].

A possible addition to the more modern printing techniques would be to print cell adhesion molecules using micro-contact printing before delivering the cells, effectively organising the growth of the cells into the desired shape [35].

Microarray spotting is similar to some of the more modern techniques, in that it employs a computer controlled xyz motion stage to move the biological material. The pen itself operates in the same way as a quill-type ink pen and is used to pick up small volumes of biological material from multi-well plates and depositing (or spotting) them in the desired location on the substrate [91].

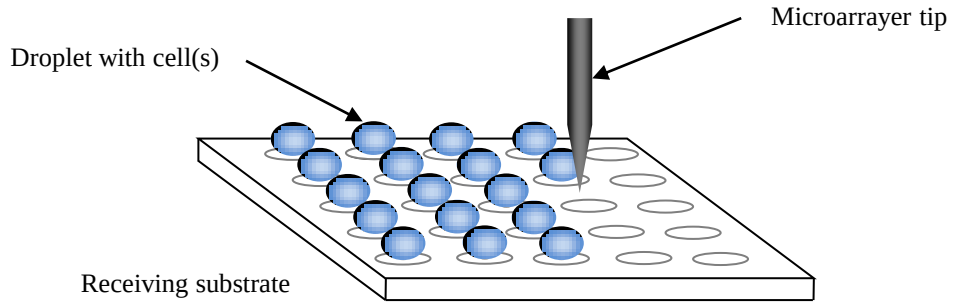

Figure 2.23 *– Schematic of the Microarray spotting technique (adapted from [92]).*

Providing that the substrate is a flat, solid surface, printing is reliable and repeatable. However, if the substrate is a membrane or uneven, then problems can arise such as missed spots or surface indentations [91]. Microarray spotting techniques have several inherent limitations, including heating and viscosity effects, variable volume transfer, clogging, and contamination (if multiple biological materials are used) [11,91].

Photolithography, also known as optical or UV lithography, is a microfabrication technique that uses light to remove parts of a thin film or substrate. The desired pattern is transferred using light from a photo mask to a light-sensitive chemical photoresist on the substrate [93,94]. A series of chemicals are applied which etch the exposure pattern onto the substrate. Photolithography is used in the semiconductor industry to create complex integrated circuits.

With slight modification, the photolithographic process can be used to pattern cells. By depositing cell attachment factors onto a substrate previously coated with agar (which retards cell adhesion) and applying a pattern using photolithography, the resulting surface will only permit cells to grow in the desired pattern. This method has been successfully used to pattern fibroblasts, cardiomyocytes and HeLa cells with a spatial resolution of ±3 µm [90,93].

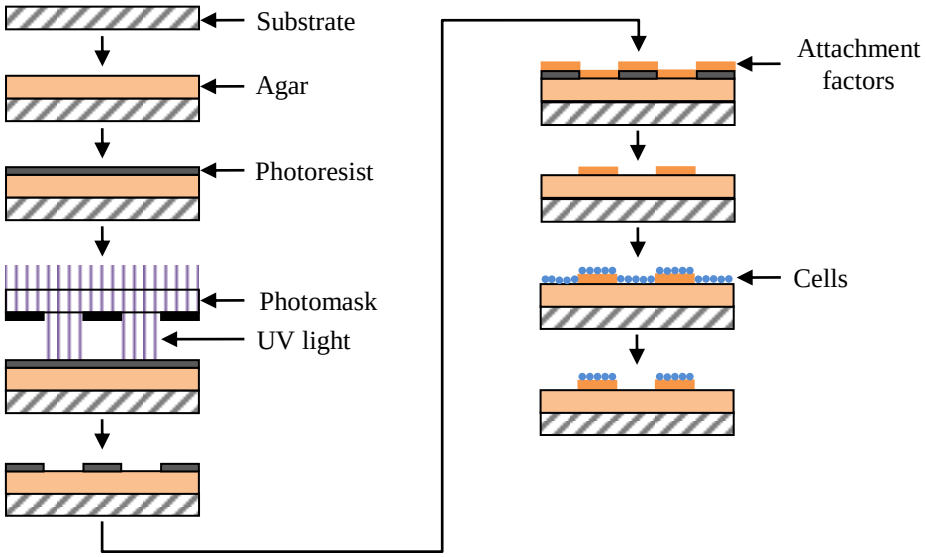

Figure 2.24 *– Schematic of Photolithographic cell patterning technique*

Photolithography is an extremely useful micro-fabrication technique: so much so that it is often used to supplement some of the other techniques described here – for example, making patterned substrates to print cells onto [95] or stamps to print cells with [90]. Unfortunately it is also an extremely expensive process, and is unable to pattern non-planar surfaces [90].

2.2.9 Applications of Biological Cell Printing

During my investigation into the techniques used in biological cell printing, it became apparent that there are a wide range of useful applications. These applications range from *in vitro* drug screening to organ printing, including tissue engineering and stem cell and cancer research.

2.2.9.1 Tissue engineering

From the very first paper that was published investigating cell printing, tissue engineering was identified as a major application for this new technology [96]. Cell printers that are only able to create two-dimensional cellular constructs are useful for some applications such as printing skin [97], but a number of studies have shown that certain cells require a three-dimensional structure in order to function properly. Dunn et al. showed that hepatocytes cultured as a monolayer lost many of their liver-specific functions after a few days, but those cultured with a layer collagen gel in a "sandwich configuration" were able to retain their liver-specific functions for several weeks [98]. Therefore, if more complex structures such as organs and organelles were to be printed

the cell printer would need the ability to transfer mesoscopic patterns of viable cells of multiple cell lines into well-defined three-dimensional arrays that closely mimic the tissue structure.

Three-dimensional multicellular culture would enable more in-depth investigations into the mechanisms and chemical signalling that occurs within *in vivo* systems and allow for the creation of predesigned synthetic tissue for repair, replacement and rejuvenation. As many cell printing techniques have proven to be compatible with stem cell transfer, this will open the door for the creation of autologous three-dimensional tissues generated from patient specific cells directed to differentiate into both organ specific and non-organ specific cells [72].

2.2.9.2 In vitro drug screening

Those same three-dimensional multicellular arrays could also be adapted and further developed for use in high throughput *in vitro* drug screening studies of a wide range of drugs. By incorporating microfluidics techniques, micro-tissue-laden chips called "organ-on-a-chip" devices [99] could be created, which produce the same physiological reaction that the entire organ would but on a much smaller scale. This development would result in faster and more reliable results (due to a much larger testing population and less inter-sample variability), better drugs, and an end to animal model-based studies, ultimately resulting in a more humane research paradigm [100].

2.2.9.3 Cell-sorting and research

One of the most important requirements for studying components of any biological system, either molecules in a cell or cells in an organ, is having pure populations of different types of living cells from the biological system being studied [101]. These isolated components can them be characterised before being recombined under controlled conditions.

Table 2.3 *– A comparison of the demonstrated capabilities of the different biological cell printing techniques*

	Spot size or resolution (µm)	Deposition speed	Drop size	Cell viability (%)	Bio-ink viscosity range (mPa·s)	Advantages/*limitations*	References
Optical Tweezers	5×10^{-3}	1 MHz	-	100	Not reported	Single cell resolution, *Single plane transport only*	[1–3]
Laser-based	10-120	5 kHz 9×10^{-8} mL/s	12 fL – 90 nL	95-100	2-300	Nozzle-free, *Expensive, Radiation*	[6,8–12,19–21]
Inkjet	10-85	3.6 kHz 5×10^{-4} mL/s	1-130 pL	75-90	1-20	Expandable, Multi-ink, Cheap, *Nozzle-based, Heat/Viscosity*	[34,44–48]
Valve-based	150	0.3 kHz 1.4×10^{-3} mL/s	≥2 nL	>95	1-18	Gentle, Expandable, Multi-ink, *Nozzle-based*	[52–54]
Bio-extrusion	1200	1.4 mL/s	-	40-80	100-2000	Continuous streams, Expandable *Nozzle-based*	[58,102]
Electrohydrodynamic Jet	~2-1000	1×10^{-2} mL/s	2-10 pL	100	22	Continuous streams, *Non-fixed droplet sizes*	[69–71]
Acoustics	~12	10 kHz	5-50 nL	>90	0.3-10	Nozzle-free, Multi-ink *Cell concentration variance*	[82,84,85]

The ability to create precise *in vitro* cultures of cells is essential for replicating the *in vivo* microenvironment. For example, a culture of cancer cells can help us to gain further understanding of the influence of spatial and geometric locations on cancer induction, proliferation, and metastasis [8]. Cell-to-cell communication between healthy normal cells and carcinomas could also be studied in cultures. A cell-based model that emulates the *in vitro* behaviour offers obvious advantages over traditional drug testing techniques saving time, money and increasing predictability [103].

2.3 Human Stem Cell Biology

Pluripotent stem cells, which can be divided into embryonic stem cells (ESCs) and induced pluripotent stem cells (iPSCs), have the ability to self-renew indefinitely and the potential to differentiate into cells constituting all three somatic germ layers (or all cells found in an adult) [104–108]. Mouse ESCs were first isolated from early mouse blastocysts in 1981 [109,110], followed soon after by human ESCs (hESCs) in 1998 [111]. In 2006 Takahashi et al. discovered that iPSCs can be derived from somatic cells by retrovirally transducing them with four transcription factors – Oct3/4, Sox2, Klf4 and C-myc [112,113]. These cells have the same self-renewal and differentiation capabilities as ESCs but with the added advantage that iPSCs can be used for autogenic therapies.

These unique potency characteristics make hESCs and iPSCs ideal for use in a number of applications, such as modelling early embryonic development. The potentially limitless numbers of differentiated hESC progeny can also be used for clinical tissue engineering/replacement applications such as novel drug discovery and testing for the pharmaceutical industry [104,105,114,115]. Controlled and reproducible methods for the directed differentiation of hESCs or iPSCs are essential if these cells are to be used for tissue engineering or regenerative medicine applications. Differentiation of pluripotent stem cells is performed in two main ways: monolayer culture or through a cell aggregate intermediate step [104,116].

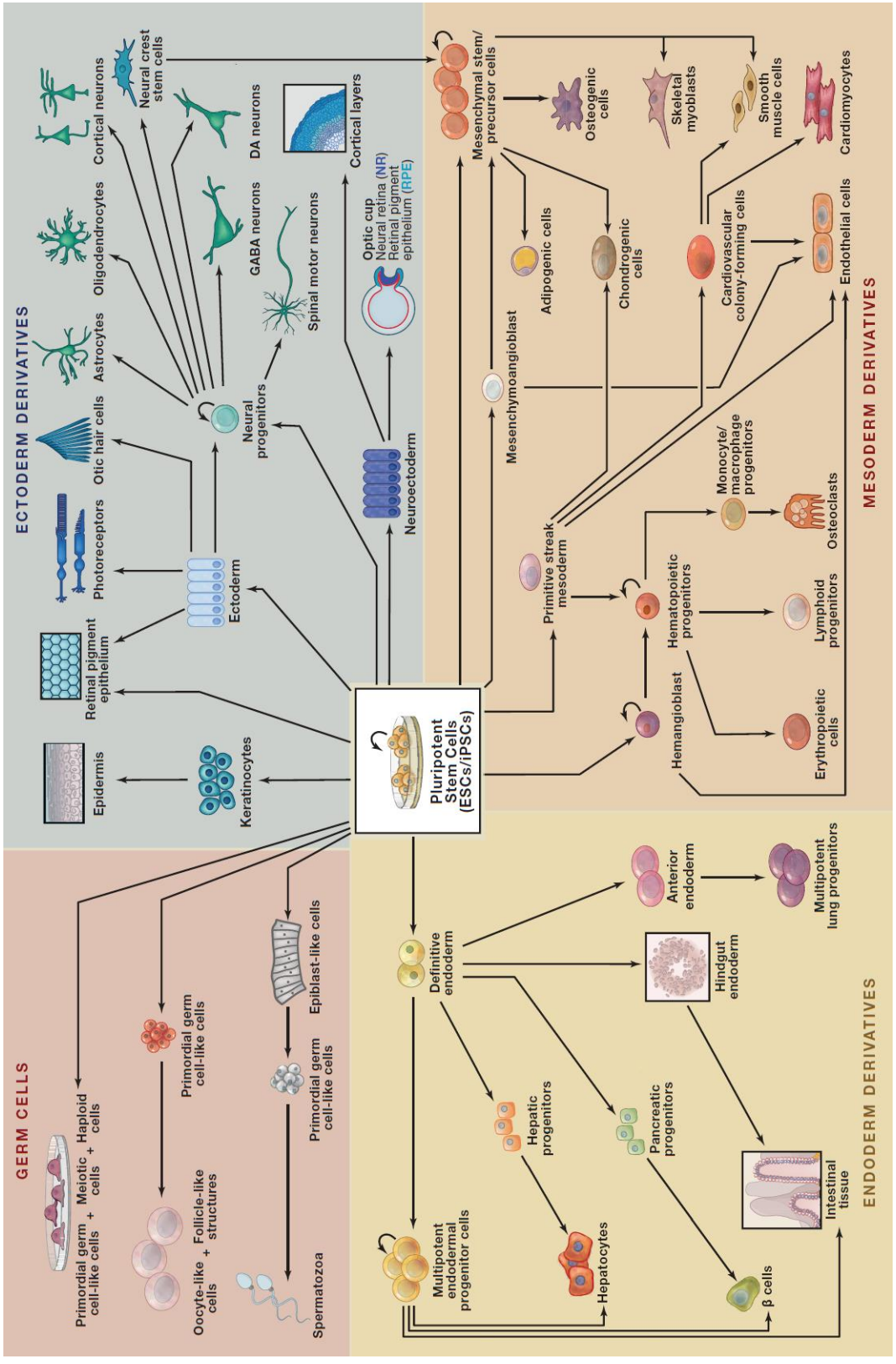

***Figure 2.25** – Schematic illustration of the differentiation potential of hPSCs. This cell type has the potential to differentiate to all three germ layers, endoderm, mesoderm, and ectoderm, or to the germ line cells. Some of the different cell types are exemplified by simple illustrations [117].*

The use of stem cells rather than adult cells is important as harvested adult cells rapidly lose important function and can fail to create new tissues with the other cells, whereas stem cells which have been directed to differentiate into the same tissue-specific cells result in foetal-like populations, which are more likely to create new tissues [118,119].

2.3.1 Cell Aggregates

In vitro, hESCs typically cluster together to form 3-dimensional spheroid aggregates when cultured in medium that had the growth factors removed, which maintains them in a non-adherent and undifferentiated state [120]. After the spheroids have formed, the medium can be replaced by one which allows the hESCs to differentiate, and the spheroids are now commonly known as embryoid bodies (EBs). Descendants of all three germ layers can be generated from hESCs following EB formation including hepatic, hemopoietic, pancreatic, cardiac, neural, and even germ cells. The efficiency with which specific cell types are generated within the EB is partly determined by the size of the spheroid used to create the EB. A lack of uniformity in EB size can lead to asynchronous and heterogeneous differentiation [121,122]. Consequently, the ability to reliably create uniform EBs of specific sizes is required to generate the correct cell-cell signals needed to produce particular cell types such as cardiomyocytes [123].

2.3.1.1 Static suspension

Static suspension culture is the most basic method used to create cellular aggregates and EBs. A suspension of ESCs are placed in an ultra-low adherence Petri-dish and simply allowed to spontaneously form aggregates as shown in Figure 2.26 [106,124]. Itskovitz-Eldor et al. demonstrated that human EBs created in suspension culture acquire molecular markers specific to the three embryonic germ layers [106], therefore various lineages can be created in this manner.

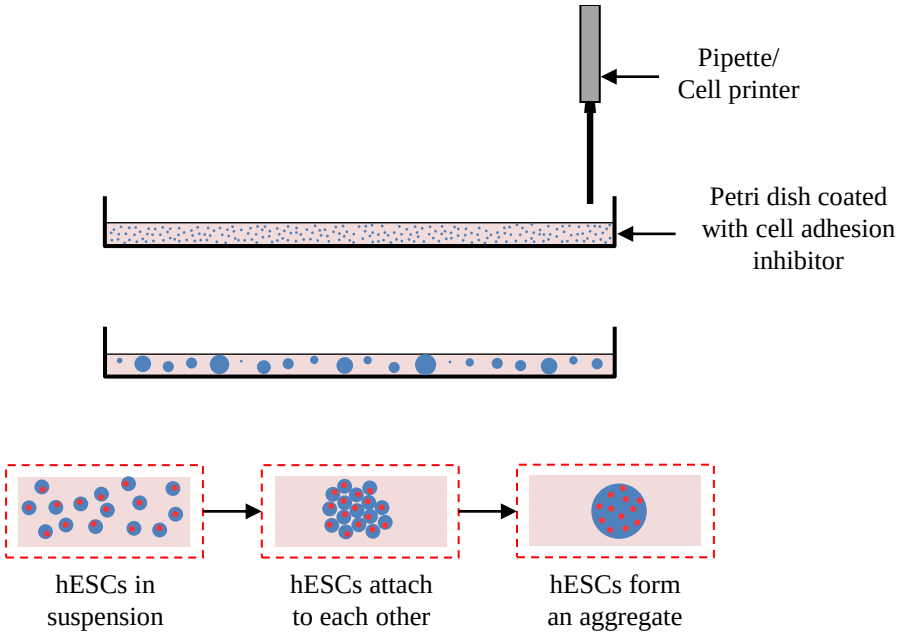

Figure 2.26 *– Schematic of the static suspension aggregation technique*

This is an extremely simple method which is popular for neuronal cells [125], however there is little to no control over the size and shape of the aggregates [124]. Since the suspended cells are not compartmentalised, aggregates frequently agglomerate into irregular large aggregates, thus the subsequent differentiation results in heterogeneous populations [106,120,124,126].

2.3.1.2 Rotary mass suspension

There are several different techniques that fall into this category, including spinner flasks, rotary orbital culture and combinations and modifications of these techniques. The main difference between these techniques and the others described here is that the large scale production of EBs with homogeneous size, which is only possible with bioreactor techniques [126].

Spinner flasks are simple systems that utilise paddle-impellers to drive the suspended cells to clump together and aggregate into EBs. The *in vitro* environment can be continuously monitored and regulated (pH, shear forces, medium exchange rate etc.) [124].

Orbital shakers are a similar technique to spinner flasks, but the rotary movement is supplied by moving the entire container which serves to reduce the maximum shear

force that is applied to the cells. EBs created using this technique were reported to differentiate more easily than those created using static suspension culture [126].

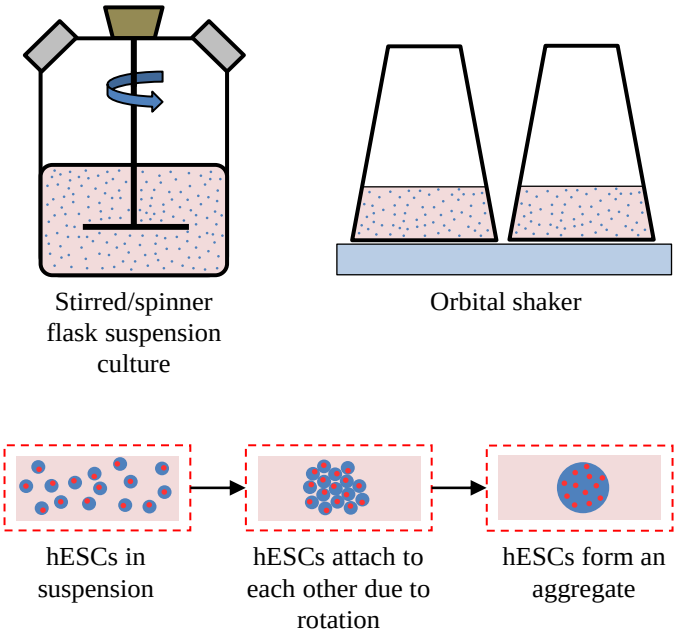

Figure 2.27 *– Schematic of the rotary mass suspension aggregation technique*

Rotary mass suspension culture is a very simple and scalable technique that allows for continuous monitoring and control of the physical and chemical environment, which is difficult to achieve by traditional methods [124]. Spheroids with homogeneous size distribution can be created with this technique, but the flow environment created by the process may damage the hESCs and disrupt cell signalling which could affect subsequent cell differentiation [120,123,127].

2.3.1.3 Gel encapsulation

Gel encapsulation is a technique which bridges the gap between hanging drop and static suspension culture; it encapsulates the suspended cells into small pockets of suspended cells in an effort to improve the homogeneity of aggregate sizes. A Petri dish is pre-loaded with hydrogels (such as alginate or methylcellulose) and droplets of suspended ESCs are jetted into the hydrogel to form isolated colonies which are physically separated but share a common nutrient supply via the hydrogel [124].

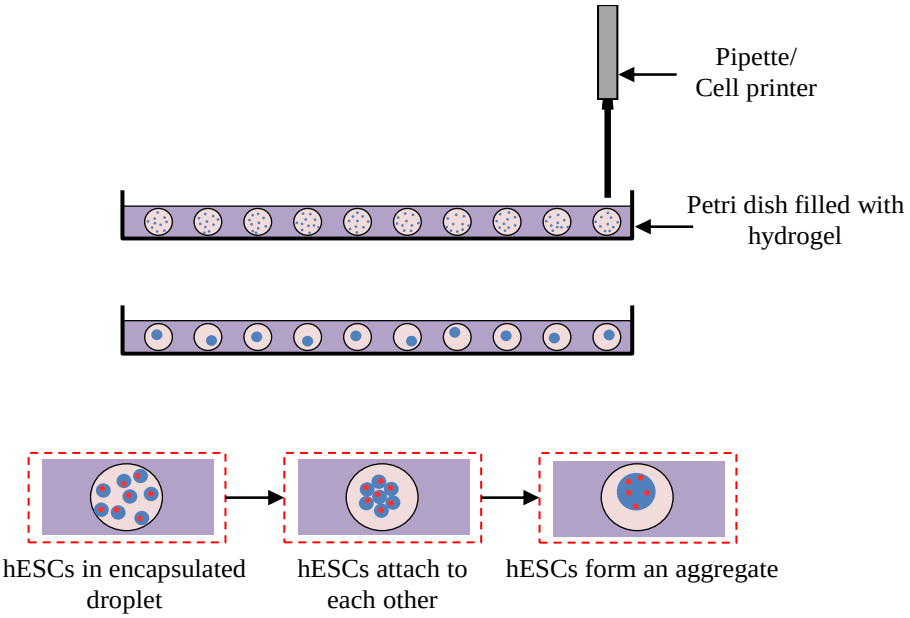

Figure 2.28 *– Schematic of the gel encapsulation aggregation technique*

EBs created in this way have improved synchrony and size reproducibility (and therefore differentiation reproducibility) [124]. Different hydrogels can be used to create different microenvironments for the ESCs and therefore elicit different responses from the ESCs, including inducing or preventing differentiation [128]. However, media changes and the retrieval of generated EBs are difficult due to the presence of the hydrogel material [120]

2.3.1.4 Non-adhesive micro-well arrays

Non-adhesive microwell plates have been developed in various dimensions and shapes (i.e. U and V shaped wells) in order to control the size and shape of the resulting spheroids. The surface of the wells is modified using a variety of techniques, such as plasma treatment, chemicals etc. to make them hydrophobic. Defined numbers of cells are deposited into the wells and, since they cannot attach to the surface of the well, they attach to each other and form an aggregate [124].

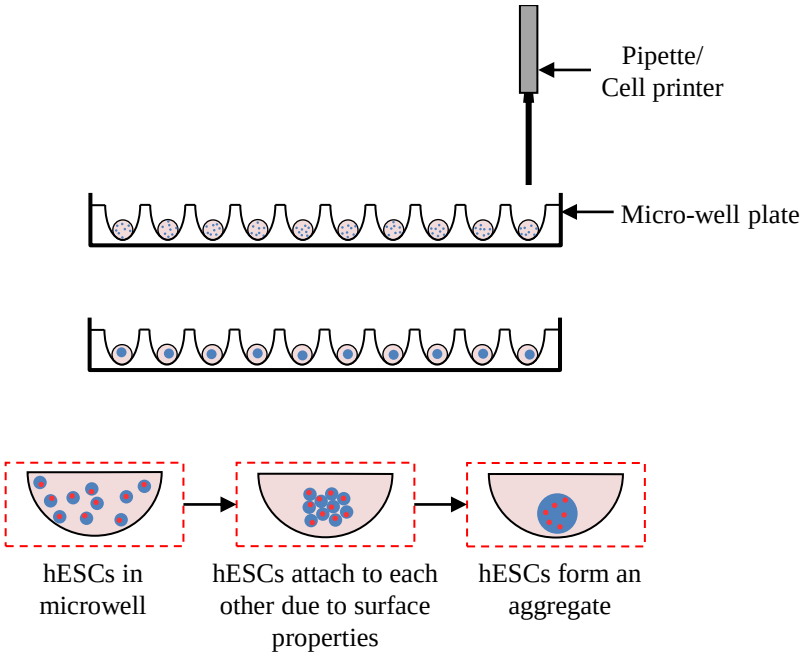

Figure 2.29 *– Schematic of the non-adhesive micro-well array aggregation technique*

The process is much faster than the other techniques and results in uniform size aggregates; however, the resulting aggregates are mechanically forced into a disk shape which is unstable, and the cells in the resulting EB form different cell lineages when re-suspended [121,123,124].

2.3.1.5 Adhesive stencils

In the adhesive stencils method, PDMS stamps are made using soft lithography with specified pattern geometries. The stamps are sterilised, inked with an aqueous solution of pH 5 1:30 growth factor-reduced Matrigel (GFR-MG), and then rinsed with sterile ddH_2O, and finally dried with sterile N_2, leaving a monolayer of protein on the surface [129]. This layer is transferred to the substrate using the stamp, the surface of which has been pre-treated to prevent protein adsorption and cell attachment to unpatterned regions of the substrate [130]. Cells are then seeded onto the substrate and are cultured in medium to allow them to attach to the patterned regions; unattached cells are subsequently removed by washing. Cells grow to confluence in the patterned regions and form flat aggregates.

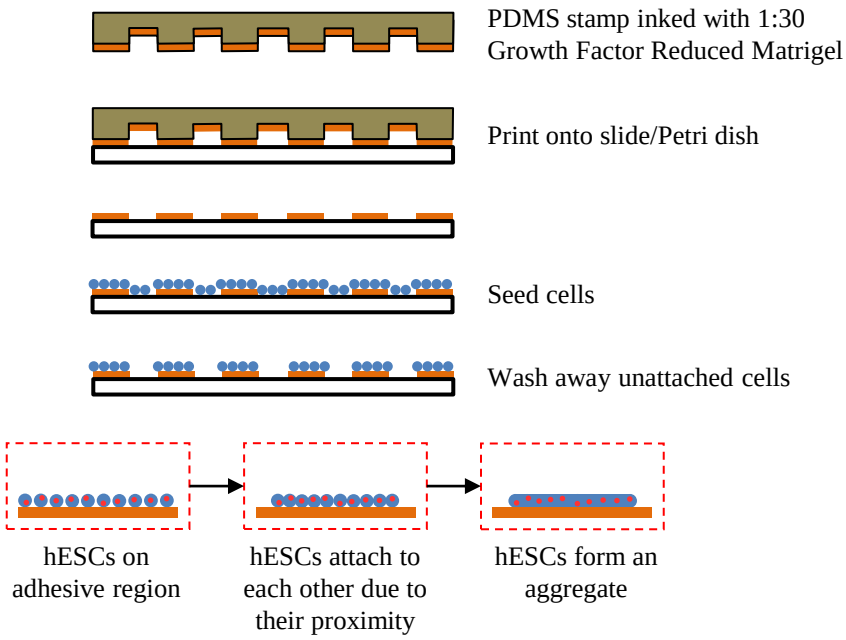

Figure 2.30 *– Schematic of the adhesive stencil aggregation technique*

This is an extremely simple and well established technique which can be scaled up very easily to be high throughput. However, adhesive stencils and other surface modification techniques are only able to control the initial size of EBs and the aggregates are only two-dimensional disks – not the 3D spheroids that are usually required [129].

2.3.1.6 Hanging-drop

In hanging-drop culture, cells in suspension are dispensed onto the underside of the lid of a Petri dish. The lid is inverted, creating a micro-environment without a surface for the cells to attach to which causes them to attach to each other forming a spheroid aggregate at the free liquid-air interface. The droplets are held in place by surface tension.

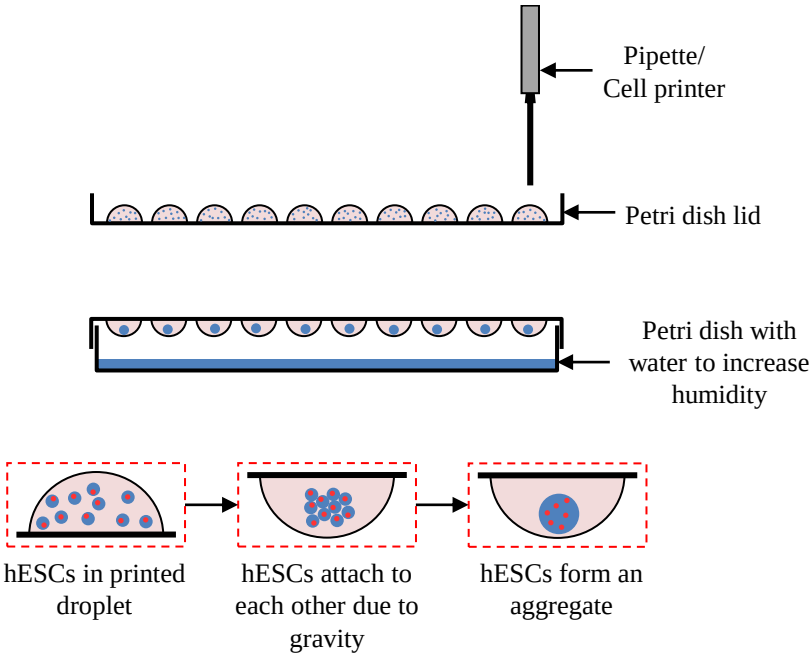

Figure 2.31 *– Schematic of the hanging-drop aggregation technique*

The hanging drop technique is a common method that is able to create uniform spheroid aggregates of specific sizes and cell numbers [131,132]. Another advantage is that it does not require any modification of the substrate surface, as the aggregates are gravity-induced and the substrate is inverted so there are no surfaces for the cells to adhere to. However, the resulting EBs can vary in size, mostly due to variations in droplet volume and cell concentrations in each droplet during pipetting, and due to the manual nature of this method is can be very time consuming and liable to human error [107,133].

Long-term culture is a challenge with this technique as fresh culture media will need to be added in order to keep the cells supplied with medium. Using a cell printer to deposit the droplets overcomes this issue since each droplet is in a known location, so it would be a very simple matter to flip the plate and overprint with fresh medium. An innovative new solution to this problem has been devised by a company called 3D Biomatrix which specialises in 3D cell culture products: Perfecta3D® Hanging Drop Plates [134]. These plates have standard well plate format but with the addition of an access hole at the bottom of the well (as shown in Figure 2.32) which eliminates the need to flip the plate to deposit the cells or add fresh media.

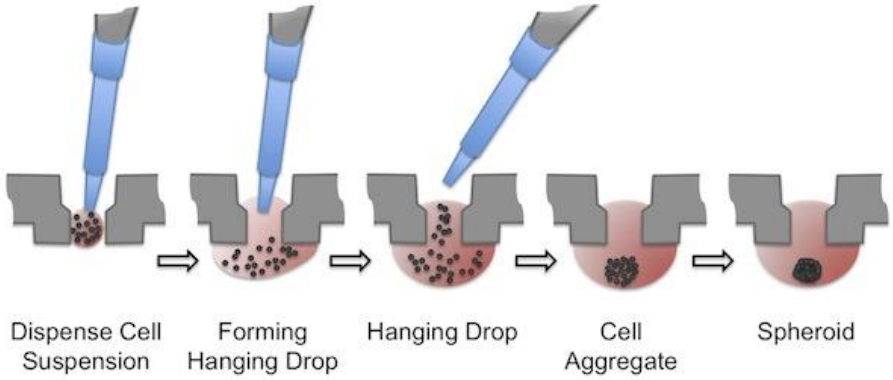

Figure 2.32 *– Cross section detail of the Perfecta3D® well geometry and the modified hanging droplet spheroid creation scheme [134]*

Table 2.4 *– A comparison of the demonstrated capabilities of the different cell aggregate creation techniques*

	Homogeneity of EB	Scalable production of EB	Controlled monitoring	Integrated culture	Easy to manage	Heterogeneity of EB	Small scale production of EB	Labour-intensive procedure	Difficult to manage	Requires a lot of medium	Shear force	References
Static Suspension					X	X						[124]
Rotary Mass Suspension		X	X		X	X				X	X	[124]
Gel Encapsulation	X							X	X	X		[120]
Non-adhesive Microwells	X				X		X					[127]
Adhesive Stencils		X			X	X	X					[124]
Hanging Drop	X	X					X	X	X			[120,128]

2.3.2 Bioengineering Livers

The pharmaceutical industry faces many challenges in the development of new medicines. It can take decades to successfully develop new drugs and only a very small number of candidate drugs are approved for human use [135–137]. There are several possible causes for this low success rate including externally applied restrictions and the increasing complexity of diseases. The majority of pre-clinical testing models currently in use are of non-human origin, leading to different responses when tested on humans late in the clinical phase of the trial or at market which, in the case of thalidomide for example, can have disastrous results [138]. Cell-based *in vitro* assays with high human relevance would serve to increase the efficiency of drug development but as primary cells rapidly lose their function in isolation, other possibilities must be considered [118,119].

A possible solution to this is the directed differentiation of human pluripotent stem cells and the creation of micro-tissues from these cells which would mimic the physiological reaction of an entire organ but at a much smaller scale. Cells from a single source or multiple hPSC lines can be used to test individual or population responses to novel drugs in high-throughput tests [118]. However, if these cells are to be used for these kind of applications, their differentiation must be reproducibly directed to the required lineages for each tissue. Unfortunately, homogeneous cellular differentiation of hPSCs into specific germ layers has proven to be hard to accomplish [139,140].

The most important cell types for drug discovery are considered to be hepatocytes, cardiomyocytes, and neuronal cells [118]. While cardiotoxicity is a common adverse effect of some drugs and neurons can be used to develop screening assays and establishing drug-target interactions [141], the liver is the most important organ for testing drug candidates. Unexpected drug metabolism, drug-induced injury of the liver and alteration of liver function are some of the major causes of drug candidate exclusion [142,143].

2.3.2.1 Differentiation of hPSCs into hepatocytes

The first article describing the generation of hepatocyte-like cells from hESCs was published in 2003 [144]. The core protocol, guiding cells to differentiate through definitive endoderm and early hepatic development by attempting to mimic the embryonic development of the liver, was used by several groups with slight

modifications. The resulting cells morphologically closely resemble hepatocytes and exhibit other hepatic functions such as albumin production, glycogen storage, ICG uptake and release and urea synthesis [145–147].

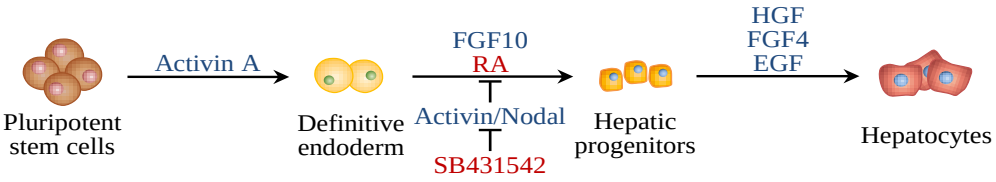

Figure 2.33 *– Schematic illustration of the differentiation pathway from hPSC to hepatocytes. Key growth and differentiation factors for each pathway are highlighted in blue and small molecules in red*

However, the generated cells in many studies are not truly functional, only a few studies demonstrate significant levels of enzymatic activity and so far no study has shown activity levels of multiple Cytochrome P450 (CYP) enzymes close to that of *in vivo* (or freshly isolated) human primary hepatocytes [139,140,148]. Obtaining fully functional cells from hESCs is a major challenge, one which has only just begun to be addressed.

2.3.2.2 Creation of liver micro-tissues

In vitro studies by Dunn et al. and Mauriel have shown that hepatocytes cultured as a monolayer lost many of their liver-specific functions after a few days [98,149]. Therefore harvested primary hepatocytes or hPSC-derived hepatocytes would need to be organised and cultured in three-dimensions, using a 3D matrix such as a hydrogel, to maintain their function over a longer timeframe [63]. The addition of supporting cells which are present in the adult liver could also serve to reproduce more of the functions of an adult liver in an *in vitro* construct.

The construction of an entire adult liver *in vitro* would constitute an almost insurmountable task with the technology of the day due to the numbers of cells that would be required and the highly vascular nature of the liver [63]. Therefore a smaller tissue construct such as a micro-tissue or organ bud would be a more reasonable aim.

Ramaiahgari et al. (2014) created spheroid aggregates from human hepatoma (HepG2) cells using hydrogel and allowing the cells to self-organise [143]. They observed that the HepG2 cells in the spheroids re-acquired lost hepatocyte functions such as the formation of structures resembling bile canaliculi, storage of glycogen and transport of bile salts, in addition to this the spheroids also exhibited an increase in the expression of

albumin, urea, xenobiotic transcription factors, phase I and II drug metabolism enzymes and transporters during long-term (28 days) culture [143]. These spheroids could easily be used for high-throughput long-term toxicity screening assays, but HepG2 cells and hepatocytes are different – which could result in differences in their responses.

For many years, it was believed that liver organogenesis was not possible to reproduce *in vitro*, but recently all that changed. Takebe et al. (2013) were able to construct a liver bud in a Petri dish from two-dimensionally cultured hiPSC-derived hepatic endoderm cells (iPSC-HEs) with human umbilical vein endothelial cells (HUVECs) and human mesenchymal stem cells (hMSCs) [150]. Although the cells were initially cultured in 2D, after around six days they were able to self-assemble into manipulatable, macroscopically visible, mechanically stable, three-dimensional cell clusters – hiPSC-derived liver buds [150]. It should be noted that there was no development of an external bile network, which means these liver buds do not perform all the functions of an adult liver [151].

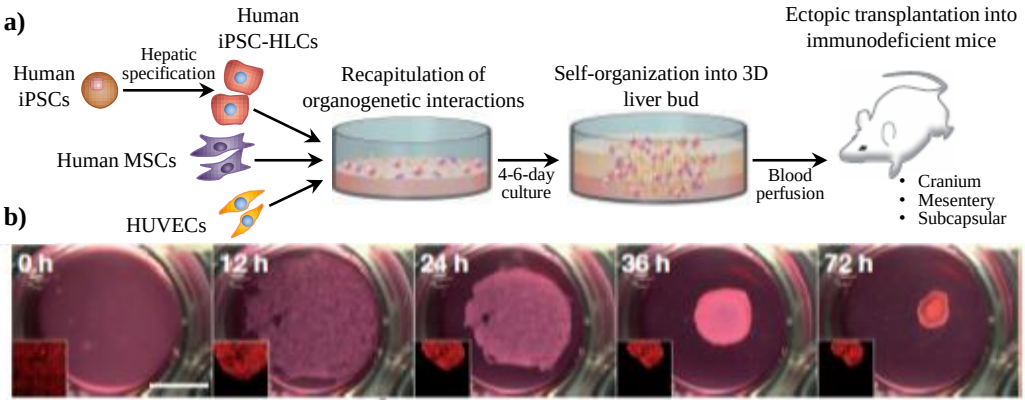

Figure 2.34 *– Generation of liver buds from hiPSCs: a) Schematic representation of the process; b) Self-organisation of liver buds from co-culture of hiPSC-HLCs with HUVECs and hMSCs (adapted from [150])*

2.4 Hydrogels for 3D Cell Patterning

The use of biodegradable scaffolds for tissue engineering started in the late 1980s as a method to increase the efficiency of transplanted cells using porous scaffolds made from biodegradable polymers, which they termed "chimeric neomorphogenesis" [152]. Cells (sometimes along with proteins and genes) are cultured within porous biodegradable 3D scaffolds which act as the extracellular matrix (ECM) to which cells attach, grow, and form new tissues [153]. As the cells start to create their own ECM, the biopolymer which the scaffold is made from should start to degrade, allowing the new tissue to

support itself [154]. In scaffold design one must consider mass-transport requirements for cell nutrition, migration and waste removal, as well as surface features to facilitate cell attachment, all of which necessitate a porous scaffold structure [27,153,155].

Traditionally, cells and other biomaterials are seeded onto the pre-prepared scaffolds and cultured in a bioreactor [36,156], however this approach has various limitations and challenges including inflammatory responses to the polymer materials [153,154], non-uniform cell density [36,157–159], undesired triggering of stem cell differentiation [160] and the creation of a vascular network is as yet unsolved [36,157,158]. Therefore an alternative technique was developed to address these issues which create the 3D porous structure from cell-laden hydrogels in a layer-by-layer approach.

Hydrogels are three-dimensional cross-linked networks of hydrophilic polymer chains, which can be either natural or synthetic in origin, that can absorb substantial amounts of water, up to 20 times its molecular weight [161–164]. The mechanical and structural properties of hydrogels, which are dependent on the crosslink junctions between the polymer chains, are comparable to the extracellular matrix (ECM) of many tissues [163–168]. The polymer networks contain pores between the polymer chains which enhance the supply of nutrients and oxygen throughout the structure in addition to providing room for cells and newly forming tissue [169,170].

The formation of the polymer chain networks, commonly referred to as crosslinking or gelation, can be triggered or modified by the addition of light, chemicals or thermal transitions (depending on the hydrogel). Hydrogels used as biomaterials are typically biodegradable [163]; they are also extremely customizable, with a very large selection of available synthetic and natural components, fabrication techniques, and synthesis methodologies which result in tuneable properties such as pore size and mechanical strength [163,166]. Encapsulating cells in hydrogels enables three-dimensional cell patterning and direct organ (or organoid) printing [169]. Other benefits of using hydrogels for 3D cell culture include: biocompatibility, injectability, ease of modification, and growth factors which can be released at programmed intervals to assist tissue formation or growth [161]. However, degradation and digestion of the hydrogel at a complimentary rate to that of ECM formation is not trivial to program [169].

When human ES cells (hESCs) are encapsulated within a 3D hyaluronic acid hydrogel, the hESCs maintained their undifferentiated state while remaining pluripotent [171]. In contrast, hESCs encapsulated in 3D dextran hydrogel are induced to differentiate demonstrating that different hydrogels act as microenvironments which can maintain or trigger differentiation of stem cells [124,128].

2.4.1 Natural Hydrogels

There are several natural derived hydrogel forming polymers including hyaluronic acid, alginate, chitosan, fibrin, collagen and gelatin. Each natural polymer has specific properties depending on their origin and composition which make them more suited to certain applications. A number of polymers are derived from components of the ECM such as collagen and fibrin. Collagen gels are the main component of mammalian tissue ECM and make up 25% of the total protein mass of most mammals [163,164]. Hyaluronic acid is a polysaccharide that can be found in most mammalian tissues. Alginate and agarose are also polysaccharides, but they are derived from marine algae.

Hyaluronan, also known as hyaluronic acid (HA) or hyaluronate, is an anionic, non-sulfated, long unbranched polysaccharide which is a major constituent of ECM where it regulates cell motility and adhesion, as well as mediating cell proliferation and differentiation [163,172,173]. Hyaluronate consists of repeating disaccharide blocks of (1,4)-linked β-$_D$-guluronic acid and $_N$-acetyl-β-$_D$-glucosamine units [163,172]. Gelation of hyaluronate can be achieved by attaching thiols, methacrylates or tyramines [171]. However, hyalurnate hydrogels can suffer from poor cell attachment due to its hydrophilic and polyanionic properties. This can be remedied by modifying the hydrogel, as Shu et al. (2003) did, by adding peptides to enhance cell proliferation within the hydrogel [172].

Alginic acid, commonly known as alginate, is a naturally occurring anionic polysaccharide isolated from the cell walls of brown algae. Alginate is a copolymer with linear blocks of (1,4)-linked β-$_D$-mannuronate (M) acid and α-$_L$-guluronic acid (G) residues covalently linked in different combinations of consecutive M-blocks, consecutive G-blocks or alternating MG-blocks [59,174]. Gelation of sodium alginate is easily achieved through selective binding of carboxylic groups on G-blocks with divalent cations such as calcium or barium, subsequently forming bonds with adjacent chains, creating an egg-box structure [175,176]. The viscosity of the prepared alginate

solution is dependent on the concentration of the polymer, molecular weight (M_W), average chain segment ratio (G to M ratio), temperature and the pH of the solution [59,163,165,166,175,177].

Chitosan (Ct) is a linear polysaccharide which can be extracted from arthropod exoskeletons by deacetylation of chitin [163,178]. Chitosan consists of β-(1,4)-linked $_D$-glucosamine with randomly located $_N$-acetyl-$_D$-glucosamine units [163,173]. Due to the structural similarity with mammalian ECM components, chitosan is degradable by human enzymes [163]. The crystallinity is determined by the degree of deacetylation with maximum crystallinity at 0% and 100% [163,173]. The amount of deacetylation also controls the degradation rates with higher deacetylation resulting in lower degradation rates [173]. The stable crystal structure of chitosan makes it insoluble in solutions above pH 7 but soluble in solutions below pH 5 [173]. Chitosan gelation is achieved through hydrogen bonding triggered by exposure to high pH solutions [173].

Collagen comes in many different types, but the basic structure is composed of three polypeptide chains (called alpha peptides) in a triple helix with hydrogen and covalent bonds [163]. Collagen I is an $\alpha1(I)_2\alpha2(I)$ heterotrimer (two of the chains are identical while the third differs slightly in chemical composition), unlike collagen II and collagen III, which are α1 homotrimers (all three chains are identical) [179]. The mechanical properties of collagen fibres can be modified in several ways including: physical cross-linking (i.e. with UV irradiation, thermal changes) [180,181]; chemical cross-linking (i.e. with formaldehyde, glutaraldehyde, carbodiimide) [180,182]; combination with other polymers (i.e. HA, fibrin, PVA) [183,184].

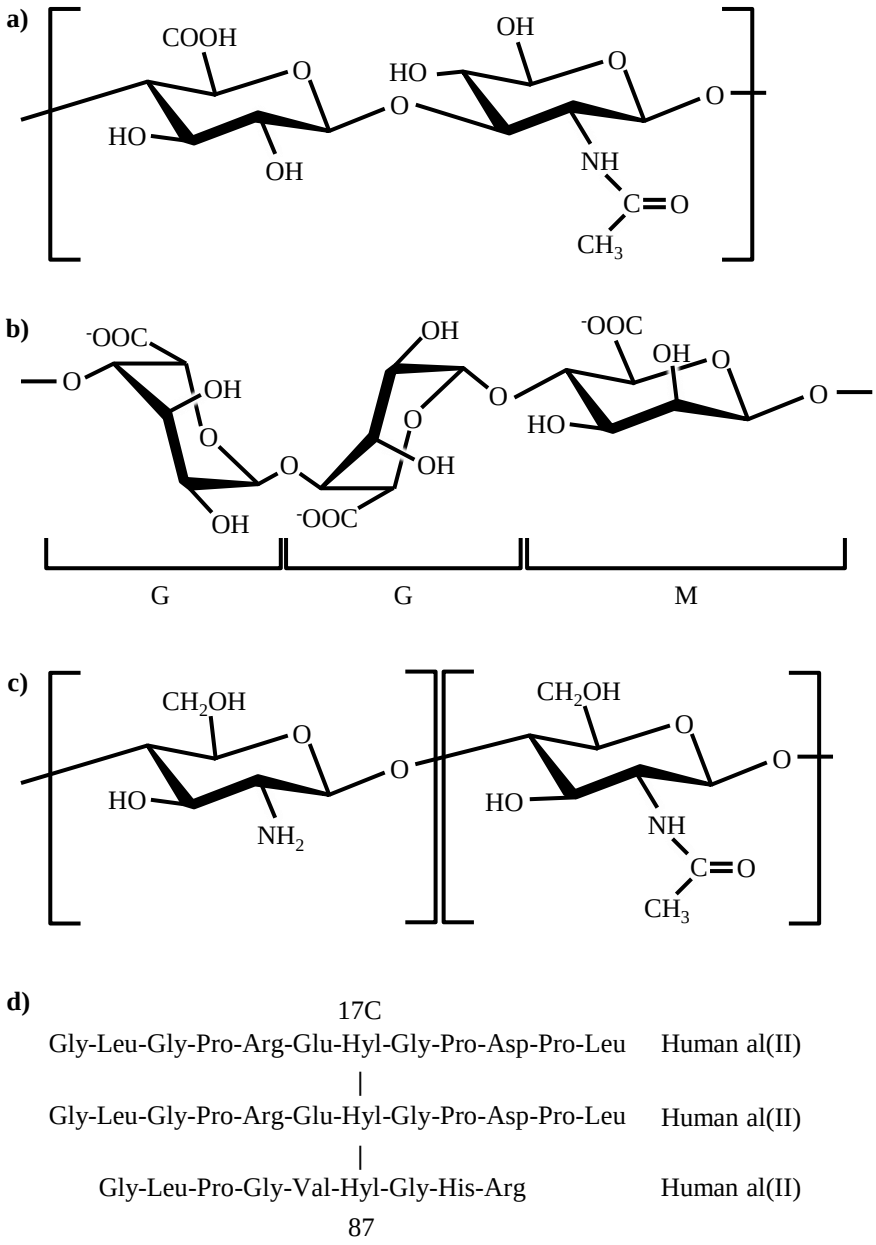

Figure 2.35 *– Chemical structure of naturally derived hydrogel polymers: a) HA; b) alginate; c) chitosan; d) human type II collagen fibrils described in [185]*

Natural polymers possess an inherent biocompatibility and have often exhibited positive cell interaction, but can suffer from large variations batch-to-batch and a lack of adaptability [170].

2.4.2 Synthetic Hydrogels

Despite the large numbers of available natural hydrogel forming polymers sometimes none of them quite meet all the requirements for a particular application. Synthetic hydrogels can be designed with controllable and reproducible chemical structure, molecular weight, degradable linkages, crosslinking modes and mechanical properties

[163]. In order to modify the properties of the gel, synthetic polymers can also be combined with natural hydrogels including: degradability, porosity, stiffness and hydrophilicity [164]. Novel hydrogel materials should possess the ability to survive sterilisation procedures and it would be advantageous if they were tailored to be compatible with specific bioprinting techniques to enable use in advanced tissue and organ fabrication [169]. Examples of synthetic hydrogel materials include PEG and PVA.

Poly(ethylene glycol) (PEG), also known as polyethylene oxide (PEO) or polyoxyethylene (POE) depending on its molecular weight, is a polyether compound with a wide variety of applications in industry and medicine. The term PEG is used for polymers with a molecular mass below 20,000 g/mol, while PEO refers to polymers with a higher molecular mass [186]. PEG/PEO is a hydrophilic polymer that can be modified to crosslink in a variety of ways, including photo-crosslinking by adding acrylates to the ends of the fibres and mixing with an appropriate photoinitiator [163,187]. Thermally reversible hydrogels have also been created synthesising block copolymers of PEG/PEO and poly($_L$-lactic acid) (PLLA) [163]. PEG-based hydrogels are extremely popular due to their biocompatibility and the versatility of the material [169]. The structural properties, and hence the subsequent transport characteristics, of the hydrogel structure can be controlled by changing the molecular weight or the concentration of the polymer [187]. Kraehenbuel et al. (2008) showed that PEG-based hydrogels can direct the differentiation of pluripotent P19 embryonal carcinoma cells along a cardiac lineage *in vitro* [188].

Poly(vinyl alcohol) (PVA, PVOH, or PVA1) (not to be confused with polyvinyl acetate) is a hydrophilic polymer that is widely used in biomedical applications including drug delivery and tendon repair [163,189]. PVA tends to spontaneously form weak physically cross-linked hydrogels which are unsuitable for most applications, therefore additional chemical crosslinks are used for longer term applications [169]. This additional cross-linking can be achieved through freeze-thaw processes, chemical cross-linking or radiation [163,189]. Unfortunately, these processes result in harsh environments within the forming hydrogel that are not compatible with cells [189]. PVA can be modified to be photo-crosslinkable by grafting crosslinkable groups onto the fibres, hydrogels can then be formed in minutes at physiological conditions which allows cells to be present during formation and *in situ* formation, resulting in

homogeneous seeding throughout the structure [189]. While PVA hydrogels possess similar water content to articular cartilage, the mechanical properties are not sufficient to withstand the typical loading conditions [190].

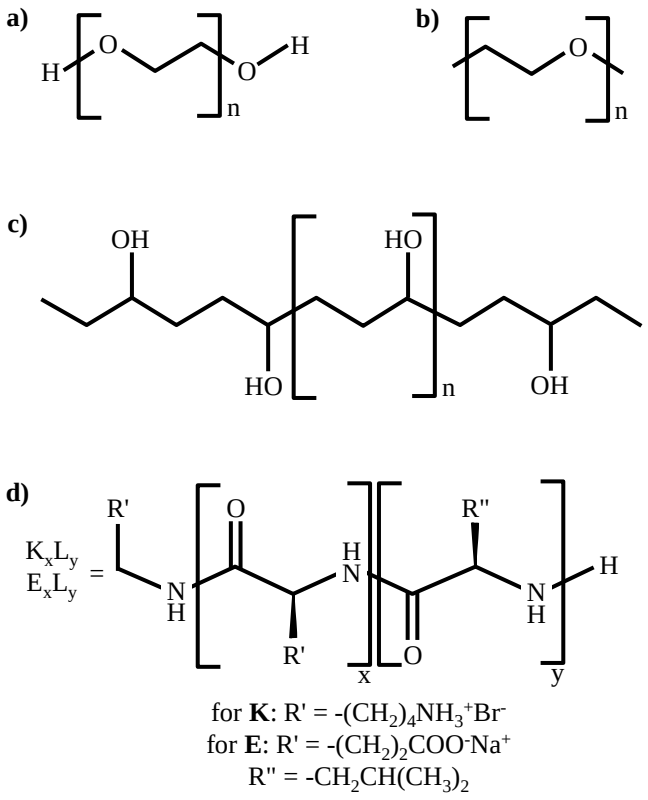

Figure 2.36 *– Chemical structure of synthetically derived hydrogel polymers: a) PEG; b) PEO; c) PVA; and d) a diblock co-polypeptide hydrogel described in [191]*

Censi et al. (2011) used a photopolymerisable, thermosensitive and biodegradable synthetic hydrogel based on PEG and HPMAm-lactate to engineer cartilage, the polymer exhibited similar characteristics to collagen and encapsulated chondrocytes were highly viable [170].

Synthetic polymers have well-defined, tuneable structures, are less-prone to issues with remaining by-products and batch-to-batch variations which can be an issue with some natural hydrogel materials [169,170]. However, biocompatibility and biodegradability often present a challenge [170,189].

2.4.2.1 Synthetic Peptide Hydrogels

Polymeric hydrogels, both natural and synthetic, can suffer from a number of limitations including poorly defined structure and irreversible bonds [192–194]. In

recent years synthetic self-assembling peptide-based hydrogels have been developed which are composed of short oligomers that tend to aggregate in aqueous solution and form distinct sheet structures with charged amino acids on the outside, which enable further interactions with ions contained in physiological fluids [169,195]. Peptide-based hydrogels show much promise due to their biocompatibility, biodegradability, easy incorporation of functional groups and well-defined sub-structures [191,196–199].

2.4.3 Printing with Hydrogels

By utilising a bioprinting technique to pattern hydrogels, highly porous cell-laden 3D constructs with complex tissue-mimicking geometries and reproducible control over cell placement can be constructed in a high throughput layer-by-layer approach [159,164,170,184]. Several different cell types could be incorporated and the structure could be designed to precisely fit into an existing defect to facilitate regeneration. Bioprinted hydrogel structures can be used to assist the regeneration of a number of different tissues including liver [200], cartilage [170,184], bone [201] and skin [202]. Hydrogel structures created with a bioprinter have several advantages over those created using other techniques: there will be much increased repeatability between structures as compared to those created using other techniques such as particulate leaching, gas foaming or solvent casting; also, complex internal architectures can be designed in computer aided design software using data from medical scans as a template [63,155].

Typically, hydrogels are formed from long chains, which result in high viscosity gels with non-Newtonian characteristics [203]. However this is usually higher than the viscosity range of most bioprinting techniques [34,45,58,67], therefore non-cross-linked precursor solutions are usually dispensed separately to be cross-linked post-printing in a layer-by-layer self-assembly process to build up a 3D structure from 2D slices [203]. It is important to note that in order to create structures with geometric fidelity using a bioprinter, the viscosity and gelling speed have to meet very specific requirements that depend on the application [159]. In certain situations this is not possible as the hydrogel is a single component such as collagen which is a gel at room temperature; in this case it is possible to cool the gel to lower the viscosity to a printable range [57]. This has its drawbacks as the temperature would need to be raised after each layer to allow it to gel sufficiently to support the next layer which drastically increases the time required to print a 3D structure.

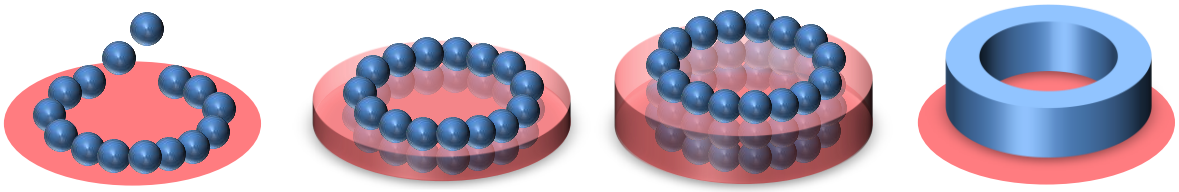

Figure 2.37 *– Schematic of the layer-by-layer hydrogel-assisted bioprinting technique (adapted from [158])*

Schuurman et al. (2011) used a bioprinter to create a 3D hybrid hydrogel and thermoplastic structure with encapsulated human immortalized chondrocytes. Polycaprolactone (PCL) and C20A4-laden alginate was printed in a layer by layer fashion with the PCL supporting the alginate which would be challenging to print alone at low viscosities. The post-printing viability of the cells was significantly lower than the control which is possibly due to residual heat from the PCL [159].

Boland et al. (2003) introduced a new scheme for organ and tissue printing using hydrogels. They proposed using preformed cellular aggregates as building blocks with hydrogels added to support and direct their self-assembly [36]. Aggregates are placed on the surface of the hydrogel so that they are in contact with their neighbours and allowed to fuse into contiguous structures; extra hydrogel can be added to facilitate the creation of 3D structures. This new scheme has several advantages, including lower stress experienced by cells during dispensing, minimisation of required hydrogel material, large scale tissues that can be created quickly through the process of aggregate fusion, a cellular environment which is closer to the *in vivo* environment so cells will work better, and sensitive stem cells are less likely to re-differentiate and lose their function [158,204].

2.5 Summary and Conclusion

In this review, several different topics were covered: techniques for printing viable biological cells were reviewed and summarised; a background in human stem cell biology was provided with descriptions of differentiation, aggregate creation and the creation of liver tissue; and hydrogels including their use in 3D cell patterning was presented. Table 2.3 compares the capabilities of the different biological cell printing techniques described in this review.

There are many different approaches to cell printing, but simply described, it is a rapid transfer technique that is easily customised in terms of cell types, printed patterns and application. Many of the techniques utilise CAD/CAM technology (be it software or machinery) and have achieved, or are very close to, single cell resolution. Cells, and other biomaterials, can be deposited onto a homogeneous growth surface to ensure cellular proliferation is controlled by normal cell-cell interactions. Precise patterns of cells can be deposited to form co-cultures and multi-cultures. Three dimensional printing is possible by depositing cells layer-by-layer, either by repeated deposition of cells onto a single point or by the addition of matrix layers. The majority of cell printing techniques are capable of printing high percentages of viable cells quickly and reliably. However, the viability and function of printed cells are affected by different factors in each technique, such as shear forces in the nozzle, heat applied during dispensing and impact on the substrate surface, each of which need to be optimised separately to minimise cell damage.

Human stem cell biology is far too large a subject to be described in full in this thesis, but the relevant topics of this field were described here. Pluripotent stem cells (PSCs) have the capability to differentiate into any of the cells found in the adult body and have the ability to self-renew indefinitely but differentiation *in vitro* can be hard to control. There are two types of PSC: embryonic stem cells and induced pluripotent stem cells. A number of differentiation protocols have been developed that give specific instructions to PSCs and direct them to differentiate down a specific lineage pathway to the desired cell type. Cell-based *in vitro* assays with human liver cells could be used to increase the efficiency of drug development. PSCs can be directed to differentiate into hepatocytes which demonstrate many of the functions of *in vivo* cells; these cells could be bioprinted with hydrogels to create 3D liver micro-tissues that replicate the response and functions of a human liver but on a much smaller scale. If multiple different hPSC lines are used then high-throughput population testing of novel drugs would be possible.

Hydrogels are three-dimensional cross linked networks of hydrophilic polymer chains that can absorb substantial amounts of water; the mechanical and structural properties of hydrogels are comparable to extracellular matrix (ECM). Cells can be cultured in 3D hydrogel structures and since the networks are porous the cells can grow and get access to nutrients. The hydrogel acts like a scaffold for the cells while they grow and should degrade when the cells start to create their own ECM. An advantage of using hydrogels

instead of traditional scaffolds is that they can be created in a layer-by-layer approach and do not suffer from the biocompatibility and mechanical incongruity with tissue. There are several types of hydrogel, both natural and synthetic, which cross-link in a variety of different ways and are extremely customizable. Hydrogel precursor solutions are typically aqueous and can therefore be deposited with a bioprinter in a layer-by-layer approach to create porous cell-laden 3D constructs with tissue-mimicking geometries and high spatial control over cell placement.

2.6 References

[1] Ashkin A, (1970). "Acceleration and Trapping of Particles by Radiation Pressure," *Physical Review Letters*, **24**(4), pp. 156–159.

[2] Gajraj A, and Meiners JC, (2005). "Optical tweezers," *Encyclopedia of Modern Optics*, pp. 78–86.

[3] Zhang H, and Liu K-K, (2008). "Optical tweezers for single cells," *Journal of The Royal Society Interface*, **5**(24), pp. 671–690.

[4] Enger J, Goksör M, Ramser K, Hagberg P, and Hanstorp D, (2004). "Optical tweezers applied to a microfluidic system," *Lab on a Chip*, **4**(3), pp. 196–200.

[5] Liu Y, Cheng DK, Sonek GJ, Berns MW, Chapman CF, and Tromberg BJ, (1995). "Evidence for Localized Cell Heating Induced by Infrared Optical Tweezers," *Biophysical Journal*, **68**, pp. 2137–2144.

[6] Odde DJ, and Renn MJ, (1999). "Laser-guided direct writing for applications in biotechnology," *Trends in Biotechnology*, **17**(10), pp. 385–389.

[7] Chrisey DB, Pique A, Fitz-Gerald J, Auyeung RCY, McGill RA, Wu HD, and Duignan M, (2000). "New approach to laser direct writing active and passive mesoscopic circuit elements," *Applied Surface Science*, **154**, pp. 593–600.

[8] Schiele NR, Corr DT, Huang Y, Raof NA, Xie Y, and Chrisey DB, (2010). "Laser-based direct-write techniques for cell printing," *Biofabrication*, **2**(3), p. 032001.

[9] Barron JA, Ringeisen BR, Kim H, Spargo BJ, and Chrisey DB, (2004). "Application of laser printing to mammalian cells," *Thin Solid Films*, **453-454**, pp. 383–387.

[10] Barron JA, Spargo BJ, and Ringeisen BR, (2004). "Biological laser printing of three dimensional cellular structures," *Applied Physics A*, **79**, pp. 1027–1030.

[11] Barron JA, Wu P, Ladouceur HD, and Ringeisen BR, (2004). "Biological laser printing: a novel technique for creating heterogeneous 3-dimensional cell patterns," *Biomedical microdevices*, **6**(2), pp. 139–147.

[12] Guillotin B, Souquet A, Catros S, Duocastella M, Pippenger B, Bellance S, Bareille R, Rémy M, Bordenave L, Amédée J, and Guillemot F, (2010). "Laser assisted bioprinting of engineered tissue with high cell density and microscale organization," *Biomaterials*, **31**(28), pp. 7250–7256.

[13] Duocastella M, Colina M, Fernández-Pradas JM, Serra P, and Morenza JL, (2007). "Study of the laser-induced forward transfer of liquids for laser bioprinting," *Applied Surface Science*, **253**(19), pp. 7855–7859.

[14] Barron JA, Rosen R, Jones-Meehan J, Spargo BJ, Belkin S, and Ringeisen BR, (2004). "Biological laser printing of genetically modified Escherichia coli for biosensor applications," *Biosensors and Bioelectronics*, **20**(2), pp. 246–252.

[15] Hopp B, Smausz T, Antal Z, Kresz N, Bor Z, and Chrisey D, (2004). "Absorbing film assisted laser induced forward transfer of fungi (Trichoderma conidia)," *Journal of Applied Physics*, **96**(6), pp. 3478–3481.

[16] Banks DP, Grivas C, Mills JD, Eason RW, and Zergioti I, (2006). "Nanodroplets deposited in microarrays by femtosecond Ti:sapphire laser-induced forward transfer," *Applied Physics Letters*, **89**(19), pp. 193107–193113.

[17] Catros S, Fricain J-C, Guillotin B, Pippenger B, Bareille R, Remy M, Lebraud E, Desbat B, Amédée J, and Guillemot F, (2011). "Laser-assisted bioprinting for creating on-demand patterns of human osteoprogenitor cells and nano-hydroxyapatite," *Biofabrication*, **3**(2), p. 025001.

[18] Ringeisen BR, Chrisey DB, Pique A, Young HD, Modi R, Bucaro M, Jones-Meehan J, and Spargo BJ, (2002). "Generation of mesoscopic patterns of viable *Escherichia coli* by ambient laser transfer," *Biomaterials*, **23**, pp. 161–166.

[19] Wu PK, Ringeisen BR, Krizman DB, Frondoza CG, Brooks M, Bubb DM, Auyeung RCY, Piqué A, Spargo B, McGill RA, and Chrisey DB, (2003). "Laser transfer of biomaterials: Matrix-assisted pulsed laser evaporation (MAPLE) and MAPLE Direct Write," *Review of Scientific Instruments*, **74**(4), pp. 2546–2557.

[20] Catros S, Guillotin B, Bačáková M, Fricain J-C, and Guillemot F, (2011). "Effect of laser energy, substrate film thickness and bioink viscosity on viability of endothelial cells printed by Laser-Assisted Bioprinting," *Applied Surface Science*, **257**(12), pp. 5142–5147.

[21] Barron JA, Krizman DB, and Ringeisen BR, (2005). "Laser Printing of Single Cells: Statistical Analysis, Cell Viability, and Stress," *Annals of Biomedical Engineering*, **33**(2), pp. 121–130.

[22] Gruene M, Unger C, Koch L, Deiwick A, and Chichkov B, (2011). "Dispensing pico to nanolitre of a natural hydrogel by laser-assisted bioprinting," *Biomed Eng Online*, **10**(1), pp. 19–30.

[23] Oishi Y, Taniguchi K, Matsumoto H, Ishihara A, Ohira Y, and Roy RR, (2003). "Differential responses of HSPs to heat stress in slow and fast regions of rat gastrocnemius muscle," *Muscle Nerve*, **28**(5), pp. 587–594.

[24] Ringeisen BR, (2009). "43: The Evolution of Cell Printing," Fundamentals of tissue engineering and regenerative medicine, Springer, Berlin, pp. 613–631.

[25] Nahmias Y, Schwartz RE, Verfaillie CM, and Odde DJ, (2005). "Laser-guided direct writing for three-dimensional tissue engineering," *Biotechnology and Bioengineering*, **92**(2), pp. 129–136.

[26] Ozbolat I, and Yu Y, (2013). "Bioprinting towards organ fabrication: challenges and future trends," *IEEE Transactions on Biomedical Engineering*, **60**(3), pp. 691–699.

[27] Guillotin B, and Guillemot F, (2011). "Cell patterning technologies for organotypic tissue fabrication," *Trends in Biotechnology*, **29**(4), pp. 183–190.

[28] Wilson WC, and Boland T, (2003). "Cell and organ printing 1: Protein and cell printers," *The Anatomical Record*, **272A**(2), pp. 491–496.

[29] Roth EA, Xu T, Das M, Gregory C, Hickman JJ, and Boland T, (2004). "Inkjet printing for high-throughput cell patterning," *Biomaterials*, **25**(17), pp. 3707–3715.

[30] Campbell PG, and Weiss LE, (2007). "Tissue engineering with the aid of inkjet printers," *Expert opinion on biological therapy*, **7**(8), pp. 1123–1127.

[31] Huang J, Cai R, and Zhang K, (2012). "Experiments and Analysis of Drop on Demand Cell Printing," *Research Journal of Applied Sciences*, **4**(2), pp. 93–96.

[32] Derby B, (2010). "Inkjet Printing of Functional and Structural Materials: Fluid Property Requirements, Feature Stability, and Resolution," *Annual Review of Materials Research*, **40**(1), pp. 395–414.

[33] Ozaeta JR, (2008). "Development of a Cell Depositing System Using Inkjet Technology," MSc Thesis, California Polytechnic State University.

[34] Zhang H, Massingill JL, and Woo JT, (2000). "Low VOC, low viscosity UV cationic radiation-cured ink-jet ink system," *Journal of Coatings Technology*, **72**(6), pp. 45–52.

[35] Xu T, Jin J, Gregory C, Hickman JJ, and Boland T, (2005). "Inkjet printing of viable mammalian cells," *Biomaterials*, **26**(1), pp. 93–99.

[36] Boland T, Mironov V, Gutowska A, Roth EA, and Markwald RR, (2003). "Cell and organ printing 2: Fusion of cell aggregates in three-dimensional gels," *The Anatomical Record*, **272A**(2), pp. 497–502.

[37] Wang X, (2008). "Drop-on-demand inkjet deposition of complex fluid on textiles," PhD Thesis, Georgia Institute of Technology.

[38] Hanson E, (2009). "How an ink jet printer works," *Imaging.org* [Online]. Available: http://www.imaging.org/ist/resources/tutorials/inkjet_printer.cfm. [Accessed: 15-Jan-2011].

[39] Saunders RE, Gough JE, and Derby B, (2008). "Delivery of human fibroblast cells by piezoelectric drop-on-demand inkjet printing," *Biomaterials*, **29**(2), pp. 193–203.

[40] Yamaguchi S, Ueno A, Akiyama Y, and Morishima K, (2011). "Cell Patterning using Ink Jet Technology to Eject a Single Cell in a Single Droplet," Proceedings of the International Conference on Biofabrication 2011, Toyama, Japan, p. 59.

[41] Kamisuki S, Hagata T, Tezuka C, Nose Y, Fujii M, and Atobe M, (1998). "A low power, small, electrostatically-driven commercial inkjet head," Micro Electro Mechanical Systems, 1998. MEMS 98. Proceedings., The Eleventh Annual International Workshop on, IEEE, pp. 63–68.

[42] Murata K, (2003). "Super-fine ink-jet printing for nanotechnology," MEMS, NANO and Smart Systems, 2003. Proceedings. International Conference on, IEEE, pp. 346–349.

[43] SIJTechnology Inc., (2010). "Technology | SIJTechnology, Inc. of super-fine inkjet technology" [Online]. Available: http://www.sijtechnology.com/en/technology/index.html. [Accessed: 14-Nov-2010].

[44] Di Biase M, Saunders RE, Tirelli N, and Derby B, (2011). "Inkjet Printing and Cell Seeding Thermoreversible Photocurable Gel Structures," *Soft Matter*, **7**(6), pp. 2639–2646.

[45] Derby B, (2012). "Printing and Prototyping of Tissues and Scaffolds," *Science*, **338**(6109), pp. 921–926.

[46] Nakamura M, Nishiyama Y, and Henmi C, (2008). "3D Micro-fabrication by inkjet 3D biofabrication for 3D tissue engineering," Micro-NanoMechatronics and Human Science, 2008. MHS 2008. International Symposium on, IEEE, pp. 451–456.

[47] Nakamura M, Kobayashi A, Takagi F, Watanabe A, Hiruma Y, Ohuchi K, Iwasaki Y, Horie M, Morita I, and Takatani S, (2005). "Biocompatible inkjet printing technique for designed seeding of individual living cells," *Tissue Eng.*, **11**(11-12), pp. 1658–1666.

[48] Cui X, Dean D, Ruggeri ZM, and Boland T, (2010). "Cell damage evaluation of thermal inkjet printed Chinese hamster ovary cells," *Biotechnology and Bioengineering*, **106**(6), pp. 963–969.

[49] Pardo L, Wilson WC, and Boland T, (2003). "Characterization of Patterned Self-Assembled Monolayers and Protein Arrays Generated by the Ink-Jet Method †," *Langmuir*, **19**(5), pp. 1462–1466.

[50] Hugenschmidt S, Planas-Bohne F, and Taylor DM, (1993). "On the toxicity of low doses of tetrasodium-ethylenediamine-tetraacetate (Na-EDTA) in normal rat kidney (NRK) cells in culture," *Arch Toxicol*, **67**(1), pp. 76–78.

[51] Calvert P, (2001). "Inkjet Printing for Materials and Devices," *Chemistry of Materials*, **13**(10), pp. 3299–3305.

[52] Moon S, Lin P-A, Keles HO, Yoo S-S, and Demirci U, (2007). "Cell Encapsulation by Droplets," *J Vis Exp*, **8**.

[53] Demirci U, and Montesano G, (2007). "Cell encapsulating droplet vitrification," *Lab on a Chip*, **7**(11), p. 14281433.

[54] Xu F, Emre AE, Turali ES, Hasan SK, Moon S, Nagatomi J, Khademhosseini A, and Demirci U, (2009). "Cell proliferation in bioprinted cell-laden collagen droplets," Bioengineering Conference, 2009 IEEE 35th Annual Northeast, IEEE, pp. 1–2.

[55] Weiss LE, Amon CH, Finger S, Miller ED, Romero D, Verdinelli I, Walker LM, and Campbell PG, (2005). "Bayesian computer-aided experimental design of heterogeneous scaffolds for tissue engineering," *Computer-Aided Design*, **37**(11), pp. 1127–1139.

[56] Xu F, Celli J, Rizvi I, Moon S, Hasan T, and Demirci U, (2011). "A three-dimensional in vitro ovarian cancer coculture model using a high-throughput cell patterning platform," *Biotechnology Journal*, **6**(2), pp. 204–212.

[57] Moon S, Hasan SK, Song YS, Xu F, Keles HO, Manzur F, Mikkilineni S, Hong JW, Nagatomi J, and Haeggstrom E, (2009). "Layer by layer three-dimensional tissue epitaxy by cell-laden hydrogel droplets," *Tissue Engineering Part C: Methods*, **16**(1), pp. 157–166.

[58] Vozzi G, Previti A, De Rossi D, and Ahluwalia A, (2002). "Microsyringe-Based Deposition of Two-Dimensional and Three-Dimensional Polymer Scaffolds with a Well-Defined Geometry for Application to Tissue Engineering," *Tissue Engineering*, **8**(6), pp. 1089–1098.

[59] Chung JHY, Naficy S, Yue Z, Kapsa R, Quigley A, Moulton SE, and Wallace GG, (2013). "Bio-ink properties and printability for extrusion printing living cells," *Biomater. Sci.*, **1**(7), pp. 763–773.

[60] Cohen DL, Malone E, Lipson HOD, and Bonassar LJ, (2006). "Direct freeform fabrication of seeded hydrogels in arbitrary geometries," *Tissue Engineering*, **12**(5), pp. 1325–1335.

[61] EnvisionTEC, (2014). "3D-Bioplotter®," *EnvisionTEC* [Online]. Available: http://envisiontec.com/products/3d-bioplotter/. [Accessed: 17-May-2014].

[62] Invetech, (2014). "Organovo: NovoGen MMX Bioprinter™" [Online]. Available: http://www.invetech.com.au/portfolio/life-sciences/3d-bioprinter-world-first-print-human-tissue/. [Accessed: 17-May-2014].

[63] Yan Y, Wang X, Xiong Z, Liu H, Liu F, Lin F, Wu R, Zhang R, and Lu Q, (2005). "Direct Construction of a Three-dimensional Structure with Cells and Hydrogel," *Journal of Bioactive and Compatible Polymers*, **20**(3), pp. 259–269.

[64] Norotte C, Marga FS, Niklason LE, and Forgacs G, (2009). "Scaffold-free vascular tissue engineering using bioprinting," *Biomaterials*, **30**(30), pp. 5910–5917.

[65] Shim J-H, Lee J-S, Kim JY, and Cho D-W, (2012). "Bioprinting of a mechanically enhanced three-dimensional dual cell-laden construct for osteochondral tissue engineering using a multi-head tissue/organ building system," *Journal of Micromechanics and Microengineering*, **22**(8), p. 085014.

[66] Nair K, Gandhi M, Khalil S, Yan KC, Marcolongo M, Barbee K, and Sun W, (2009). "Characterization of cell viability during bioprinting processes," *Biotechnology Journal*, **4**(8), pp. 1168–1177.

[67] Melchels FPW, Domingos MAN, Klein TJ, Malda J, Bartolo PJ, and Hutmacher DW, (2012). "Additive manufacturing of tissues and organs," *Progress in Polymer Science*, **37**(8), pp. 1079–1104.

[68] Telegraph Media Group Ltd., (2010). "Science Obituaries: Professor John Fenn," *The Telegraph* [Online]. Available: http://www.telegraph.co.uk/news/obituaries/science-obituaries/8226026/Professor-John-Fenn.html. [Accessed: 10-Apr-2010].

[69] Park J-U, Hardy M, Kang SJ, Barton K, Adair K, Mukhopadhyay DK, Lee CY, Strano MS, Alleyne AG, Georgiadis JG, Ferreira PM, and Rogers JA, (2007). "High-resolution electrohydrodynamic jet printing," *Nature Materials*, **6**(10), pp. 782–789.

[70] Eagles PAM, Qureshi AN, and Jayasinghe SN, (2006). "Electrohydrodynamic jetting of mouse neuronal cells," *Biochemical Journal*, **394**(2), pp. 375–378.

[71] Jayasinghe SN, Qureshi AN, and Eagles PAM, (2006). "Electrohydrodynamic Jet Processing: An Advanced Electric-Field-Driven Jetting Phenomenon for Processing Living Cells," *Small*, **2**(2), pp. 216–219.

[72] Poncelet D, de Vos P, Suter N, and Jayasinghe SN, (2012). "Bio-electrospraying and Cell Electrospinning: Progress and Opportunities for Basic Biology and Clinical Sciences," *Advanced Healthcare Materials*, **1**(1), pp. 27–34.

[73] Jayasinghe SN, (2013). "Cell electrospinning: a novel tool for functionalising fibres, scaffolds and membranes with living cells and other advanced materials for regenerative biology and medicine," *Analyst*, **138**(8), pp. 2215–2223.

[74] Wang DZ, Jayasinghe SN, Edirisinghe MJ, and Luklinska ZB, (2007). "Coaxial electrohydrodynamic direct writing of nano-suspensions," *J Nanopart Res*, **9**(5), pp. 825–831.

[75] Bartolovic K, Mongkoldhumrongkul N, Waddington SN, Jayasinghe SN, and Howe SJ, (2009). "The differentiation and engraftment potential of mouse hematopoietic stem cells is maintained after bio-electrospray," *Analyst*, **135**(1), pp. 157–164.

[76] Coppola S, Vespini V, Grilli S, and Ferraro P, (2011). "Self-assembling of multi-jets by pyro-electrohydrodynamic effect for high throughput liquid nanodrops transfer," *Lab on a Chip*, **11**(19), pp. 3294–3298.

[77] Rogers JA, and Paik U, (2010). "Nanofabrication: Nanoscale printing simplified," *Nature Nanotechnology*, **5**(6), pp. 385–386.

[78] Townsend-Nicholson A, and Jayasinghe SN, (2006). "Cell electrospinning: a unique biotechnique for encapsulating living organisms for generating active biological microthreads/scaffolds," *Biomacromolecules*, **7**(12), pp. 3364–3369.

[79] Jayasinghe SN, and Townsend-Nicholson A, (2006). "Stable electric-field driven cone-jetting of concentrated biosuspensions," *Lab Chip*, **6**(8), pp. 1086–1090.

[80] Ferraro P, Coppola S, Grilli S, Paturzo M, and Vespini V, (2010). "Dispensing nano–pico droplets and liquid patterning by pyroelectrodynamic shooting," *Nature Nanotechnology*, **5**(6), pp. 429–435.

[81] Wood RW, and Loomis AL, (1927). "The physical effects of high-frequency sound waves of great intensity," *Philosophical Magazine*, **7**, pp. 417–433.

[82] Ellson R, Mutz M, Browning B, Lee Jr. L, Miller MF, and Papen R, (2003). "Transfer of low nanoliter volumes between microplates using focused acoustics - automation considerations," *Journal of the Association for Laboratory Automation*, **8**(5), pp. 29–34.

[83] Al-Sueimani Y, Yule AJ, and Collins AP, (1999). "How orderly is ultrasonic atomization?," Proc. of ILASS-Europe'99, Toulouse, France, pp. 1–6.

[84] Elrod SA, Hadimioglu B, Khuri-Yakub BT, Rawson EG, Richley E, Quate CF, Mansour NN, and Lundgren TS, (1989). "Nozzleless droplet formation with focused acoustic beams," *Journal of Applied Physics*, **65**(9), pp. 3441–3447.

[85] Demirci U, and Montesano G, (2007). "Single cell epitaxy by acoustic picolitre droplets," *Lab on a Chip*, **7**(9), pp. 1139–1145.

[86] Demirci U, (2006). "Acoustic Picoliter Droplets for Emerging Applications in Semiconductor Industry and Biotechnology," *Journal of Microelectromechanical Systems*, **15**(4), pp. 957–966.

[87] Tasoglu S, and Demirci U, (2013). "Bioprinting for stem cell research," *Trends in Biotechnology*, **31**(1), pp. 10–19.

[88] Fink J, Théry M, Azioune A, Dupont R, Chatelain F, Bornens M, and Piel M, (2007). "Comparative study and improvement of current cell micro-patterning techniques," *Lab on a Chip*, **7**(6), pp. 672–680.

[89] Folch A, Jo B-H, Hurtado O, Beebe DJ, and Toner M, (2000). "Microfabricated elastomeric stencils for micropatterning cell cultures," *Journal of biomedical materials research*, **52**(2), pp. 346–353.

[90] Kane RS, Takayama S, Ostuni E, Ingber DE, and Whitesides GM, (1999). "Patterning proteins and cells using soft lithography," *Biomaterials*, **20**(23), pp. 2363–2376.

[91] MicroFab Technologies Inc., (2009). "Microarrays (presynthesized)" [Online]. Available: http://www.microfab.com/technology/biomedical/MicroarraysPreSyn.html. [Accessed: 04-Apr-2011].

[92] Fernandes TG, Diogo MM, Clark DS, Dordick JS, and Cabral JMS, (2009). "High-throughput cellular microarray platforms: applications in drug discovery, toxicology and stem cell research," *Trends in Biotechnology*, **27**(6), pp. 342–349.

[93] Rohr S, Flückiger-Labrada R, and Kucera JP, (2003). "Photolithographically defined deposition of attachment factors as a versatile method for patterning the growth of different cell types in culture," *Pflügers Archiv European Journal of Physiology*, **446**(1), pp. 125–132.

[94] Mooney JF, Hunt AJ, McIntosh JR, Liberko CA, Walba DM, and Rogers CT, (1996). "Patterning of functional antibodies and other proteins by photolithography of silane monolayers," *Proceedings of the National Academy of Sciences*, **93**(22), pp. 12287–12291.

[95] Lee CJ, Huie P, Leng T, Peterman MC, Marmor MF, Blumenkranz MS, Bent SF, and Fishman HA, (2002). "Microcontact Printing on Human Tissue for Retinal Cell Transplantation," *Archives of Opthalmology*, **120**(12), pp. 1714–1718.

[96] Klebe RJ, (1988). "Cytoscribing: a method for micropositioning cells and the construction of two-and three-dimensional synthetic tissues," *Experimental cell research*, **179**(2), pp. 362–373.

[97] Binder KW, Zhao W, Park GY, Xu T, Dice D, Atala A, and Yoo JJ, (2010). "In situ bioprinting of the skin for burns [Poster]," Advanced Technology Applications for Combat Casualty Care (ATACCC), Florida, USA.

[98] Dunn JC, Yarmush ML, Koebe HG, and Tompkins RG, (1989). "Hepatocyte function and extracellular matrix geometry: long-term culture in a sandwich configuration.," *The FASEB journal*, **3**(2), pp. 174–177.

[99] Huh D, Matthews BD, Mammoto A, Montoya-Zavala M, Hsin HY, and Ingber DE, (2010). "Reconstituting Organ-Level Lung Functions on a Chip," *Science*, **328**(5986), pp. 1662–1668.

[100] Chapman K, and Robinson S, (2007). "Challenging the regulatory requirement for acute toxicity studies in the development of new medicines."

[101] Herzenberg LA, Sweet RG, and Herzenberg LA, (1976). "Fluorescence-activated Cell Sorting," *Scientific American*, **234**(3), pp. 108–117.

[102] Khalil S, Nam J, and Sun W, (2005). "Multi-nozzle deposition for construction of 3D biopolymer tissue scaffolds," *Rapid Prototyping Journal*, **11**(1), pp. 9–17.

[103] Bhadriraju K, and Chen CS, (2002). "Engineering cellular microenvironments to improve cell-based drug testing," *Drug Discovery Today*, **7**(11), pp. 612–620.

[104] Murry CE, and Keller G, (2008). "Differentiation of Embryonic Stem Cells to Clinically Relevant Populations: Lessons from Embryonic Development," *Cell*, **132**(4), pp. 661–680.

[105] Fenno LE, Ptaszek LM, and Cowan CA, (2008). "Human embryonic stem cells: emerging technologies and practical applications," *Current Opinion in Genetics & Development*, **18**(4), pp. 324–329.

[106] Itskovitz-Eldor J, Schuldiner M, Karsenti D, Eden A, Yanuka O, Amit M, Soreq H, and Benvenisty N, (2000). "Differentiation of human embryonic stem cells into embryoid bodies compromising the three embryonic germ layers.," *Mol Med*, **6**(2), pp. 88–95.

[107] Xu F, Sridharan B, Wang S, Gurkan UA, Syverud B, and Demirci U, (2011). "Embryonic stem cell bioprinting for uniform and controlled size embryoid body formation," *Biomicrofluidics*, **5**(2), pp. 22207–15.

[108] Gage FH, (2000). "Mammalian Neural Stem Cells," *Science*, **287**(5457), pp. 1433–1438.

[109] Evans MJ, and Kaufman MH, (1981). "Establishment in culture of pluripotential cells from mouse embryos," *Nature*, **292**(5819), pp. 154–156.

[110] Martin GR, (1981). "Isolation of a pluripotent cell line from early mouse embryos cultured in medium conditioned by teratocarcinoma stem cells," *PNAS*, **78**(12), pp. 7634–7638.

[111] Thomson JA, Itskovitz-Eldor J, Shapiro SS, Waknitz MA, Swiergiel JJ, Marshall VS, and Jones JM, (1998). "Embryonic Stem Cell Lines Derived from Human Blastocysts," *Science*, **282**(5391), pp. 1145–1147.

[112] Takahashi K, Tanabe K, Ohnuki M, Narita M, Ichisaka T, Tomoda K, and Yamanaka S, (2007). "Induction of Pluripotent Stem Cells from Adult Human Fibroblasts by Defined Factors," *Cell*, **131**(5), pp. 861–872.

[113] Takahashi K, and Yamanaka S, (2006). "Induction of Pluripotent Stem Cells from Mouse Embryonic and Adult Fibroblast Cultures by Defined Factors," *Cell*, **126**(4), pp. 663–676.

[114] McNeish J, (2004). "Embryonic stem cells in drug discovery," *Nat Rev Drug Discov*, **3**(1), pp. 70–80.

[115] Wu DC, Boyd AS, and Wood KJ, (2007). "Embryonic stem cell transplantation: potential applicability in cell replacement therapy and regenerative medicine," *Front. Biosci.*, **12**, pp. 4525–4535.

[116] Doetschman TC, Eistetter H, Katz M, Schmidt W, and Kemler R, (1985). "The in vitro development of blastocyst-derived embryonic stem cell lines: formation of visceral yolk sac, blood islands and myocardium," *J Embryol Exp Morphol*, **87**(1), pp. 27–45.

[117] Williams LA, Davis-Dusenbery BN, and Eggan KC, (2012). "SnapShot: Directed Differentiation of Pluripotent Stem Cells," *Cell*, **149**(5), pp. 1174–1174.e1.

[118] Jensen J, Hyllner J, and Björquist P, (2009). "Human embryonic stem cell technologies and drug discovery," *J. Cell. Physiol.*, **219**(3), pp. 513–519.

[119] Trounson A, and DeWitt ND, (2012). "Stem cell biology: Towards the reality of cell therapeutics," *Nature Cell Biology*, **14**(4), pp. 331–331.

[120] Dang SM, Kyba M, Perlingeiro R, Daley GQ, and Zandstra PW, (2002). "Efficiency of embryoid body formation and hematopoietic development from embryonic stem cells in different culture systems," *Biotechnol. Bioeng.*, **78**(4), pp. 442–453.

[121] Park J, Cho CH, Parashurama N, Li Y, Berthiaume F, Toner M, Tilles AW, and Yarmush ML, (2007). "Microfabrication-based modulation of embryonic stem cell differentiation," *Lab on a Chip*, **7**(8), pp. 1018–28.

[122] Kim PTW, and Ong CJ, (2012). "Differentiation of Definitive Endoderm from Mouse Embryonic Stem Cells," Mouse Development, J.Z. Kubiak, ed., Springer Berlin Heidelberg, pp. 303–319.

[123] Mohr JC, Zhang J, Azarin SM, Soerens AG, de Pablo JJ, Thomson JA, Lyons GE, Palecek SP, and Kamp TJ, (2010). "The microwell control of embryoid body size

in order to regulate cardiac differentiation of human embryonic stem cells," *Biomaterials*, **31**(7), pp. 1885–1893.

[124] Rungarunlert S, Techakumphu M, Pirity MK, and Dinnyes A, (2009). "Embryoid body formation from embryonic and induced pluripotent stem cells: Benefits of bioreactors," *World J Stem Cells*, **1**(1), pp. 11–21.

[125] Suslov ON, Kukekov VG, Ignatova TN, and Steindler DA, (2002). "Neural stem cell heterogeneity demonstrated by molecular phenotyping of clonal neurospheres," *PNAS*, **99**(22), pp. 14506–14511.

[126] Carpenedo RL, Sargent CY, and McDevitt TC, (2007). "Rotary Suspension Culture Enhances the Efficiency, Yield, and Homogeneity of Embryoid Body Differentiation," *STEM CELLS*, **25**(9), pp. 2224–2234.

[127] Ng ES, Davis RP, Azzola L, Stanley EG, and Elefanty AG, (2005). "Forced aggregation of defined numbers of human embryonic stem cells into embryoid bodies fosters robust, reproducible hematopoietic differentiation," *Blood*, **106**(5), pp. 1601–1603.

[128] Nonaka J-I, Yoshikawa M, Ouji Y, Matsuda R, Nishimura F, Yamada S, Nakase H, Moriya K, Nishiofuku M, Ishizaka S, and Sakaki T, (2008). "CoCl2 inhibits neural differentiation of retinoic acid-treated embryoid bodies," *Journal of Bioscience and Bioengineering*, **106**(2), pp. 141–147.

[129] Bauwens CL, Peerani R, Niebruegge S, Woodhouse KA, Kumacheva E, Husain M, and Zandstra PW, (2008). "Control of Human Embryonic Stem Cell Colony and Aggregate Size Heterogeneity Influences Differentiation Trajectories," *STEM CELLS*, **26**(9), pp. 2300–2310.

[130] Tan JL, Liu W, Nelson CM, Raghavan S, and Chen CS, (2004). "Simple approach to micropattern cells on common culture substrates by tuning substrate wettability," *Tissue Eng.*, **10**(5-6), pp. 865–872.

[131] Lin R-Z, Lin R-Z, and Chang H-Y, (2008). "Recent advances in three-dimensional multicellular spheroid culture for biomedical research," *Biotechnol J*, **3**(9-10), pp. 1172–1184.

[132] Kelm JM, and Fussenegger M, (2004). "Microscale tissue engineering using gravity-enforced cell assembly," *Trends in Biotechnology*, **22**(4), pp. 195–202.

[133] Kurosawa H, Imamura T, Koike M, Sasaki K, and Amano Y, (2003). "A simple method for forming embryoid body from mouse embryonic stem cells," *Journal of Bioscience and Bioengineering*, **96**(4), pp. 409–411.

[134] 3D Biomatrix, (2014). "Features," *Perfecta3D Hanging Drop Plate Features* [Online]. Available: https://3dbiomatrix.com/features/. [Accessed: 02-Jun-2014].

[135] Dickson M, and Gagnon JP, (2009). "The Cost of New Drug Discovery and Development," *Discovery Medicine*, **4**(22), pp. 172–179.

[136] Kaitin K, (2010). "Deconstructing the Drug Development Process: The New Face of Innovation," *Clin Pharmacol Ther*, **87**(3), pp. 356–361.

[137] Paul SM, Mytelka DS, Dunwiddie CT, Persinger CC, Munos BH, Lindborg SR, and Schacht AL, (2010). "How to improve R&D productivity: the pharmaceutical industry's grand challenge," *Nature Reviews Drug Discovery*, **9**, pp. 203–214.

[138] Kolaja K, (2014). "Stem Cells and Stem Cell-derived Tissues and Their Use in Safety Assessment," *J. Biol. Chem.*, **289**(8), pp. 4555–4561.

[139] Hay DC, Fletcher J, Payne C, Terrace JD, Gallagher RCJ, Snoeys J, Black JR, Wojtacha D, Samuel K, Hannoun Z, Pryde A, Filippi C, Currie IS, Forbes SJ, Ross JA, Newsome PN, and Iredale JP, (2008). "Highly efficient differentiation of hESCs to functional hepatic endoderm requires ActivinA and Wnt3a signaling," *PNAS*, **105**(34), pp. 12301–12306.

[140] Hay DC, Zhao D, Fletcher J, Hewitt ZA, McLean D, Urruticoechea-Uriguen A, Black JR, Elcombe C, Ross JA, Wolf R, and Cui W, (2008). "Efficient Differentiation of Hepatocytes from Human Embryonic Stem Cells Exhibiting Markers Recapitulating Liver Development In Vivo," *STEM CELLS*, **26**(4), pp. 894–902.

[141] Dage J, and Merchant K, (2012). "The application of iPS cells and differentiated neuronal cells to advance drug discovery," *Drug Discovery World*, **13**(2), pp. 21–26.

[142] Kola I, and Landis J, (2004). "Can the pharmaceutical industry reduce attrition rates?," *Nat Rev Drug Discov*, **3**(8), pp. 711–716.

[143] Ramaiahgari SC, den Braver MW, Herpers B, Terpstra V, Commandeur JNM, van de Water B, and Price LS, (2014). "A 3D in vitro model of differentiated HepG2 cell spheroids with improved liver-like properties for repeated dose high-throughput toxicity studies," *Arch Toxicol*, **88**(4), pp. 1–13.

[144] Rambhatla L, Chiu C-P, Kundu P, Peng Y, and Carpenter MK, (2003). "Generation of Hepatocyte-Like Cells From Human Embryonic Stem Cells," *Cell Transplantation*, **12**(1), pp. 1–11.

[145] Cai J, Zhao Y, Liu Y, Ye F, Song Z, Qin H, Meng S, Chen Y, Zhou R, Song X, Guo Y, Ding M, and Deng H, (2007). "Directed differentiation of human embryonic stem cells into functional hepatic cells," *Hepatology*, **45**(5), pp. 1229–1239.

[146] Agarwal S, Holton KL, and Lanza R, (2008). "Efficient Differentiation of Functional Hepatocytes from Human Embryonic Stem Cells," *STEM CELLS*, **26**(5), pp. 1117–1127.

[147] Baharvand H, Hashemi SM, and Shahsavani M, (2008). "Differentiation of human embryonic stem cells into functional hepatocyte-like cells in a serum-free adherent culture condition," *Differentiation*, **76**(5), pp. 465–477.

[148] Söderdahl T, Küppers-Munther B, Heins N, Edsbagge J, Björquist P, Cotgreave I, and Jernström B, (2007). "Glutathione transferases in hepatocyte-like cells derived from human embryonic stem cells," *Toxicology in Vitro*, **21**(5), pp. 929–937.

[149] Maurel P, (1996). "The use of adult human hepatocytes in primary culture and other in vitro systems to investigate drug metabolism in man," *Advanced Drug Delivery Reviews*, **22**(1–2), pp. 105–132.

[150] Takebe T, Sekine K, Enomura M, Koike H, Kimura M, Ogaeri T, Zhang R-R, Ueno Y, Zheng Y-W, Koike N, Aoyama S, Adachi Y, and Taniguchi H, (2013). "Vascularized and functional human liver from an iPSC-derived organ bud transplant," *Nature*, **499**(7459), pp. 481–484.

[151] Franco D, (2014). "Towards a bioengineered liver," *Journal of Hepatology*, **60**(2), pp. 455–456.

[152] Vacanti JP, Morse MA, Saltzman WM, Domb AJ, Perez-Atayde A, and Langer R, (1988). "Selective cell transplantation using bioabsorbable artificial polymers as matrices," *Journal of Pediatric Surgery*, **23**(1), pp. 3–9.

[153] Hollister SJ, (2005). "Porous scaffold design for tissue engineering," *Nat Mater*, **4**(7), pp. 518–524.

[154] Leor J, Aboulafia-Etzion S, Dar A, Shapiro L, Barbash IM, Battler A, Granot Y, and Cohen S, (2000). "Bioengineered Cardiac Grafts : A New Approach to Repair the Infarcted Myocardium?," *Circulation*, **102**(Supplement 3), pp. III–56–III–61.

[155] Khalil S, and Sun W, (2009). "Bioprinting Endothelial Cells With Alginate for 3D Tissue Constructs," *Journal of Biomechanical Engineering*, **131**(11), p. 111002.

[156] Langer R, and Vacanti JP, (1993). "Tissue Engineering," *Science*, **260**(5110), pp. 920–926.

[157] Khademhosseini A, Langer R, Borenstein J, and Vacanti JP, (2006). "Microscale technologies for tissue engineering and biology," *Proceedings of the National Academy of Sciences of the United States of America*, **103**(8), pp. 2480–2487.

[158] Mironov V, Visconti RP, Kasyanov V, Forgacs G, Drake CJ, and Markwald RR, (2009). "Organ printing: Tissue spheroids as building blocks," *Biomaterials*, **30**(12), pp. 2164–2174.

[159] Schuurman W, Khristov V, Pot MW, van Weeren PR, Dhert WJA, and Malda J, (2011). "Bioprinting of hybrid tissue constructs with tailorable mechanical properties," *Biofabrication*, **3**(2), p. 021001.

[160] Engler AJ, Sen S, Sweeney HL, and Discher DE, (2006). "Matrix Elasticity Directs Stem Cell Lineage Specification," *Cell*, **126**(4), pp. 677–689.

[161] Singh A, Sharma PK, Garg VK, and Garg G, (2010). "Hydrogels: A review," *Int J Pharmaceut Sci Rev Res*, **4**(2), pp. 97–105.

[162] Peppas NA, (2013). "2.5 Hydrogels," Biomaterials Science, Academic Press, pp. 35–42.

[163] Drury JL, and Mooney DJ, (2003). "Hydrogels for tissue engineering: scaffold design variables and applications," *Biomaterials*, **24**(24), pp. 4337–4351.

[164] Geckil H, Xu F, Zhang X, Moon S, and Demirci U, (2010). "Engineering hydrogels as extracellular matrix mimics," *Nanomedicine*, **5**(3), pp. 469–484.

[165] Peppas NA, Hilt JZ, Khademhosseini A, and Langer R, (2006). "Hydrogels in Biology and Medicine: From Molecular Principles to Bionanotechnology," *Advanced Materials*, **18**(11), pp. 1345–1360.

[166] Slaughter BV, Khurshid SS, Fisher OZ, Khademhosseini A, and Peppas NA, (2009). "Hydrogels in Regenerative Medicine," *Advanced Materials*, **21**(32-33), pp. 3307–3329.

[167] Hoffman AS, (2002). "Hydrogels for biomedical applications," *Advanced Drug Delivery Reviews*, **54**(1), pp. 3–12.

[168] Burdick JA, and Murphy WL, (2012). "Moving from static to dynamic complexity in hydrogel design," *Nat Commun*, **3**, p. 1269.

[169] Teßmar J, Brandl F, and Göpferich A, (2009). "37: Hydrogels for Tissue Engineering," Fundamentals of tissue engineering and regenerative medicine, Springer, Berlin, pp. 493–515.

[170] Censi R, Schuurman W, Malda J, di Dato G, Burgisser PE, Dhert WJA, van Nostrum CF, di Martino P, Vermonden T, and Hennink WE, (2011). "A Printable Photopolymerizable Thermosensitive p(HPMAm-lactate)-PEG Hydrogel for Tissue Engineering," *Advanced Functional Materials*, **21**(10), pp. 1833–1842.

[171] Gerecht S, Burdick JA, Ferreira LS, Townsend SA, Langer R, and Vunjak-Novakovic G, (2007). "Hyaluronic acid hydrogel for controlled self-renewal and differentiation of human embryonic stem cells," *PNAS*, **104**(27), pp. 11298–11303.

[172] Shu XZ, Ghosh K, Liu Y, Palumbo FS, Luo Y, Clark RA, and Prestwich GD, (2004). "Attachment and spreading of fibroblasts on an RGD peptide–modified injectable hyaluronan hydrogel," *J. Biomed. Mater. Res.*, **68A**(2), pp. 365–375.

[173] Francis Suh J-K, and Matthew HWT, (2000). "Application of chitosan-based polysaccharide biomaterials in cartilage tissue engineering: a review," *Biomaterials*, **21**(24), pp. 2589–2598.

[174] Mirshafiey A, Khodadadi A, Rehm BH, Khorramizadeh MR, Eslami MB, Razavi A, and Saadat F, (2005). "Sodium Alginate as a Novel Therapeutic Option in Experimental Colitis," *Scandinavian Journal of Immunology*, **61**(4), pp. 316–321.

[175] Kong H-J, Lee KY, and Mooney DJ, (2002). "Decoupling the dependence of rheological/mechanical properties of hydrogels from solids concentration," *Polymer*, **43**(23), pp. 6239–6246.

[176] Marriott AS, Bergström E, Hunt AJ, Thomas-Oates J, and Clark JH, (2014). "A natural template approach to mesoporous carbon spheres for use as green chromatographic stationary phases," *RSC Advances*, **4**(1), pp. 222–228.

[177] Fedorovich NE, Alblas J, de Wijn JR, Hennink WE, Verbout AJ, and Dhert WJA, (2007). "Hydrogels as Extracellular Matrices for Skeletal Tissue Engineering: State-of-the-Art and Novel Application in Organ Printing," *Tissue Engineering*, **13**(8), pp. 1905–1925.

[178] Azab AK, Orkin B, Doviner V, Nissan A, Klein M, Srebnik M, and Rubinstein A, (2006). "Crosslinked chitosan implants as potential degradable devices for brachytherapy: In vitro and in vivo analysis," *Journal of Controlled Release*, **111**(3), pp. 281–289.

[179] Kuznetsova NV, McBride Jr DJ, and Leikin S, (2003). "Changes in Thermal Stability and Microunfolding Pattern of Collagen Helix Resulting from the Loss

of α2(I) Chain in Osteogenesis Imperfecta Murine," *Journal of Molecular Biology*, **331**(1), pp. 191–200.

[180] Lee CR, Grodzinsky AJ, and Spector M, (2001). "The effects of cross-linking of collagen-glycosaminoglycan scaffolds on compressive stiffness, chondrocyte-mediated contraction, proliferation and biosynthesis," *Biomaterials*, **22**(23), pp. 3145–3154.

[181] Schulz Torres D, M. Freyman T, Yannas IV, and Spector M, (2000). "Tendon cell contraction of collagen–GAG matrices in vitro: effect of cross-linking," *Biomaterials*, **21**(15), pp. 1607–1619.

[182] Oliver RF, Grant RA, Cox RW, and Cooke A, (1980). "Effect of aldehyde cross-linking on human dermal collagen implants in the rat," *Br J Exp Pathol*, **61**(5), pp. 544–549.

[183] Scotchford CA, Cascone MG, Downes S, and Giusti P, (1998). "Osteoblast responses to collagen-PVA bioartificial polymers in vitro: the effects of cross-linking method and collagen content," *Biomaterials*, **19**(1–3), pp. 1–11.

[184] Xu T, Binder KW, Albanna MZ, Dice D, Zhao W, Yoo JJ, and Atala A, (2013). "Hybrid printing of mechanically and biologically improved constructs for cartilage tissue engineering applications," *Biofabrication*, **5**(1), p. 015001.

[185] Eyre DRD, (2005). "Methods of detecting collagen degradation" Patent Number EP1560026 A1, August 3, 2005.

[186] Peppas NA, Keys KB, Torres-Lugo M, and Lowman AM, (1999). "Poly(ethylene glycol)-containing hydrogels in drug delivery," *Journal of Controlled Release*, **62**(1–2), pp. 81–87.

[187] Weber LM, He J, Bradley B, Haskins K, and Anseth KS, (2006). "PEG-based hydrogels as an in vitro encapsulation platform for testing controlled β-cell microenvironments," *Acta Biomaterialia*, **2**(1), pp. 1–8.

[188] Kraehenbuehl TP, Zammaretti P, Van der Vlies AJ, Schoenmakers RG, Lutolf MP, Jaconi ME, and Hubbell JA, (2008). "Three-dimensional extracellular matrix-directed cardioprogenitor differentiation: Systematic modulation of a synthetic cell-responsive PEG-hydrogel," *Biomaterials*, **29**(18), pp. 2757–2766.

[189] Schmedlen RH, Masters KS, and West JL, (2002). "Photocrosslinkable polyvinyl alcohol hydrogels that can be modified with cell adhesion peptides for use in tissue engineering," *Biomaterials*, **23**(22), pp. 4325–4332.

[190] Stammen JA, Williams S, Ku DN, and Guldberg RE, (2001). "Mechanical properties of a novel PVA hydrogel in shear and unconfined compression," *Biomaterials*, **22**(8), pp. 799–806.

[191] Deming TJ, (2007). "Synthetic polypeptides for biomedical applications," *Progress in Polymer Science*, **32**(8–9), pp. 858–875.

[192] Appel EA, del Barrio J, Loh XJ, and Scherman OA, (2012). "Supramolecular polymeric hydrogels," *Chemical Society Reviews*, **41**(18), p. 6195.

[193] Yan X, Wang F, Zheng B, and Huang F, (2012). "Stimuli-responsive supramolecular polymeric materials," *Chemical Society Reviews*, **41**(18), p. 6042.

[194] Dankers PYW, Hermans TM, Baughman TW, Kamikawa Y, Kieltyka RE, Bastings MMC, Janssen HM, Sommerdijk NAJM, Larsen A, van Luyn MJA, Bosman AW, Popa ER, Fytas G, and Meijer EW, (2012). "Hierarchical Formation of Supramolecular Transient Networks in Water: A Modular Injectable Delivery System," *Adv. Mater.*, **24**(20), pp. 2703–2709.

[195] Zhang S, (2003). "Fabrication of novel biomaterials through molecular self-assembly," *Nat Biotech*, **21**(10), pp. 1171–1178.

[196] Chen Y, Pang X-H, and Dong C-M, (2010). "Dual Stimuli-Responsive Supramolecular Polypeptide-Based Hydrogel and Reverse Micellar Hydrogel Mediated by Host–Guest Chemistry," *Adv. Funct. Mater.*, **20**(4), pp. 579–586.

[197] Kyle S, Felton SH, McPherson MJ, Aggeli A, and Ingham E, (2012). "Peptide-Based Biomaterials: Rational Molecular Design of Complementary Self-Assembling Peptide Hydrogels (Adv. Healthcare Mater. 5/2012)," *Advanced Healthcare Materials*, **1**(5), pp. 679–679.

[198] Cheng Y, He C, Xiao C, Ding J, Cui H, Zhuang X, and Chen X, (2013). "Versatile Biofunctionalization of Polypeptide-Based Thermosensitive Hydrogels via Click Chemistry," *Biomacromolecules*, **14**(2), pp. 468–475.

[199] Khan W, Muthupandian S, Farah S, Kumar N, and Domb AJ, (2011). "Biodegradable Polymers Derived From Amino Acids," *Macromol. Biosci.*, **11**(12), pp. 1625–1636.

[200] Yan Y, Wang X, Pan Y, Liu H, Cheng J, Xiong Z, Lin F, Wu R, Zhang R, and Lu Q, (2005). "Fabrication of viable tissue-engineered constructs with 3D cell-assembly technique," *Biomaterials*, **26**(29), pp. 5864–5871.

[201] Reichert JC, Heymer A, Berner A, Eulert J, and Nöth U, (2009). "Fabrication of polycaprolactone collagen hydrogel constructs seeded with mesenchymal stem cells for bone regeneration," *Biomedical Materials*, **4**(6), p. 065001.

[202] Chen R-N, Ho H-O, Tsai Y-T, and Sheu M-T, (2004). "Process development of an acellular dermal matrix (ADM) for biomedical applications," *Biomaterials*, **25**(13), pp. 2679–2686.

[203] McCallum D, Ferris C, Calvert P, and Wallace G, (2010). "Printed hydrogel materials," Nanoscience and Nanotechnology (ICONN), 2010 International Conference on, IEEE, pp. 257–260.

[204] Jakab K, Norotte C, Marga F, Murphy K, Vunjak-Novakovic G, and Forgacs G, (2010). "Tissue engineering by self-assembly and bio-printing of living cells," *Biofabrication*, **2**(2), p. 022001.

Chapter 3 – Experimental Methods

3.1 Introduction

Myriad experiments were performed in the course of this research in subjects ranging from initial testing and characterisation to stem cell culture and micro-tissue engineering. The experimental methods for all of these experiments are described in this chapter. Section 3.2 presents the valve-based deposition system that is at the centre of bioprinting platform. Section 3.3 describes the procedures used to test the bioprinting platforms' compatibility with biological cells including human embryonic stem cells. Section 3.4 presents the techniques used to fabricate the novel components for the bioprinters. Finally, Section 3.5 covers the technique used to create the two component solutions used to print hydrogels.

3.2 Valve-based Deposition System

Regardless of changes in the surrounding systems – the mechanical motion mechanism, control electronics, firmware and software – one system remains largely unchanged throughout all the experiments in this thesis: the valve-based deposition system.

As shown in Figure 3.1, each nanolitre dispensing system is comprised of a solenoid valve (VHS 25+ Nanolitre Dispense Valve, Lee Products Ltd) with a Teflon coated nozzle (Minstac Nozzle, Lee Products Ltd) controlled by a digital spike signal. Flexible tubing connects the solenoid valve to a static pressure reservoir (like an ink cartridge in a standard printer) for the bio-ink solution (i.e. cells in suspension, staining solution or just ordinary water for testing purposes) via a custom designed pressure manifold block.

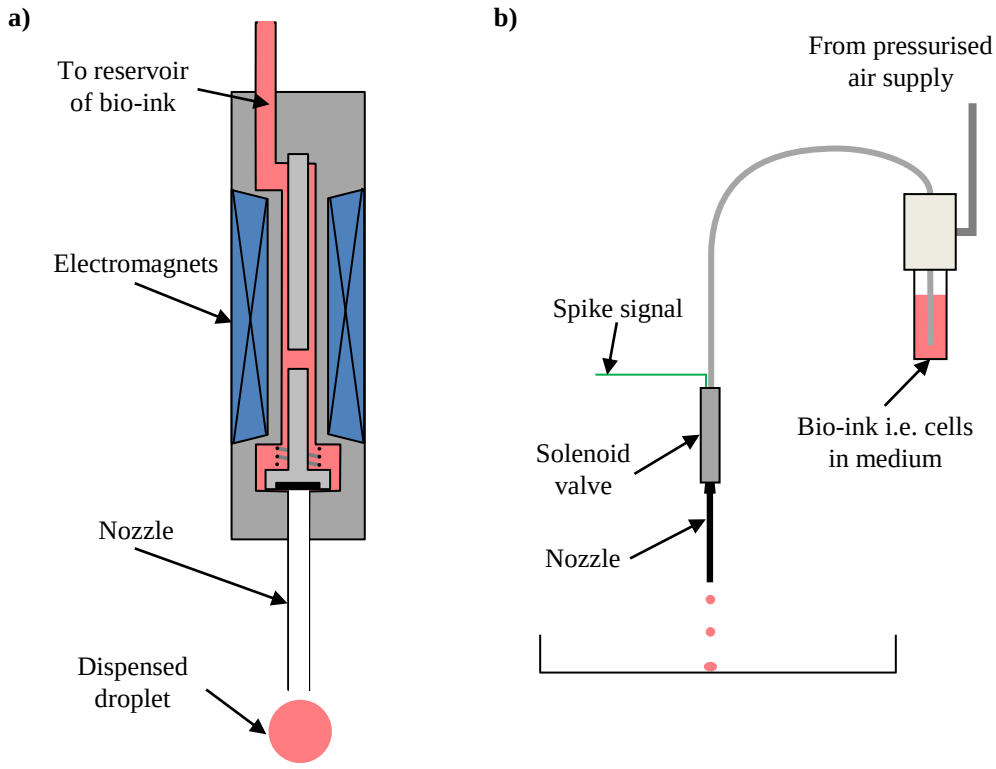

Figure 3.1– *a) Detailed schematic of the solenoid valve mechanism; b) Schematic of the valve-based nanolitre dispensing system.*

Bio-ink is dispensed by opening and closing the valve. The volume of dispensed fluid is affected by several factors: the properties of the fluid (i.e. viscosity, surface tension, concentration of suspended particles such as cells.); the internal diameter of the nozzle orifice; the valve on-time; and the static pressure applied to the bio-ink reservoir.

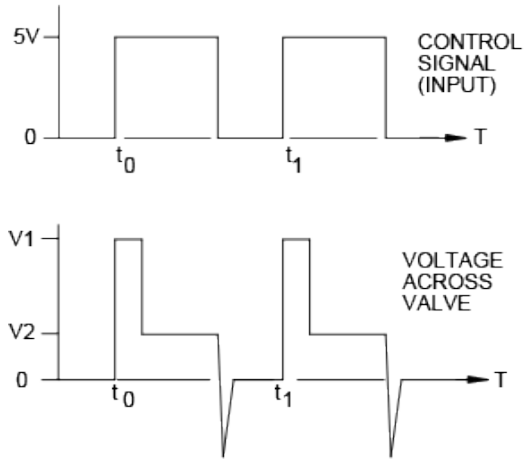

Figure 3.2 *– Valve operating signals: a) control signal input to the valve driver, b) the output signal to the valve. When the voltage across the valve is 24V (V1) the valve is open.*

3.3 Biological Techniques

The experiments were performed in collaboration with Jason King, John Gardner, Sebastian Greenhough, Catherine Fyfe and Helen Bradburn from Roslin Cellab. All cell culturing was provided by them, in addition to the various different cell media types used in the following experiments.

3.3.1 Cell Culture

A frozen sample of cells was taken from the freezer, thawed out, suspended in medium and centrifuged for a few minutes to separate any large aggregates of cells. The medium was removed and the cells were re-suspended in fresh medium. By pipetting the solution up and down multiple times the cells were separated into single cells. The suspended cells were then transferred to a T25 flask. When observed under a microscope the cells were observed to be circular with "hands" and therefore healthy. The flask was then placed inside an incubator at 36.0-37.5°C, 5.0±0.5% CO_2.

To prevent the cells from becoming over confluent they need to be split every few days. When subjected to typsin/EDTA, the cells lose contact with the T25 flask but remain in contact with each other. By pipetting the dislodged cells up and down a few times the cells can be returned to a single cell suspension and can be split into the required amounts.

3.3.2 Optical Cell Viability

It is very important to determine if the cells suffered any damage as a result of the printing process and, if so, how much. A solution containing suspended cells was loaded into the reservoir of one of the cell deposition systems. The printing process was then performed into the wells of a multi-well plate and a small amount of solution that was kept separate and manually pipetted onto the plate provided a non-printed control.

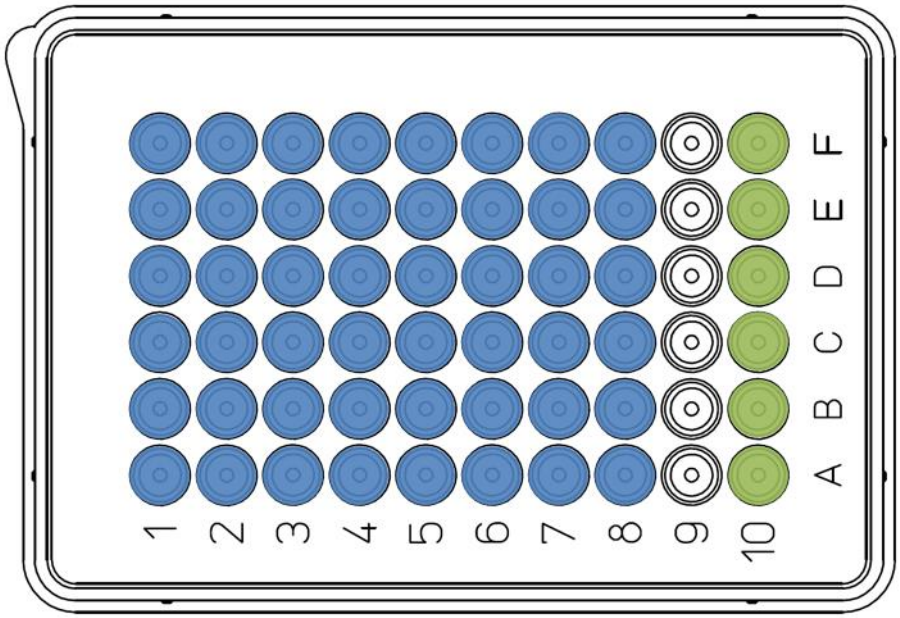

Figure 3.3 *– Printing scheme for the optical cell viability test with printed wells shown in blue and control shown in green*

The viability of the printed and non-printed cells was assessed via trypan blue exclusion. A 0.4% solution of trypan blue (T8154, Sigma-Aldrich) in phosphate-buffered saline (PBS, pH 7.2, Life Technologies) was prepared. 0.1 mL per 1 mL of trypan blue solution was added to each printed and non-printed sample. Cell viability was measured by viewing bright-field images under the microscope (fl0015000m Trinocular Fluorescence Microscopes) both immediately and at 24 hours after printing. The numbers of live and dead cells were counted using ImageJ. Between these times the control and printed cells were kept in a CO_2 incubator (Galaxy S+, RS Biotech) at 36.0-37.5°C, 5.0±0.5% CO_2.

3.3.3 Fluorescence-Activated Cell Sorting

Fluorescence-activated cell sorting (FACS) is the most popular type of flow cytometry. It is a process for sorting heterogeneous suspensions of biological cells into separate containers, based upon the specific light scattering and fluorescent characteristics of each cell [1].

Specific cells within a mixture are labelled using fluorescently tagged antibodies that bind selected cell-surface molecules (Figure 3.4a). The cell suspension is delivered in a rapid, thin stream into the centre of a second moving steam of fluid called the sheath flow [2]. The two fluids do not mix due to differences in viscosity and density resulting in a stable bi-layer stream. The tube through which the stream flows narrows into a

funnel, constricting the flow and resulting in a narrower stream with the cells spaced out individually.

The stream is actuated with a vibrating mechanism which causes it to break up into individual droplets each containing one cell. Each cell passes through a laser beam, where its fluorescent properties are measured using two detectors. The forward scatter channel provides information on the cells' size and viability, while the side scatter channel provides information on the fluorescence and granularity of the cell, which can be used to identify the cell type. Depending upon which antibody it carries, the droplet is given a certain electrical charge. The charged droplet then passes between a pair of charged metal plates, which diverts droplets into different containers based upon their charge (Figure 3.4b).

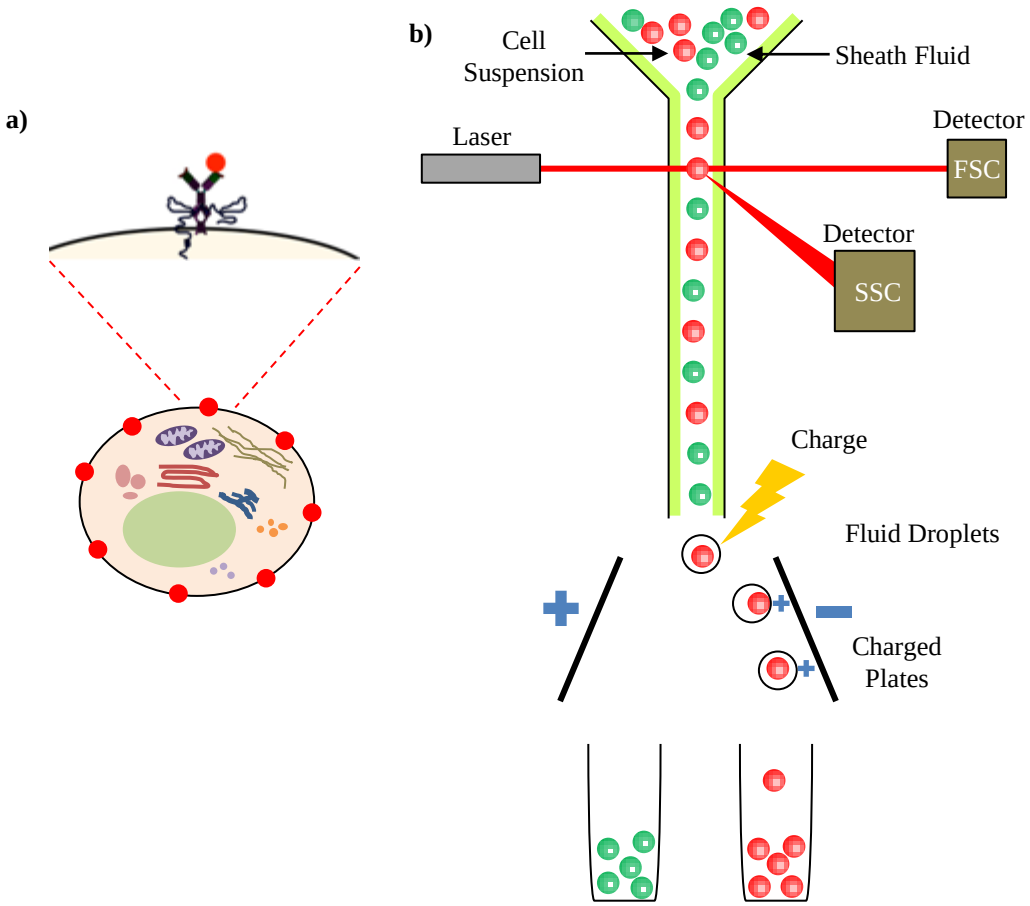

Figure 3.4 *– Schematic of fluorescence-activated cell sorting a) detail view of the fluorescent tag on the cell surface, b) diagram of the FACS technique (adapted from [1,2])*

BD's FACSCalibur flow cytometer was used to perform cell analysis for this research. Advantages of this system include its high speed and the depth of the data it outputs.

Figure 3.5 *– BD FACSCalibur*

3.3.4 Multi-marker Pluripotency Validation

Viability alone is insufficient when printing pluripotent stem cells; printed cells must not only be viable but also morphologically unchanged by the printing process. In other words, they need to still be pluripotent stem cells post-printing; the bioprinting process must not trigger the cells to differentiate. Pluripotency can be validated by testing cells for the presence of certain biomarkers including SSEA-3, SSEA-4, OCT3/4, SOX2, NANOG and many others [3,4].

3.3.4.1 OCT3/4 Optical Validation

Human ES cells were printed out and kept in a CO_2 incubator (Galaxy S+, RS Biotech) at 36.0-37.5°C, 5.0±0.5% CO_2 for 48 hours. The now adherent hESCs were washed once with PBS and fixed using a 4% solution of paraformaldehyde for 20 minutes at room temperature (RT). Cells were permeabilised by washing once with PBS and then incubating with 100% ethanol for 5 minutes at RT. Cells were then washed three times with PBS and blocked using 1% normal goat serum (Sigma G9023) in PBST (PBS plus 0.1% Tween 20) for 1 hour at RT. Blocking buffer was then replaced with fresh blocking buffer containing the primary antibody (goat anti-OCT-4, Santa Cruz SC-5279) at a dilution of 1:200. This was incubated on a rocker table at RT for 2 hours or overnight at +4 °C. The primary antibody was removed by washing three times with PBST for 5 minutes each at RT. An Alexa-fluor conjugated secondary antibody (rabbit anti-goat, Life Technologies, A-11078) was diluted 1:200 in 1% normal rat serum (Sigma R9133)/PBST and used for 30 minutes at RT in the dark on a rocker table.

Unbound antibody was removed during three 5 minute PBST washes on a rocker table at RT in the dark. Salt was removed by washing twice with double distilled water. Excess water was removed and the sample embedded with Vectashield containing DAPI according to manufacturer's instructions. Samples were allowed to set at RT in the dark overnight before being analysed on a fluorescence microscope.

3.3.4.2 Multi-marker FACS Validation

Human ES cells were printed out and kept in a CO_2 incubator (Galaxy S+, RS Biotech) at 36.0-37.5°C, 5.0±0.5% CO_2 for one week. The now adherent hESCs were washed once with PBS and trypsin/EDTA was added to detach the cells from T25 flask. By pipetting the dislodged cells up and down a few times the cells were returned to a single cell suspension. A sample was viewed under the microscope to confirm the presence of single cells. Cells were then washed three times with PBS and centrifuged at 300*g* for 5 minutes before being re-suspended in an appropriate volume of PBS for the required cell concentration.

Cells were fixed using a 4% solution of paraformaldehyde for 20 minutes at room temperature (RT). Cells were permeabilised by washing twice with 1X BD Perm/Wash buffer (centrifuging at 500*g* for 5 minutes), re-suspended in 1X BD Perm/Wash buffer at 1×10^7 cells/mL and then incubated for 10 minutes at RT.

Two polystyrene tubes were prepared, each containing 100 µL of permeabilised cells at 1×10^7 cells/mL, one labelled "specific stain" and one "isotype control". 20µL each of PerCP-Cy5.5 Oct3/4, PE SSEA-1 and Alexa Fluor® 647 SSEA-4 components were added to the specific stain tube, while 20µL each of PerCP-Cy5.5 isotype control, PE isotype control and Alexa Fluor® 647 isotype control components were added to the isotype control tube. The tubes were mixed gently and incubated for 30 minutes at RT in the dark. Four new tubes were labelled "Negative", "PerCP", "PE" and "Alexa 647". To each of these tubes were added 100 µL of Perm/Wash buffer, negative beads and anti-mouse beads (except for the negative tube which only had buffer and negative beads). 20µL of the relevant stain were added to the tubes (one for each except the negative tube). The four tubes were vortexed and incubated for 30 minutes at RT in the dark. All six tubes were washed twice with 1X BD Perm/Wash buffer (centrifuging at 500*g* for 5 minutes), cells and beads were re-suspended in 300 µL of Foetal Bovine Serum.

The beads were run through the FACS machine to confirm the application settings according to manufacturer's instructions. Finally the cells were run through the FACS machine and the data was recorded.

3.4 Bioprinter Parts Fabrication

3.4.1 CO_2 Laser Machining

The carbon dioxide (CO_2) laser was invented in 1964 by Kumar Patel [5]. They are the highest power continuous wave lasers that exist and they have a reasonably high efficiency.

The active laser medium is composed of carbon dioxide (CO_2), nitrogen (N_2), hydrogen (H_2), helium (He) and (sometimes) xenon (Xe). These gases are mixed and fill the discharge tube and energy is pumped through the gas in the form of an electrical discharge. Electron impacts excite the nitrogen molecules into a metastable vibrational state. This excitation energy is transferred to the carbon dioxide molecules during collisions. Helium molecules serve to control the temperature and the other components help to reoxidise the carbon monoxide molecules – which were formed in the discharge – back to carbon dioxide. The discharge tube is located between two mirrors, creating a laser resonator that continuously amplifies the generated laser light. One of the mirrors is partially permeable to the specific desired output wavelength and allows some of the laser light of this wavelength to escape. Laser light can then be passed through a lens to focus it into a laser beam with an extremely high energy density.

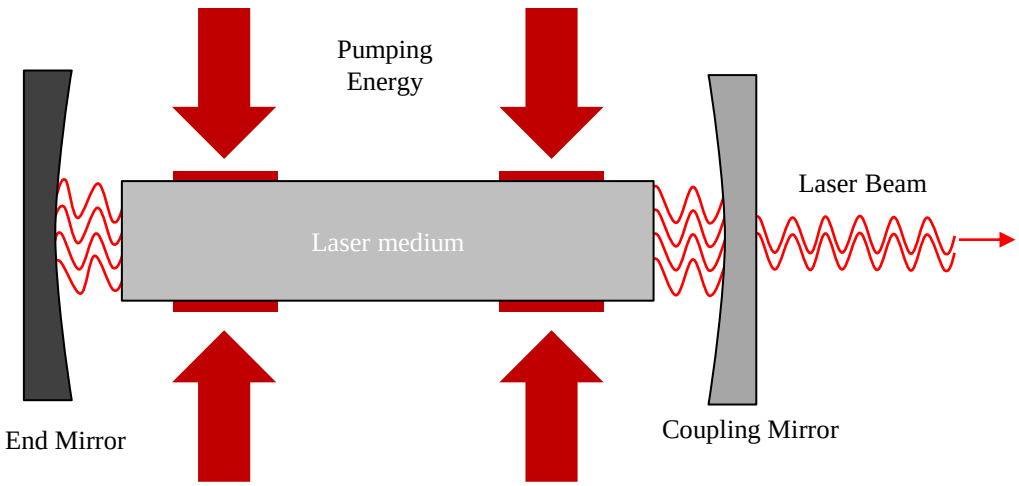

Figure 3.6 *– Schematic of a basic laser system*

Trotec's Speedy 300 was used to laser cut the acrylic panels which formed part of the bioprinters developed during this research. The advantages of this system are its high speed, excellent beam quality, large work area and superior linear motion systems. The system was also very easy to use and accepted designs easily in standard DXF format.

Figure 3.7 *– Trotec Speedy 300 CO2 Laser engraving machine*

3.4.2 Additive Manufacturing (3D Printing)

Fused filament fabrication (FFF), otherwise known as fused deposition modelling (FDM) was invented by S. Crump in 1989 [6]. It is one of the most popular additive manufacturing techniques due to the simplicity of the mechanism.

As with all additive manufacturing techniques, a 3D model file (usually in STL format) is orientated and scaled. The file is separated into thin (usually 100 µm) slices in the Z-direction and tool paths for each slice are calculated for the model (and support structures if required).

A coil of thermoplastic is unwound and fed into the extruder mechanism, which uses a driven toothed drive gear and a roller to feed and retract the filament at a controlled rate into and out of the heater block. The heater block heats the filament beyond its glass transition temperature and small beads of thermoplastic material are extruded from the

nozzle to form layers as the material hardens. The nozzle traces out the calculated tool-paths, and the model is built up from the bottom up, layer by layer.

Several materials can be used with this technology. The most popular are Acrylonitrile Butadiene Styrene (ABS) and Polylactic acid (PLA), and others include:

- Nylon
- High Density Polyethylene (HDPE)
- Polycaprolactone (PCL)
- Polycarbonate

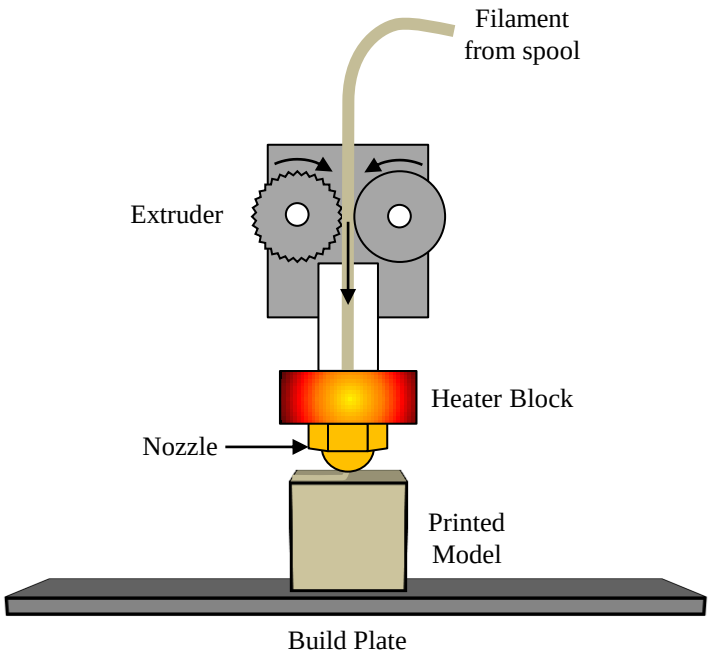

Figure 3.8 *– Schematic of the fused filament fabrication method of additive manufacturing*

Makerbot's Replicator/Replicator 2X were used to 3D print the extra components used to create the bioprinters for this research. The advantages of these systems are their relatively low cost, reasonable part resolution, large work area and simple mechanisms which enable easy repair and servicing. The system was also very easy to use and accepted designs easily in standard STL format.

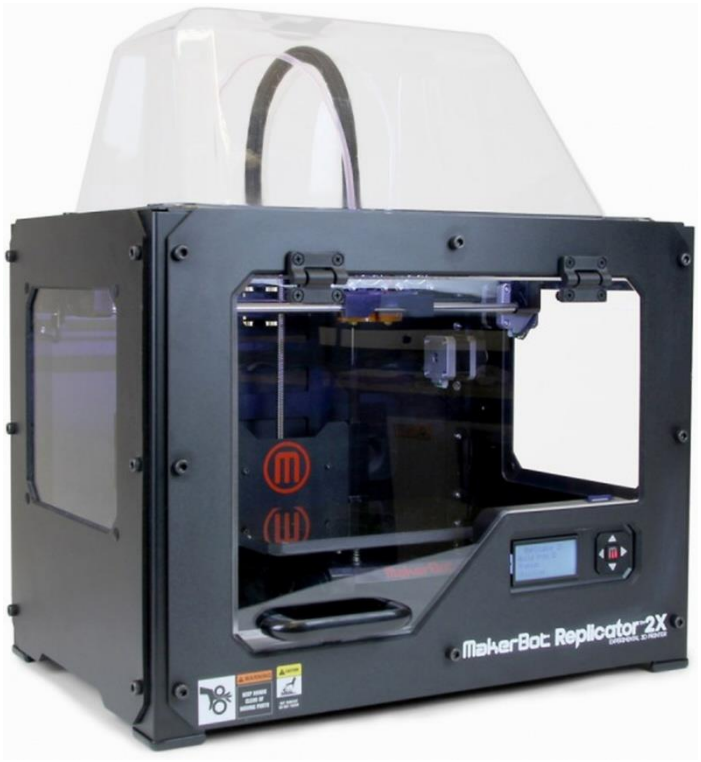

Figure 3.9 *– Makerbot Replicator 2X 3D printer*

3.5 Hydrogel Material Preparation

Alginic acid, commonly known as alginate, is a naturally occurring anionic polysaccharide derived from the cell walls of brown algae. Alginate is a copolymer with linear blocks of (1,4)-linked β-$_D$-mannuronate (M) acid and α-$_L$-guluronic acid (G) residues covalently linked in different combinations of consecutive M-blocks, consecutive G-blocks or alternating MG-blocks [7,8]. Gelation of sodium alginate is easily achieved through selective binding of carboxylic groups on G-blocks with divalent calcium cations, subsequently forming bonds with adjacent chains creating an egg-box structure [9,10]. The viscosity of the prepared alginate solution is dependent on the concentration of the polymer, molecular weight (M_W), average chain segment ratio (G to M ratio), and the pH of the solution [7,11].

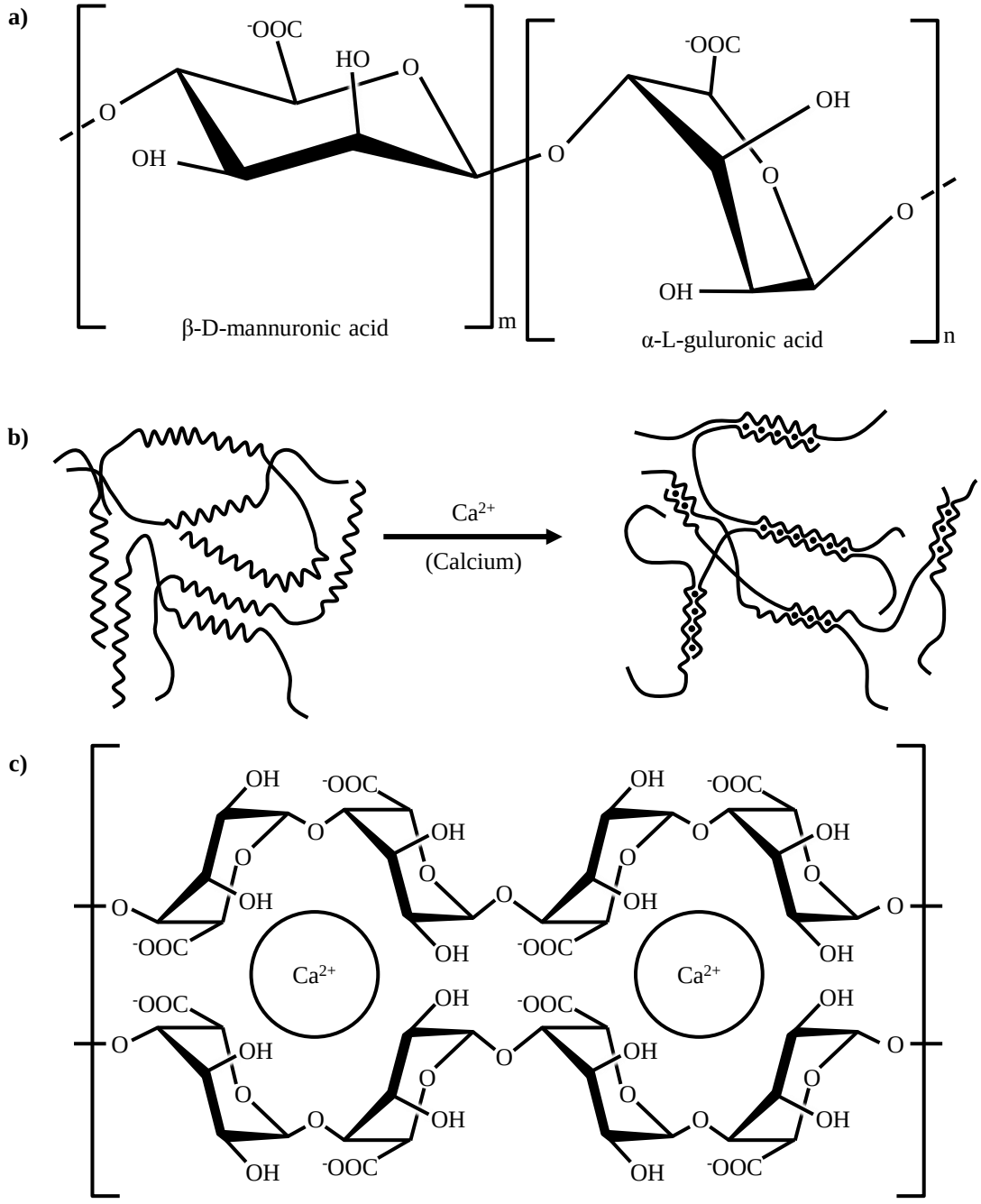

Figure 3.10 *– Alginate hydrogel structure: a) alginate monomers; b-c) representation of "egg-box" model binding of monomer blocks to calcium ions (adapted from [10])*

The alginate hydrogel used for this research was formed by mixing two solutions: sodium alginate and calcium chloride, varying the volume and concentration ratios of these two solutions yielded hydrogels with different mechanical properties. The procedures for creating 2% sodium alginate and 5% calcium chloride solutions are provided as an example of the process.

1.0 g of Sodium alginate (W201502, Sigma-Aldrich) was measured and added to a 50 mL centrifuge tube to which was added 50 mL of deionized water. The centrifuge tube was submerged in an ultrasonic bath at approximately 60 °C for approximately one hour (or until the solid had dissolved) before further agitation on a vortex spinner to provide a more uniform solution.

2.5 g of calcium chloride dehydrate (223506, Sigma-Aldrich) was added to 50 mL of deionized water in a 50 mL centrifuge tube and allowed to dissolve.

3.6 Plasma Surface Treatment

Plasma treatment was used to modify the surface wettability of materials used as bioprinting substrates. Oxygen plasma removes organic contaminants by chemical reaction with highly reactive oxygen radicals and through ablation by energetic oxygen ions; it also promotes surface oxidation and hydroxylation which serves to increase surface wettability [12].

Samples (glass microscope slides) were placed inside the chamber of the plasma treatment machine and the vacuum pump evacuates the chamber creating a low pressure environment. At a pressure of approximately 0.1 mbar the process gas (i.e. oxygen) is fed into the chamber. When the working pressure is reached, the process gas is ignited creating the plasma which treats the exposed surfaces of the workpiece. Gas is continuously refreshed and contaminated gas is removed. When the treatment is complete the chamber is vented and the treated workpiece can be removed.

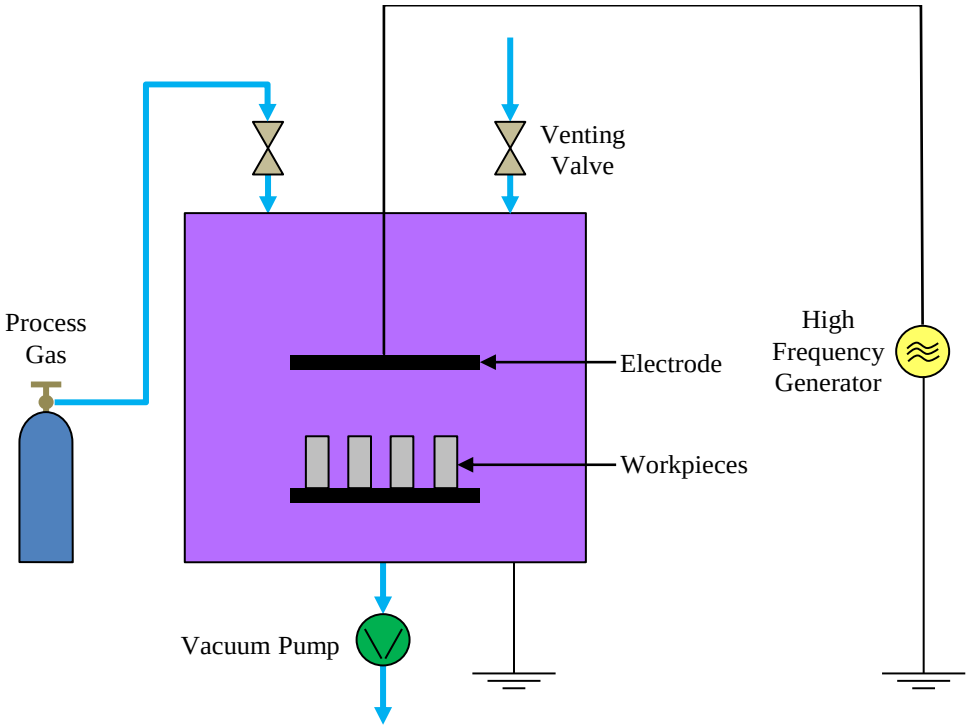

Figure 3.11 *– Schematic of the plasma system (adapted from [13])*

Diener Electronic's Zepto plasma system was used to treat the glass microscope slides used as bioprinting substrates for this research. The advantages of this system are its low cost, suitable chamber volume and ease of use.

Figure 3.12 *– Diener electronic Zepto plasma system*

3.7 References

[1] Willis RC, (2004). "Sorting out the mess," *Modern Drug Discovery*, **7**(11), pp. 29–32.

[2] Sabban S, (2011). "Development of an in vitro model system for studying the interaction of Equus caballus IgE with its high- affinity FcεRI receptor," PhD Thesis, The University of Sheffield.

[3] Takahashi K, Tanabe K, Ohnuki M, Narita M, Ichisaka T, Tomoda K, and Yamanaka S, (2007). "Induction of Pluripotent Stem Cells from Adult Human Fibroblasts by Defined Factors," *Cell*, **131**(5), pp. 861–872.

[4] Chen L, and Daley GQ, (2008). "Molecular basis of pluripotency," *Human Molecular Genetics*, **17**(R1), pp. R23–R27.

[5] Patel CKN, (1964). "Continuous-Wave Laser Action on Vibrational-Rotational Transitions of CO2," *Phys. Rev.*, **136**(5A), pp. A1187–A1193.

[6] Crump SS, (1992). "Apparatus and method for creating three-dimensional objects" Patent Number US5121329 A, June 9, 1992.

[7] Chung JHY, Naficy S, Yue Z, Kapsa R, Quigley A, Moulton SE, and Wallace GG, (2013). "Bio-ink properties and printability for extrusion printing living cells," *Biomater. Sci.*, **1**(7), pp. 763–773.

[8] Mirshafiey A, Khodadadi A, Rehm BH, Khorramizadeh MR, Eslami MB, Razavi A, and Saadat F, (2005). "Sodium Alginate as a Novel Therapeutic Option in Experimental Colitis," *Scandinavian Journal of Immunology*, **61**(4), pp. 316–321.

[9] Kong H-J, Lee KY, and Mooney DJ, (2002). "Decoupling the dependence of rheological/mechanical properties of hydrogels from solids concentration," *Polymer*, **43**(23), pp. 6239–6246.

[10] Marriott AS, Bergström E, Hunt AJ, Thomas-Oates J, and Clark JH, (2014). "A natural template approach to mesoporous carbon spheres for use as green chromatographic stationary phases," *RSC Advances*, **4**(1), pp. 222–228.

[11] Drury JL, and Mooney DJ, (2003). "Hydrogels for tissue engineering: scaffold design variables and applications," *Biomaterials*, **24**(24), pp. 4337–4351.

[12] Harrick Plasma, (2013). "Plasma Applications: Surface Activation and Modification," *Harrick Plasma* [Online]. Available: http://www.harrickplasma.com/applications_activation.php. [Accessed: 30-Apr-2014].

[13] Diener electronic, (2007). "Plasma Technology" [Online]. Available: http://www.plasmasurfacetechnology.eu/media/Plasmatechnik_en_web.pdf. [Accessed: 30-Apr-2014].

Chapter 4 – Development of Novel Valve-based 3D Cell Printing Platforms

4.1 Introduction

Based on the findings of the literature review, the valve-based technique was chosen over the other printing techniques described in Chapter 2 because it is cheaper and more expandable than laser printing, gentler for cells, and able to use materials with a wider range of viscosities than inkjet, has greater control over droplet size and location than electrohydrodynamic jetting; and is less prone to heating than acoustics.

The development of a valve-based bioprinter, including improvements and challenges encountered, are described in this chapter. Section 4.2 presents the first generation bioprinter. Section 4.3 details the creation of a portable valve-based deposition system. Section 4.4 describes an improved bioprinter that corrects some of the issues encountered in the first generation model. Finally, Section 4.5 presents the final version of the bioprinter developed in the course of this research.

4.2 Mark I

4.2.1 A Single Nozzle System

There have been several different generations of the cell printer setup from the very first to the current setup. The first version was a very crude proof-of-concept system. A single valve-based deposition system was mounted to a 3-axis CNC machine (High-Z S-400 CNC Machine, Heiz CNC-Step) with the valve assembly and some control electronics mounted to the tool head, while the bio-ink reservoir – which at this point was a small reagent bottle with tubing passing through holes drilled into the lid and sealed with glue – was located on the worktop next to the CNC machine (Figure 4.1).

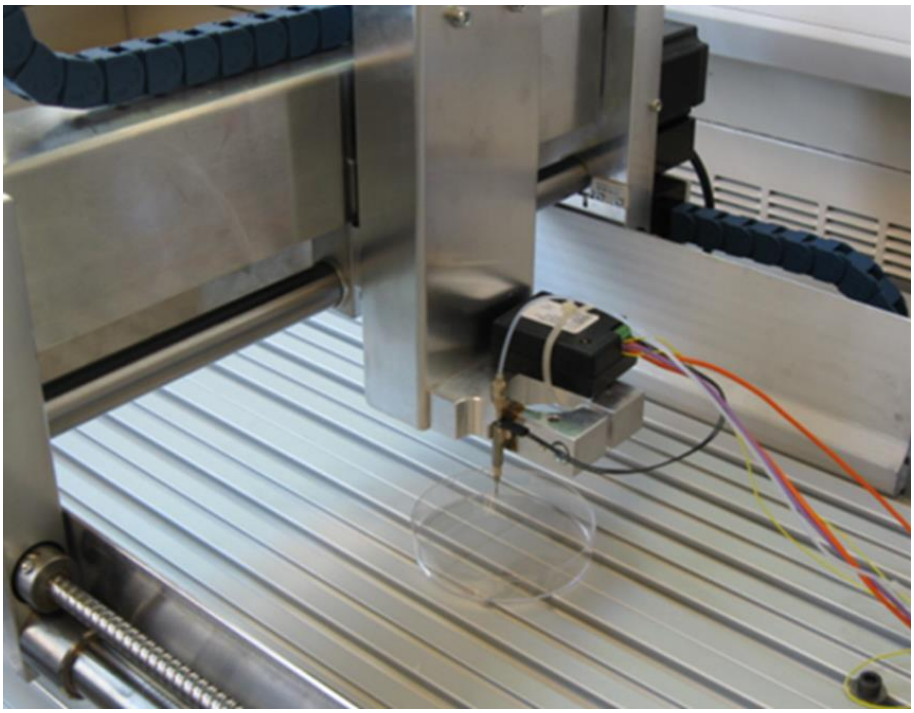

Figure 4.1 *– Single nozzle system setup*

The CNC machine uses G-code to define its movements, so an algorithm was developed in MATLAB which takes the coordinates of the target points as an input and outputs a G-code file that can be read by the CNC machine. First, the algorithm takes in the target point coordinates in the form of a binary image with 1 representing a target point and 0 a non-target point (as shown in Figure 4.2 below). The coordinates of all the target points are then stored in a 2 column array. The array of target points is analysed and an optimal order is calculated using a Travelling Salesman algorithm, which passes through each point only once in the shortest path. The MATLAB algorithm stores the G-code commands in a text file for each target point in the calculated order, which can be used to instruct the cell printer to follow the calculated path, pausing at every target point to allow for printing by manually triggering the deposition system.

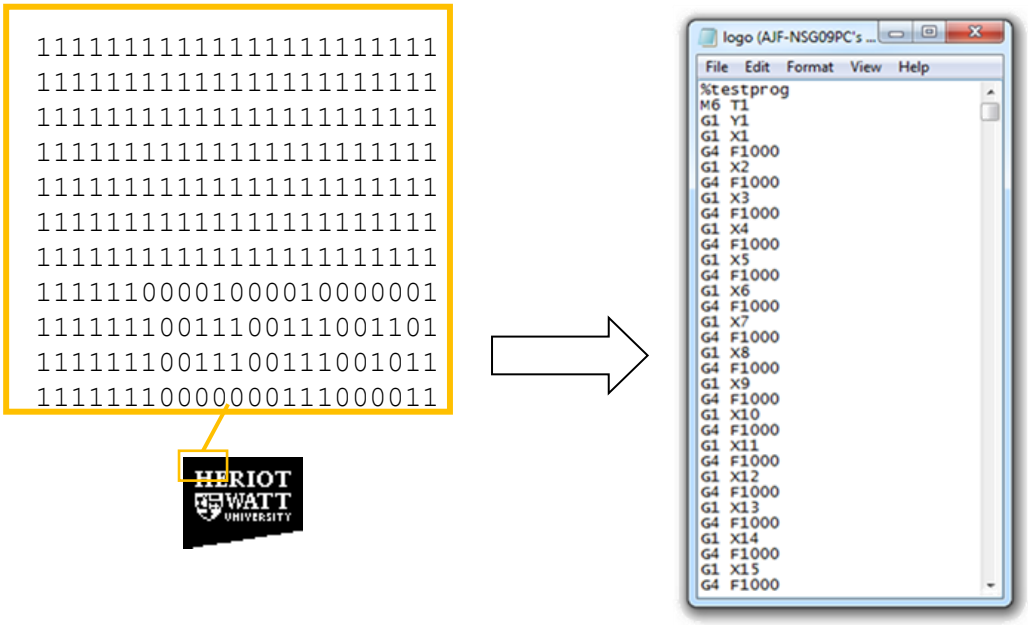

Figure 4.2 *– Target point coordinates to G-code*

This initial version performed reasonably well but suffered from a number of usability issues. Firstly, the system ran on two completely separate control systems (Figure 4.3) – the CNC machine controller did not communicate with the deposition system in any way. The only way to print an array of droplets was therefore to either manually program each movement of the CNC machine before manually triggering the deposition system or to program the entire array pattern – including pauses at each dispense position – and manually trigger the deposition system when the CNC machine paused. This meant that even simple patterns were extremely time consuming to set up and to run. Secondly, the deposition control system was a LabVIEW program which ran on the lab computer and was quite slow to respond, so was not capable of outputting signals with small enough pulse widths and high standard of accuracy and repeatability to dispense the small volumes which would be required for bioprinting.

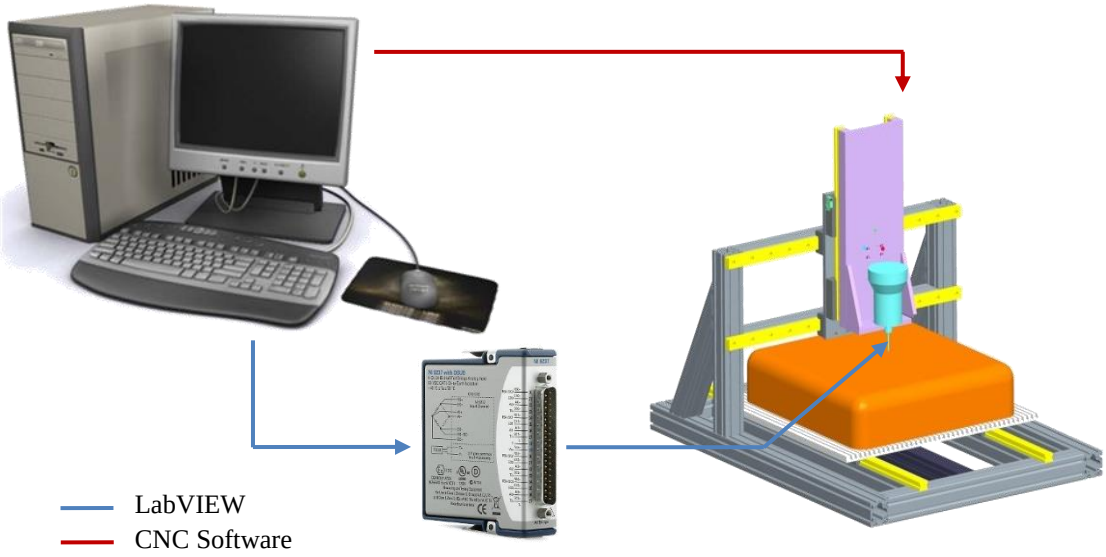

Figure 4.3 *– Pictographic Diagram of experimental setup for the Mark Ia bioprinter*

4.2.2 Switching from LabVIEW to Arduino and MATLAB

In order to address some of the issues encountered with the first version, a number of refinements were added to the bioprinter. The main alteration was the replacement of the LabVIEW control system with a new control program running on a microcontroller (Arduino UNO, Arduino) to generate the control signals for the deposition system. A series of new MATLAB and Arduino programs were created to control the cell printer using this new hardware setup.

The first program developed was an algorithm written in C code for the Arduino which triggers the dispense cycle by sending a short impulse signal to the valve driver, opening and closing the valve and allowing the bio-ink to be dispensed at the cell printers current location. This program allowed for various volumes to be dispensed either by varying the width of the generated signal or specifying a number of droplets to dispense in quick succession.

The signal to trigger the dispensing of a droplet was initially sent by pressing a button attached to the Arduino for testing purposes. As the aim was to create a single control system for the cell printer, the dispense trigger signal needed to be sent from the computer over the serial line. The algorithm therefore required the ability to handshake with the computer to agree on a communications protocol. The dispensing program was modified accordingly to enable serial communication with a new MATLAB program which ran on the lab PC and could trigger the deposition system through the Arduino.

4.2.3 An Optical Vision System

The next upgrade was the addition of a USB microscope for visual inspection of the target substrate during the printing process. Due to the type of deposition system used, a direct line-of-sight view through the nozzle was not possible, so the USB microscope had to be mounted at an offset angle from the valve assembly. A support frame was constructed from perforated zinc sheeting and jubilee clips and mounted to the tool head of the CNC, as shown in Figure 4.4.

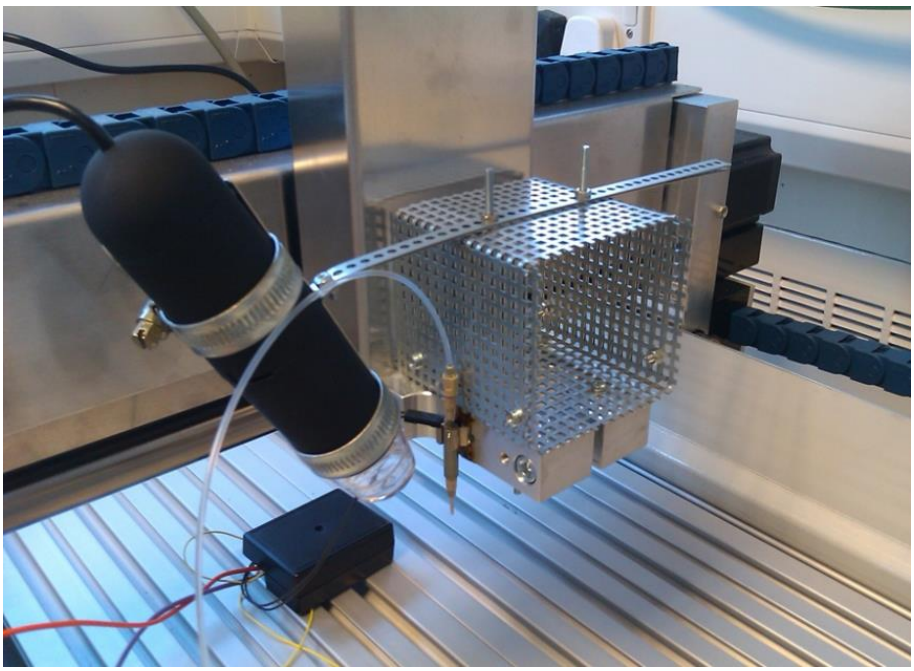

Figure 4.4 *– Single nozzle system with USB microscope*

While also useful for simply observing the printing process during experiments, the main purpose of the USB microscope was an attempt to tie together the two separate control systems. The first idea was to have single closed-loop control system with the USB microscope supplying the feedback as shown in Figure 4.5. By scanning over the area to be printed and capturing several images sufficient to describe the entire area, it is possible to join the images together like a mosaic and create an image of the entire target region. Features, such as the wells on a microfluidic device, can be extracted from this image and their coordinates saved in array. This control system would send the movement commands to the CNC machine over the parallel line from the computer and the dispense signals over the serial line to the Arduino.

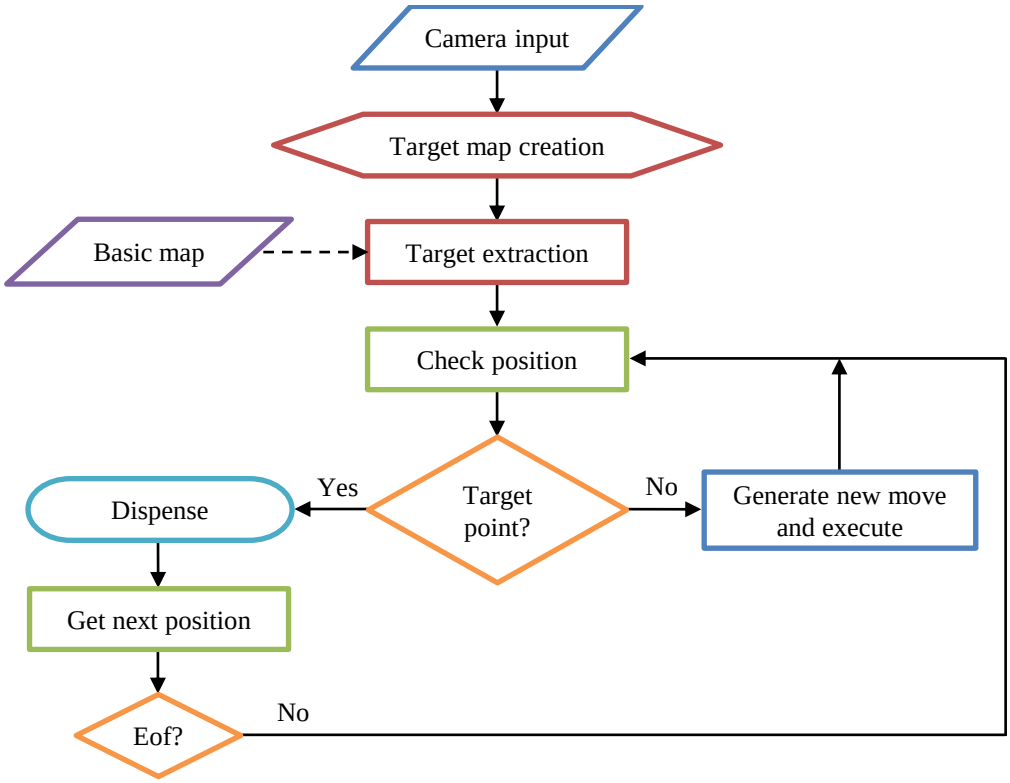

Figure 4.5 *– Flow diagram of the proposed MATLAB vision based control system for the Mark I bioprinter*

Unfortunately, the communications protocol used by the CNC machine proved difficult to mimic, so a different program had to be devised. The final algorithm was developed in MATLAB, using the USB microscope to identify the pauses of the CNC machine as the points to dispense bio-ink. The program captures real-time images from the USB microscope and compares them to previous frames to determine whether or not the CNC machine tool head is in motion. If the absolute difference between the two frames is below a pre-set threshold (determined experimentally), then the algorithm designates the current position as a target point and sends a signal to the Arduino to trigger the dispensing of a droplet of bio-ink. Some timers were added to the algorithm to ensure that target points weren't accidentally assigned in incorrect locations: for example, if the tool head was moving too slowly it could be possible for two frames to be similar enough to trigger an erroneous dispense. The timers also ensure that the cell printer dispenses only one droplet at each target point, regardless of how long the CNC machine dwells at a single location. In order to simplify the printing process, this algorithm runs continuously until the CNC machine stops moving (the dwell timer measures an extremely long pause). Furthermore, to prevent the algorithm triggering the dispense of a droplet before the CNC machine has moved to the first target point, an

enable signal was added which activates after the first movement is detected. A flowchart for this control system is shown in Figure 4.6.

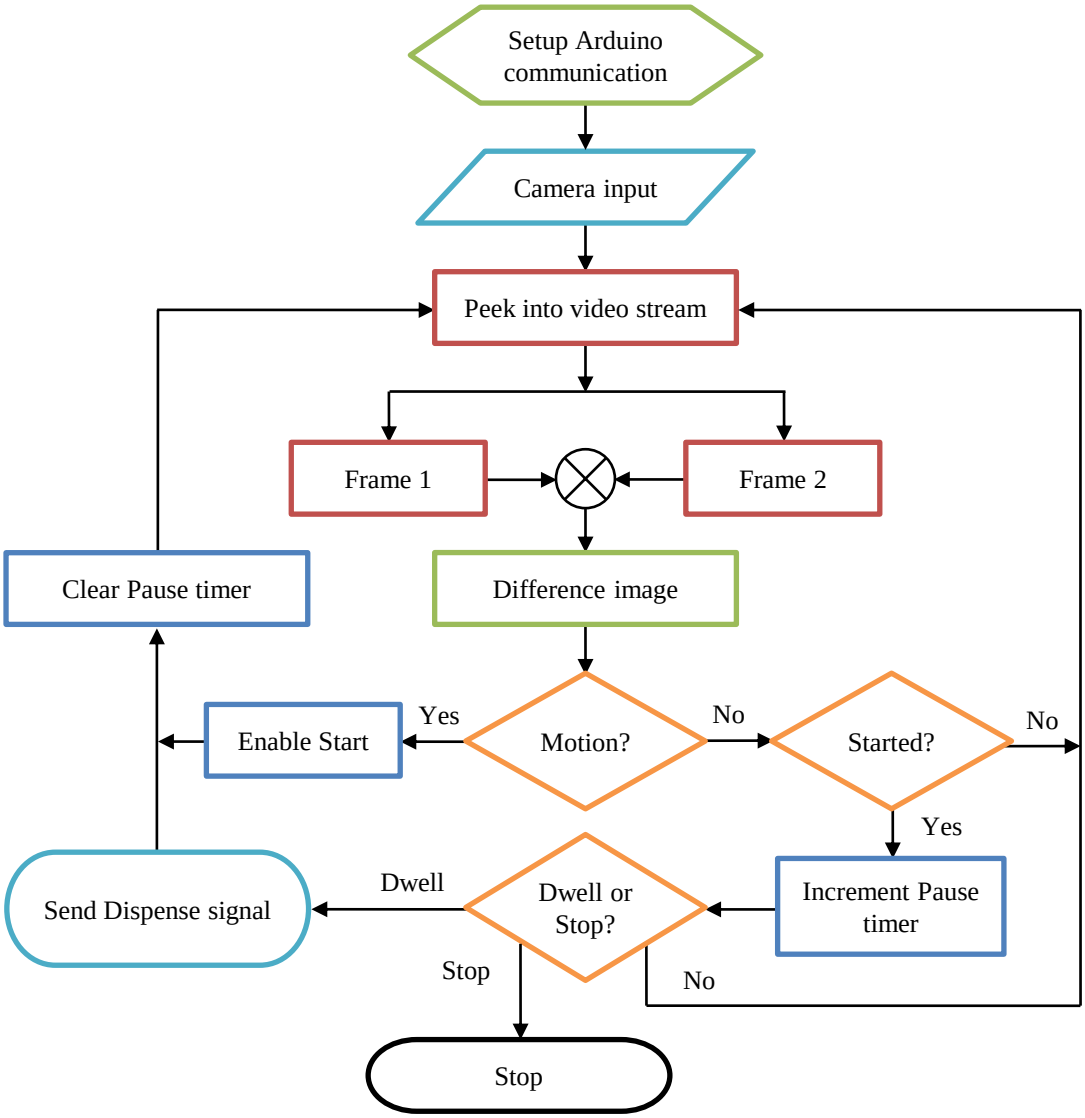

Figure 4.6 *– Flow diagram of the implemented MATLAB vision based control system for the Mark I bioprinter*

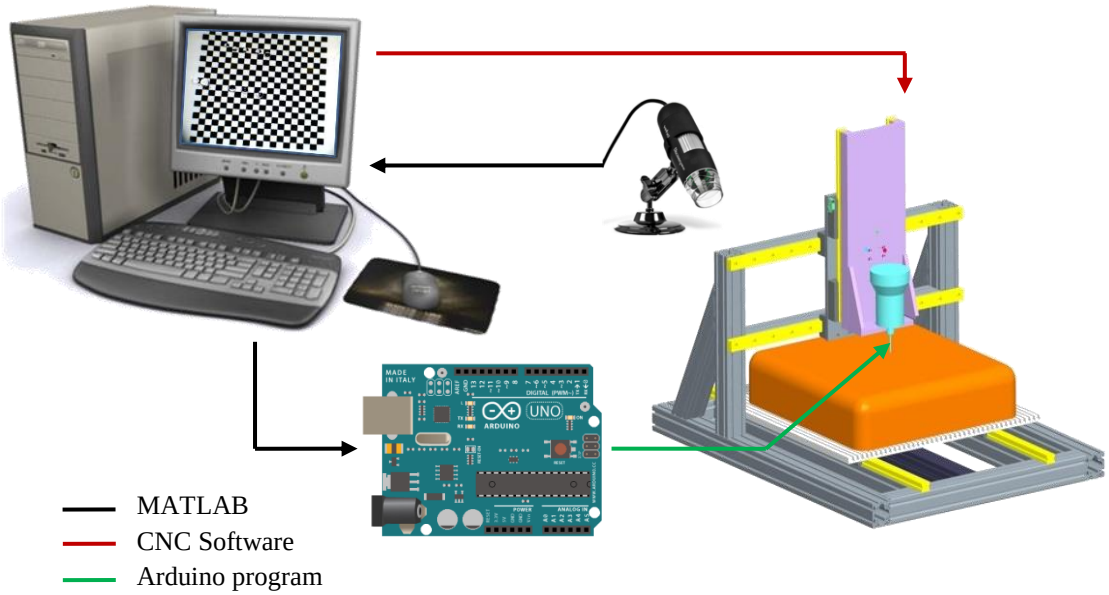

Figure 4.7 *– Pictographic Diagram of experimental setup for the Mark Ib bioprinter*

While these upgrades greatly improved the printing resolution and speed of the system, there were still a few issues upon which to improve. The mount for the USB microscope was too unstable and wobbled violently whenever the CNC machine was in motion; this, coupled with the defocusing of the USB microscope due to the vibration, meant that the USB microscope could not be used to reliably monitor or control the printer. Another issue was that the length of the tubing between the valve and the bio-ink reservoir was far too large. This meant that the system took a long time to sterilise and load new bio-inks and this large dead volume created a lot of wasted biomaterials. Finally, the vision based control system was too Heath Robinson; it worked inefficiently and the system was slower than it could be. Improvements could be made; for instance a direct communication between the CNC machine controller and the deposition system.

4.2.4 Arduino – CNC Machine Communication

Happily, an error in development led to an alteration that greatly improved the system. While attempting to rationalise the wiring of the system, one of the stepper motors was inadvertently disconnected from the CNC machine controller while the system was powered-on which unfortunately damaged the CNC machine controller beyond repair.

Building a new CNC machine controller allowed for much greater control over the system and tied the separate control systems together more effectively. A 4-axis stepper motor driver (G540, Geckodrive Motor Controls) and a suitable 36V 20A power supply (S-360-36, MeanWell) were mounted in an enclosure (LC540-4A, Camtronics Inc.). This new controller had a few outputs that could be triggered by G-code which meant that the CNC controller could finally connect directly to the deposition system controller and the entire system could therefore be run using a single G-code file.

Figure 4.8 *– Replacement CNC machine controller*

There were a few issues to overcome: the triggerable outputs operated at 36V but the Arduino operated at 5V, so some electrical relays were added to the outputs and connected to a 5V power supply in such a way that when the outputs went high a 5V signal also went high. The deposition system could then be triggered by the CNC machine controller with the appropriate G-code.

Initially the trigger system operated simply by triggering the dispense cycle on the rising edge of the control signal. However, the relay is a rather slow component and took time to physically switch between states. In order to speed up the system, the deposition system controller was programmed to trigger the dispense cycle on both the rising and the falling edge of the control signal as shown in Figure 4.9, cutting the wait time in half.

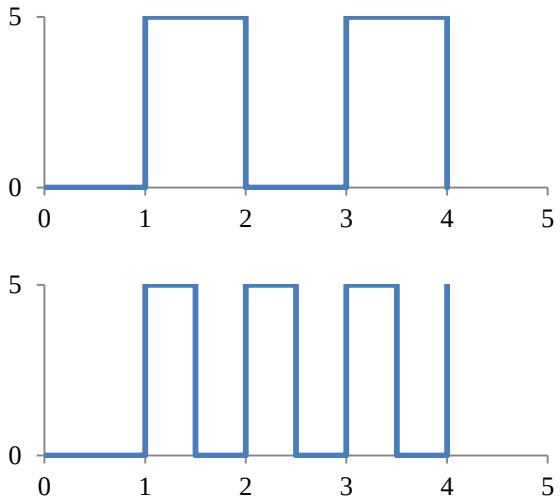

Figure 4.9 *– CNC deposition trigger signals illustrating the halving of the dispensing wait time: a) CNC machine controller output, b) the control signal output to the valve.*

4.2.5 Dual Nozzle System with On-board Bio-Ink Reservoirs

More complex experiments that were being planned required more than one bio-ink to be printed in a single experiment, so a second cell deposition system was added to the CNC machine tool head.

The reagent bottle that was being used as a bio-ink reservoir was replaced by two 50 mL centrifuge tubes which were repositioned onto the CNC machine tool head to shorten the length of tubing between the solenoid valve and the reservoir. This served to decrease the amount of time required to purge the system of a bio-ink after it has been used and to prime the system with the next bio-ink to be used. The tubes were passed through holes drilled into the lids of the tubes and sealed with epoxy resin.

The USB microscope mount was augmented with the addition of an extra supporting beam to reduce the vibration caused during movement.

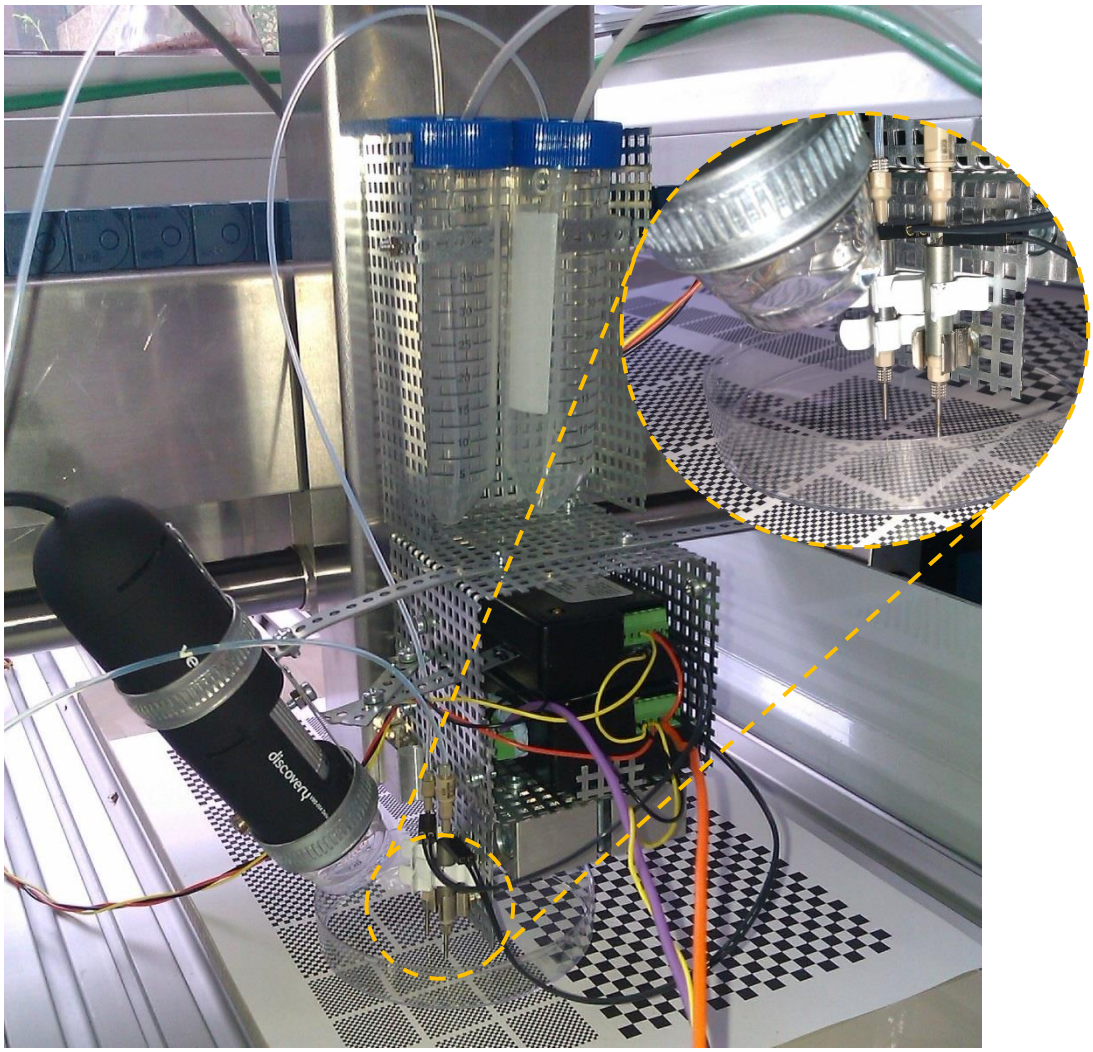

Figure 4.10 *– Dual nozzle system with USB microscope and integrated bio-ink reservoirs*

This version has the capability to print two different biological materials independently of each other in the same pre-programmed pattern.

Unfortunately, the seal on the centrifuge tubes was insufficient and there were periodic leaks when higher pressures were used. These leaks were not always immediately obvious, which meant that if went undetected it could waste a lot of time and bio-ink during an experiment.

4.2.6 A Laser-cut Tool Head Mount

The existing tool head mount performed reasonably well but a more robust tool head mount was needed for the dual deposition systems to improve the reliability of the system and reduce the unwanted vibrations of the USB microscope. A new, sleeker mount was designed in CorelDRAW and fabricated from 4 mm thick clear Acrylic sheet on a laser cutter (Trotec Speedy 300 CO2 Laser Engraver, Trotec).

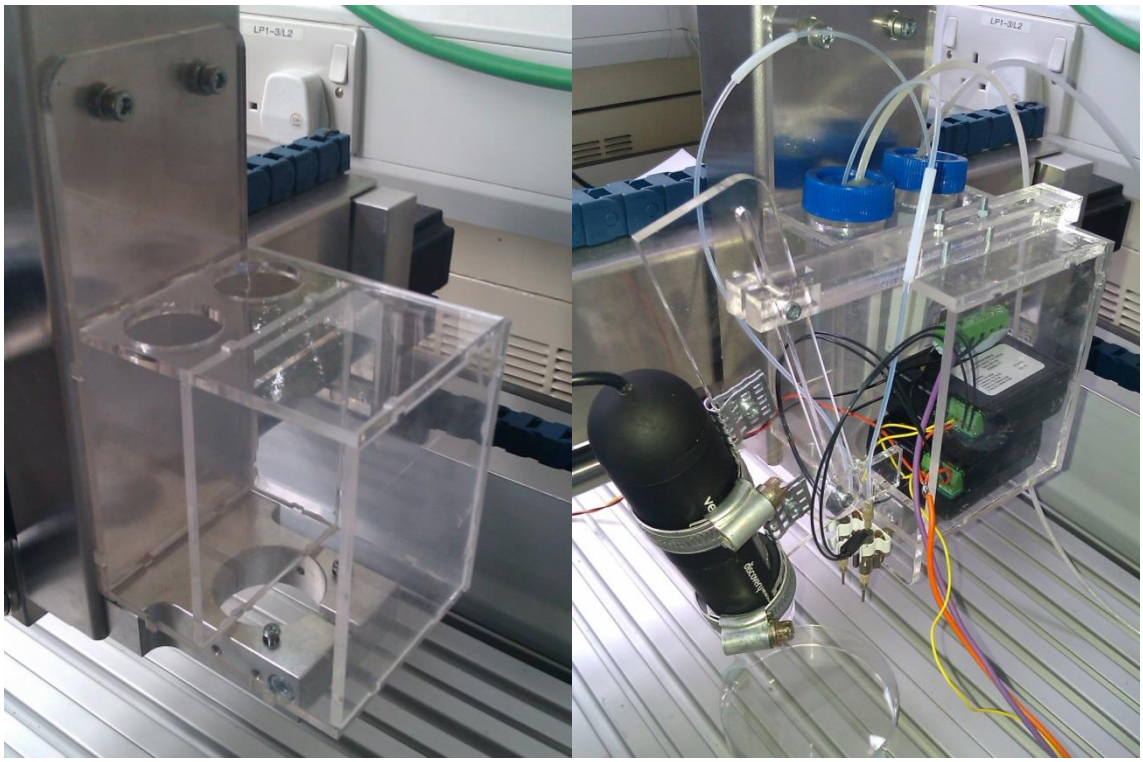

Figure 4.11 *– A laser-cut tool head mount*

After the new tool head was finished, a number of other refinements were made, which included new valve mounting clips which ensured that the valves remained vertical and at a fixed relative distance apart. A more important change was the addition of new pressure manifolds (Fluiwell-1C-15 mL, Fluigent S.A.) that provided a pressure seal between the bio-ink reservoirs and the tubing that goes to the valves and the pressure regulators. The bio-ink reservoir centrifuge tubes were replaced with 15 mL versions as Fluiwell does not manufacture manifolds to fit the 50 mL tubes and such large volumes are not normally required for the experiments conducted in this course of research.

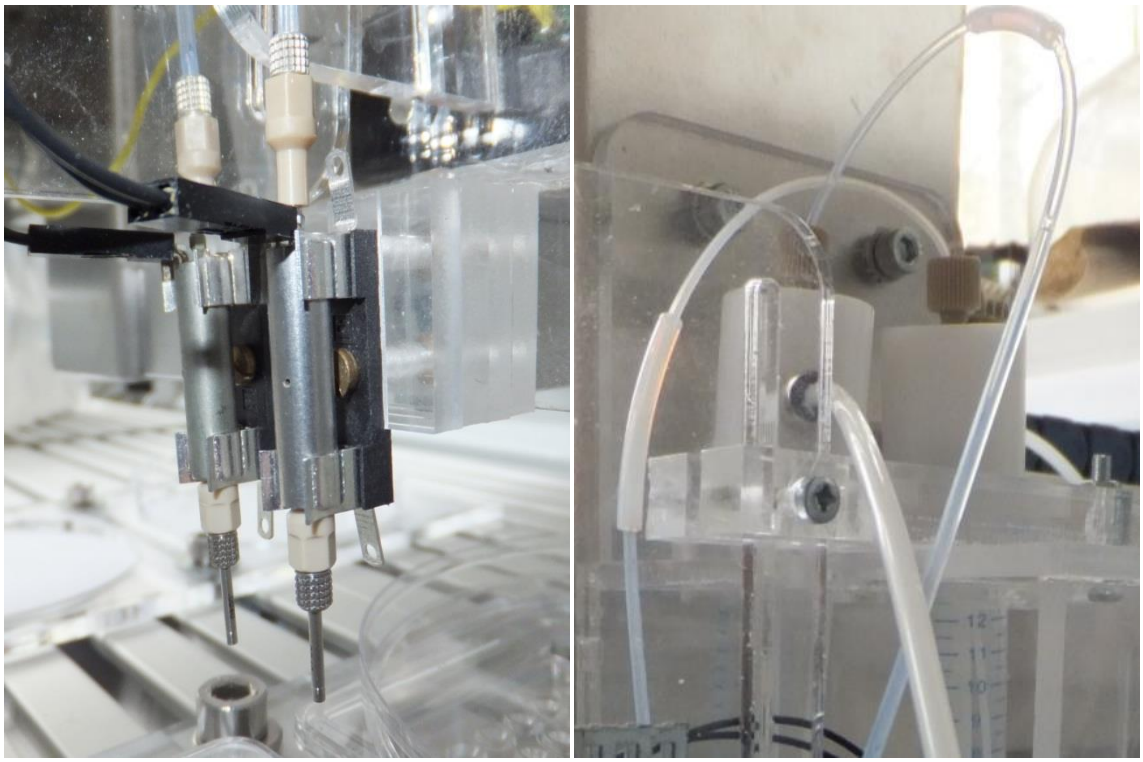

Figure 4.12 *– Final hardware upgrades to the Mark I bioprinter*

4.2.7 Graphical User Interface

The bioprinter uses G-codes to define the movement and droplet patterns to dispense. These files were manually written in Notepad, meaning that new patterns would take a long time to create. For that reason a new program was created to automatically generate the G-code files.

The Graphical User Interface (GUI) program had an axis where dispense points could be plotted by clicking with the mouse. In addition to their location, plotted points stored a variable to control the droplet volume at that point; this variable could be altered by selecting the point, and points could be deleted. Since the points were likely to be added in a non-optimal order, two path planning routines were available: shortest path and raster scan path. The shortest path used a genetic algorithm implementation of the Travelling Salesman Problem to find the shortest path between every point while stopping at each point only once; this path is useful when sparse patterns were created. The raster scan path sweeps vertically bottom-to-top, then moves to the left, where it turns and sweeps out the next path top-to-bottom (the paths have been optimised slightly to speed up the system); this path is useful for more densely populated patterns are created.

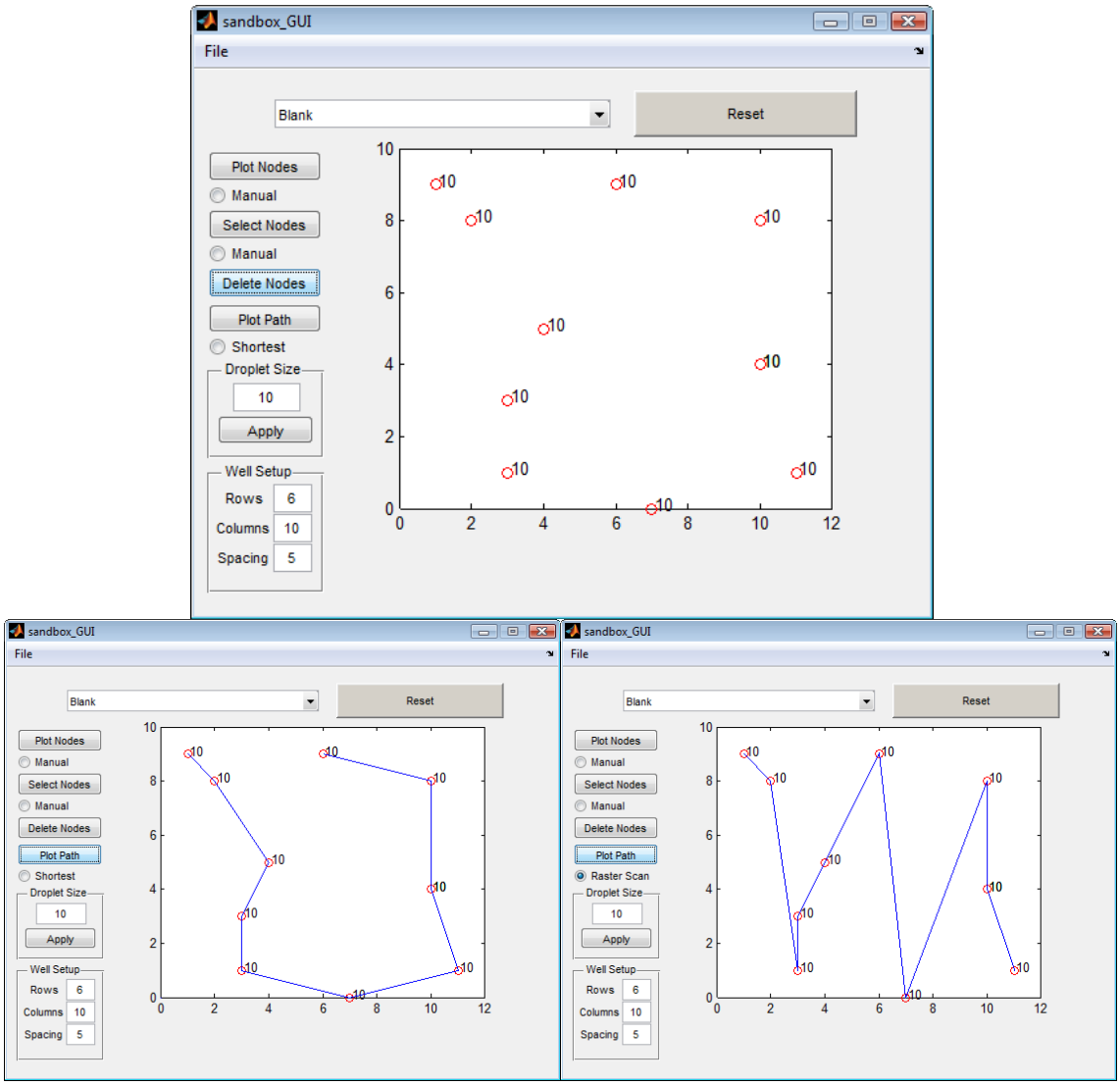

Figure 4.13 *– Graphical User Interface (GUI) program for the Mark I bioprinter in free plot mode. Points entered into the program (top), generated shortest path through these points (left) and optimised raster scan path through the points (right)*

Since several planned experiments required the use of multi-well plates, the GUI included multi-well plate options. The properties of the well plate, including the number of wells and columns as well as the well spacing, could be entered into the GUI and displayed on the plot axis. Dispense points could be added in the same manner as before, but points outside the wells would snap to the nearest well, or the wells could be automatically be populated with the current size setting.

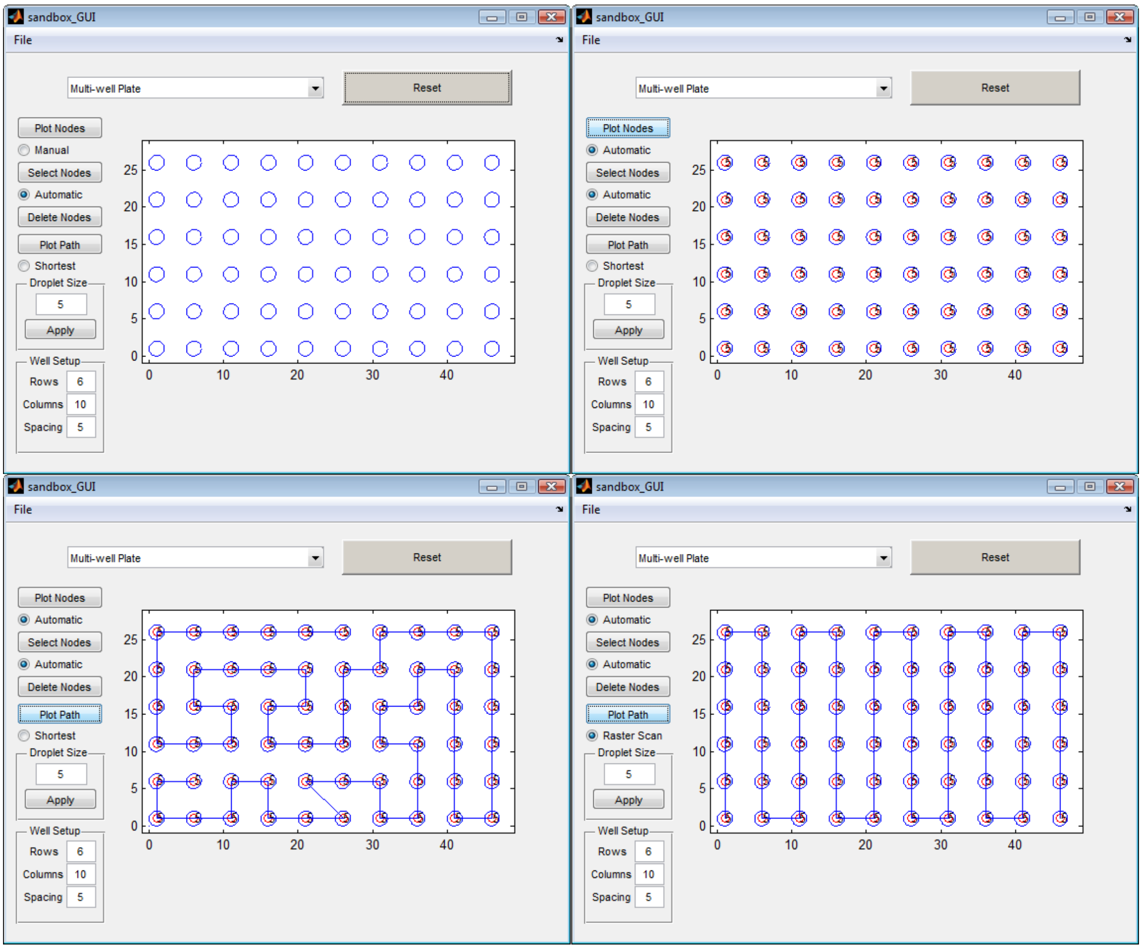

Figure 4.14 *– Graphical User Interface (GUI) program for the Mark I bioprinter in multi-well plate mode. Well coordinates generated from Well Setup (top left), points auto-populated to every well (top right), generated shortest path through these points (bottom left) and optimised raster scan path through the points (bottom right)*

4.2.8 Additional Software Development

A number of other algorithms were developed during the development of the control software. Although they were not directly used in the control software for this version of the bioprinter, they contributed to the development of the current version of the control software.

The first of these algorithms was written in C code for the Arduino and it performs a dynamic purge of the cell deposition system to remove any air bubbles that are present. Different size bubbles "break off" at different frequencies; therefore the algorithm is required to cycle through the dynamic response range of the value. This is done by rapidly opening and closing the valve at 100 Hz, 150 Hz, 200 Hz and so on up to 500 Hz for 1 second at each frequency. Depending on the system pressure and configuration, the purge cycle may need to be repeated. If the system has been unused for an extended period of time or a new bio-ink is to be used the purge cycle should be

run repeatedly with water until all the remnants of the previous bio-ink have been flushed from the system. This new purge program also allowed for the system to be cleaned and sterilised more easily than before and a sterilisation protocol was established by flowing solutions through the deposition system using the purge program:

- 2% bleach solution;
- 70% ethanol alcohol solution;
- Millipore filtered water/Sterile culture media.

This is similar to the cleaning techniques used by a number of different groups: Pardo et al. [1] and Roth et al. [2] rinse the bio-ink cartridges with ethanol and deionised water; and Boland et al. have a similar rinse procedure but the entire bioprinter assembly is placed beneath a UV lamp in a laminar flow hood and irradiated overnight. The addition of the bleach solution and the use of sterile culture media before printing serves to speed-up the procedure and ensure that there are no left-over salts in the deposition system.

4.2.8.1 Optical Control Software Development

Due to the offset positioning of the USB microscope, the view the control system receives of the substrate is oblique, so a vision algorithm was written in MATLAB that corrected the perspective view. The algorithm corrects the view by identifying the side of the image that is furthest from the USB microscope and stretching it so that it matches up with the side that is closest to the USB microscope. An exemplar input and output is shown in Figure 4.15 using an ideal input image. Unfortunately, this algorithm takes too long to execute (an average time of ~1.2 seconds per frame) and as it would ideally be used on every frame it would severely limit the ability of the control program to run in real time. Therefore it was ultimately removed from the main control system algorithm.

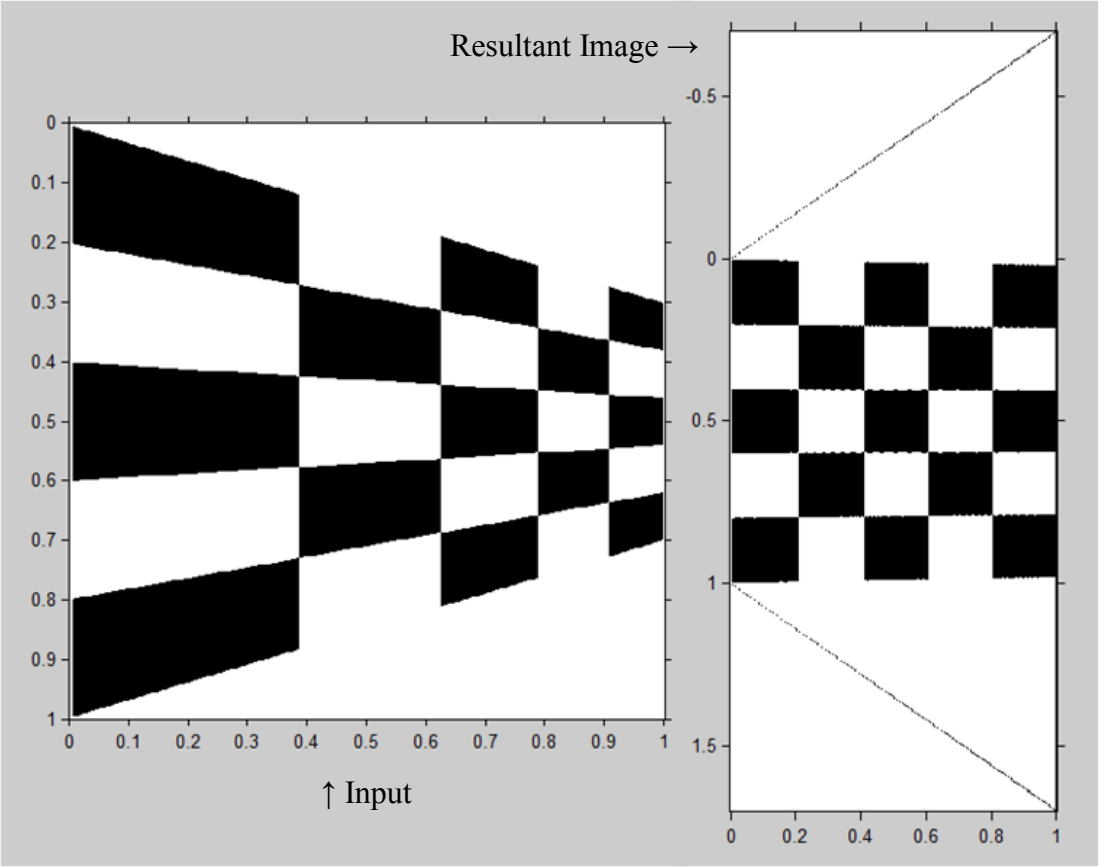

Figure 4.15 *– Exemplar input and output from the perspective correction algorithm*

Another algorithm was developed to allow the control program to check the coordinates of a target point before dispensing bio-ink to ensure it was not erroneous. The algorithm determines the location of the nozzle by comparing the current camera view to a generated target area map (which is a composite image made up of different views of the target area). This algorithm was abandoned with the perspective correction algorithm due to their time requirements. An exemplar input and output is shown in Figure 4.16 using test images.

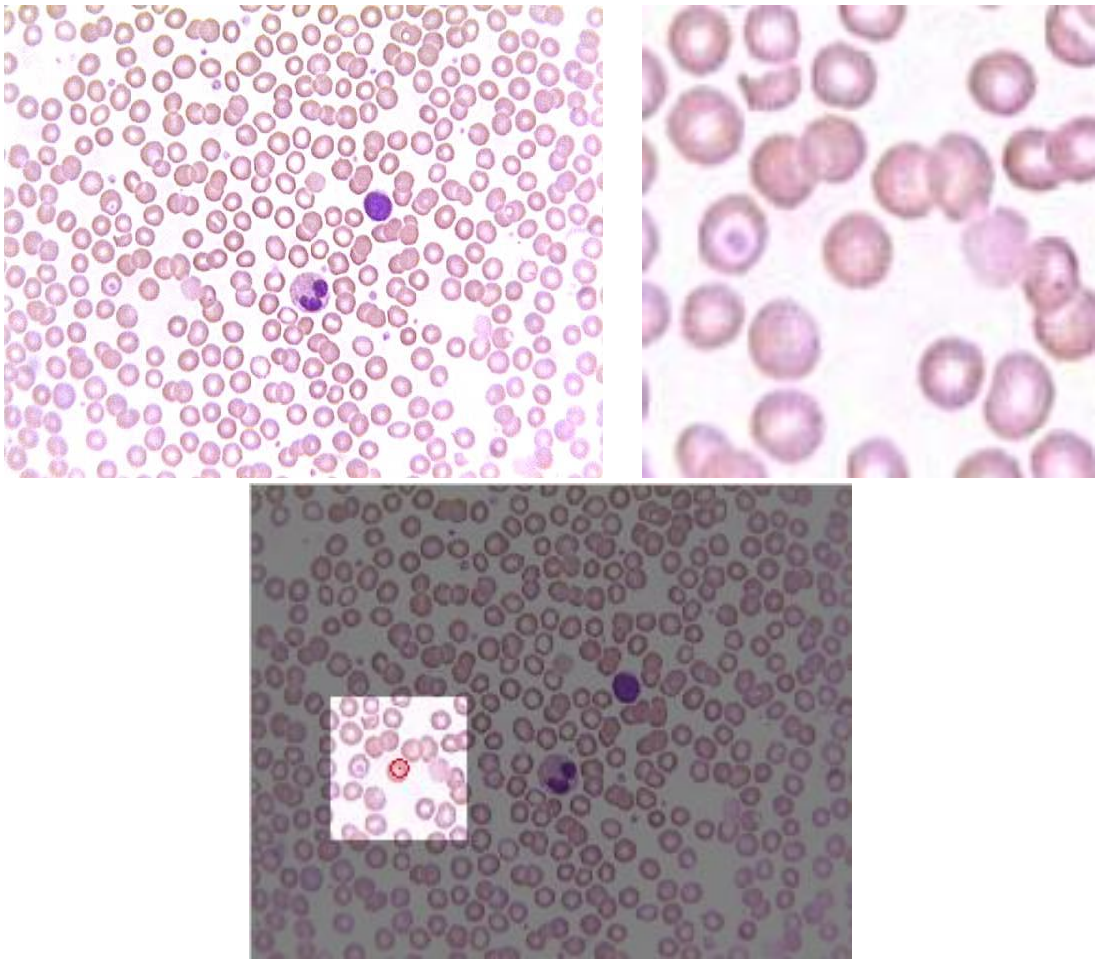

Figure 4.16 *– Nozzle coordinate calculation using exemplar data, Top left: target area map; Top right: current view; Bottom: calculated location within target area*

4.3 A Portable Deposition System

Not all experiments required the use of the entire printer; occasionally, only the deposition systems were required, so a portable deposition system was created that could be handheld for ease of transportation.

A single valve, bio-ink reservoir and microregulator were mounted on a small boss-clamp stand and connected together with tubing; this would be the basis of the system. Up until this point the bioprinting systems had always been connected to the lab compressed air supply; however, a portable system requires a portable air supply. This would necessitate either a small air compressor or an air cylinder; a small medical air cylinder was acquired (298123-AZ, BOC Ltd.) to ensure that the biomaterials would remain in a sterile environment without the need to filter the air coming from a compressor, and to limit the number of mains connections required by the system.

There were a number of challenges encountered while creating the portable pneumatics system. The most critical of these was a very serious error when BOC supplied an oxygen cylinder in place of the ordered medical air cylinder which could have resulted in serious and explosive consequences should it have come into contact with the lubricants and oils used in the system. Extra safety checks were implemented after this near-incident.

A new control system was created from a microcontroller (Arduino UNO, Arduino) and a valve driver with two buttons providing the interface: one button triggered a dispense cycle and the other a purge cycle. The parameters of the dispense and purge cycles can be altered via USB from a PC if required.

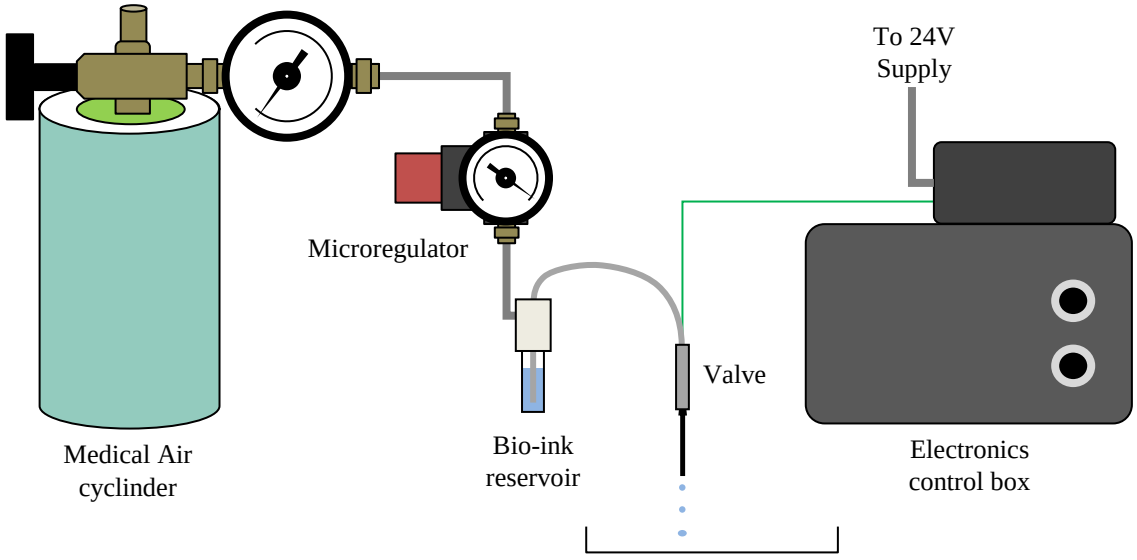

Figure 4.17 *– Schematic of the portable deposition system*

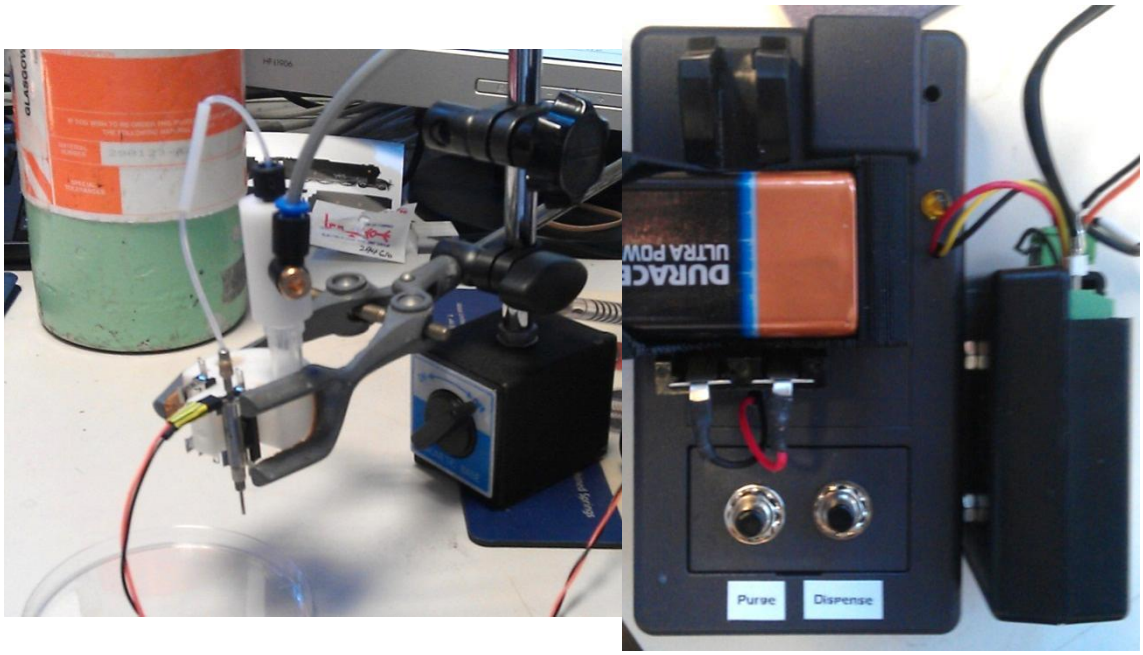

Figure 4.18 *– Portable deposition system: detailed views of the mounting system and the electronics control box*

The control system requires two different voltage inputs: 24V for the valve and 6-12V for the microcontroller. In the first version of the portable system the 24V supply was provided by a 24V 2.5A switch mode power supply unit (Model 9177, Mascot) and the microcontroller was powered by a 9V battery. However, the batteries did not seem to last very long in the system, so a DC-DC converter (SDS-030B24, Sunpower) was added to power the microcontroller from the existing 24V mains PSU.

This portable system was transferred to Roslin Cellab and has been used for a variety of cell-based experiments described in this thesis. It proved to be so useful that a second system was created as an additional testing platform.

4.4 Mark II

The Mark I bioprinter was only intended to be a proof of concept, and as such it performed excellently within its research parameters while highlighting areas requiring improvement. The most obvious of these was the size and weight of the machine, which prevented it from being moved from the lab. Since a lot of the experiments performed during the course of this research require cells from Roslin Cellab it would be useful to be able to install the bioprinter there to perform some experiments, especially those that use fragile or expensive-to-produce cells that suffer on the journey between labs. Another issue was the slow speed of the machine; if small volumes were

dispensed in a large pattern, the first droplets had quite often evaporated before the pattern was completed. With these points in mind, the second version of the bioprinter, the Mark II, was designed.

4.4.1 An Open Source Foundation

Since my background in engineering did not cover the design and construction of high resolution XYZ translation stages, it was decided that an existing off-the-shelf system should be selected as a base to build the new bioprinter. The requirements for the donor system were that it be relatively inexpensive, portable (meaning that it should be as small and light as is feasible) and that it be fully documented, or "hackable", so that the deposition electronics could be integrated into the system without too much work.

Several manufacturers produce small translation stages with high resolution, but these systems either have travel ranges which are too short for the project's requirements, or are too heavy or expensive.

Attention was then turned to the systems which already include XYZ translation stages, such as the CNC machine on which the Mark I was based. CNC machines themselves are almost always too large, heavy, or difficult to interface; with but there are other machines that include XYZ translation stages: 3D printers. Most 3D printers made by large companies such as Stratasys are just as unsuitable as CNC machines due to their large size, weight and complexity but thanks to the expiration of a key additive manufacturing patent [3] in 2009 there was an explosion of open-source 3D printers that were relatively cheap, small, lightweight and fully documented. It was therefore a simple matter to modify the hardware and software of one of these 3D printers to support bioprinting.

A Makerbot Replicator (Single) was chosen to be the base of the Mark II bioprinter over other possible machines due to its sturdy frame construction, high movement resolution and its ability to run stand-alone without being connected to a PC.

Figure 4.19 *– The Makerbot Replicator*

4.4.2 Making New Components

A number of parts on the Replicator were not required for bioprinting, so the plastic extruders, heated build plate and plastic filament management systems were immediately removed.

The Fluiwell pressure manifolds worked well on the Mark I system, so were retained for the Mark II, though with some modifications: the volumes that were used for the majority of the experiments rarely required the use of even half the capacity of the 15 mL centrifuge tubes so it was decided to switch to 2 mL micro centrifuge tubes. Rather than buy new pressure manifolds from Fluiwell to fit these new smaller tubes (Fluiwell's products were rather expensive), new pressure manifolds were designed in SolidWorks and manufactured from Delrin by the Mechanical Engineering Department's workshop technicians.

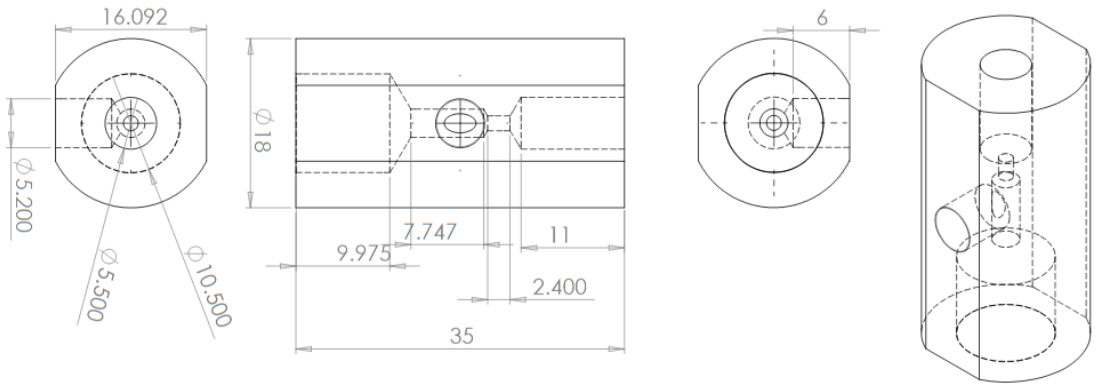

Figure 4.20 *– Original drawings for the custom designed pressure manifolds*

The three holes were tapped with the required threads for each of the connecting components to seal correctly: a finger tight ferrule is screwed into the top to seal the tubing that connects to the valve; a 2 mL micro centrifuge tube screws into the bottom to hold the bio-ink; and a 4 mm push in adapter screws into the side to connect to the pressurised air supply.

Because this version of the bioprinter was intended to be mounted into a laminar flow hood for some experiments, it needed to have the ability to be wiped down and cleaned with ethanol, meaning that the existing wooden panels were unsuitable for the bioprinter. As the Replicator is open source, the designs of the body panels are freely available. New panels were laser cut from 5 mm thick acrylic sheets, the donor 3D printer was completely dismantled and the bioprinter was assembled using the new acrylic body panels and the mechanical and electronic components from the donor machine.

The tool carriage had two mounting holes and recessed pads where the plastic extruder used to be attached. A new tool mount was designed in SolidWorks with mounting points for four valves and four bio-ink cartridges. The valves were set at exactly 10 mm apart in a square configuration to make offset calculations easier in the software later on. The tool mount was printed out on another 3D printer (Makerbot Replicator, Makerbot), assembled, and mounted to the tool carriage.

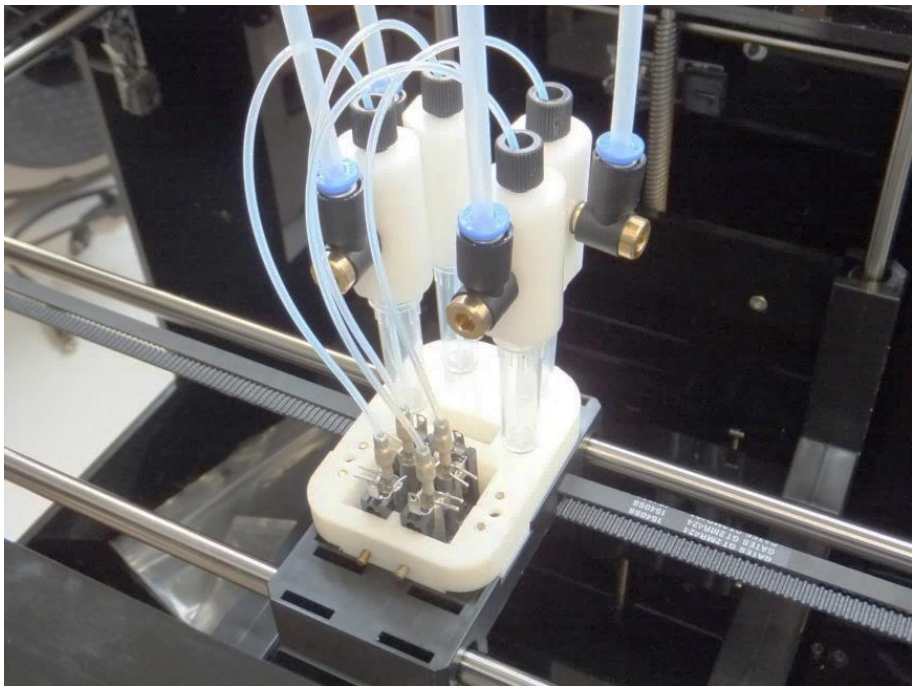

Figure 4.21 *– Quad-valve tool mount on the Mark II bioprinter*

Unfortunately the location of the X-axis endstop switch was higher up than the designed tool mount. Therefore, an extra "shoe" component that correctly triggered the endstop was designed, printed and mounted to the machine.

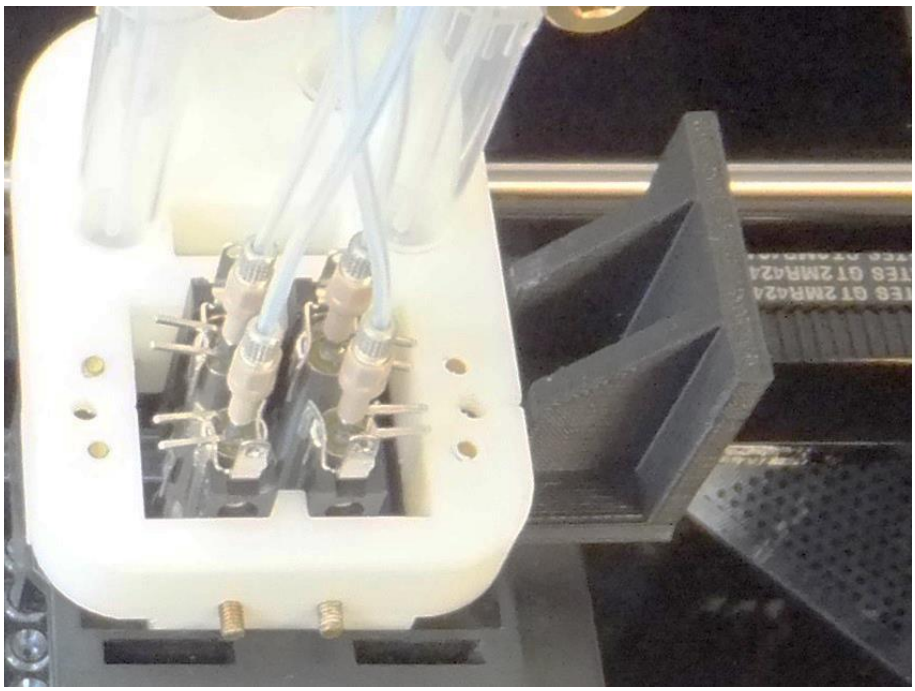

Figure 4.22 *– Endstop shoe on the Mark II bioprinter*

The microregulator that regulated the pressure of the bio-ink reservoirs on the Mark I bioprinter was never securely mounted. This was rectified on the Mark II by mounting

the microregulator to the machine with a new mounting bracket which was designed to fit into the mounting holes that used to hold the filament guides on the donor system at the top of the rear panel granting easy access to adjust the inlet pressure for the bio-ink reservoirs.

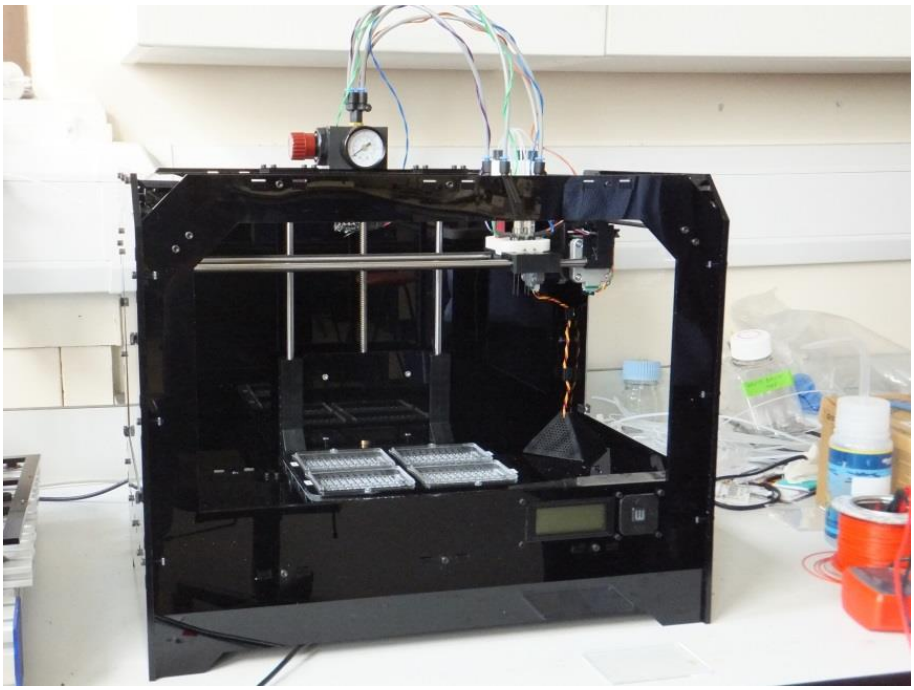

Figure 4.23 *– The completed mechanical system of the Mark II bioprinter*

A number of substrate trays were laser cut for holding a variety of different substrates including 60-well plates, 72-well plates and 90 mm petri dishes. These trays could be located on the Z-axis translational stage with four locating bolts to fix their position. The coordinates of salient reference positions were recorded for use when creating G-code programs to run on the bioprinter. Additional panels were laser cut from transparent acrylic to fully enclose the bioprinter and keep the inside free from dust and other airborne contaminants.

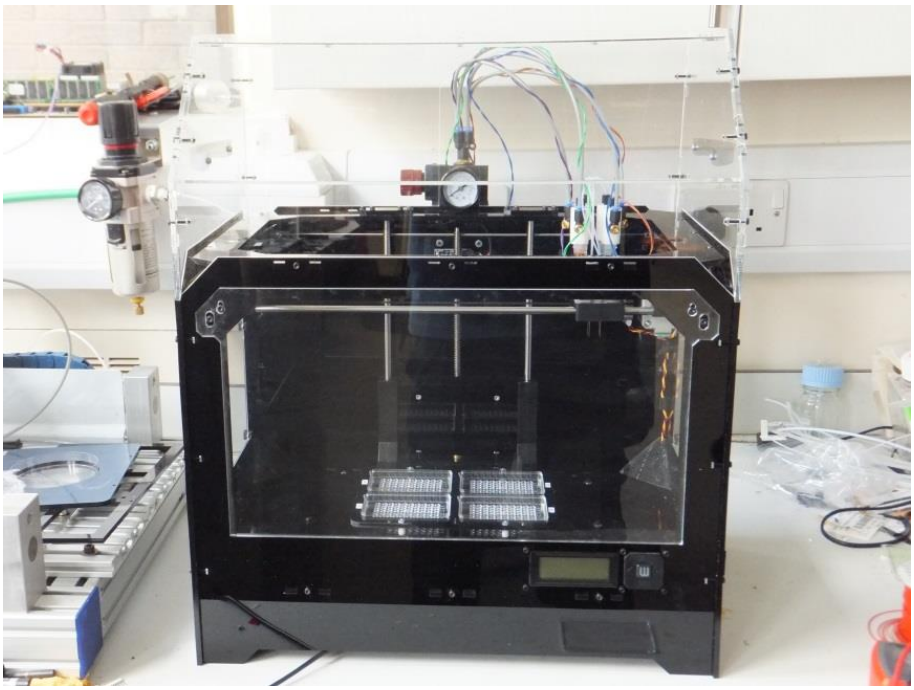

Figure 4.24 *– The Mark II bioprinter with enclosing panels*

Some of the valve control electronics were mounted on the tool head on the Mark I, which meant that there were a large number of cables trailing on the machine. On the Mark II the wiring was rationalised to streamline the machine as far as possible; therefore, all of the electronics were mounted on the underside of the machine leaving far fewer wires connecting to the tool head. It also served to reduce the travelling mass of the tool head, which should improve the positional repeatability of the system.

4.4.3 Control System Augmentations

The donor system was controlled by a single mainboard (Mightyboard Rev E, Makerbot) with open-source firmware. The original plan was to modify this firmware to incorporate new subroutines to control the deposition systems but although the firmware was open-source, it was largely undocumented, extremely convoluted, badly commented and spanned several programming languages, making it prohibitively difficult to adapt.

Since it was not possible to alter the firmware, further research into the mainboard was conducted with the aim of finding another way to augment the system. There is an output on the mainboard labelled 'Extra FET' which, when the correct G-codes are entered into the program, enabled or disabled a 24V supply – M126 enabled the output and M127 disabled it. This would provide the spike voltage required by the valves.

Now all that was required was four 5V control signal lines, one for each valve, but finding them proved to be very difficult indeed.

While investigating output pins on the mainboard with a multi-meter one of the probes shorted out the 5V power rail and the 5V regulator went up in smoke. A replacement was ordered and the mainboard was sent to the Electronics workshop for repairs. Unfortunately the damage was too severe for the technicians to repair so a replacement was needed. Regrettably, Makerbot do not sell Mightyboards separately but luckily the Makerbot support team was kind enough to provide a replacement since the damage was incurred accidentally.

Unlike other stepper motor drivers used on other 3D printer controllers, the ones used on the mainboard do not have a potentiometer to alter the current sent to the stepper motors; rather, they have a voltage reference pin to set the current. Since the plastic extruder mechanism control circuits were not required for the Mark II system, there were two empty stepper driver slots on the mainboard, each with a Vref pin. These Vref pins can be set by a G130 G-code command to any value between 0 and 255, representing a range of analogue voltages between 0 and 5V. An Arduino UNO microcontroller was wired up to these output pins and measured the voltages generated and it worked (with a small margin of error). Three voltage ranges were defined for each output pin to enable control of 4 deposition systems as shown in Table 4.1. A program was written for the Arduino that checked the voltages fell into one of three voltage ranges and triggered the corresponding deposition system as appropriate.

Table 4.1 *– Variables for triggering four deposition systems using G130 G-code command*

	Off	On1	On2
Vref A	≤63	64-126	127≥
Vref B	≤63	64-126	127≥

During the hydrogel printing experiments it was discovered that the two hydrogel components required different pressures to dispense comparable volumes; for example, the calcium solution requires much less pressure than the sodium alginate solution due to the different viscosities of the two solutions. Therefore, a second microregulator was added to the system between the existing microregulator and one of the bio-ink

reservoirs so that one bio-ink can be dispensed using reduced pressure relative to the other bio-ink reservoir.

The final addition to the Mark II system was a DC-DC converter; this was required to power the Arduino microcontroller from the mainboard 24V supply as the Arduino requires 6-12V input. Up until this point the printer had been constantly connected to the lab PC to power the Arduino, which was certainly not ideal if it was to be a portable system.

4.4.4 Second Generation Graphical User Interface

The Mark II bioprinter uses different G-code commands from the Mark I so some modifications would be required to the Mark I GUI for it to work with the Mark II. This opportunity was used to rewrite the interface program to reflect the development of my programming knowledge.

Several improvements were added, the first of which being the droplet property controls which allow the operator to specify not only the volume of each droplet but the percentage of up to four bio-inks that constitute it. The droplet volume and specified inlet pressure were used to calculate the needed valve on-time using an equation derived experimentally (Equation 5.2). The proportion of each bio-ink is displayed using a labelled pie chart.

A number of tabs were added to the program for the different substrates that the Mark II bioprinter could use: the multi-well plate system was adapted from the original GUI; a new free plot mode was created for printing onto 90 mm Petri dishes; and a new small plate mode was written for printing onto the 60/72 well Terasaki plates.

The free plot mode is similar to the one in the original GUI but it includes a circle in the plot axis defining the limits of the Petri dish. It also contains a "snap-to" setting to align user-entered points to a grid with a specified spacing.

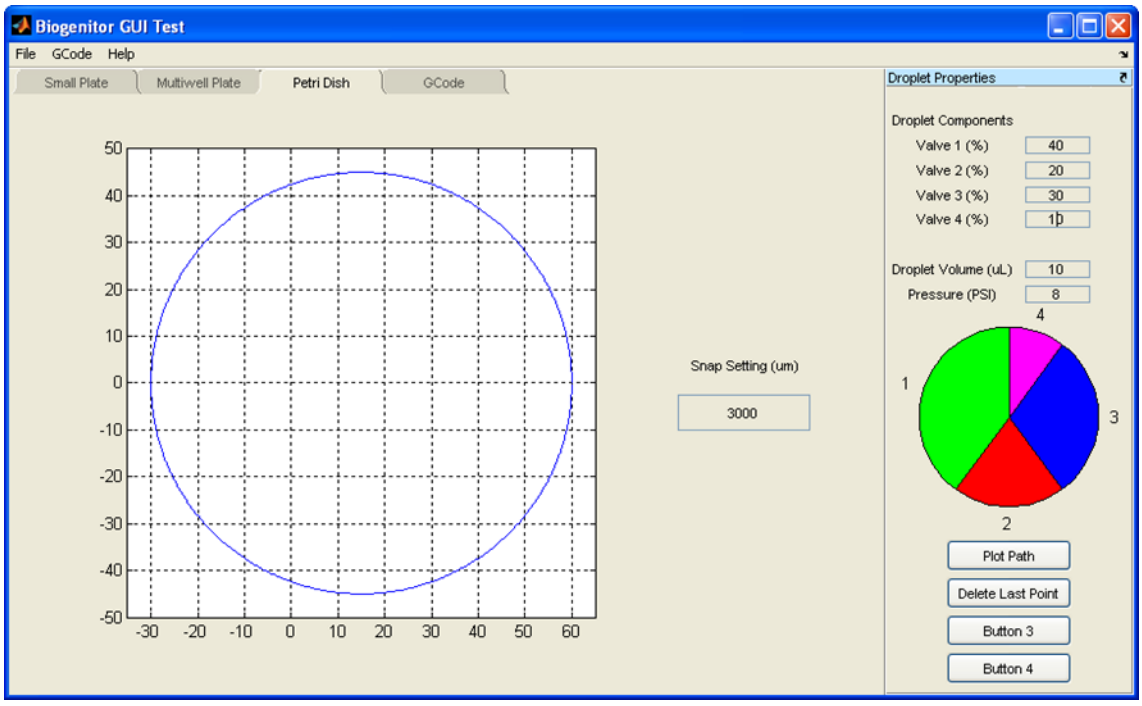

Figure 4.25 *– Graphical User Interface (GUI) program for the Mark II bioprinter in free plot mode showing the new droplet properties controls*

The small plate mode has buttons that represent each well on a plate and by selecting the buttons, the current droplet properties are applied to that well as shown in Figure 4.26. The small plate substrate tray can hold 4 Terasaki plates which can have 60 or 72 wells; the setup can be specified using the controls at the bottom of the window.

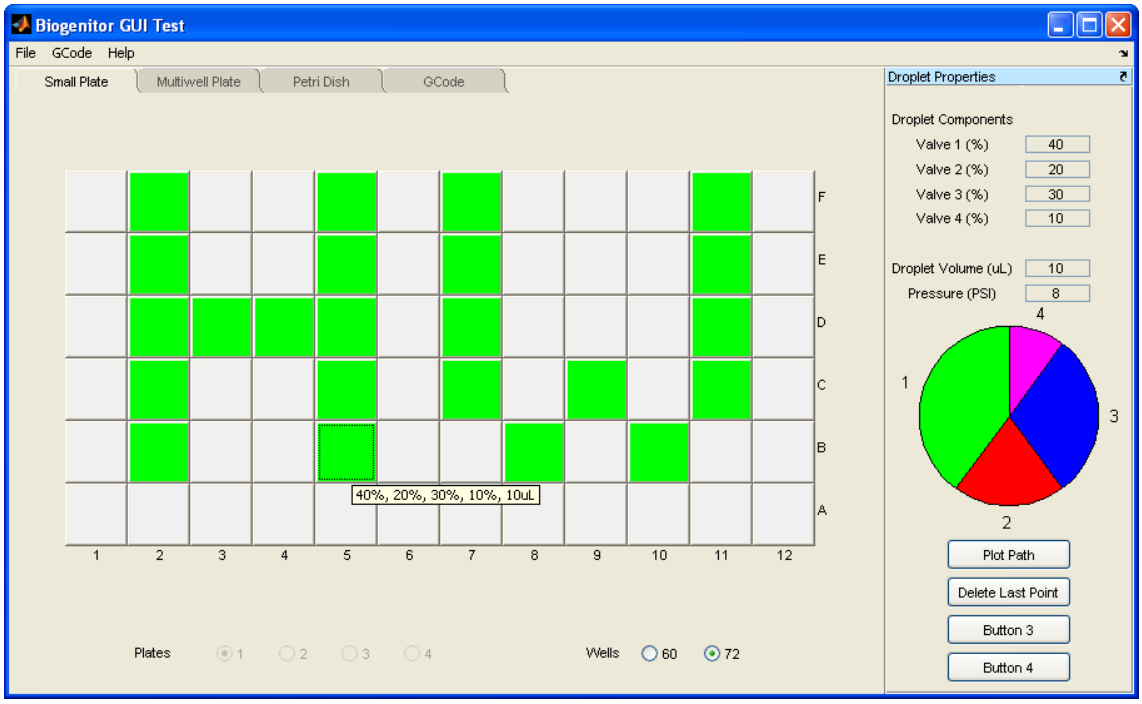

Figure 4.26 *– Graphical User Interface (GUI) program for the Mark II bioprinter in the new small plate mode. Selected target points shown highlighted in green displaying the applied droplet properties in the tooltip*

Paths can be created using a raster or shortest path in the same manner as in the original GUI; indeed, the same functions are used, though slightly modified. The G-code file with the correct commands and syntax is generated and displayed in the interface for easy error checking.

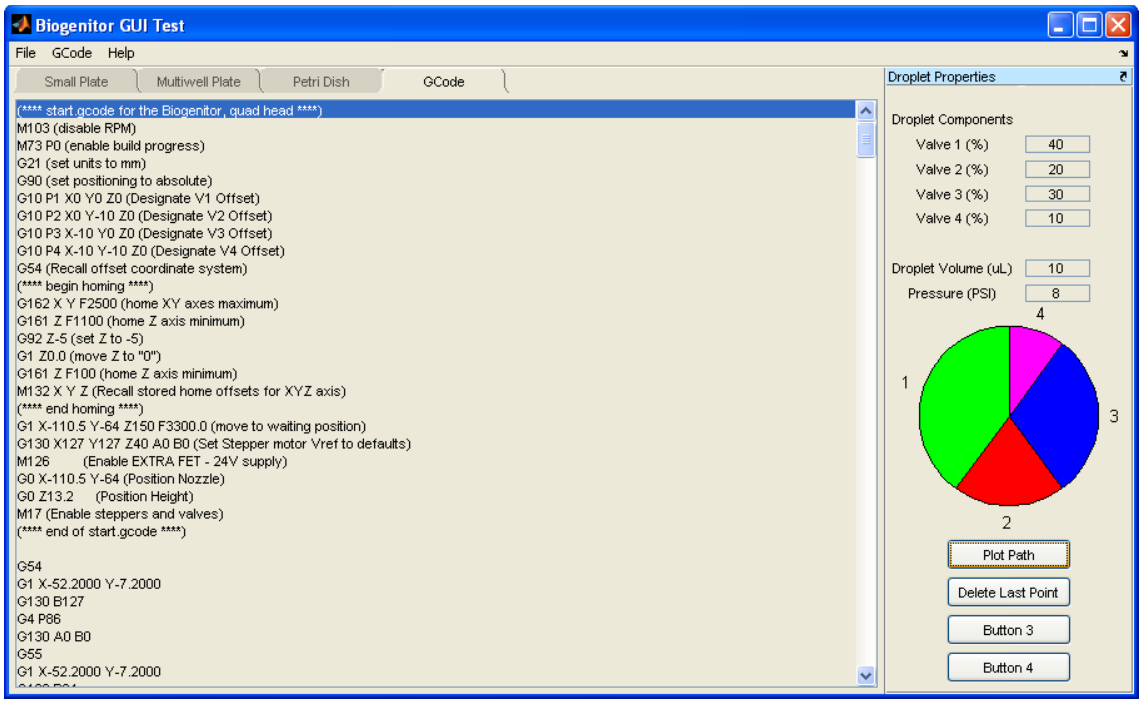

Figure 4.27 *– Graphical User Interface (GUI) program for the Mark II bioprinter showing the generated G-code for the pattern entered in the previous figure*

Before the generated G-code file could be run on the Mark II bioprinter it had to be translated into an s3g or x3g file that the firmware could understand. This was not ideal as the translation required running the G-code file through another piece of software, but it worked.

Another issue was the large plate mode; as it was copied across from the old program it had a number of issues including incorrect coordinates and the interface wasn't as clean and polished as the rest of the program. There were plenty of programming issues that were encountered during the creation of this new user interface, mostly caused by dealing with empty of zero valued variables or percentages greater than 100, but they were all located and resolved.

4.5 Mark III

The Mark II bioprinter was a generally successful machine. It managed to significantly improve and correct a large number of the shortcomings of the Mark I bioprinter, but

there still remained a number of improvements which could be made and some new problems arose. The most important new issue was the slight loss of printing resolution introduced by the new mainboard.

4.5.1 RAMPS Electronics

Since the Makerbot Mightyboard mainboard was the cause of the new issues it was replaced by a new, more open source electronics solution: the RepRap Arduino Mega Pololu Shield, or RAMPS for short. The RAMPS board sits on an Arduino Mega 2560 which uses an ATmega2560 microcontroller which has twice as much flash memory as the Mightyboard (which uses an ATmega1280); this means that there is much more space for firmware alterations.

The Mark II used the same power supply as the Makerbot Replicator, which was a cable-and-box setup. While this was perfectly adequate, it sometimes got in the way or was difficult to position without putting strain on the cables. Therefore, the Mark III has an on-board power supply unit. The valves require 24V to operate while the RAMPS electronics including the stepper motors run on 12V. Initially, two separate PSUs were used, a 12V 20A embedded switch mode power supply unit (S-240W-12, YXDY) and a 24V 2.5A switch mode power supply unit (Model 9177, Mascot) mounted to the underside of the bioprinter and connected to an IEC power connector with an integrated fuse. In order to simplify the system, the two units were replaced with a single embedded switch mode power supply (QP-320D, MeanWell) that outputs both 12V and 24V.

The same high quality NEMA 17 hybrid stepper motors from the Mark II were used for the Mark III, but interestingly the RAMPS board stepper motor connections used a different pin order than the Mightyboard, which was unexpected and took some time to correct. Instead of each wire connecting in order, the last two were reversed.

The RAMPS electronics has a number of different options for LCD interfaces. The Smart 2004 LCD controller was selected due to its popularity and screen size. It uses a combined potentiometer and momentary switch to navigate the on-board menu system in contrast to the five push buttons (4 directions and enter) which made navigation quite slow on the Mark II.

Another advantage of the RAMPS electronics over the Mightyboard is that it can read G-code files from an SD card rather than s3g or x3g files which the Mightyboard requires. The Mark II programs had to be translated from G-code before loading them onto the bioprinter but the Mark III is able to take the G-code programs directly. This makes program creation much simpler for the user.

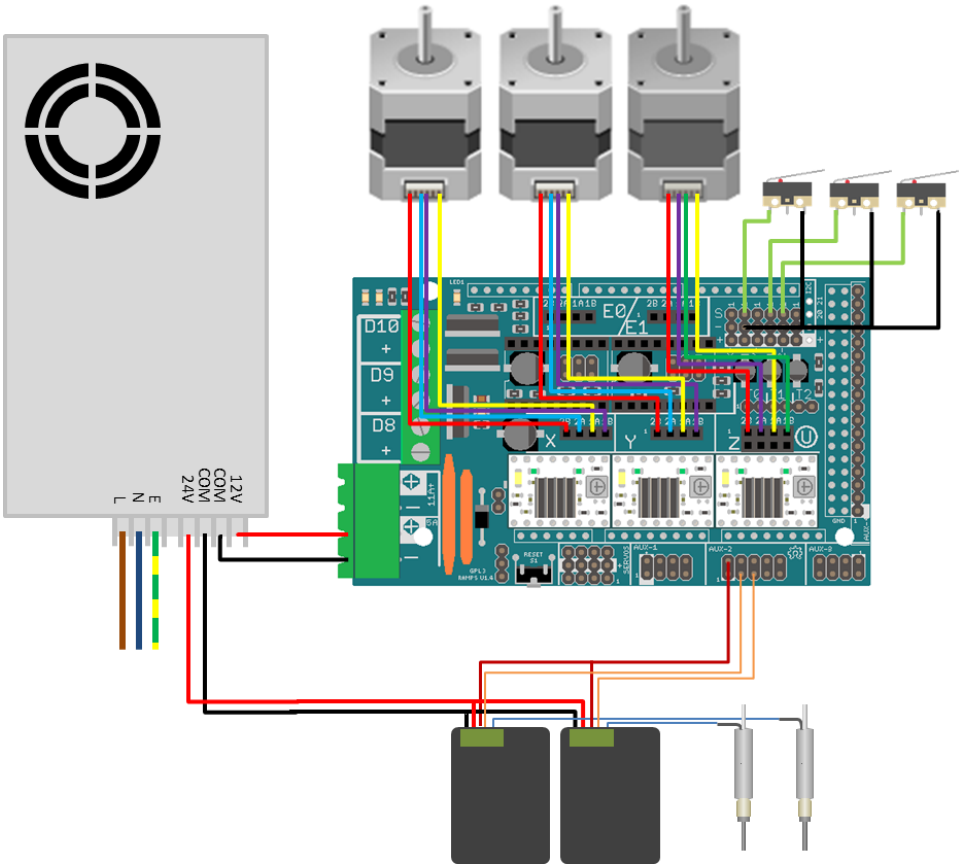

Figure 4.28 *– Schematic of the Mark III electronics system with two deposition systems*

4.5.2 Firmware

There are several available firmwares for RAMPS; the most common option is Marlin which is written entirely in C++ and is well documented. This means that alterations are easy to implement.

Two new G-code commands were added to the firmware to enable the system to control the deposition systems. The first was the variable dispense command:

```
M45 V# S#
```

This allows the user to specify the valve to use (1-4) and the duration of the dispense cycle in microseconds (≥150). The Mark III bioprinter uses a slightly modified version of the Mark II's GUI and the dispense cycle duration can be calculated from the desired volume in the same manner.

The second new G-code command triggers the dynamic purge routine:

```
M46 V#
```

This finally integrates the dynamic purge algorithm into the bioprinter control system and allows the user to purge a specified valve (1-4) without uploading the separate purge algorithm to the control system or using the portable deposition system controller (as was the case with the Mark II system).

The dynamic purge trigger command was also integrated into the LCD interface menu system to allow users to easily trigger the purge routine at the push of a few buttons.

Figure 4.29 *– The purge routines integrated into the interface menu system*

The configuration settings for the X, Y and Z translation stages were calculated by measuring the mechanical characteristics of the translation stages, including belt and acme rod pitches, the number of teeth on the pulleys and the maximum translation distances.

Initially there was some difficulty with the system refusing to store new configuration variables in the EEPROM (electrically erasable program memory), but eventually the correct variables were stored and the system operated correctly.

4.5.3 Body Redesign and Improvements

The basic mechanical layout of the X, Y and Z axes were maintained so the design of the Mark II body panels was used as the basis of the new design. A number of alterations were made to the body panels to suit the new components: the mounting holes were altered to suit the new electronics and the LCD interface board was a completely different design to the one used in the original design.

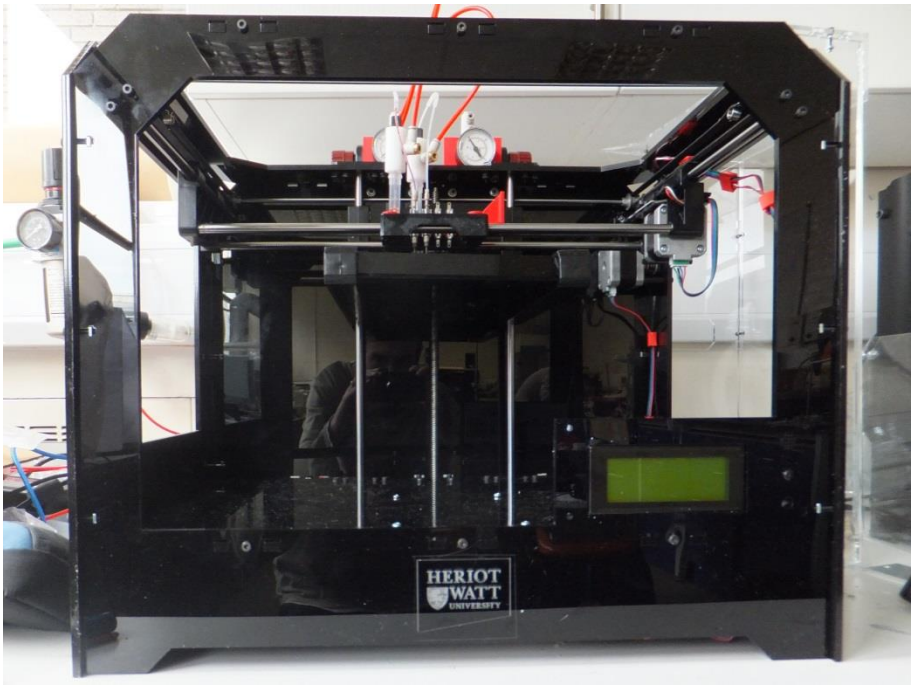

Figure 4.30 *– The redesigned Mark III bioprinter*

There was an issue with the laser-cut holes for the Arduino/RAMPS mounting not lining up exactly; this was due to contradictory information about the position of the mounting holes on the internet. This was solved by simply drilling new holes in the panel.

While printing with hydrogels using the Mark II bioprinter it was discovered that the different components had different viscosities and required different inlet pressures to allow for minimum volumes to be dispensed. The Mark III bioprinter was therefore designed with two micro-regulators to allow different pressures to be applied to

different bio-inks. The standard pneumatic tubing used on the Mark II was replaced with coiled tubing to reduce the strain on the tool carriage at the extreme edges of the movement range.

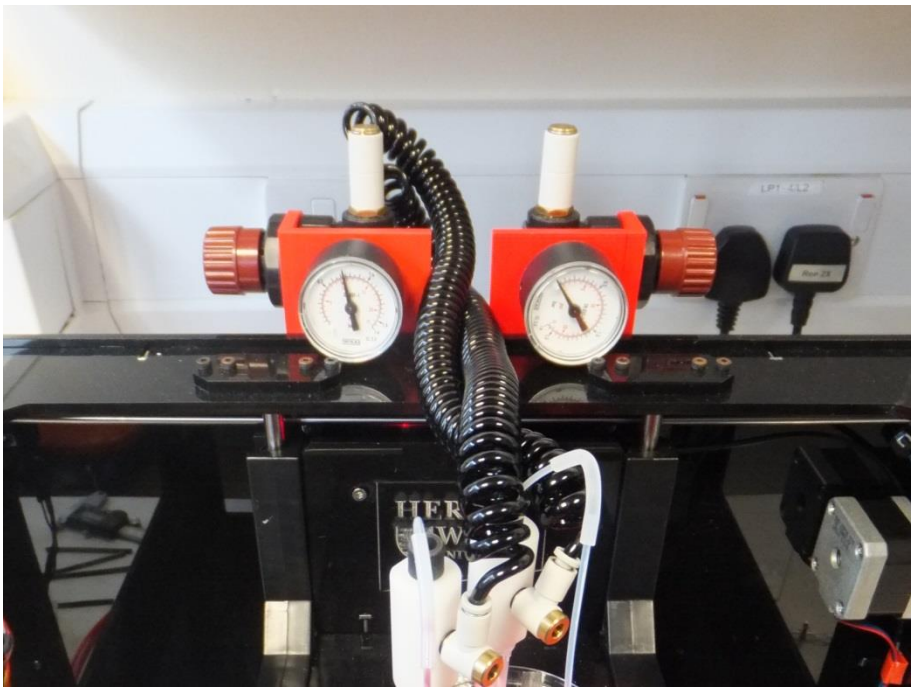

Figure 4.31 *– Two micro-regulators mounted to the Mark III bioprinter and the new coiled pneumatic tubing*

The tool mount on the Mark II worked perfectly well but was slightly restricted and changing the valves and bio-inks was difficult due to the lack of space. Therefore, a new tool mount was designed in SolidWorks for the Mark III which was much wider. The valves were set at exactly 10 mm apart in a linear configuration to make alterations and maintenance easier. The tool mount was printed out on a 3D printer, assembled and mounted to the tool carriage.

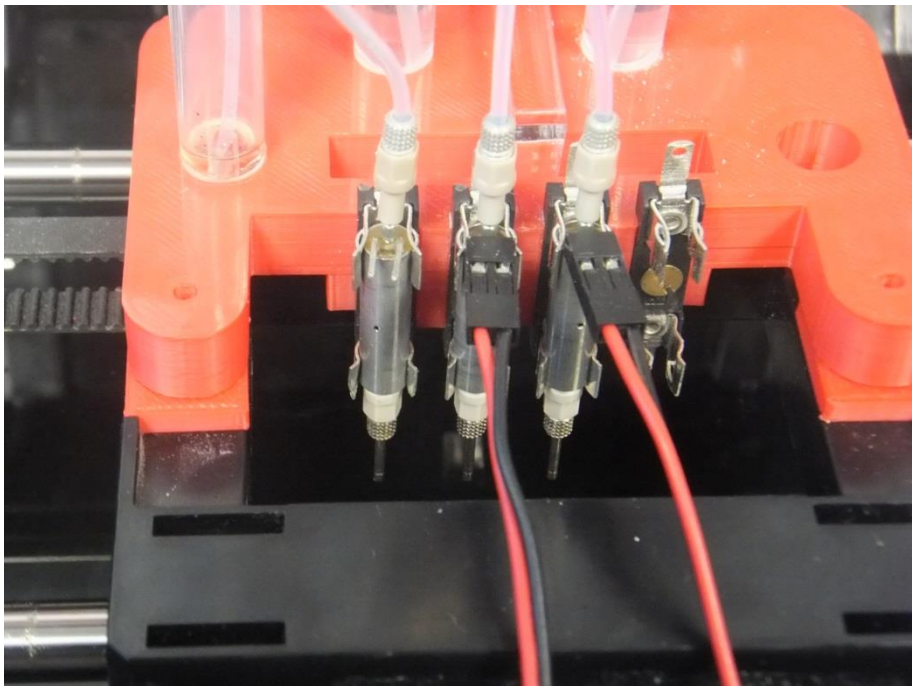

Figure 4.32 *– New quad-valve tool mount on the Mark III bioprinter*

Taking advantage of the new coiled pneumatic tubing, the hood for the Mark III bioprinter was designed to be much lower than the Mark II hood. This reduced the amount of acrylic required and made the Mark III bioprinter easier to transport, as it was slightly smaller.

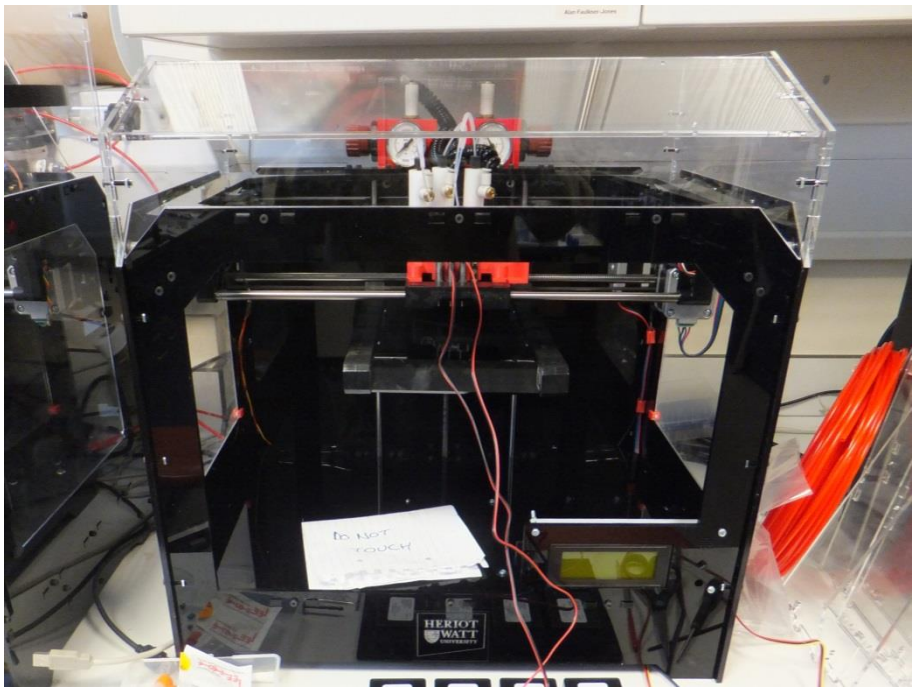

Figure 4.33 *– The Mark III bioprinter with side panels and lower profile hood*

New substrate trays were laser cut to suit the experiments carried out on the Mark III bioprinter – namely, 96-well plates and microscope slides. These substrate trays are interchangeable with the Mark II substrate trays as they use the same mounting holes. Again, the coordinates of salient reference positions were recorded for use when creating G-code programs to run on the bioprinter.

Figure 4.34 *– Interchangeable substrate trays*

4.5.4 Graphical User Interface Upgrades

With a few small modifications, the GUI for the Mark II could be used to create programs to run on the Mark III as well. An extra menu was added which allows the user to specify for which machine they are creating G-code programs. The GUI uses this to determine which style of G-code commands and which header and footer (in separate text files) to apply to the G-code program.

The multi-well plate tab that was adapted from the original GUI was replaced with a large plate mode that was similar to the small plate mode with buttons that represent each well on a plate. The large plate substrate tray can hold 1 large plate which can have a number of different well arrangements; a selection of popular options (1, 6, 96 & 384) are included allowing the user to specify which plate they are using.

In the small plate mode in the second generation GUI, when the user applied a set of droplet properties to a well, the button representing that well took the colour of the bio-ink component with the highest volume percentage of that well – green for valve 1, red for valve 2, blue for valve 3 and purple for valve 4. In this version of the GUI the colour applied to the buttons is defined by the ratio of the volumes of each bio-ink, with the valve 4 colour being replaced by white. Any colour can therefore be created using the red, green and blue percentages, and can be made lighter or darker given the percentage of white in that well. This is shown in Figure 4.35.

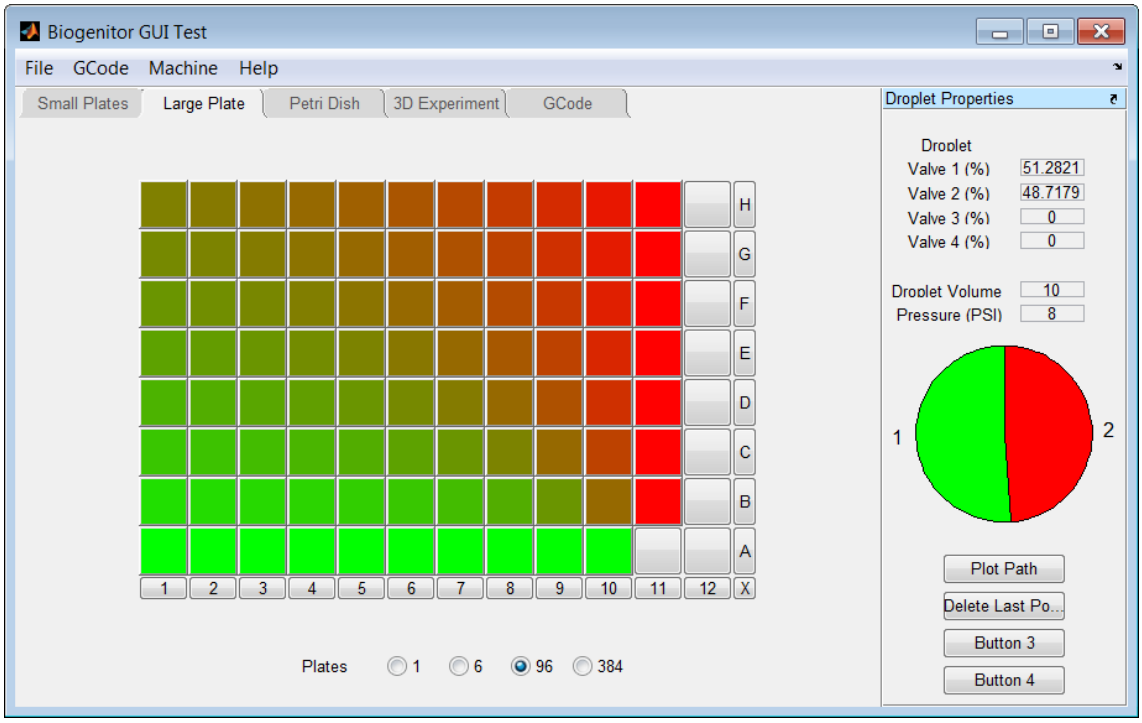

Figure 4.35 *– Graphical User Interface (GUI) program for the Mark III bioprinter in large plate mode showing the new average colour system to show droplet components*

4.5.5 Basic Interface Program

The Mark I bioprinter used a MATLAB algorithm to create G-code files from binary (black and white) images created in MS Paint. This was a very useful program for creating shapes from arrays of droplets printed onto Petri dishes and microscope slides. A refined version was created with added features which allowed users to specify the number of layers to dispense, which components to dispense, and the spacing between each pixel (to define a scale for the pattern). This new program was used for hydrogel printing and many of the simple geometric patterns were programmed using this algorithm.

4.6 References

[1] Pardo L, Wilson WC, and Boland T, (2003). "Characterization of Patterned Self-Assembled Monolayers and Protein Arrays Generated by the Ink-Jet Method †," *Langmuir*, **19**(5), pp. 1462–1466.

[2] Roth EA, Xu T, Das M, Gregory C, Hickman JJ, and Boland T, (2004). "Inkjet printing for high-throughput cell patterning," *Biomaterials*, **25**(17), pp. 3707–3715.

[3] Crump SS, (1992). "Apparatus and method for creating three-dimensional objects" Patent Number US5121329 A, June 9, 1992.

Chapter 5 – Response of Pluripotent Stem Cells to the Valve-based Bioprinting Process

5.1 Introduction

In the field of biofabrication, great advances are being made towards fabricating 3D tissue and whole organs with techniques utilising very fine spatial control of cell deposition. Rapid progress has been made in recent years in developing and testing printing techniques, including those based on laser pulses, inkjets and other – more novel – approaches. Laser based printing techniques are accurate and reliable but they are more suited to single cell deposition and could be prone to heating problems that can cause cell damage [1–8]. Inkjet printing techniques are inexpensive, easy to set up and potentially expandable but can suffer from clogging, shear forces leading to cell damage, and the bio-inks must be within a specific range of viscosity and surface tension [9–20]. Bio-extrusion techniques are able to create cell-laden 3D structures, but issues include nozzle-based disadvantages, the impossibility of printing discrete droplets within a reasonable range of volumes, and the bio-inks must be within a specific range of viscosity and surface tension [21–28]. Electrohydrodynamic Jet printing has the unique ability to create continuous streams as well as discrete droplets, but the droplet sizes and dispense location are not currently controllable [29–32]. Acoustic based printing techniques do not rely on nozzles to deliver the biological materials, preventing any clogging problems, but may have issues with overheating over longer printing sessions [33–36]. Valve-based printing techniques are one of the newest additions to this list and have the advantage of being one of the gentlest techniques for printing any number of cells, but – as with all other nozzle-based techniques – clogging is potentially an issue [37–40].

Although human mesenchymal stem cells (hMSCs) [41] and mouse embryonic stem cells (mESCs) [42] have been printed in the past, until now there have been no reports of attempts to print human embryonic stem cells (hESCs) or induced pluripotent stem cells (iPSCs). hESCs are known to be more sensitive to physical manipulation, more demanding in terms of their requirement for extracellular matrix coatings for routine cell culture, and are more difficult to transfect with plasmid DNA. However, they do have a greater potential to generate a wider variety of differentiated cell types than hMSCs, and tissues generated using iPSCs would be expected to yield better models of

human biology than those using mESCs as precursors. Here is the report of the first investigation into the response of hESCs and iPSCs to the bioprinting process.

5.2 Project Acknowledgements

The project was performed in collaboration with Jason King, John Gardner, Catherine Fyfe and Helen Bradburn from Roslin Cellab. Human Embryonic Kidney cells (line 293), Human Embryonic Stem cells (lines RC-6 and RC-10) and Human Induced Pluripotent Stem cells (line RCi-22) were provided at various concentrations. All cell culturing was provided by them, in addition to the various different cell media types used in the following experiments.

5.3 Preliminary Testing Results

In order to test the basic functionality of the system, a series of tests were performed using water. Water was used instead of cells in solution because it acts in much the same way and is much easier to work with. A number of experiments were devised and conducted to test the functionality of the cell printer in different ways, including spatial and droplet size repeatability, scope of possible droplet sizes and speed of printing. Each experiment is described in detail; the results are here presented and discussed.

5.3.1 Characterisation of Droplet Size

The first study was an investigation into the possible range of droplet sizes that could be dispensed by the cell printer, with a particular emphasis on determining the size of the smallest possible droplet. The volume of dispensed fluid is affected by several factors: the properties of the fluid (i.e. viscosity, surface tension, etc.); the diameter of the nozzle orifice; the valve on-time; and the inlet pressure. As water is being used as a substitute for cells in suspension for this preliminary study, the fluid properties are constant. The orifice of the nozzle was chosen to be the smallest available (0.0508 mm). The valve on-time was set at the smallest period of time that the hardware was rated to handle (0.3 ms); in this setup, the valve controller is the slowest component. This leaves the inlet pressure as the only remaining variable that can affect the volume of dispensed fluid. An experiment was therefore devised where the inlet pressure applied to the static pressure reservoir was set at a high value and slowly decreased, with several droplets deposited at each pressure.

Altering the inlet pressure applied to the static pressure reservoir is one method for varying the droplet sizes. However, if several different sized droplets were required in the same experiment, there would be insufficient time to alter the inlet pressure for each droplet. Therefore, another means of quickly altering the droplet sizes was required. One approach would be simplicity itself: overprinting existing droplets until they were of sufficient size, but what if there was another way? As stated at the beginning of this section, the valve on-time also affected the volume of dispensed fluid and, apart from the inlet pressure, it is the only variable remaining that is not fixed by the properties of the bio-ink or the dimensions of the nozzle. A second experiment was devised where the valve on-time was set at a small value and gradually increased, with a single droplet deposited at each separate on-time.

Measuring the volume of a single droplet directly would be quite challenging and would require recording images of the droplet from multiple angles and estimating the diameter, height and contact angle of the printed droplet, or alternatively using a high-speed camera to capture an image of the droplet before it impacted the substrate and measuring the volume from the mean diameter. A far simpler approach was adopted; the volume of the droplets was calculated from their weight and the density of the water. 10,000 droplets were deposited onto a precision micro scale (Adventurer Pro AV812, Ohaus Co) at each pressure/pulse duration combination and the weights were recorded. The volumes were calculated using the following formula:

$$Volume\ of\ 1\ droplet\ (nL) = \frac{weight\ of\ N\ droplets\ (g) \times 1.09 \times 10^6}{N} \quad (5.1)$$

The results are shown in Figure 5.1 and Figure 5.2.

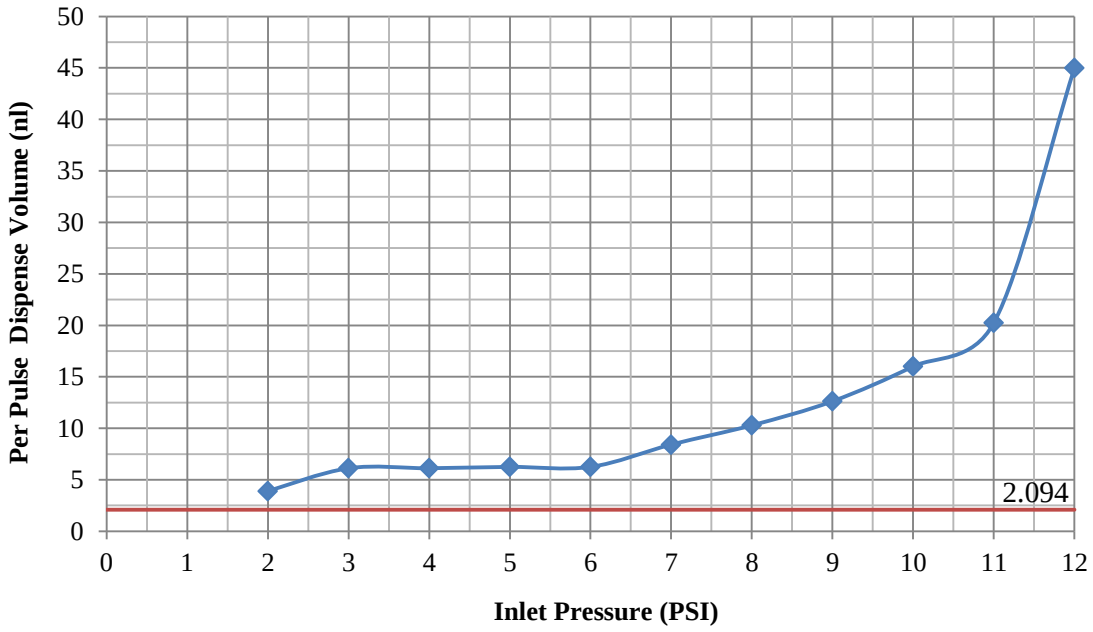

Figure 5.1 *– The results from the investigation into the relationship between inlet pressure and droplet volume*

The smallest possible droplet produced during this investigation was 2.094 nL. Due to the relationship between the inlet pressure and droplet volume, setting the inlet pressure at a particular value would be a quick way of fixing the minimum or modal droplet size for a particular application. This means that when the water is exchanged for cells in suspension the maximum number of cells that are deposited in a single droplet will be controllable.

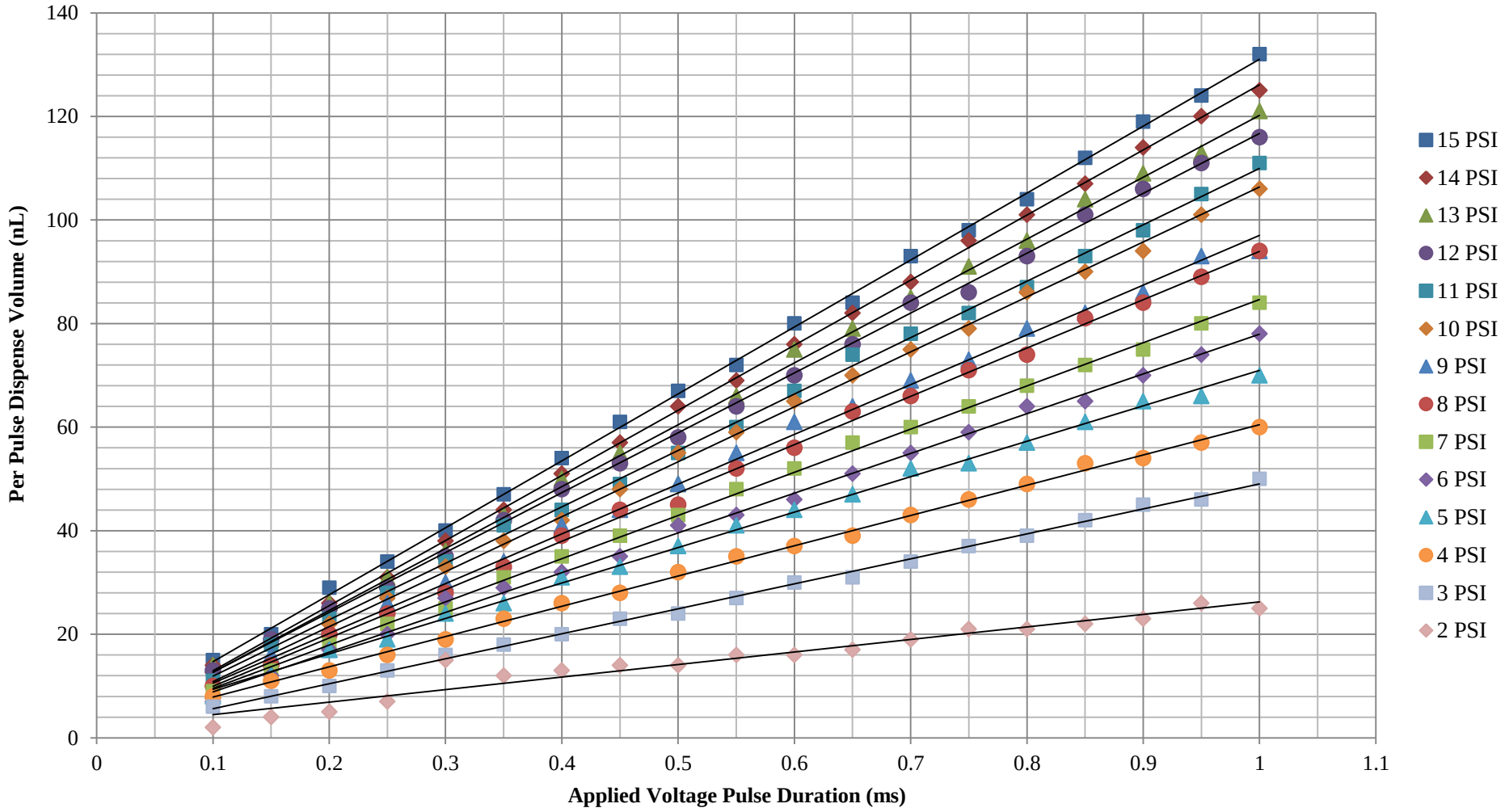

Figure 5.2 *– The results from the investigation into the relationship between inlet pressure, applied voltage pulse duration and droplet volume*

The relationship between the applied voltage pulse duration and the dispensed volume for each pressure is clearly linear but the relationship between each line is slightly more complex. The bioprinter is controlled via a graphical user interface which allows users to specify the position and properties of droplets in an array. This program calculates the required settings for each droplet using the following equation which was derived from the experimental data and describes the relationship between the inlet pressure, valve time and droplet volume:

$$t_{valve} = \frac{V_{droplet} + 1.202}{35.507 \times (\ln(P) - 0.240)} \tag{5.2}$$

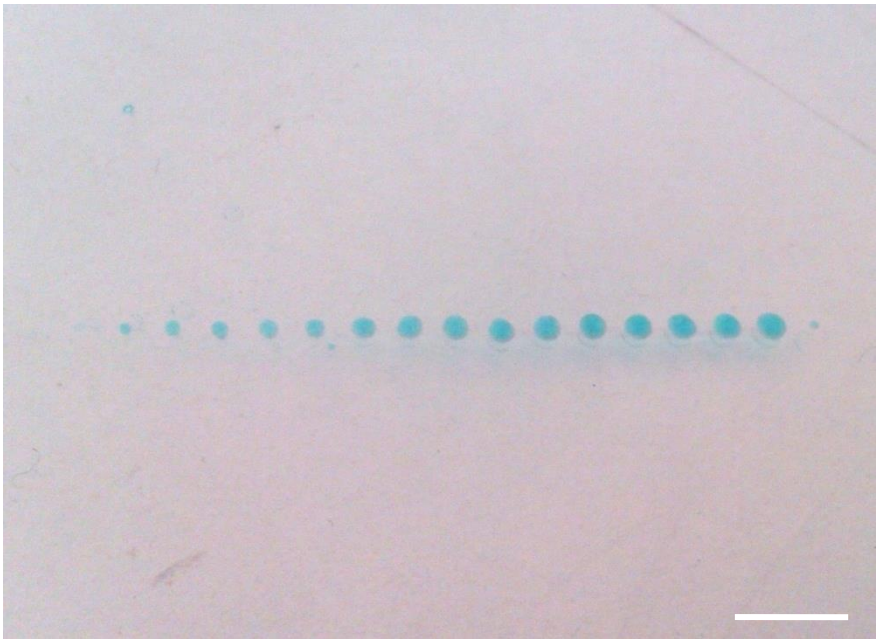

Figure 5.3 *– Dispensed droplets of varying sizes (scale bar 5 mm)*

5.3.2 Positional Repeatability

The next study was an investigation into the positional repeatability of the cell printer – in other words, was the cell printer accurate enough to allow us to return to a previous location specified by the same coordinates without drifting either in the x-direction, y-direction, or both? The CNC machine is largely responsible for the positional repeatability, but it could be affected by the lower spatial accuracy of the inkjet-based droplet deposition system. It is extremely important that the cell printer be capable of positional repeatability in order to allow printing of precise patterns and the overprinting of droplets. Overprinting droplets would be an extremely useful feature of the cell printer as it would allow other biological materials to be transfected into

dispensed cells or materials, such as oil to cover the droplets to prevent evaporation of the medium. Therefore, an experiment was devised where the cell printer was instructed to print at four locations in a repeating square grid pattern as shown at the top of Figure 5.4.

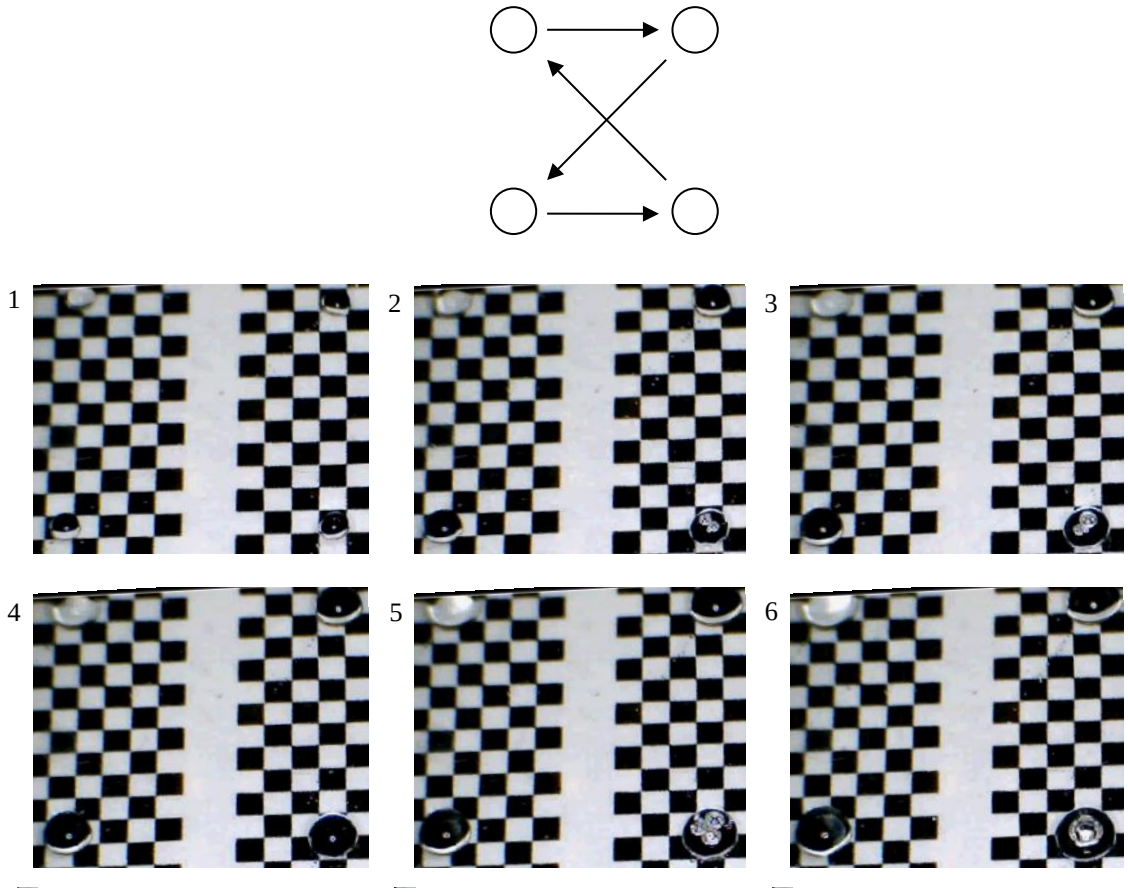

Figure 5.4 *– The results from the investigation into spatial repeatability. Top: grid pattern. Bottom: snapshots from the printing process, one taken after every pass through the grid*

This demonstrates that the cell printer has high spatial accuracy and is capable of returning to previous locations using the same coordinates. By factoring in the linear offset between the two nozzles, droplets can be overprinted, using either different materials (as mentioned above) or the same material to increase the concentration.

5.3.3 Complex Grid Printing

The next logical step would be to increase the complexity of the grid pattern to be printed. A low resolution image of the Heriot-Watt University logo was created in MS Paint with black pixels representing the dispense points. Blue food colouring was added to the water in the bio-ink reservoir to improve the visibility of the printed

droplets. A G-code file was created from the image using the dedicated MATLAB algorithm and fed into the bioprinter; the results are shown in Figure 5.5.

Figure 5.5 *– An array of droplets printed in the form of the Heriot-Watt University Logo*

This proves that not only can the cell printer print a small repeating pattern, but it can also print a large and complex pattern without drifting in either direction. An added advantage of this particular experiment was that due to its large size, there was time to measure the response time of the control software and decrease the built-in pauses for dispensing, thus speeding up the system. Unfortunately, printing such large arrays takes a relatively long time (tens of minutes) so by the time the last droplet has been printed, the first few had evaporated. This would easily be solved by printing onto a wet substrate coated with a cell culture medium such as fibrin, soy agar gel or collagen.

5.3.4 Sterility Testing

Some of the experiments conducted using the Mark II bioprinter used cells that were very expensive to produce, so it was important to ensure that not only would these cells be unaffected by the printing process, but also that no contamination entered the system which could affect the results. The Mark II system was therefore transferred to Roslin Cellab and tested for sterility. The deposition system was cleaned out with a 2% solution of Presept (Johnson and Johnson Medical) and left to stand for 30 minutes, then cleaned with a 70% solution of Ethanol and water (all micro-filtered), before bacteria-feeding broth was finally printed into the wells of a 96-well plate for testing.

The plate was examined 21 days post-printing and there was no evidence of microbial contamination present; the system was therefore deemed sterile. As the Mark II and Mark III bioprinters both share the same deposition system setup they are both sterilisable.

5.4 HEK293 Viability

The HEK293 cell line was named for Frank Graham, a scientist at a lab at the University of Leiden, who invented the calcium phosphate method for transfecting cells in 1977; it was named as such because it was Graham's 293rd experiment. The popularity of this particular cell line is due to its extreme transfectability by various techniques, including the calcium phosphate method [43].

A frozen sample of HEK293 cells (293FT, Life Technologies) was thawed out, suspended in high glucose Dulbecco's Modified Eagle Medium: Nutrient Mixture F-12 (DMEM / F-12) (Life Technologies) and centrifuged at 300 rpm for 2 minutes to separate the large clumps of cells. The medium was removed and the cells were re-suspended in fresh medium; by pipetting the solution up and down multiple times, the cells were separated into single cells. The suspended cells were then transferred to a T25 flask. When observed under a microscope the cells were observed to be circular with "hands" and therefore healthy. The flask was then placed inside an incubator at 36.0-37.5°C, 5.0±0.5% CO_2.

A single cell suspension of HEK293 cells at a concentration of approximately 1×10^5 cells/mL in DMEM was loaded into the cell printer and primed. Droplets were dispensed into a Petri dish and a control was created in a second Petri dish; Trypan Blue was applied to both dishes before being examined under the microscope. 10 random sample images were taken for both the printed and control groups and the number of live cells and dead cells were counted in each image. The results of this study are shown in Figure 5.6.

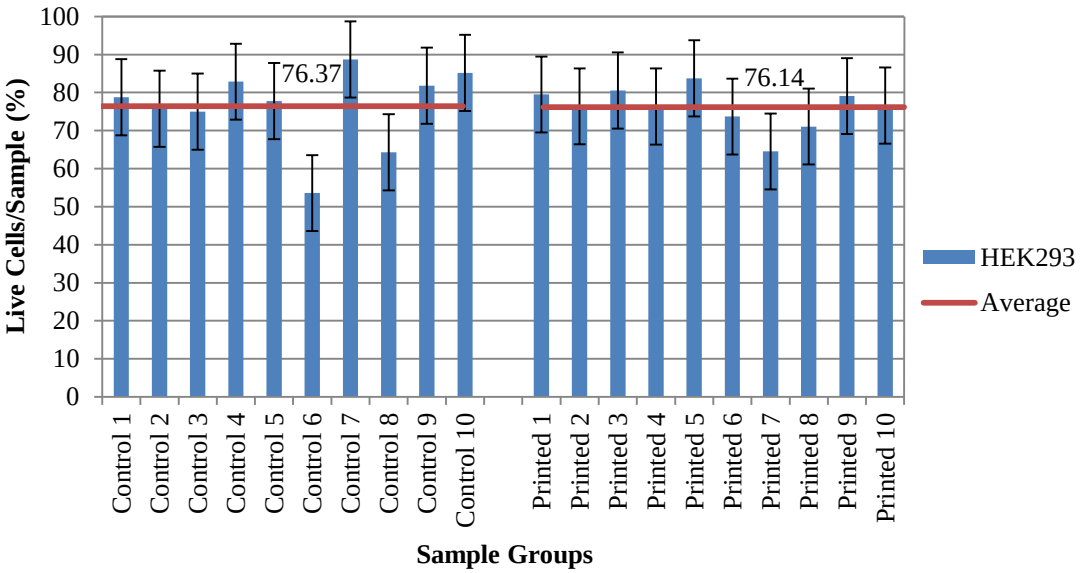

Figure 5.6 *– A graph to show the percentages of live cells per sample.*

The normalised cell viability was calculated to be >99% for the Mark I valve-based cell printer. This confirms that this printing process did not appear to damage the cells or affect the viability of the vast majority of dispensed cells.

5.5 hESCs and hiPSCs

5.5.1 Cell Culture

Human embryonic stem cell lines RC-6 and RC-10 were cultured in complete StemPro® hESC SFM (supplement, DMEM/F-12, BSA, FGF basic, and 2-mercaptoethanol) (Life Technologies) supplemented with 8 ng/mL of human basic fibroblast growth factor (hbFGF). Human induced pluripotent stem cells line RCi-22 were cultured on Geltrex matrix with Essential 8 medium (Life Technologies). Cells were stored in an incubator at 36.0-37.5°C, 5.0±0.5% CO_2. Under these conditions, the cells are maintained in an undifferentiated state.

5.5.2 hESC Viability

Human ES cells (line RC-10) were suspended in StemPro® hESC SFM to a concentration of approximately 1×10^6 cells/mL and loaded into the reservoir of one of the cell deposition systems. A program was written that dispensed approximately 1 mL of bio-ink (the volume varied with pressure); this large volume was required to allow for analysis to be carried out on a FACS machine. Different experiments sometimes require different experimental variables such as applied pressure and nozzle geometry.

Two main types of nozzle have been used for the experiments in this thesis: a shorter, thick-walled nozzle; and a longer, thin-walled nozzle. Since such a large volume was required for each pressure/nozzle combination, only 6 different pressures were used to limit the number of cells required for this experiment. Cells were printed into micro-centrifuge tubes and the unprinted cells were used as a viability control.

The printed samples were examined using a BD FACSCalibur flow cytometer at approximately 30 minutes post printing. The control sample was split in two; half were stained and used to calibrate the data thresholds. The raw data plots and a graph of the results are shown in Figure 5.7 and Figure 5.8 respectively.

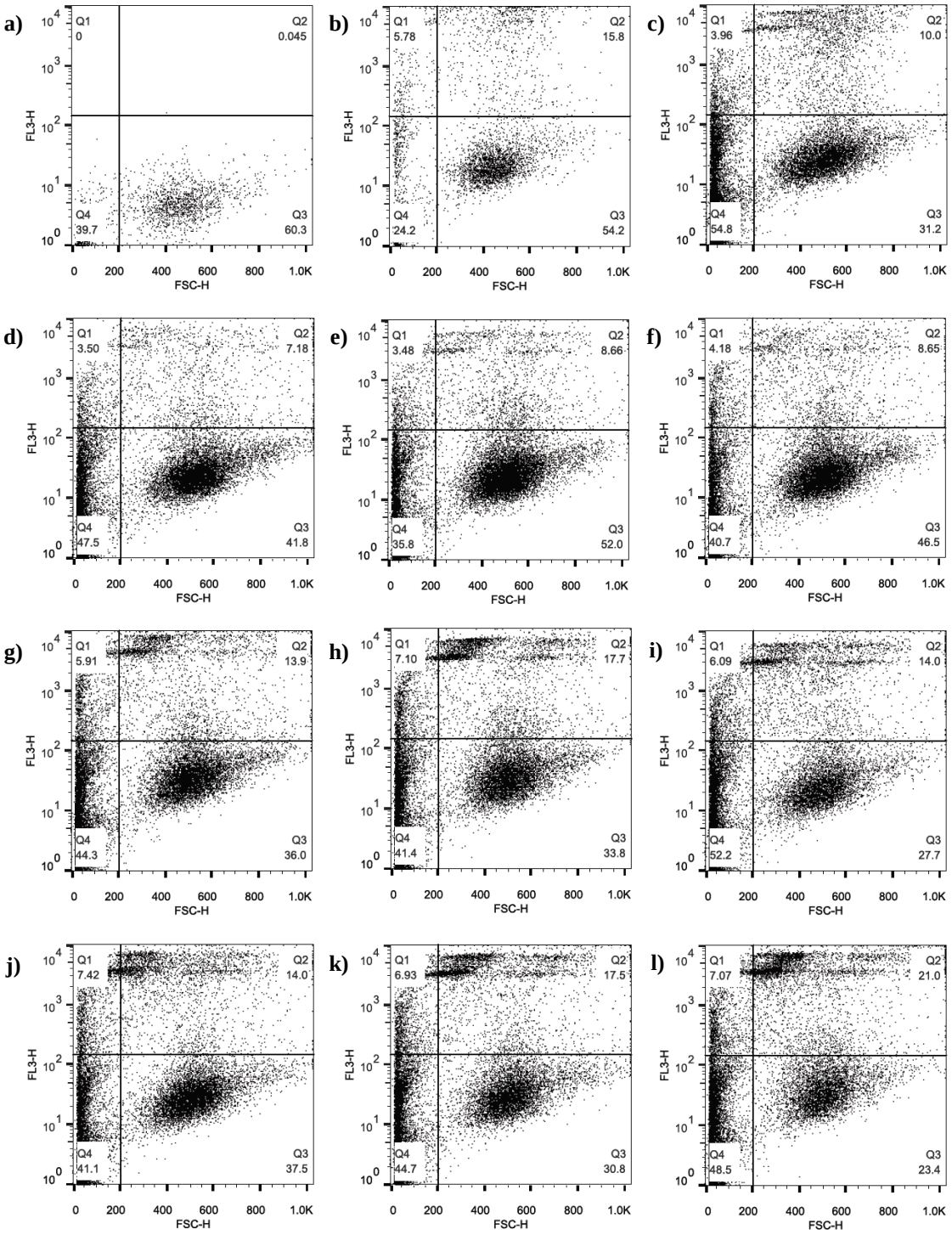

Figure 5.7 *– Raw FACS data plots showing the numbers of live hESCs per sample: a-b) controls: a) unstained control; b) stained control; c-h) short nozzle: c) 2PSI; d) 4 PSI; e) 7 PSI; f) 10 PSI; g) 15 PSI; h) 20 PSI; i-l) long nozzle: i) 7 PSI; j) 10 PSI; k) 15 PSI; l) 20 PSI*

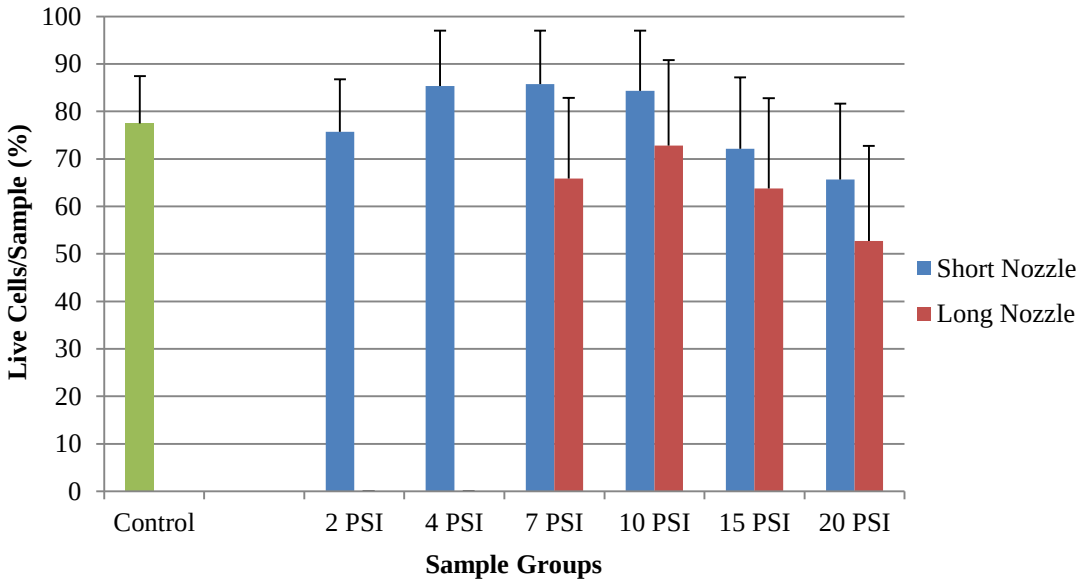

Figure 5.8 *– A graph of the FACS data to show the percentages of live hESCs per sample as a function of pressure and nozzle length*

Cell viability was calculated to be >84% for the short nozzle and >68% for the long nozzle over all pressures. This clearly shows that the viability of the cells is affected by the length of the nozzle used; this is most likely due to the increased time the cells are subject to shear forces experienced by the cells on their transit through the nozzle. However, cell viability remains high with the shorter nozzle at pressures below 15 PSI even for sensitive cells such as hESCs, which is consistent with the observations of other groups with stem cells [42,44] and other cell types using similar bioprinting approaches [37–40].

It should be noted that the viability immediately post printing is believed to be higher than the results presented here; the lower results can be attributed to the time delay between the printing and analysis of the cells and the fact that the FACS machine was not in the same location as the printing took place (it was some 15 minutes away by car). Initially, the plan was to use the FACS machine on site but it was found to be out of order so an alternative had to be used.

5.5.3 hiPSC and hESC Viability

Human iPS cells (line RCi-22) viability was measured in much the same way as the hESC viability, but without a variation in nozzle geometry or pressures. The printed samples were examined using the FACS machine.

The raw data plots and a graph of the results are shown in Figure 5.9 and Figure 5.10 respectively.

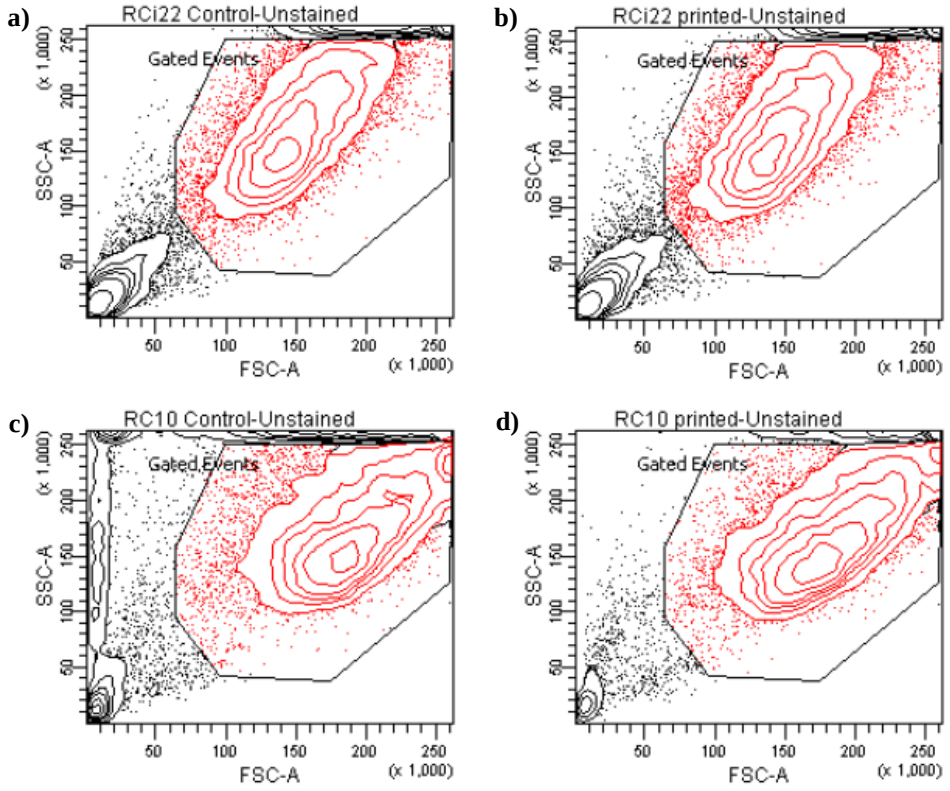

Figure 5.9 *– FACS data plots showing the numbers of live hiPSCs per sample with numbers of hESCs per sample for comparison: (a-b) hiPSC: a) control; b) printed cells; (c-d) hESC: c) control; d) printed cells*

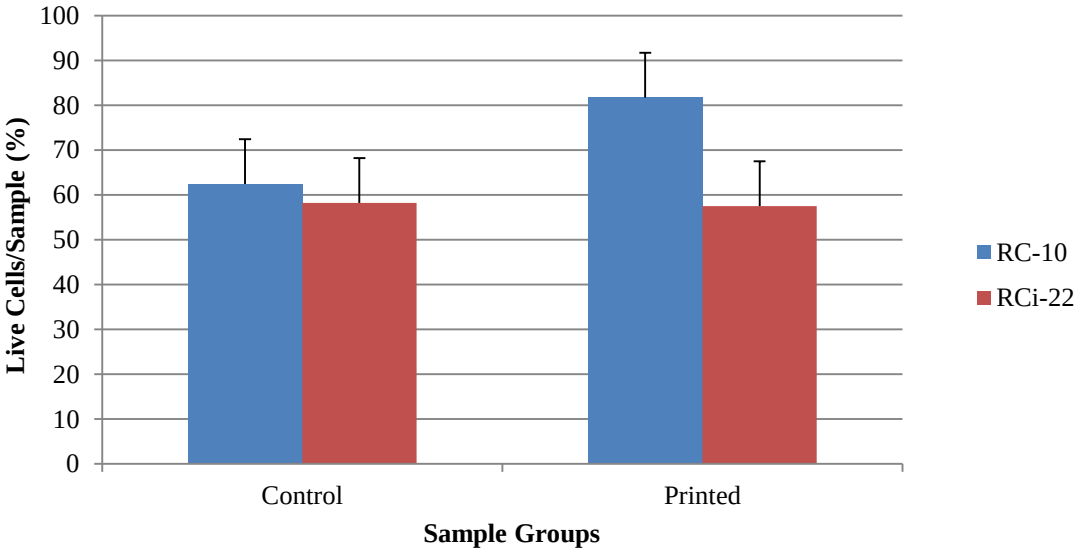

Figure 5.10 *– A graph to show the percentages of live hiPSCs per sample with hESC data for comparison*

There is negligible difference in terms of viability between the printed and non-printed hiPSCs, proving that our valve-based printing technology is compatible with hiPSC transfer without negatively affecting the viability of these fragile cells.

5.5.4 Multi-marker Pluripotency Validation

It is not sufficient to confirm only the post-printing viability of pluripotent stem cells; the printed cells should remain pluripotent in order to confirm that they are completely unaffected by the printing process. The printed cells were examined to check that they still possessed two of the most common pluripotency markers: Oct3/4 and SSEA-4. SSEA-1 (stage-specific embryonic antigen 1) was used as a negative test as it should only be expressed in differentiated cells.

Two lines of hESCs and one line of hiPSCs were tested for these markers – lines RC-6, RC-10 and RCi-22 – and cells were examined one week after printing using flow cytometry.

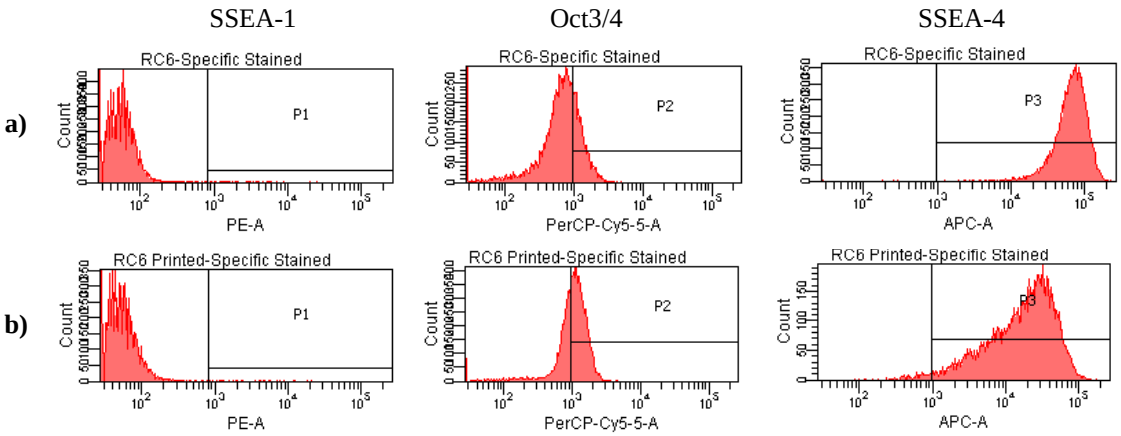

Figure 5.11 *– FACS results of multi-marker pluripotency validation: a) hESC line RC-6 non-printed control; b) hESC line RC-6 printed results*

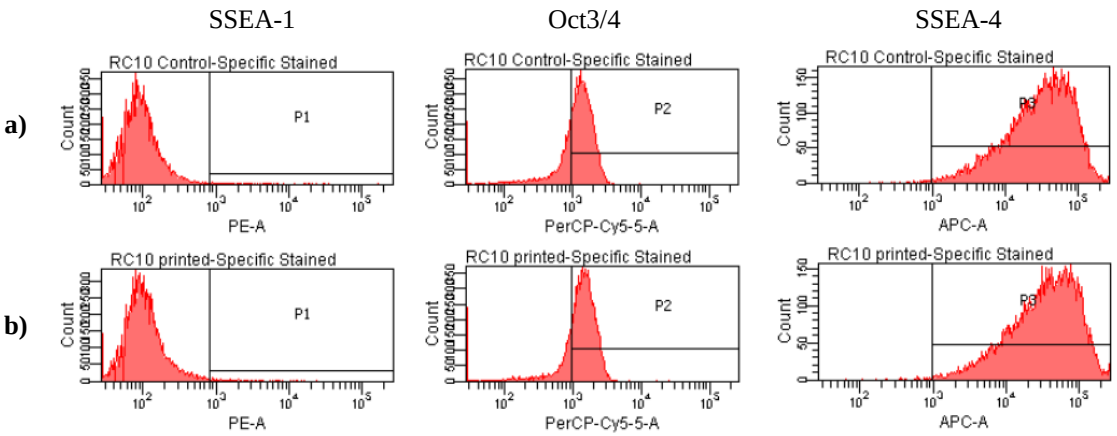

Figure 5.12 *– FACS results of multi-marker pluripotency validation: a) hESC line RC-10 non-printed control; b) hESC line RC-10 printed results*

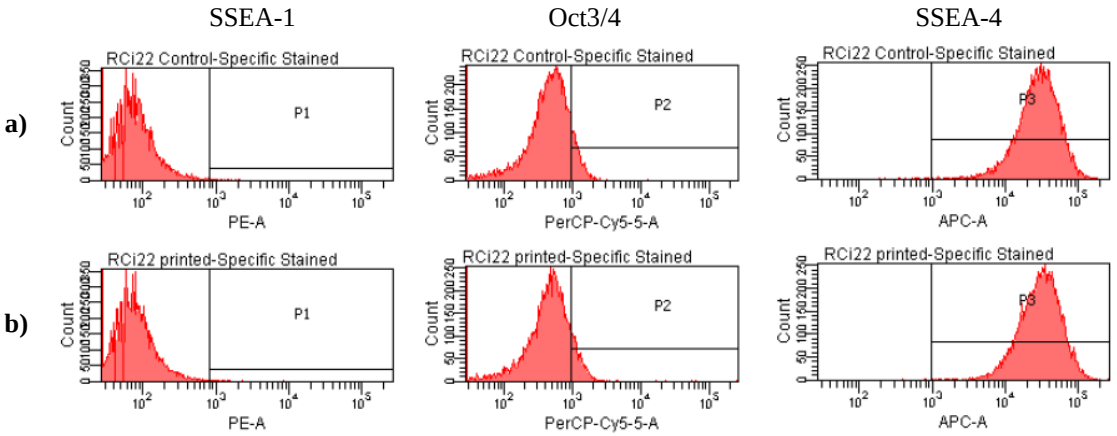

Figure 5.13 *– FACS results of multi-marker pluripotency validation: a) hiPSC line RCi-22 non-printed control; b) hiPSC line RCi-22 printed results*

At one week post-printing there is very little observable difference between the printed cells and the non-printed control, confirming that all the tested human pluripotent stem cells remain pluripotent. The Oct3/4 marker levels are lower than the normal range for pluripotency in the printed RC-10 and RCi-22, though still acceptable; in the case of the RC-10 sample, the gating may not be tight enough. In the RCi-22 sample the control exhibits a similar marker level. Also, the RC-6 SSEA-4 printed result is lower than the control, but the results are still positive as they are within an acceptable range.

5.6 Characterisation of Droplet Cell Concentration

The number of cells encapsulated within a single droplet can be controlled by changing the droplet size (by altering the parameters as previously discussed) or the initial concentration of cells in the bio-ink. The cell size also plays a part in determining cell

concentrations; the larger the cell, the smaller the number of cells that can be encapsulated within a droplet of a fixed size.

An array of the Heriot-Watt University logo was designed and 10 mL of StemPro® hESC SFM with RC-10 hESCs, suspended at a concentration of 5×10^6 cells/mL, was loaded into the reservoir of one of the cell deposition systems. 2 µL of DAPI (4′, 6-Diamidino-2-Phenylindole, Dihydrochloride) (Life Technologies) was added in order to fluorescently label the cell nuclei. The printing process was then performed and cell numbers were obtained by viewing the droplets under the microscope (fl0015000m Trinocular Fluorescence Microscopes) immediately after printing. Fluorescence images of the whole array were recorded using a 2D gel imager (ChemiDoc™, Bio-Rad Laboratories, Inc.).

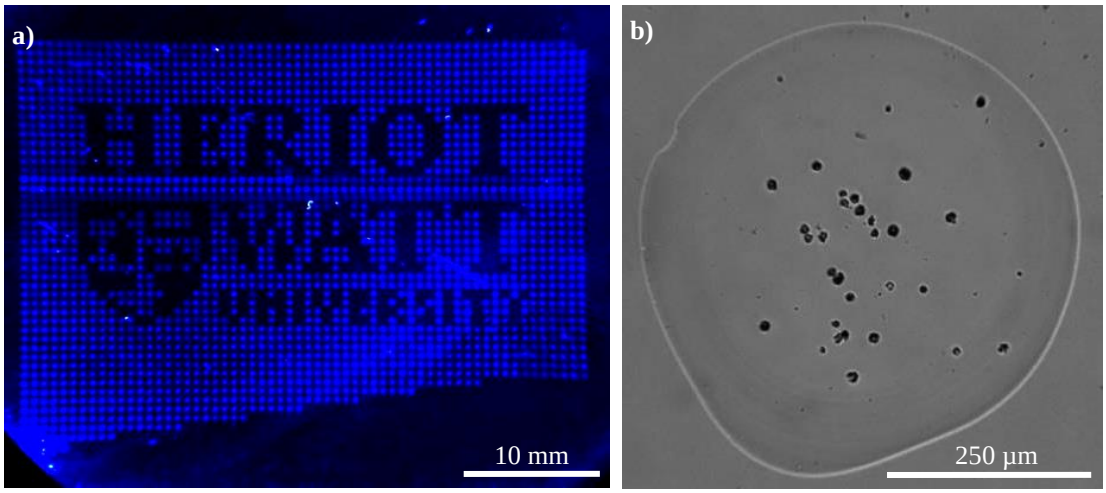

Figure 5.14 *– a) Fluorescence image of an array of Human Embryonic Stem cell droplets printed in the form of the Heriot-Watt University Logo; b) optical image of a single droplet showing the RC-10 cells.*

Each droplet was ~60 nL and it appears that around 28 RC-10 cells were transferred per printed droplet of solution. However, as the number of cells transferred per droplet is mainly determined by the concentration of cells in the bio-ink and the ratio of droplet size to cell size, these results can be altered by adjusting the droplet sizes or cell concentration.

5.7 Conclusions

Using the valve-based bioprinter the first investigation into the response of iPSCs to the printing process was undertaken and a deeper analysis of the response of hESCs including viability and pluripotency validation was made. This work demonstrates that

the valve-based printing process is gentle enough to maintain hESC and hiPSC viability and that printed cells maintain their pluripotency. The effect of nozzle geometry was investigated and the effects of nozzle length on the post-printing viability of cells were recorded; longer nozzles lower the post-printing viability of the cells. The ability to print human pluripotent stem cells (both hESCs and hiPSCs) while maintaining their pluripotency will allow us to create more accurate human tissue models, which is essential to the *in vitro* drug development and toxicity testing. Additionally, this may also lay the foundations for human stem cells to be incorporated into clinical protocols, either for patient implantation of *in vitro* regenerated organs or direct *in vivo* cell printing for tissue regeneration.

5.8 References

[1] Chrisey DB, Pique A, Fitz-Gerald J, Auyeung RCY, McGill RA, Wu HD, and Duignan M, (2000). "New approach to laser direct writing active and passive mesoscopic circuit elements," *Applied Surface Science*, **154**, pp. 593–600.

[2] Schiele NR, Corr DT, Huang Y, Raof NA, Xie Y, and Chrisey DB, (2010). "Laser-based direct-write techniques for cell printing," *Biofabrication*, **2**(3), p. 032001.

[3] Barron JA, Ringeisen BR, Kim H, Spargo BJ, and Chrisey DB, (2004). "Application of laser printing to mammalian cells," *Thin Solid Films*, **453-454**, pp. 383–387.

[4] Barron JA, Spargo BJ, and Ringeisen BR, (2004). "Biological laser printing of three dimensional cellular structures," *Applied Physics A*, **79**, pp. 1027–1030.

[5] Barron JA, Wu P, Ladouceur HD, and Ringeisen BR, (2004). "Biological laser printing: a novel technique for creating heterogeneous 3-dimensional cell patterns," *Biomedical microdevices*, **6**(2), pp. 139–147.

[6] Guillotin B, Souquet A, Catros S, Duocastella M, Pippenger B, Bellance S, Bareille R, Rémy M, Bordenave L, Amédée J, and Guillemot F, (2010). "Laser assisted bioprinting of engineered tissue with high cell density and microscale organization," *Biomaterials*, **31**(28), pp. 7250–7256.

[7] Duocastella M, Colina M, Fernández-Pradas JM, Serra P, and Morenza JL, (2007). "Study of the laser-induced forward transfer of liquids for laser bioprinting," *Applied Surface Science*, **253**(19), pp. 7855–7859.

[8] Barron JA, Rosen R, Jones-Meehan J, Spargo BJ, Belkin S, and Ringeisen BR, (2004). "Biological laser printing of genetically modified Escherichia coli for biosensor applications," *Biosensors and Bioelectronics*, **20**(2), pp. 246–252.

[9] Wilson WC, and Boland T, (2003). "Cell and organ printing 1: Protein and cell printers," *The Anatomical Record*, **272A**(2), pp. 491–496.

[10] Xu T, Jin J, Gregory C, Hickman JJ, and Boland T, (2005). "Inkjet printing of viable mammalian cells," *Biomaterials*, **26**(1), pp. 93–99.

[11] Roth EA, Xu T, Das M, Gregory C, Hickman JJ, and Boland T, (2004). "Inkjet printing for high-throughput cell patterning," *Biomaterials*, **25**(17), pp. 3707–3715.

[12] Campbell PG, and Weiss LE, (2007). "Tissue engineering with the aid of inkjet printers," *Expert opinion on biological therapy*, **7**(8), pp. 1123–1127.

[13] Pardo L, Wilson WC, and Boland T, (2003). "Characterization of Patterned Self-Assembled Monolayers and Protein Arrays Generated by the Ink-Jet Method †," *Langmuir*, **19**(5), pp. 1462–1466.

[14] Boland T, Mironov V, Gutowska A, Roth EA, and Markwald RR, (2003). "Cell and organ printing 2: Fusion of cell aggregates in three-dimensional gels," *The Anatomical Record*, **272A**(2), pp. 497–502.

[15] Kamisuki S, Hagata T, Tezuka C, Nose Y, Fujii M, and Atobe M, (1998). "A low power, small, electrostatically-driven commercial inkjet head," Micro Electro Mechanical Systems, 1998. MEMS 98. Proceedings., The Eleventh Annual International Workshop on, IEEE, pp. 63–68.

[16] Murata K, (2003). "Super-fine ink-jet printing for nanotechnology," MEMS, NANO and Smart Systems, 2003. Proceedings. International Conference on, IEEE, pp. 346–349.

[17] Calvert P, (2001). "Inkjet Printing for Materials and Devices," *Chemistry of Materials*, **13**(10), pp. 3299–3305.

[18] Guillotin B, and Guillemot F, (2011). "Cell patterning technologies for organotypic tissue fabrication," *Trends in Biotechnology*, **29**(4), pp. 183–190.

[19] Le HP, (1998). "Progress and Trends in Ink-jet Printing Technology," *Journal of Imaging Science and Technology*, **42**(1), pp. 49–62.

[20] Delaney JT, Smith PJ, and Schubert US, (2009). "Inkjet printing of proteins," *Soft Matter*, **5**(24), pp. 4866–4877.

[21] Vozzi G, Previti A, De Rossi D, and Ahluwalia A, (2002). "Microsyringe-Based Deposition of Two-Dimensional and Three-Dimensional Polymer Scaffolds with a Well-Defined Geometry for Application to Tissue Engineering," *Tissue Engineering*, **8**(6), pp. 1089–1098.

[22] Chung JHY, Naficy S, Yue Z, Kapsa R, Quigley A, Moulton SE, and Wallace GG, (2013). "Bio-ink properties and printability for extrusion printing living cells," *Biomater. Sci.*, **1**(7), pp. 763–773.

[23] Cohen DL, Malone E, Lipson HOD, and Bonassar LJ, (2006). "Direct freeform fabrication of seeded hydrogels in arbitrary geometries," *Tissue engineering*, **12**(5), pp. 1325–1335.

[24] Yan Y, Wang X, Xiong Z, Liu H, Liu F, Lin F, Wu R, Zhang R, and Lu Q, (2005). "Direct Construction of a Three-dimensional Structure with Cells and Hydrogel," *Journal of Bioactive and Compatible Polymers*, **20**(3), pp. 259–269.

[25] Norotte C, Marga FS, Niklason LE, and Forgacs G, (2009). "Scaffold-free vascular tissue engineering using bioprinting," *Biomaterials*, **30**(30), pp. 5910–5917.

[26] Shim J-H, Lee J-S, Kim JY, and Cho D-W, (2012). "Bioprinting of a mechanically enhanced three-dimensional dual cell-laden construct for osteochondral tissue engineering using a multi-head tissue/organ building system," *Journal of Micromechanics and Microengineering*, **22**(8), p. 085014.

[27] Nair K, Gandhi M, Khalil S, Yan KC, Marcolongo M, Barbee K, and Sun W, (2009). "Characterization of cell viability during bioprinting processes," *Biotechnology Journal*, **4**(8), pp. 1168–1177.

[28] Melchels FPW, Domingos MAN, Klein TJ, Malda J, Bartolo PJ, and Hutmacher DW, (2012). "Additive manufacturing of tissues and organs," *Progress in Polymer Science*, **37**(8), pp. 1079–1104.

[29] Park J-U, Hardy M, Kang SJ, Barton K, Adair K, Mukhopadhyay DK, Lee CY, Strano MS, Alleyne AG, Georgiadis JG, Ferreira PM, and Rogers JA, (2007). "High-resolution electrohydrodynamic jet printing," *Nature Materials*, **6**(10), pp. 782–789.

[30] Eagles PAM, Qureshi AN, and Jayasinghe SN, (2006). "Electrohydrodynamic jetting of mouse neuronal cells," *Biochemical Journal*, **394**(2), pp. 375–378.

[31] Jayasinghe SN, Qureshi AN, and Eagles PAM, (2006). "Electrohydrodynamic Jet Processing: An Advanced Electric-Field-Driven Jetting Phenomenon for Processing Living Cells," *Small*, **2**(2), pp. 216–219.

[32] Townsend-Nicholson A, and Jayasinghe SN, (2006). "Cell electrospinning: a unique biotechnique for encapsulating living organisms for generating active biological microthreads/scaffolds," *Biomacromolecules*, **7**(12), pp. 3364–3369.

[33] Ellson R, Mutz M, Browning B, Lee Jr. L, Miller MF, and Papen R, (2003). "Transfer of low nanoliter volumes between microplates using focused acoustics - automation considerations," *Journal of the Association for Laboratory Automation*, **8**(5), pp. 29–34.

[34] Elrod SA, Hadimioglu B, Khuri-Yakub BT, Rawson EG, Richley E, Quate CF, Mansour NN, and Lundgren TS, (1989). "Nozzleless droplet formation with focused acoustic beams," *Journal of applied physics*, **65**(9), pp. 3441–3447.

[35] Demirci U, and Montesano G, (2007). "Single cell epitaxy by acoustic picolitre droplets," *Lab on a Chip*, **7**(9), pp. 1139–1145.

[36] Demirci U, (2006). "Acoustic Picoliter Droplets for Emerging Applications in Semiconductor Industry and Biotechnology," *Journal of Microelectromechanical Systems*, **15**(4), pp. 957–966.

[37] Moon S, Lin P-A, Keles HO, Yoo S-S, and Demirci U, (2007). "Cell Encapsulation by Droplets," *J Vis Exp*, **8**.

[38] Demirci U, and Montesano G, (2007). "Cell encapsulating droplet vitrification," *Lab on a Chip*, **7**(11), p. 14281433.

[39] Xu F, Emre AE, Turali ES, Hasan SK, Moon S, Nagatomi J, Khademhosseini A, and Demirci U, (2009). "Cell proliferation in bioprinted cell-laden collagen droplets," Bioengineering Conference, 2009 IEEE 35th Annual Northeast, IEEE, pp. 1–2.

[40] Xu F, Celli J, Rizvi I, Moon S, Hasan T, and Demirci U, (2011). "A three-dimensional in vitro ovarian cancer coculture model using a high-throughput cell patterning platform," *Biotechnology Journal*, **6**(2), pp. 204–212.

[41] Koch L, Kuhn S, Sorg H, Gruene M, Schlie S, Gaebel R, Polchow B, Reimers K, Stoelting S, and Ma N, (2009). "Laser printing of skin cells and human stem cells," *Tissue Engineering Part C: Methods*, **16**(5), pp. 847–854.

[42] Xu F, Sridharan B, Wang S, Gurkan UA, Syverud B, and Demirci U, (2011). "Embryonic stem cell bioprinting for uniform and controlled size embryoid body formation," *Biomicrofluidics*, **5**(2), pp. 22207–15.

[43] Altogen Biosystems, (2010). "HEK293 Cell Line Origins, Cytogenetics, and Expression," *HEK293* [Online]. Available: http://hek293.com/. [Accessed: 01-May-2011].

[44] Raof NA, Schiele NR, Xie Y, and Chrisey DB, (2011). "The maintenance of pluripotency following laser direct-write of mouse embryonic stem cells.," *Biomaterials*, **32**(7), pp. 1802–1808.

Chapter 6 – Generation of Human Embryonic Stem Cell Spheroids

6.1 Introduction

The rapidly developing field of regenerative medicine aims to repair, replace, and regenerate damaged cells, tissues or organs through stem cell therapy. Human embryonic stem cells (hESCs) and induced pluripotent stem cells (iPSCs) have the ability to self-renew indefinitely and the potential to differentiate into any cell type [1–5]. Totipotent stem cells can differentiate into all cell types found in an organism, whereas pluripotent stem cells can only differentiate into those cells which are found in an adult [5]. These unique potency characteristics make hESCs ideal for use in a number of applications, such as modelling early embryonic development. The potentially limitless numbers of differentiated hESC progeny can also be used for clinical tissue engineering and replacement applications, such as novel drug discovery and testing for the pharmaceutical industry [1,2,6,7]. *In vitro*, hESCs typically cluster together to form 3-dimensional spheroid aggregates when cultured in medium that has the growth factors removed, which maintains them in a non-adherent and undifferentiated state. After the spheroids have formed, the medium is replaced by one which allows the hESCs to differentiate, and the spheroids are now commonly known as embryoid bodies (EBs). The efficiency with which specific cell types are generated within the EB is partly determined by the size of the spheroid used to create the EB. A lack of uniformity in EB size can lead to asynchronous and heterogeneous differentiation [8]. Consequently, the ability to reliably create uniform EBs of specific sizes is required to generate the correct cell-cell signals needed to produce particular cell types such as cardiomyocytes [9].

Various techniques can be used to create spheroid aggregates, including static suspension, rotary mass suspension, non-adhesive microwell arrays, adhesive stencils, and the hanging-drop method; however, it is still difficult to obtain uniform specific sized spheroids in a controllable manner. Static suspension has limited control over the size of cell aggregates that are formed, and the subsequent differentiation results in heterogeneous populations [3,10]. Rotary mass suspension successfully creates homogeneous size distribution of spheroids, but the process may damage the hESCs and disrupt cell signalling which could affect subsequent cell differentiation [9,11,12]. Non-adhesive microwell plates have been developed in various dimensions and shapes (i.e. U and V shaped wells) in order to control the size and shape of the resulting

spheroids; however, the resulting EBs were mechanically forced into a disk shape and were found to be unstable, forming different cell lineages when re-suspended [8,9]. Adhesive stencils and other surface modification techniques are only able to control the initial size of EBs [13]. The hanging-drop method is a common method to form EBs using hESCs, despite the fact that the resulting EBs can vary in size, mostly due to variations in droplet volume and cell concentrations in each droplet during pipetting. Further issues include the time consuming manual method, which is also liable to human error [4,14].

A new cell printing platform has been developed which is capable of depositing hESCs with precise quantity and high cellular viability, whilst maintaining their pluripotency. The combined methods of hanging-drop spheroid formation with valve-based cell deposition systems were used for the controllable and repeatable creation of uniform human embryonic stem cell spheroids of specific sizes. The combination of a single valve-based deposition system and the hanging-drop technique has recently been shown to be effective in producing spheroids from mESCs using a single nozzle system [4]. This chapter presents the development of a dual nozzle system which enables combinatorial printing of hESCs and results in a system with increased throughput, as multiple bio-inks can be printed simultaneously. In addition, the combined technique was further improved by printing cells directly into the wells of micro-well plates. This allowed the spheroids to form *in situ* without the need to transfer them to a well plate after they have formed, lowering the amount of stress applied to the cells during the aggregation procedure. The response of hESCs to the aggregation procedure was investigated to determine whether it differed in any way to that of other stem cells.

6.2 Project Acknowledgements

The project was performed in collaboration with Jason King, John Gardner, Catherine Fyfe and Helen Bradburn from Roslin Cellab. Human Embryonic Stem cells (line RC-10) were provided at a concentration of 3×10^6 cells/mL. All cell culturing was provided by them, in addition to the various different cell media types used in the following experiments. The School of Life Sciences at Heriot-Watt University provided access to and use of an incubator and optical microscope for the later experiments.

6.3 Pluripotent Stem Cell Testing

6.3.1 hESC Viability

The hESCs were cultured in complete StemPro® hESC SFM (supplement, DMEM/F-12, BSA, FGF basic, and 2-mercaptoethanol) (Life Technologies) supplemented with 8 ng/mL of human basic fibroblast growth factor (hbFGF). Cells were stored in an incubator at 36.0-37.5°C, 5.0±0.5% CO_2. Under these conditions the cells are kept in an undifferentiated state.

hES cells were suspended in StemPro® hESC SFM to a concentration of approximately 2×10^6 cells/mL and loaded into the reservoir of one of the cell deposition systems. The valve-on time was set at 8000 ms to allow for a significant volume to be dispensed, improving the reliability of the results. Due to the fact that different pressures are often used in different experiments, cellular viability was investigated at a number of pressures to give a more accurate indication of viability for various circumstances. Several droplets were dispensed at each pressure onto microscope slides; the unprinted cells were used as a control.

The slides were examined under the microscope at 24 and 72 hours post printing and sample images were recorded. The number of live and dead cells was counted using the ImageJ image processing program and the results are shown in Figure 5.8.

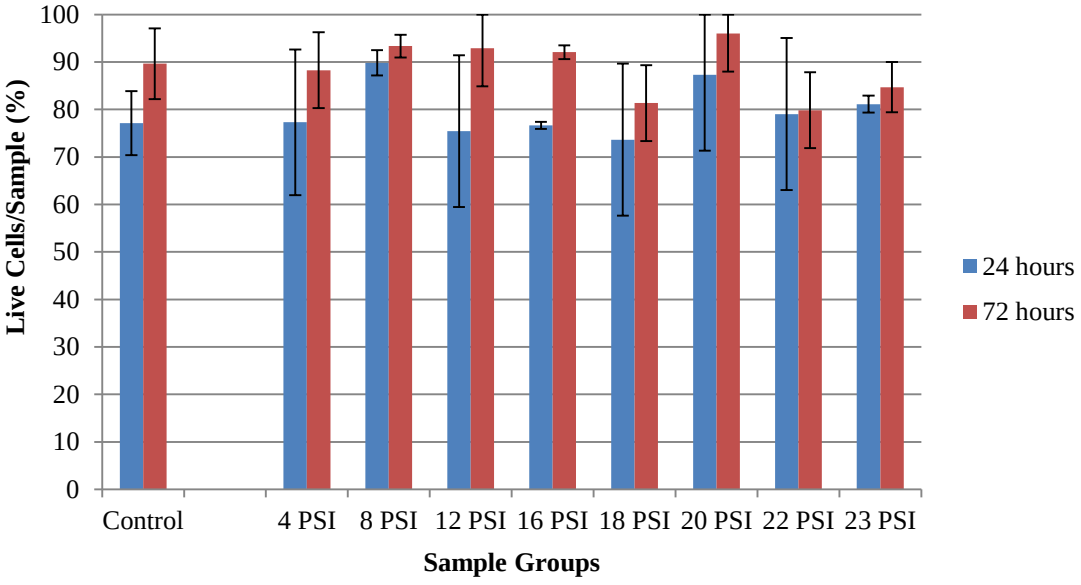

Figure 6.1 *– A graph to show the percentages of live cells per sample as a function of pressure.*

The normalised cell viability was calculated to be >95% after 24 hours and >89% after 72 hours for all pressures. This confirms that this technique does not affect the short and longer term viability of cells even those as sensitive as hESCs. This is consistent with the observations of other groups [4,15–18].

6.3.2 Oct-4 Immunofluorescence

In order to confirm that the hESCs were still pluripotent post-printing, they were examined to check that they still possessed one of the pluripotency markers: octamer-binding transcription factor 4 (Oct4). After performing the procedure detailed in section 3.3.4, the cells were examined under the microscope 72 hours after printing. The results are shown in Figure 6.2.

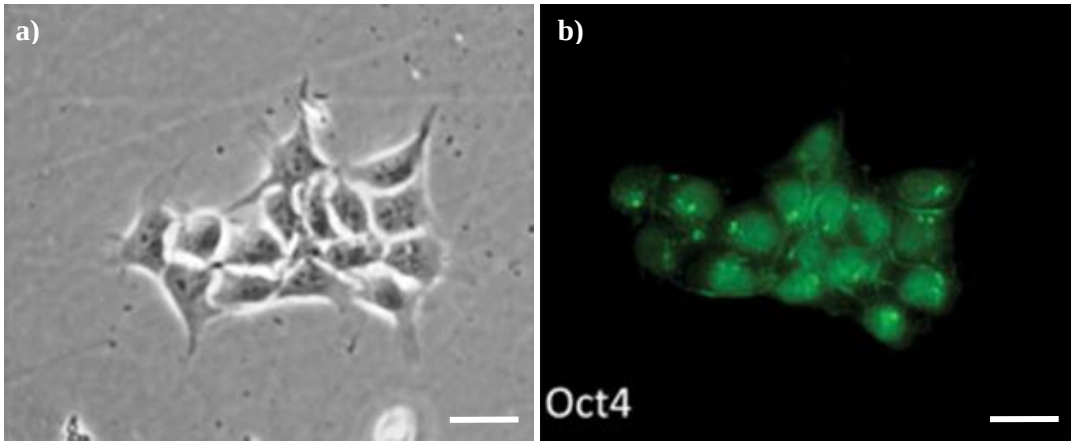

Figure 6.2 *– Detailed views of hES cells 72 hours after printing: a) optical image; b) fluorescence image (scale bar 10 µm)*

Three days after printing, hESCs remained positive for the Oct-4 pluripotency marker, which confirms that the printing process does not affect the pluripotency of hES cells.

The results presented here clearly show that even fragile cells like hESCs are unaffected by the printing process. Another advantage of the cell printing approach is the increased speed of the technique: the cell printer can deposit ~50 distinct droplets per minute and could therefore populate an entire 96-well plate in less than 2 minutes, whereas a manual approach would take significantly longer. As a consequence of this decreased time and the graphical user interface, the cell printer is a high throughput and user-friendly operation.

6.4 Combinatorial Printing Scheme for Spheroidal Aggregate Creation

Due to the fact that the size of an EB will influence the differentiation path of the hESC within it, by altering one or more of these characteristics it may be possible to discover how much influence they have over hESC differentiation and perhaps discover the perfect conditions required to produce different lineages. The size of an EB is determined by the number of cells from which it was formed and the time the cells were cultured for.

The droplet volume is easily controllable by the bioprinter and the number of cells present in each dispensed droplet can be set by the concentration of cells in the bio-ink and the volume of the dispensed droplet as discussed in section 5.3.1. Therefore, it is possible to create a gradient of cell numbers by depositing a gradient of droplet volumes. By overprinting a similar gradient of medium in the opposite direction, the resulting array will have a constant volume but a gradient of cell concentrations. Such an array could be used to create EBs with controllable sizes and show the minimum cell concentration required to create a stable aggregate.

Prior to using cells to create aggregates, DMEM (medium) was used to check that the cell printer could print a gradient of droplet volumes. Programs were written for the cell printer that would create an 11×11 array of droplets with gradients of droplet volumes. The droplet spacing was set at 1 mm, taking into account surface properties (such as hydrophobicity) and maximum droplet volume to ensure that they remained isolated and did not merge with neighbouring droplets. The first program created a decreasing gradient of droplet volumes in each row from 1.5-0 µL (no bio-ink was dispensed on the 11^{th} row); the resulting array is shown in Figure 6.3a. The second program created the reverse (increasing) gradient in each row from 0-1.5 µL (no bio-ink was dispensed on the 1^{st} row). When the two programs were run consecutively, the resulting array of droplets had a constant volume of 1.5 µL but a gradient ratio between the two different bio-inks. Since the two programs omit one row each, a pure row of each bio-ink is present in the final array. The results are shown in Figure 6.3.

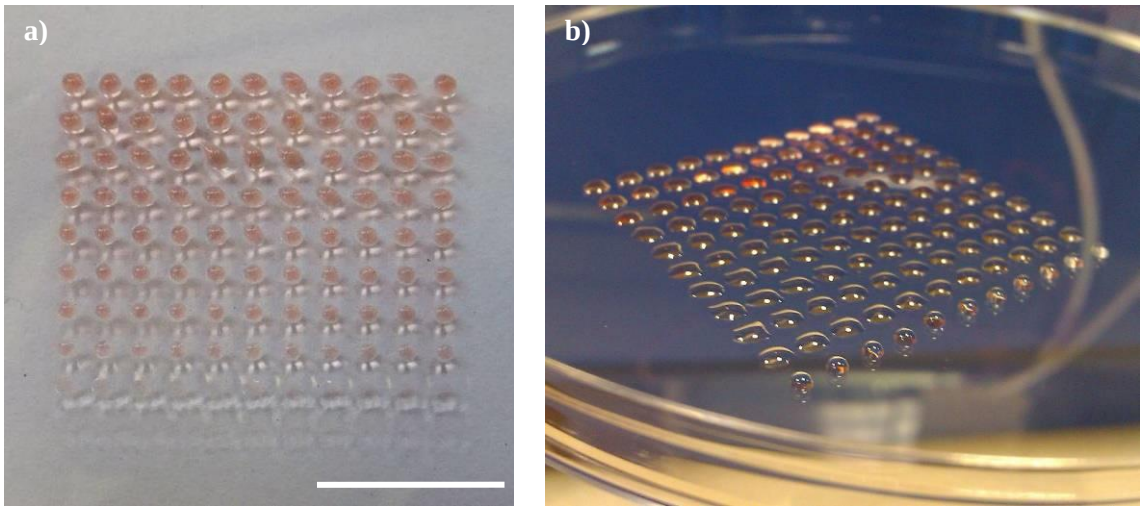

Figure 6.3 *– a) An array of DMEM (with red dye for clarity) with a gradient of droplet sizes (1.5 – 0 μL); b) the same array with an opposing gradient of water overprinted to create uniform volume droplets with a gradient of DMEM (scale bar 10 mm)*

These results show that the printer is able to create an array with a volume gradient and overprint an opposing volume gradient on top to create a constant volume array with two opposing gradients. The last row of the array in Figure 6.3b contains only water which is why they are a different shape.

6.4.1 Printing Hanging Droplets

The hanging drop method of culturing embryoid bodies customarily suspends the physically separated droplets of cells suspended in medium from the lid of a Petri dish, which can lead to problems when the dish is inverted. There are also issues with production scale and the amount of labour required to manually create the array [10,19]. Other disadvantages include the limitation on droplet volume (<50 μL) due to maintaining the droplets on the substrate surface by surface tension and the practical impossibility of medium exchange [20].

To overcome these drawbacks, the bioprinter was used to print the droplets, improving the homogeneity and repeatability of the created EBs. The Petri dish lid was replaced with 60-well Terasaki plates (653102, Greiner bio-one). These particular plates were chosen due to their flat bottomed conical well profile, angled at 56°, which both lowers the surface area of the hanging droplet and removes the unwanted corners at the bottom of most standard well plates. This increases the droplets resistance to drying and potentially induces the cells to aggregate quicker, lowering the likelihood of multiple aggregates. In order to further reduce the amount of media evaporation of the small

(tens of µL or fewer) volume deposited in each well, the lid of the multi-well plate is filled with water to act as a reservoir.

An additional benefit of printing into the wells of a multi-well plate is that the droplet locations, and hence the EB locations, are indexed. Therefore if long-term culture is required, fresh media can be added to each well very quickly and accurately to keep the EBs supplied with nutrients.

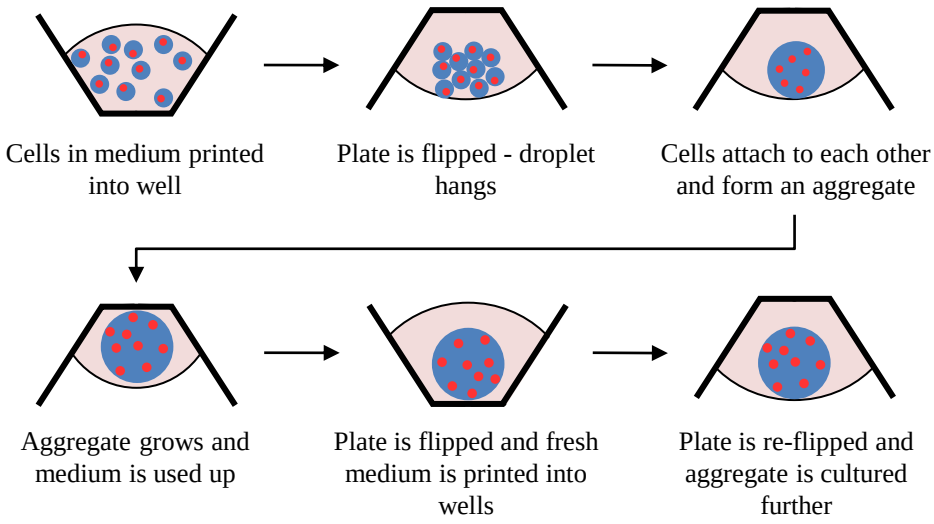

Figure 6.4 *– Schematic of the printing process for aggregate creation and culture*

In the research performed by Xu et al. [4] aggregates were formed in hanging droplets on the lid of a Petri dish and then transferred to a microwell plate for further culture. The process described here improves on existing techniques as it eliminates the need for moving the aggregates after they have formed, enabling the investigation into the effects of external agents (i.e. nanoparticles or chemicals) on different sized aggregates in the same array. Keeping the aggregates in the microwells where they formed eliminates a source of possible contamination and reduced the stress encountered by the cells and the spheroid, decreasing the chances of the spheroids fragmenting.

6.4.2 Gradient of Cell Concentration

In order to confirm the repeatability of the creation of a cell gradient array, an experiment was devised using the printed hanging-drop method and the combinatorial printing process for creating arrays with concentration gradients.

60-well Terasaki plates were used as the substrate for this experiment. The wells were coated in a thin layer of CELLStart™ to assist in maintaining the pluripotency of the hESCs. The multi-well plates were transferred to an incubator and allowed to incubate for 1 hour before the extra CELLStart™ was removed.

One of the bio-ink reservoirs was loaded with cells suspended in medium, while the other was loaded with medium alone. An array of droplets containing cells was printed onto the wells of the multi-well plate with the size of the droplets decreasing by a set amount for each column, thus creating a gradient of droplet sizes and hence a gradient of cell concentration. An opposing gradient of droplets which contained only medium was dispensed over the existing array, resulting in an array of droplets with uniform size but a cell concentration gradient. The completed array was then inverted, making the droplets hang down from the surface and forcing the cells to aggregate.

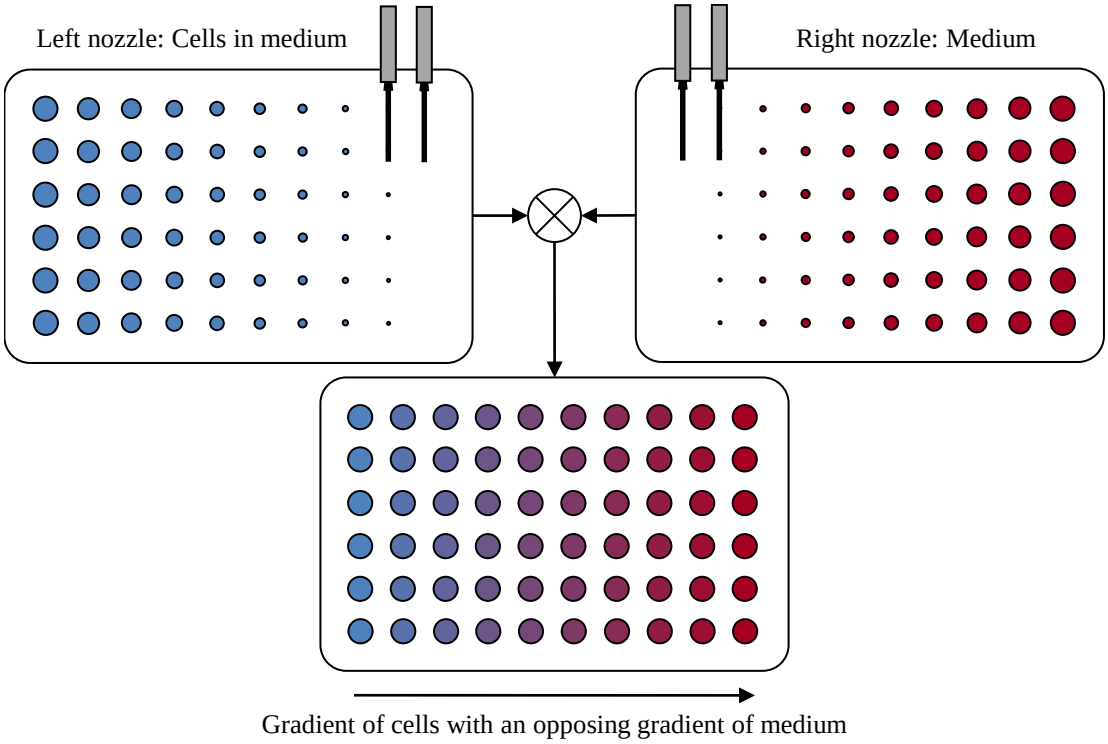

Figure 6.5 *– Schematic of the combinatorial printing process for aggregate creation*

Based on the results in Figure 5.8, the inlet pressure was set at 8 PSI as it resulted in a higher viability than the other pressures during that experiment. Using the existing valve time settings, 8 PSI also resulted in the desired volume of ~4 µL.

Firstly, the program was run to check that cell concentration gradients were being created correctly. Human ESCs were suspended in complete StemPro® hESC SFM to a concentration of approximately 1×10^6 cells/mL and loaded into the left reservoir. The other reservoir was loaded with complete StemPro® hESC SFM. The gradient of medium was printed into the wells of a 60-well plate first in order to reduce potential impact on the cells. Next, the opposing gradient of cells in medium was printed over the medium droplets, resulting in droplets of uniform size in every well (~4 µL). The cells were monitored under the microscope (fl0015000m Trinocular Fluorescence Microscopes) immediately and at 24 hours after printing. Between these times the cells were kept in a CO_2 incubator (Galaxy S+, RS Biotech) at 36.0-37.5°C, 5.0±0.5% CO_2.

Two plates were populated and examined under the microscope before being placed into an incubator. The results are shown in Figure 6.6 and Figure 6.7.

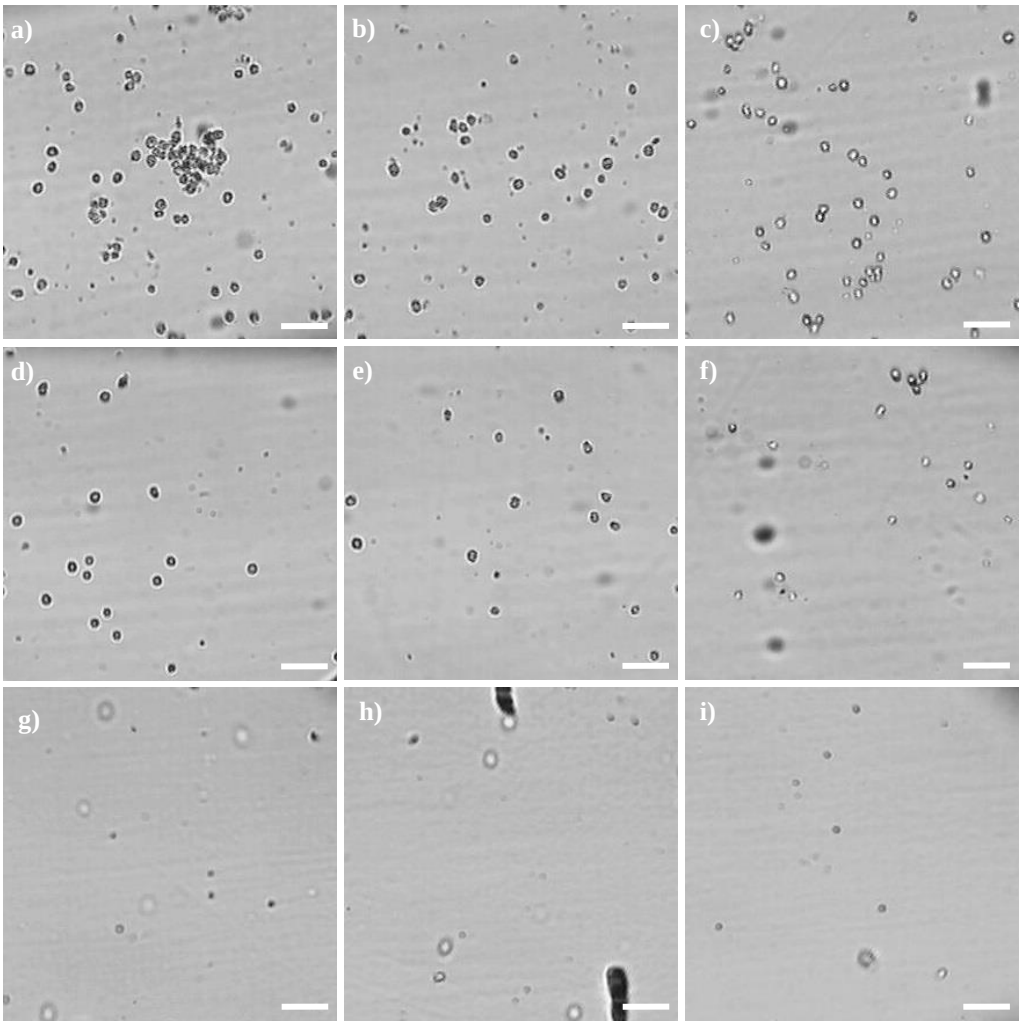

Figure 6.6 *– Detailed views of selected wells of the printed array immediately after printing: a) 1st column; b) 2nd column; c) 3rd column; d) 4th column; e) 5th column; f) 6th column; g) 7th column; h) 8th column; i) 9th column (scale bars 250 µm)*

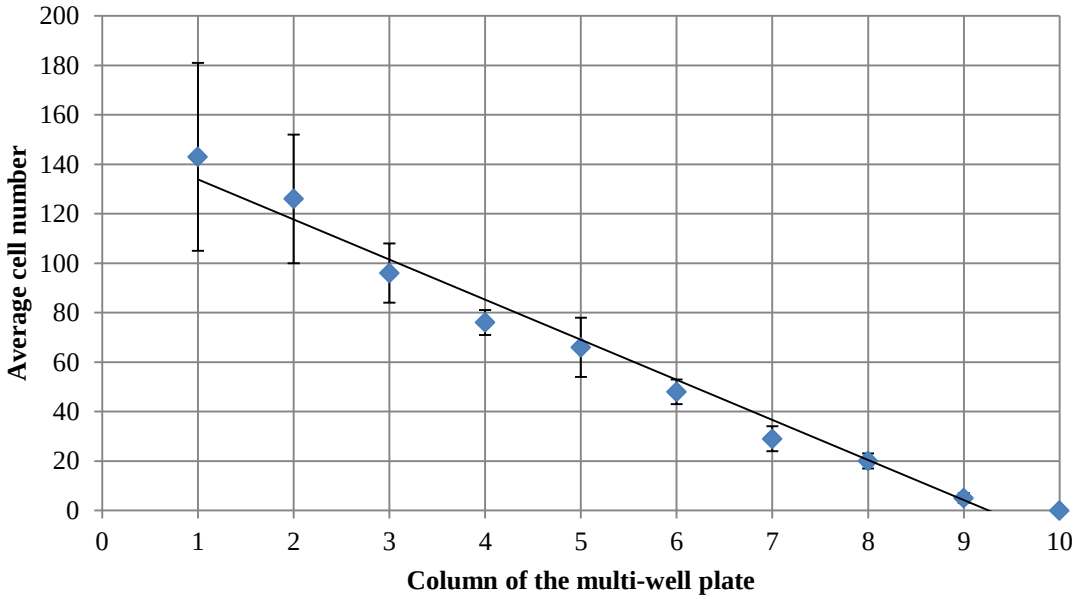

Figure 6.7 *– A graph to show the average cell numbers in each column after printing.*

These results show that a gradient of cell concentration can be created using this approach. The error bars are very small, indicating that the data is highly reliable and correct; furthermore, the relationship is linear, which means that specific cell concentrations could easily be specified for future experiments.

The original plan was to perform one long experiment in one day, wherein cells were printed and analysed immediately post printing, then measure the resulting aggregate sizes at 24 and 48 hours post printing. Unfortunately, upon examination of the cells after 24 hours post printing, it became apparent that the incubator had failed, and a large number of the cells had consequently died due to the evaporation of the medium. The experiment was not a complete loss, however as we had confirmed that it was possible to print a gradient of cell concentrations.

The error bars in Figure 6.7 for the cell numbers in the first and second columns are larger since there was insufficient volume of suspended cells to fully populate two multi-well plates. The cell counts for these two columns are taken mostly from the first multi-well plate and a small number of wells from the second plate and the larger error bars reflect the increased uncertainty.

A further issue arose when initially analysing the plates, as it transpired that the microscopes had insufficient optical magnification to view all the cells in the wells clearly. Multiple images were therefore taken and stitched together.

6.4.3 Gradient of Spheroid Aggregate Sizes

In order to combat some of the problems encountered in the previous attempt, the experiment was repeated with several modifications. Complete StemPro® hESC SFM with hES cells suspended at a concentration of 3×10^6 cells/mL were loaded into the left reservoir. The other reservoir was loaded with complete StemPro® hESC SFM. As before, the two opposing gradients of medium and cells in medium were printed onto a 60-well plate, resulting in droplets of uniform size in every well. The volume printed in each was increased to ~10 µL instead of 4 µL in order to combat the quick evaporation encountered previously. This plate was then placed into an incubator and the procedure was repeated on a second plate which was also placed into the same incubator. As the immediate cell concentration results had been verified previously, the plates were examined under the microscope 24 and 48 hours after printing. The results are shown in Figure 6.8 and Figure 6.9.

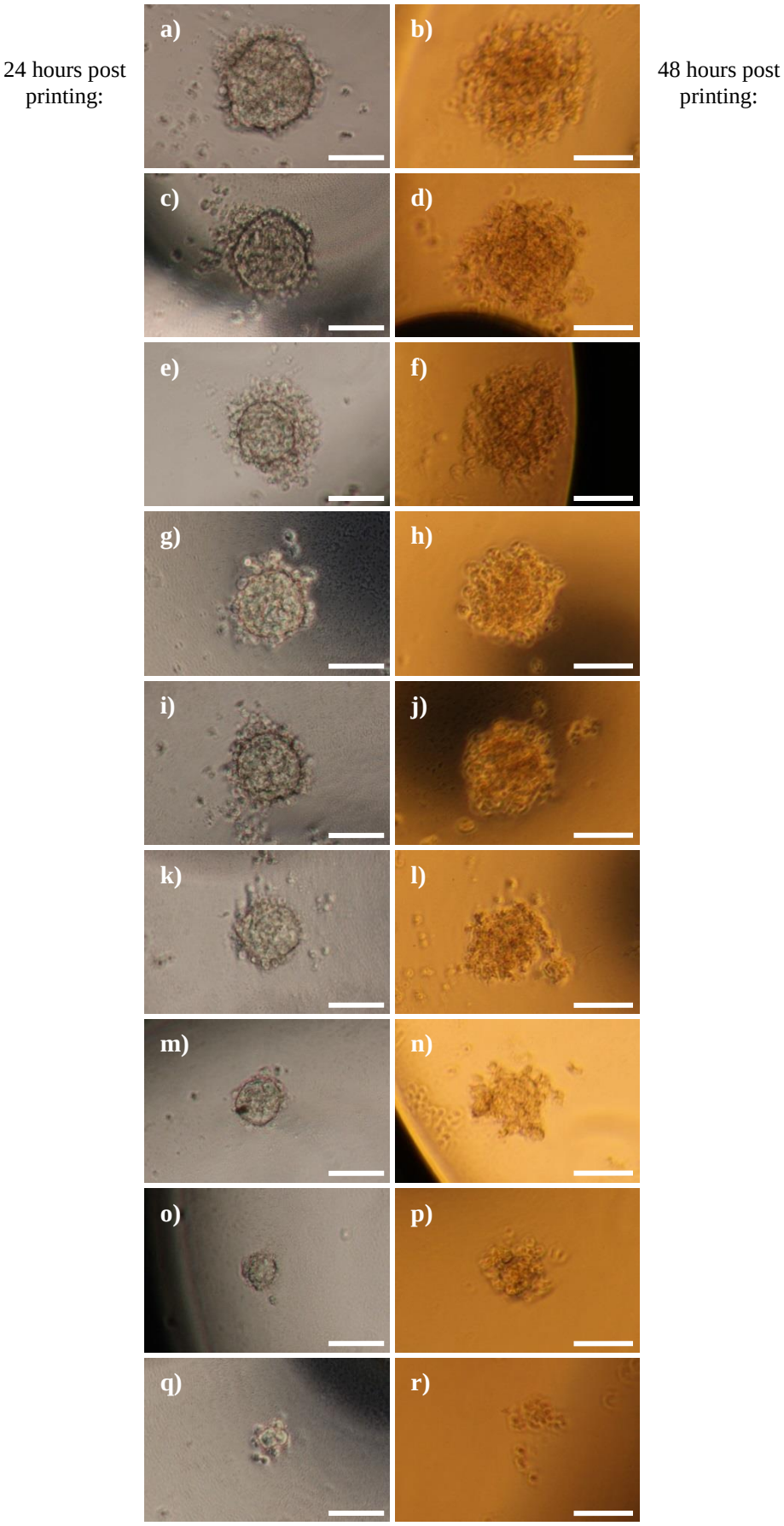

Figure 6.8 *– Detailed views of selected aggregates 24 and 48 hours after printing: a-b) 1st column; c-d) 2nd column; e-f) 3rd column; g-h) 4th column; i-j) 5th column; k-l) 6th column; m-n) 7th column; o-p) 8th column; q-r) 9th column (scale bars 250 μm)*

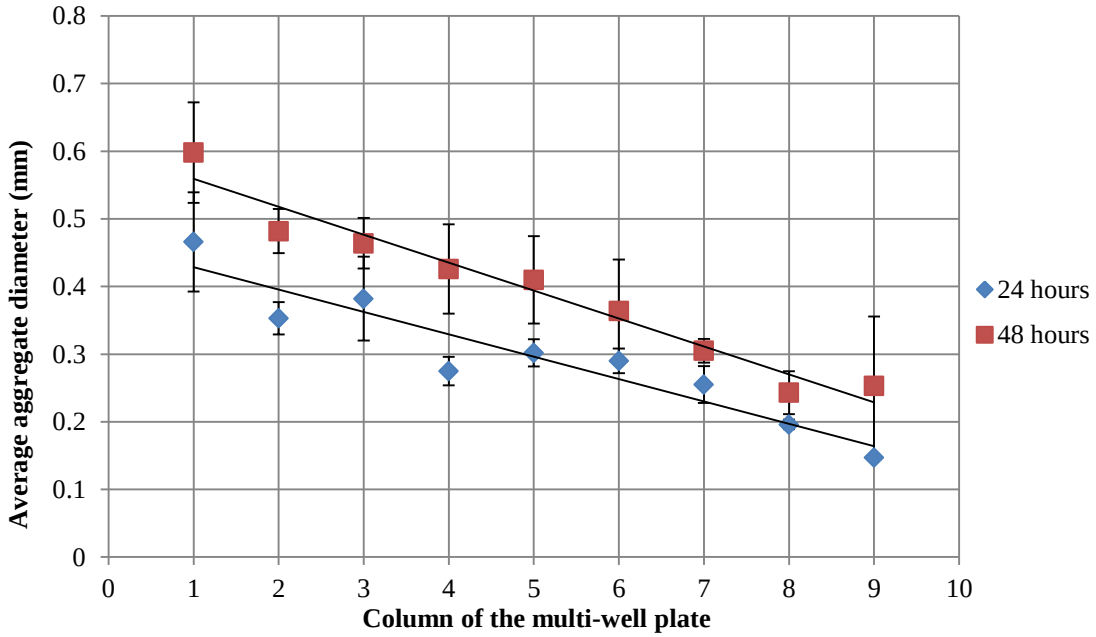

Figure 6.9 *– A graph to show average sizes of cellular aggregates in each column measured 24 and 48 hours after printing.*

In order to quantitatively evaluate the aggregate sizes, a best fit ellipse was used to calculate diameters. It was observed that a gradient in the initial concentration of cells yields aggregates with a similar gradient of sizes. In addition, higher concentrations of cells tended to yield larger aggregates, and these larger aggregates exhibited more growth over the 48 hours than smaller aggregates. This confirms that the cells are still viable, even those inside the aggregates, as the larger aggregates would not have exhibited the increased growth indicated in these results if any cells had died. This confirms results in previously reported research [21,22]. An alternative explanation for the increased growth is the re-aggregation of the smaller spheroids into larger ones [23].

An unexpected result was that multiple aggregates had formed in some of the wells. Although this did not occur very often, the data seems to suggest that it will occur more often in the wells with lower initial concentrations of cells. Another interesting result was that the multi-aggregates that formed were similar in size to those in the same column where only single aggregates had formed. Two possible explanations exist for this phenomenon: either there is a relationship between cell density and cell mobility, and there comes a point where the cells are too widely spread to form a single aggregate; or this may be a quirk of human ESCs. An example of multi-aggregate formation is shown in Figure 6.10.

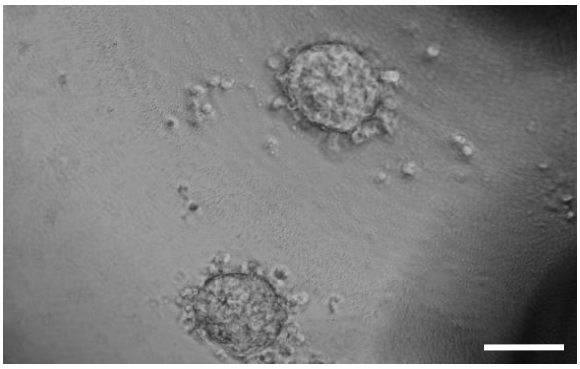

Figure 6.10 *– An example of multiple aggregates forming in the same well (scale bar 250 μm)*

The results presented here clearly show that aggregates can be created with a reasonable degree of control of their size by varying the initial cell concentration and culture time. The standardisation of aggregate sizes is much greater than those achievable by manual pipetting due to the inherently heterogeneous nature of manual pipetting, especially with regards to droplet sizes and therefore initial cell concentrations. Further work is required to fully characterise the spheroids formed using this technique.

6.5 Conclusions

This work demonstrates that the valve-based printing process is accurate enough to produce spheroids of uniform size. Due to the dual nozzle setup, the system is also able to create gradients of cells and other bio-inks which, when used in conjunction with the hanging droplet technique, yields gradients of cellular aggregates. The resulting aggregates are uniform and have repeatable sizes or size ranges, meaning that they can be made for specific applications such as the production of macrophages or other blood cells that require going through an EB phase en route to the eventual terminally differentiated cell type. Unlike previous studies, this project printed directly onto the micro-well plate, allowing the creation and culture of spheroid aggregates without the need to transfer them after formation, lowering the amount of stress applied to the cells during the aggregation procedure, increasing viability and successful aggregation formation rate.

The ability to print human embryonic stem cells for the generation of 3D structures will allow for the creation of more accurate functional human organ tissue models by incorporating programmed differentiation to increase the efficiency. These tissue models would increase the accuracy and reliability of existing *in vitro* drug development and toxicity-testing.

Additionally, this may also pave the way for human stem cells to be incorporated into clinical protocols either for patient implantation of *in vitro* regenerated organs or direct *in vivo* cell printing for tissue regeneration.

6.6 References

[1] Murry CE, and Keller G, (2008). "Differentiation of Embryonic Stem Cells to Clinically Relevant Populations: Lessons from Embryonic Development," *Cell*, **132**(4), pp. 661–680.

[2] Fenno LE, Ptaszek LM, and Cowan CA, (2008). "Human embryonic stem cells: emerging technologies and practical applications," *Current Opinion in Genetics & Development*, **18**(4), pp. 324–329.

[3] Itskovitz-Eldor J, Schuldiner M, Karsenti D, Eden A, Yanuka O, Amit M, Soreq H, and Benvenisty N, (2000). "Differentiation of human embryonic stem cells into embryoid bodies compromising the three embryonic germ layers.," *Mol Med*, **6**(2), pp. 88–95.

[4] Xu F, Sridharan B, Wang S, Gurkan UA, Syverud B, and Demirci U, (2011). "Embryonic stem cell bioprinting for uniform and controlled size embryoid body formation," *Biomicrofluidics*, **5**(2), pp. 22207–15.

[5] Gage FH, (2000). "Mammalian Neural Stem Cells," *Science*, **287**(5457), pp. 1433–1438.

[6] McNeish J, (2004). "Embryonic stem cells in drug discovery," *Nat Rev Drug Discov*, **3**(1), pp. 70–80.

[7] Wu DC, Boyd AS, and Wood KJ, (2007). "Embryonic stem cell transplantation: potential applicability in cell replacement therapy and regenerative medicine," *Front. Biosci.*, **12**, pp. 4525–4535.

[8] Park J, Cho CH, Parashurama N, Li Y, Berthiaume F, Toner M, Tilles AW, and Yarmush ML, (2007). "Microfabrication-based modulation of embryonic stem cell differentiation," *Lab on a Chip*, **7**(8), pp. 1018–28.

[9] Mohr JC, Zhang J, Azarin SM, Soerens AG, de Pablo JJ, Thomson JA, Lyons GE, Palecek SP, and Kamp TJ, (2010). "The microwell control of embryoid body size in order to regulate cardiac differentiation of human embryonic stem cells," *Biomaterials*, **31**(7), pp. 1885–1893.

[10] Rungarunlert S, Techakumphu M, Pirity MK, and Dinnyes A, (2009). "Embryoid body formation from embryonic and induced pluripotent stem cells: Benefits of bioreactors," *World J Stem Cells*, **1**(1), pp. 11–21.

[11] Ng ES, Davis RP, Azzola L, Stanley EG, and Elefanty AG, (2005). "Forced aggregation of defined numbers of human embryonic stem cells into embryoid bodies fosters robust, reproducible hematopoietic differentiation," *Blood*, **106**(5), pp. 1601–1603.

[12] Dang SM, Kyba M, Perlingeiro R, Daley GQ, and Zandstra PW, (2002). "Efficiency of embryoid body formation and hematopoietic development from embryonic stem cells in different culture systems," *Biotechnol. Bioeng.*, **78**(4), pp. 442–453.

[13] Bauwens CL, Peerani R, Niebruegge S, Woodhouse KA, Kumacheva E, Husain M, and Zandstra PW, (2008). "Control of Human Embryonic Stem Cell Colony and Aggregate Size Heterogeneity Influences Differentiation Trajectories," *STEM CELLS*, **26**(9), pp. 2300–2310.

[14] Kurosawa H, Imamura T, Koike M, Sasaki K, and Amano Y, (2003). "A simple method for forming embryoid body from mouse embryonic stem cells," *Journal of Bioscience and Bioengineering*, **96**(4), pp. 409–411.

[15] Moon S, Lin P-A, Keles HO, Yoo S-S, and Demirci U, (2007). "Cell Encapsulation by Droplets," *J Vis Exp*, **8**.

[16] Demirci U, and Montesano G, (2007). "Cell encapsulating droplet vitrification," *Lab on a Chip*, **7**(11), p. 14281433.

[17] Xu F, Emre AE, Turali ES, Hasan SK, Moon S, Nagatomi J, Khademhosseini A, and Demirci U, (2009). "Cell proliferation in bioprinted cell-laden collagen droplets," Bioengineering Conference, 2009 IEEE 35th Annual Northeast, IEEE, pp. 1–2.

[18] Xu F, Celli J, Rizvi I, Moon S, Hasan T, and Demirci U, (2011). "A three-dimensional in vitro ovarian cancer coculture model using a high-throughput cell patterning platform," *Biotechnology Journal*, **6**(2), pp. 204–212.

[19] Tung Y-C, Hsiao AY, Allen SG, Torisawa Y, Ho M, and Takayama S, (2011). "High-throughput 3D spheroid culture and drug testing using a 384 hanging drop array," *The Analyst*, **136**(3), p. 473.

[20] Kurosawa H, (2007). "Methods for inducing embryoid body formation: in vitro differentiation system of embryonic stem cells," *Journal of Bioscience and Bioengineering*, **103**(5), pp. 389–398.

[21] Lin R-Z, Lin R-Z, and Chang H-Y, (2008). "Recent advances in three-dimensional multicellular spheroid culture for biomedical research," *Biotechnol J*, **3**(9-10), pp. 1172–1184.

[22] Alvarez-Pérez J, Ballesteros P, and Cerdán S, (2005). "Microscopic images of intraspheroidal pH by 1H magnetic resonance chemical shift imaging of pH sensitive indicators," *MAGMA*, **18**(6), pp. 293–301.

[23] Landry J, Bernier D, Ouellet C, Goyette R a, and Marceau N, (1985). "Spheroidal aggregate culture of rat liver cells: histotypic reorganization, biomatrix deposition, and maintenance of functional activities.," *The Journal of cell biology*, **101**(3), pp. 914–923.

Chapter 7 – 3D Bioprinting towards the Creation of Liver Tissue

7.1 Introduction

In order to create engineered tissue structures, the ability to create precise *in vitro* microenvironments with 3D, chemical and spatial control over cells is required. A number of studies have shown that certain cells such as hepatocytes require a three-dimensional structure in order to function properly [1–3]. *In vitro* studies by Dunn et al. have shown that hepatocytes cultured as a monolayer lost many of their liver-specific functions after a few days, but those cultured with a layer of collagen gel in a "sandwich configuration" were able to retain their liver-specific functions for several weeks [4]. *In vivo,* the extracellular matrix (ECM) is the natural scaffold material that serves to maintain the 3D tissue structure, control cell proliferation, motility and migration [5].

Various techniques have been developed to position cells in three-dimensions in order to create three-dimensional tissue constructs, some of which make use of aggregates similar to those created in Chapter 6. The methods include: scaffolds, bottom-up self-assembly, cell sheets and de-/recellularisation. Bottom-up self-assembly of cells or cellular aggregates in hydrogel addresses the main limitations of the older techniques and it is the best suited technique for the creation of micro-tissues [6].

Hydrogels are important building materials for tissue engineering due to their similarities to extracellular matrix (ECM); they are also inherently biocompatible due to their hydrophilicity, and they very closely resemble the 3D biological environment required for cell culture [7–11]. They are extremely customizable, with a very large selection of available synthetic and natural components, fabrication techniques, and synthesis methodologies, which result in tuneable properties such as pore size and mechanical strength [9,10]. For these reasons, hydrogels have been used extensively in many biological and clinical applications, including 3D tissue and organ engineering.

As noted in section 1.1.2, new drug development can take from 10 to 20 years with an estimated average of about 9 to 12 years [12,13]. In addition, only around 16% of the drugs that begin preclinical testing are approved for human use [14]. Some of this low success rate can be attributed to the different responses that animals and humans have to the drugs being tested; some drugs may be dropped that would have worked on humans because they didn't have the desired effect on animals, while drugs such as thalidomide were accepted with disastrous results [15]. One possible solution to this is the creation

of human pluripotent stem cell-derived micro-tissues which could be used with organ-on-a-chip devices [16]. These micro-tissues should produce the same physiological reaction that the entire organ would, but on a much smaller scale. This would result in faster results, better drugs and an end to animal testing and vivisection. Human pluripotent stem cells (hPSCs) are the ideal cells to use for this application due to their ability to self-renew, which enables large populations of cells to be created easily, and their pluripotency, which means that they can differentiate into any required adult cell type [17–21]. However, if these cells are to be used for these kinds of applications, their differentiation must be reproducibly directed to the required lineages for each tissue. Unfortunately, homogeneous cellular differentiation of hPSCs into specific germ layers has proven to be difficult to accomplish [22,23].

If more complex structures such as those found in organs were to be printed, the bioprinter would need the ability to transfer mesoscopic patterns of viable cells into clearly-defined three-dimensional patterns. This chapter describes the application of the valve-based bioprinting platform to the creation of 3D cell-laden hydrogel structures and the directed differentiation and printing of hPSC-derived hepatocyte-like cells (HLCs) as a precursor to the creation of multi-cellular liver micro-tissues. This includes an in-depth study into the printability of alginate hydrogels of various concentrations and volume ratios, the viability and compatibility of 3D hydrogel structures with cells, and the investigation of the HLCs to verify their hepatic functions.

7.2 Project Acknowledgements

The project was performed in collaboration with Juan Jin, Chuang Li and Yijie Wang from Tsinghua University, Beijing, China, and Jason King, John Gardner, Catherine Fyfe, Sebastian Greenhough and Helen Bradburn from Roslin Cellab. Human Embryonic Stem cells (lines RC-6, RC-7, RC-8, RC-9, and RC-10) and Human Induced Pluripotent Stem cells (line RCi-22) were provided by Roslin Cellab at various concentrations. All stem cell culturing was provided by Roslin Cellab, in addition to the various different cell media types used in the following experiments. Experiments involving HLCs were carried out by Roslin Cellab.

7.3 Alginate Printing

Alginate is a natural linear polysaccharide copolymer which is extracted from brown seaweed algae. Due to their biocompatibility, non-immunogenicity, low toxicity and

hydrophilic nature, alginate hydrogels have many attractive features for biomedical applications [24]. The mechanical properties of a gelled alginate solution, including viscosity and overall stiffness, depend on the concentration of the polymer and its molecular weight distribution [9,25]. Crosslinking between the polymer chains depends on the amount of polymer chains and multivalent cations (e.g. Ca^{2+}, Ba^{2+}) present in the solution and the temperature [7,9,24,25]. *In vitro*, alginates typically degrade by approximately 40% within 9 days; this is most likely due to the diffusion of ions into the surrounding medium [26].

Sodium alginate (W201502, Sigma-Aldrich Co. LLC) and calcium chloride dehydrate (223506, Sigma-Aldrich Co. LLC) were used to form alginate hydrogels. Alginate hydrogel structures are bioprinted by dispensing an array of droplets of alginate solution from the left nozzle and then overprinting droplets of calcium solution from the right. After a few seconds, the alginate chains start to bond with the calcium ions, forming a complete hydrogel matrix in around a minute. If adjacent droplets overlap they gel together and form a single continuous layer.

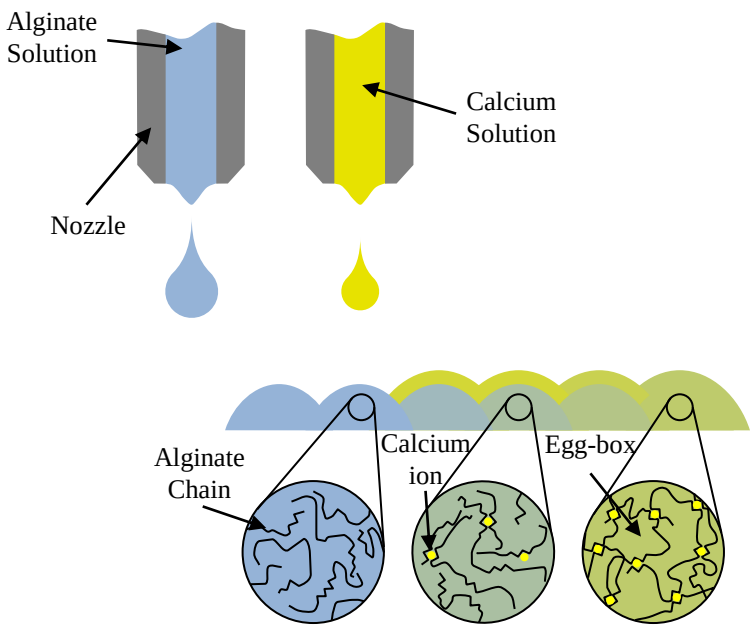

Figure 7.1 *– Schematic of the combinatorial printing process for alginate hydrogel creation.*

7.3.1 Hydrogel Spot Size Investigation

The first task was to explore the properties of the hydrogel components and determine the optimum pressure, concentration and volume ratios required to generate hydrogel.

To this end, a series of solutions with different concentrations of sodium alginate and calcium solutions were prepared and mixed.

Sodium alginate solutions with concentrations from 0.1% to 5% were successfully dispensed using the custom bioprinter described in Chapter 4 at inlet pressures of 2-15 PSI. The calcium solution has a much lower viscosity and should therefore be dispensed at much lower pressures in order to avoid flooding the printed hydrogel structure with excess calcium solution.

In order to determine the range of sizes of hydrogel droplets that can be created, an experiment was devised with a varying volume ratio of alginate and calcium solutions. Solutions of each component were created with 1% volume concentration and loaded into the bioprinter. A variety of different ratios were tested and the resulting droplets were viewed under the microscope to measure their dimensions; the properties of the resulting hydrogels were then examined. In each case a number of layers of alginate were dispensed before a single layer of calcium was added to cross-link the hydrogel.

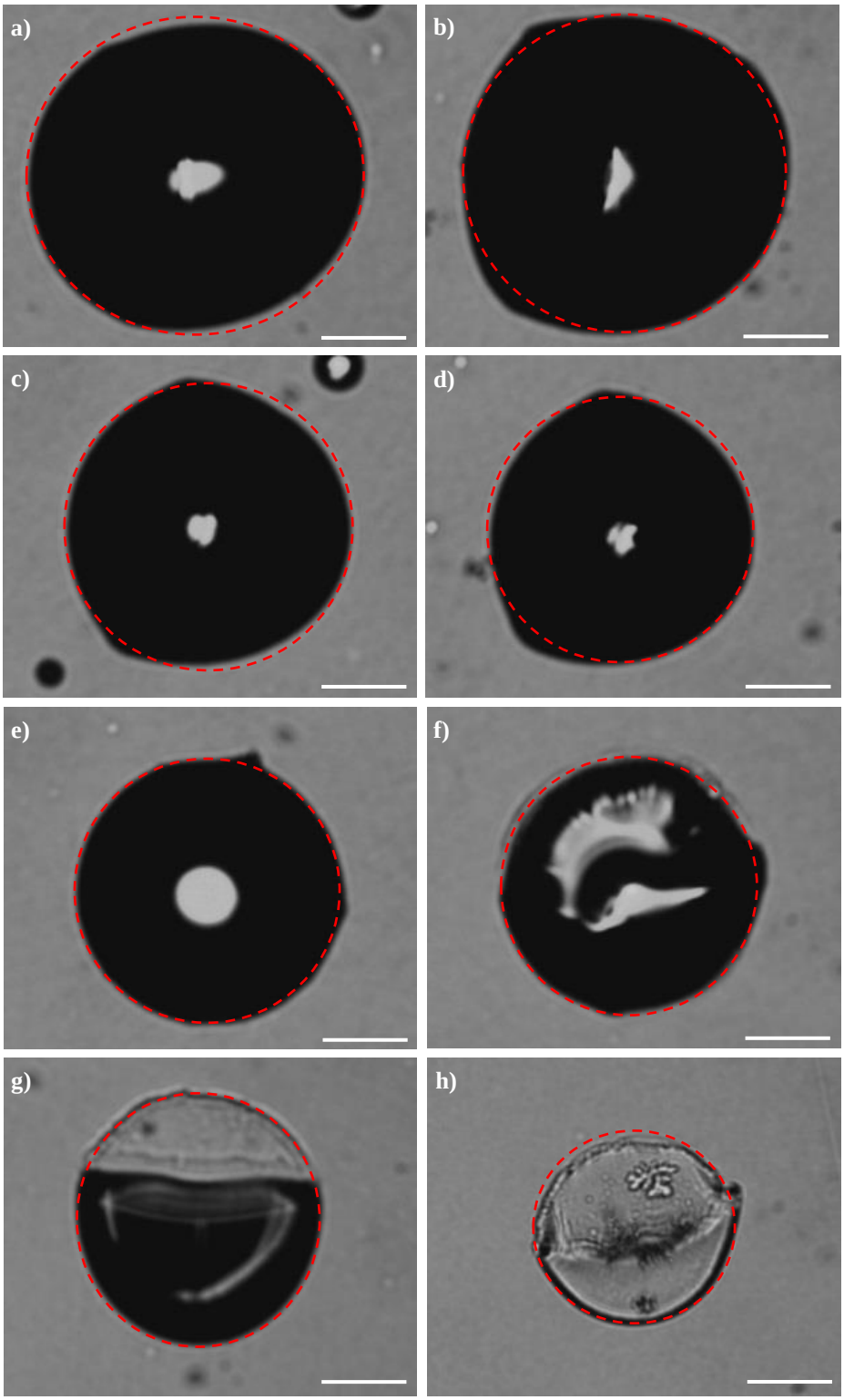

Figure 7.2 *– Results of the alginate droplet spot size investigation: a) 8 layers of alginate; b) 7 layers of alginate; c) 6 layers of alginate; d) 5 layers of alginate; e) 4 layers of alginate; f) 3 layers of alginate; g) 2 layers of alginate; h) 1 layer of alginate (scale bars 250 µm)*

The resulting droplets ranged in size from 960 to 620 µm in diameter and followed an expected linear increase in size. It was noted that all the droplets contained cross-linked hydrogels, but the volume ratio of approximately 4:1 alginate to calcium was found to

create the best hydrogel. These results were used to configure all subsequent alginate-based hydrogel experiments.

7.3.2 3D Hydrogel Bioprinted Structures

In most of the experiments undertaken thus far, droplets were dispensed separately and discretely. In contrast, these experiments required the droplets to merge together to form contiguous structures. The spacing between droplets was set to approximately half the dispensed droplet diameter to ensure that they merged. Again, 1% concentration solutions of sodium alginate and calcium chloride were used for these experiments.

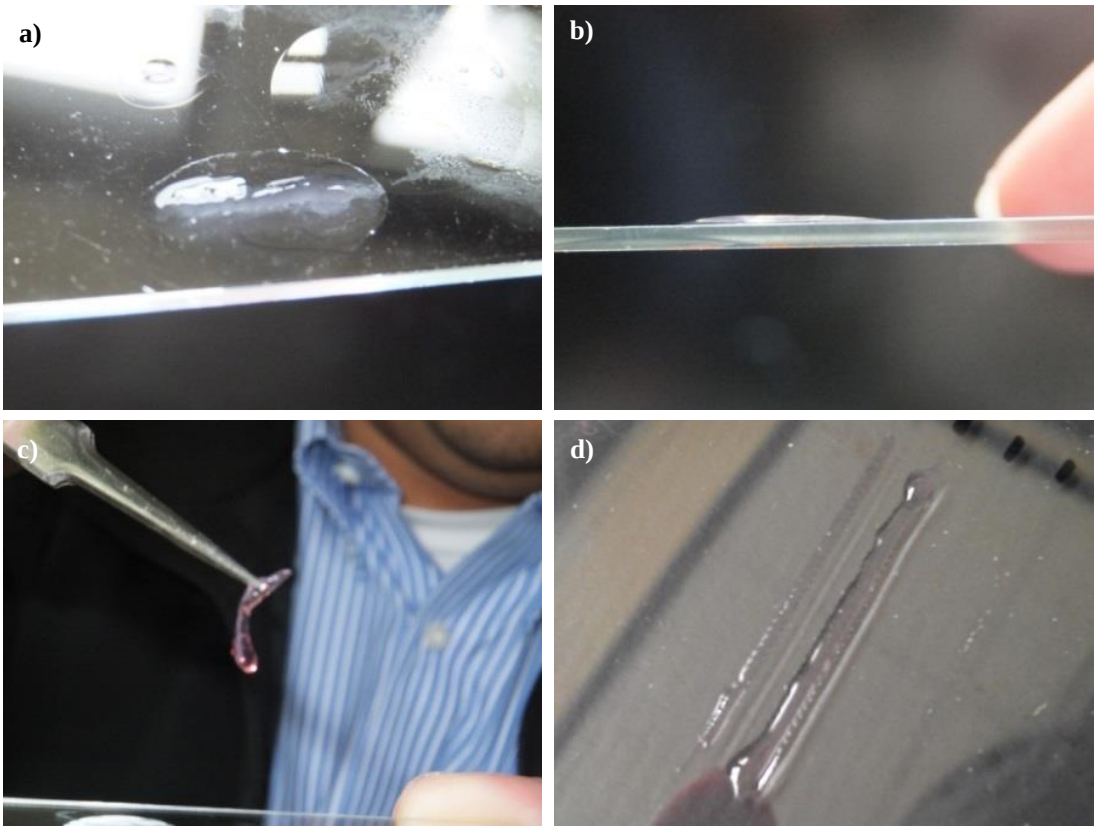

Figure 7.3 *– Simple linear printed alginate structures: a-c) 10 mm ten layer structure on a microscope slide viewed from above and the side, and being held with tweezers; d) two single layer linear hydrogel structures with different droplet sizes resulting in different line widths*

The bioprinter was able to deposit multiple alternating layers of alginate and calcium solutions in a contiguous linear structure. The resulting gel structures exhibited strong mechanical properties, were manipulatable and could even be removed from the substrate without fragmenting. Several different substrate surfaces were tested, including standard plastic Petri dishes and glass microscope slides, and it was noted that the droplets drift away from the intended target locations if the surface is too

hydrophobic, greatly reducing the spatial accuracy and repeatability of the bioprinter. However, if the surface is too hydrophilic, the droplets spread too much, reducing the resolution of the printed structures; it is therefore important to find the right surface on which to print accurate structures.

These structures are composed of a single layer of alginate and calcium solutions which form thin hydrogel structures. By depositing more alginate and calcium on top of these structures in the same pattern, three-dimensional structures can be built up layer-by-layer. Some simple circular patterns were designed with various diameters and number of layers. The results are shown in Figure 7.4.

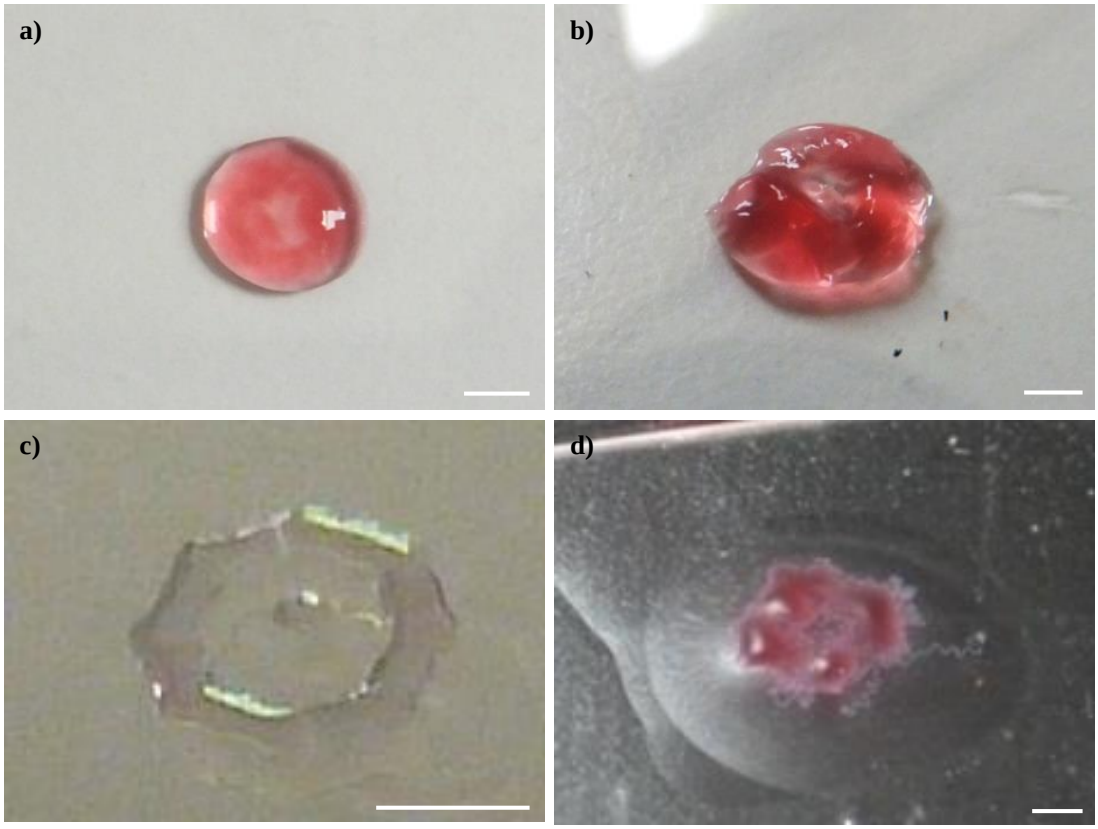

Figure 7.4 *– Simple circular printed alginate structures with red dye for improved visibility: a) 5 layer 5 mm diameter structure before the excess calcium solution was removed; b) 10 layer 5 mm diameter structure drained of excess calcium; c) 2 layer 3 mm diameter structure; d) resulting structure of reversed protocol: alginate printed onto calcium (scale bars 2 mm)*

The resulting structures were slightly more octagonal than circular and there were problems with the hydrogel spreading further as more layers were added (to the point that in some cases the hole in the centre was filled in). Another issue was that the structures were sometimes disjointed; this mainly occurred when the surface was too

hydrophobic, but it also happened at the beginning/end of the circle as shown in Figure 7.4b.

During one experiment the alginate and calcium solutions were reversed in order to determine if printing alginate onto the calcium solution would yield better structures. Figure 7.4d shows that this is not the case; the structure is more disjointed than the others and there are undesired superfluous tendrils of hydrogel leading away from the structure.

In order for this technique to be useful for tissue engineering applications, structures need to be taller to be considered truly three-dimensional. In order to increase the height of the printed structures, the concentration of alginate solution was increased from 1% to 2% to improve the mechanical strength of the hydrogel and allow it to support further layers. Square and circular structures with a large number of layers were designed and printed out. These resulting structures were photographed for analysis.

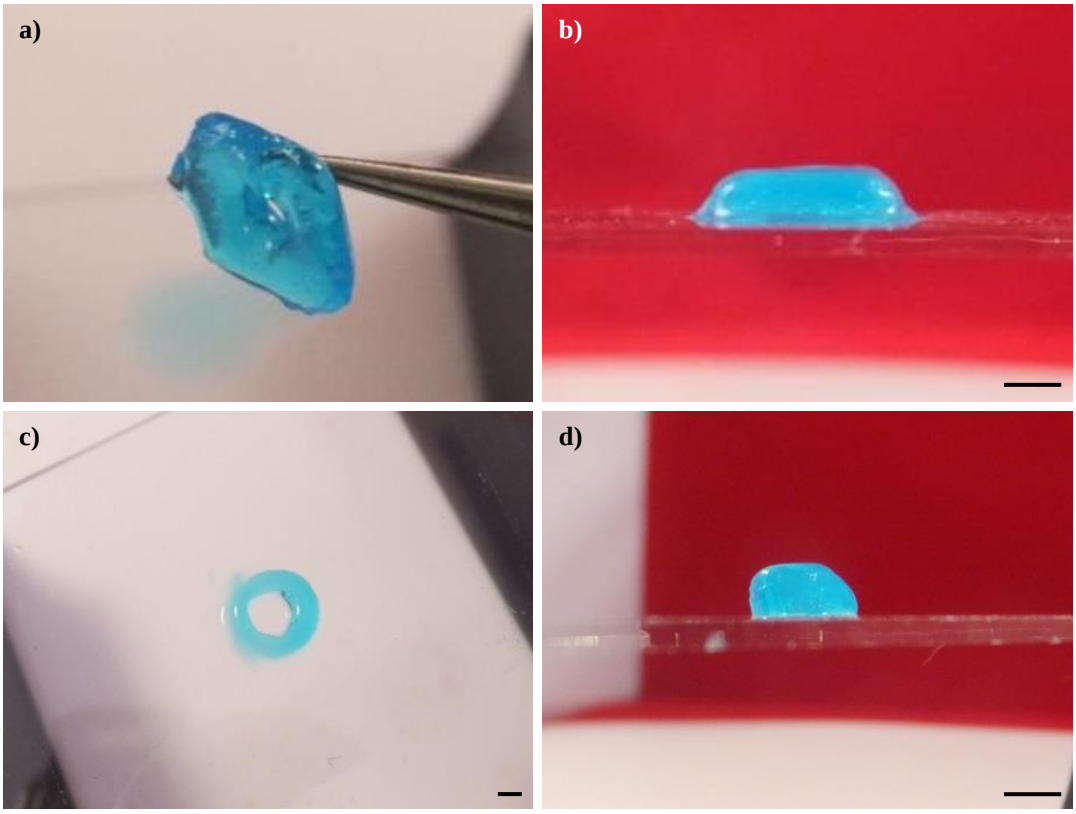

Figure 7.5 *– Tall 3D printed alginate structures with 20 layers: a-b) a 10 mm square shown being held with tweezers a) and from the side; and c-d) a 6 mm diameter circle shown from above and from the side (scale bars 2 mm)*

These taller structures were printed out in under twenty minutes. The square structure was strong enough to be physically manipulated with tweezers without deforming (as seen in Figure 7.5a); this demonstrates the high strength of the hydrogel. The structures spread slightly, but by slightly altering the volume ratio, concentrations and surface properties this spreading can be reduced.

7.3.3 Spot Size Shrinking

In order to examine the impact on the size of printed droplets, the concentration of alginate was reduced from 1% to 0.2% and the substrate surface was modified to be more hydrophilic using a plasma treatment machine (Zepto, Diener electronic). 0.2% alginate has many of the same characteristics as the DNA-based hydrogels used in chapter 8, most important of which is a similar viscosity range ensuring printed droplets would be a similar size.

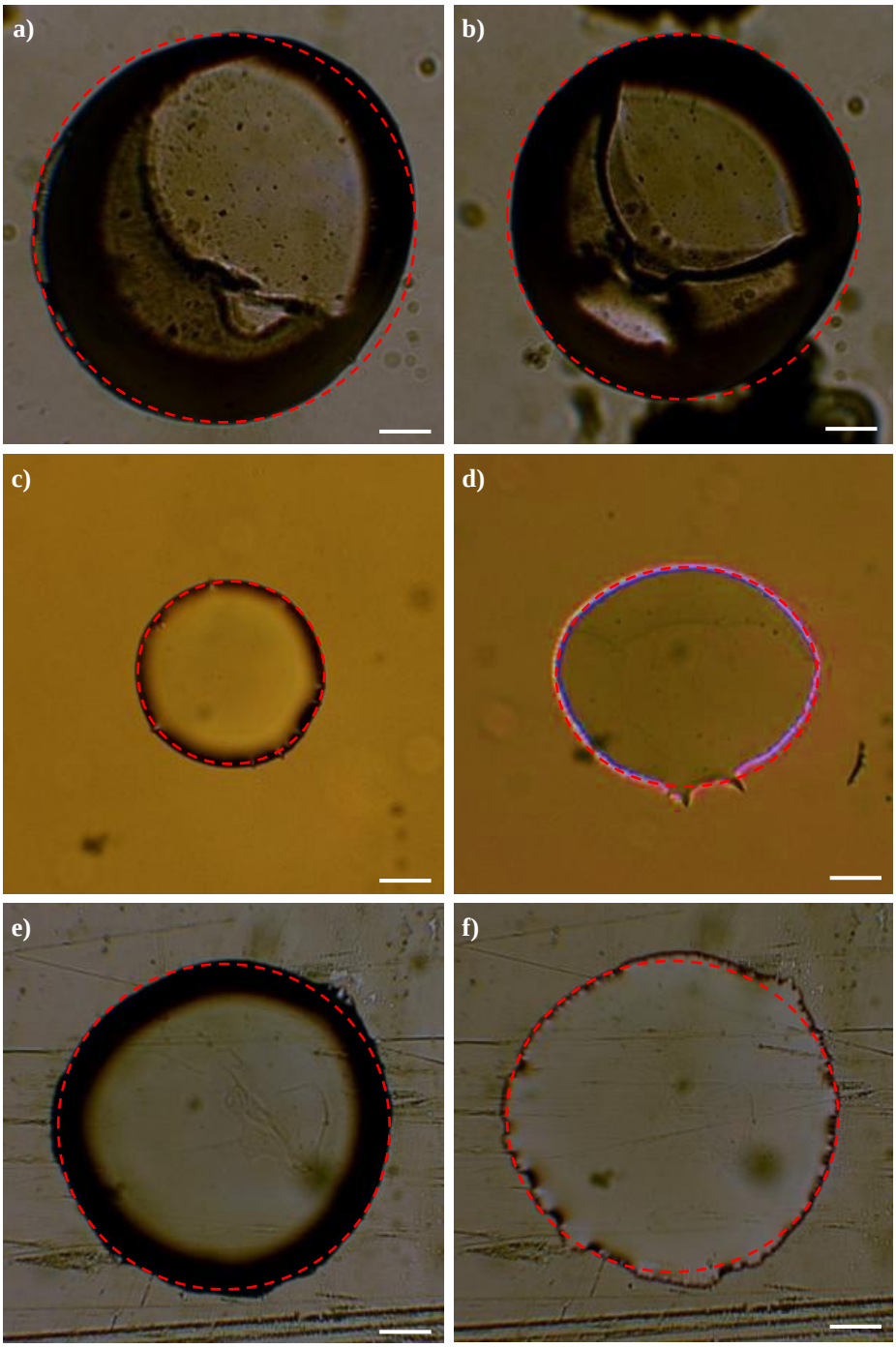

Figure 7.6 *– Results of the spot size shrinking experiment: a-b) 1% alginate on a Petri dish; c-d) 0.2% alginate on a Petri dish; e-f) 0.2% alginate on modified glass slide (scale bars 100 µm)*

As expected, on a Petri dish the 1% alginate droplets produced droplets approximately 715 µm in diameter whereas the 0.2% alginate droplets measured ~408 µm; smaller concentrations of alginate produce smaller hydrogel droplets. When this lower concentration of alginate was dispensed onto a glass substrate that had previously been plasma treated to be hydrophilic, the diameter of the droplets was much larger (~625 µm) due to spreading on the surface.

7.3.4 Hydrophilic Surface Modification

An attempt was made to improve the quality of the print, primarily the straightness and thickness of the hydrogel lines, by modifying the substrate surface. Slotted masks were laser cut with a variety of slot widths (2 mm, 1 mm, 0.8 mm, 0.6 mm, 0.4 mm, 0.2 mm and 0.1 mm); these masks were fixed to the surface of glass microscope slides before being treated with a plasma treatment machine (Zepto, Diener electronic). The resulting substrate had a hydrophobic surface with hydrophilic patches. Hydrogel lines were printed onto these patches and measured under a bright-field microscope.

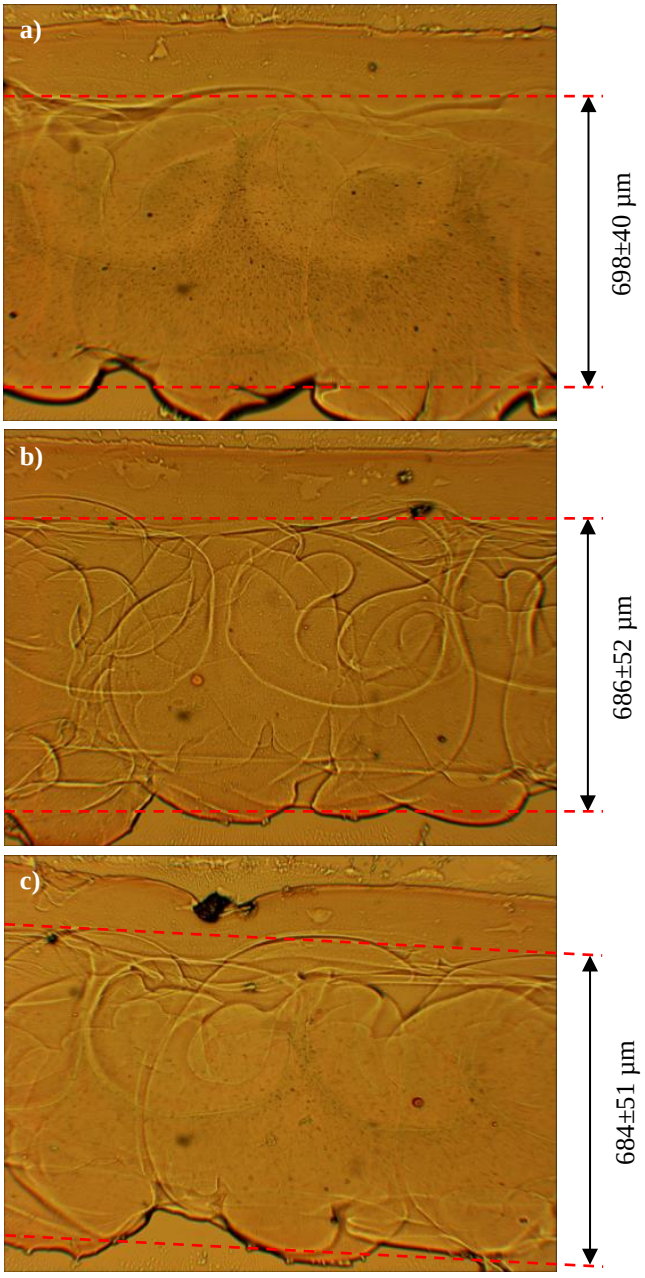

Figure 7.7 *– Printed hydrogel lines on hydrophilic treated patches: a) 0.8 mm; b) 0.7 mm; and c) 0.6 mm*

After printing, it was observed that each printed hydrogel line has almost the same width, regardless of the width of the hydrophilic patch. The hydrogel lines are also off-centre, even though the droplets are visibly in the center of the hydrophilic patches: this could be due to the nozzles used for this experiment, which were extremely thin and more flexible than desired; it is possible they were not precisely aligned in the x-axis. The lines themselves were straighter than those printed previously on uniform substrates.

It was apparent that printing out structures with different numbers of layers would result in different widths as well as different heights, but it was not clear how this would affect the final structure. Three different programs were created which described hydrogel lines with 3, 5 and 10 layers, which were printed out and analyzed using an electron microscope.

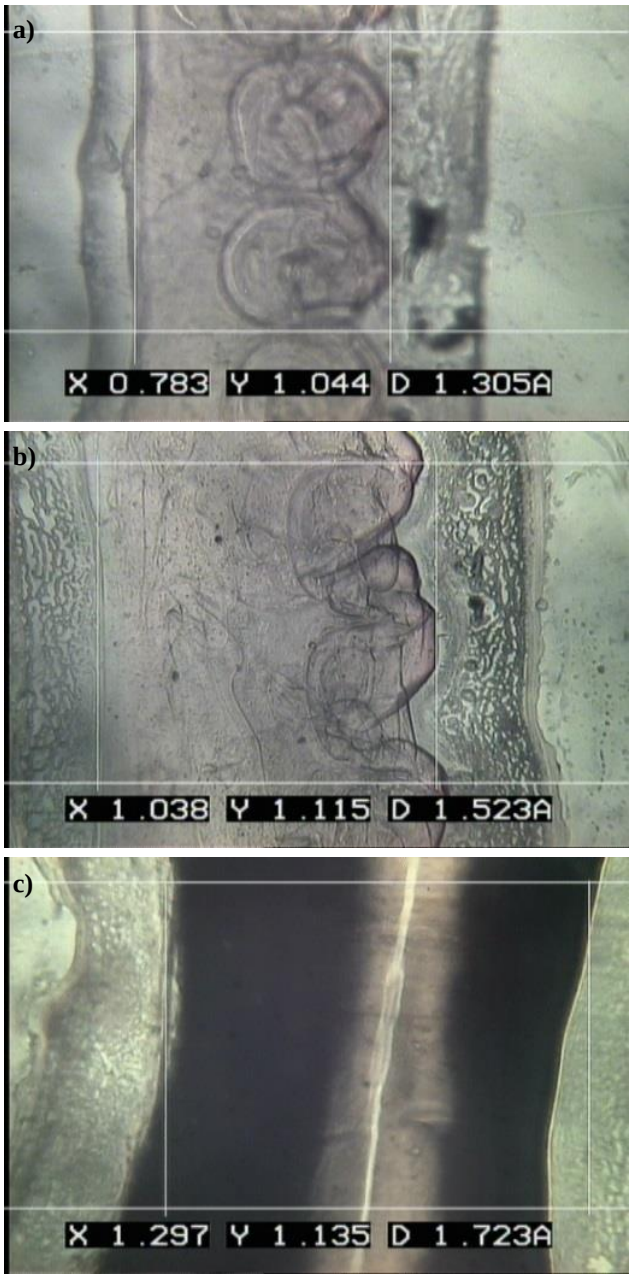

Figure 7.8 *– Images of multi-layer alginate hydrogel lines taken with an electron microscope: a) 3 layers = 0.81±0.06 mm; b) 5 layers =1.10±0.12 mm; c) 10 layers = 1.41±0.25 mm*

It is obvious that the lines are indeed spreading with increased number of layer but this increase is small; therefore, taller structures should not deform too much as the number of layers increases. The relationship can be expressed in the form of an equation:

$$w = 0.085(n) + 0.5633 \tag{7.1}$$

where *w* is the line width (in mm) and *n* is the number of layers.

7.3.5 Cell-laden Alginate Printing

As a simple first test of the bioprinters ability to pattern cells-laden hydrogels, HeLa cells were suspended in 0.2% sodium alginate solution and loaded into one of the deposition systems, with calcium solution in a second deposition system. Individual droplets were dispensed and viewed under the microscope immediately post-printing.

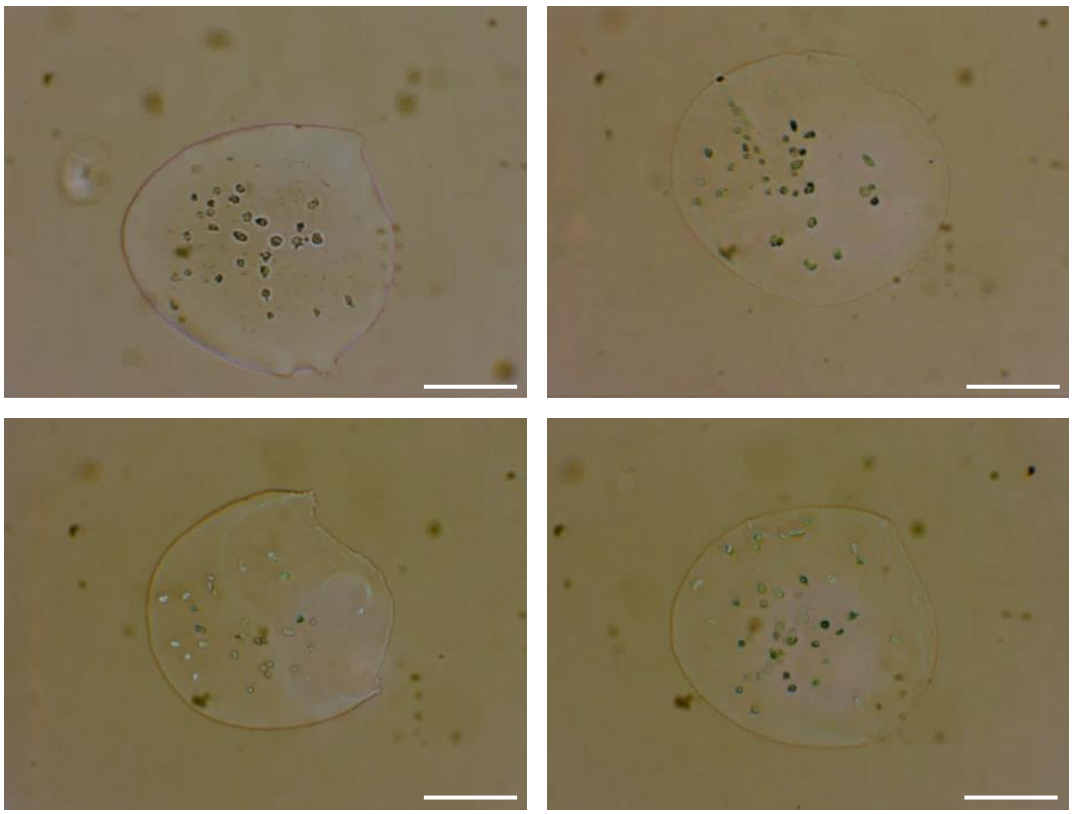

Figure 7.9 *– 0.2% alginate with HeLa cells (scale bars 250 µm)*

When observed under a microscope the cells were observed to be morphologically normal and healthy. No cellular debris was observed and the addition of cells to the hydrogel did not negatively affect the printer.

In order to verify that cells can indeed be patterned in 3D using hydrogel, a torus ring structure was designed with two different cell types (HeLa and 3T3) occupying different layers of the structure. Three deposition systems were used for this experiment: the first was loaded with HeLa cells suspended in 0.2% sodium alginate solution; the second was loaded with 3T3 cells suspended in 0.2% sodium alginate solution; and the third was loaded with calcium solution. The printed structure was observed through a bright-field microscope to check the position of the different cells.

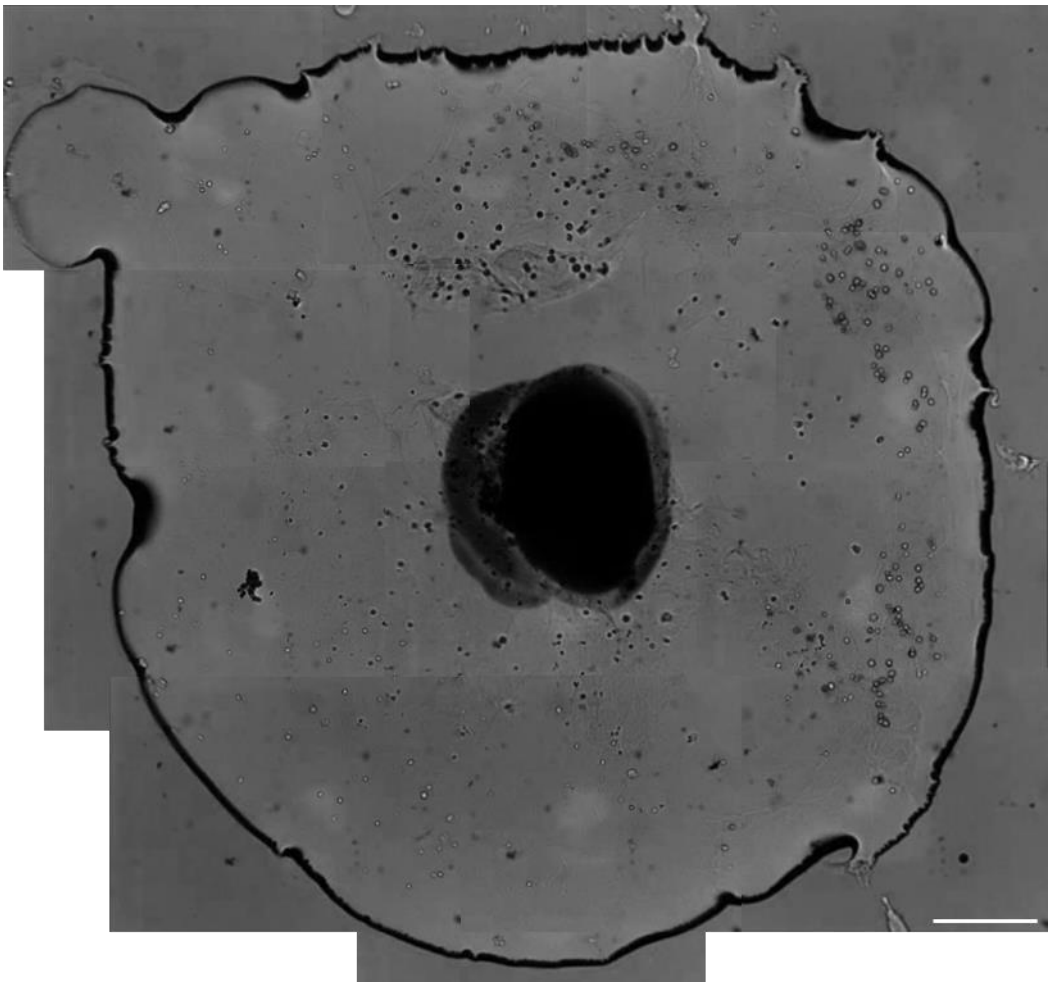

Figure 7.10 *– Multi-layer torus with HeLa and 3T3 cells suspended on different layers of the structure (scale bar 500 µm)*

By scanning through the height of the structure at different focal depths, the two different cells were found to be occupying different layers of the structure, proving that cells can be positioned at different heights as well as horizontal positions within a 3D bioprinted structure.

7.3.6 Complex Hydrogel Well Array

Hydrogel can also be used to create walled chambers for the separate culturing of multiple cell types on the same substrate. The hydrogel would allow for nutrient and chemical signal transfer whilst keeping the cells physically separate. Several programs were created with different numbers of chambers based on an overall square outline of 12 × 12 mm. These structures were printed out onto unmodified glass microscope slides.

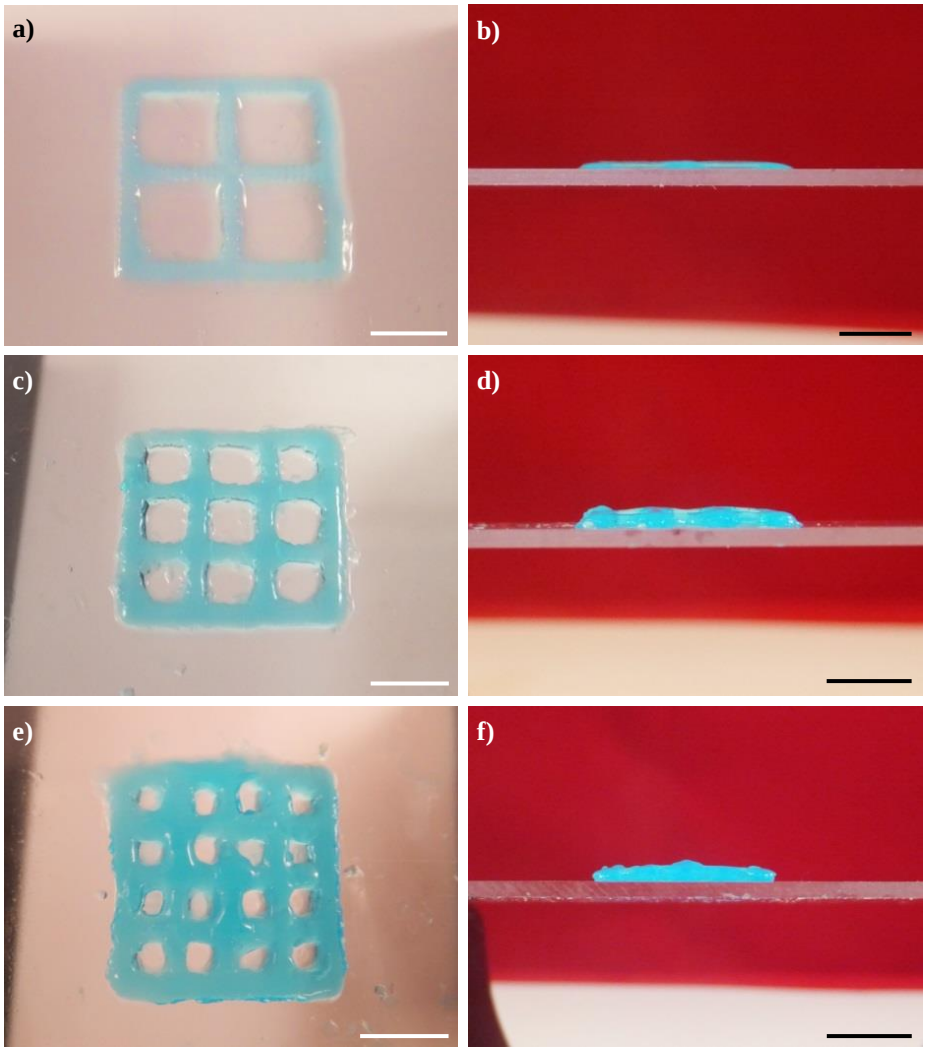

Figure 7.11 *– Hydrogel well array structures: a-b) 10 layer 2x2 viewed from a) the top and b) the side; c-d) 20 layer 3x3 viewed from c) the top and d) the side; e-f) 20 layer 4x4 viewed from e) the top and f) the side (scale bars 5 mm)*

The resulting complex well array structures were of reasonable quality, excess calcium solution having been manually drained with a pipette before imaging. The excess calcium served to support the structure as the hydrogel cross-linked which increased the resolution of the structure by preventing the hydrogel from spreading too far. This higher resolution is evident in Figure 7.11a, c and e as the line widths are almost unchanged, even though the height increases with double the number of layers.

Some minor deformation is visible in the structures, but this occurred post-printing during the excess calcium solution removal.

7.4 Hepatocyte-like Cell Creation

7.4.1 Cell Culture

Human embryonic stem cell lines RC-6, RC-7, RC-8, RC-9 and RC-10 and human induced pluripotent stem cell line RCi-22 were supplied by Roslin Cells Ltd for this research. The hES cells were cultured in complete StemPro® hESC SFM (supplement, DMEM/F-12, BSA, FGF basic, and 2-mercaptoethanol) (Life Technologies) supplemented with 8 ng/mL of human basic fibroblast growth factor (hbFGF) and the hiPS cells were cultured on Geltrex matrix with Essential 8 medium (Life Technologies). Cells were cultured in a laboratory incubator set at 36.0-37.5°C, 5.0±0.5% CO_2. Under these conditions the cells are maintained in an undifferentiated state.

7.4.2 Initial EB differentiation testing of hESC lines

Before hESCs can differentiate into mature hepatocytes, they must first become definitive endoderm. The first stage-specific hepatic marker the cells must produce is α-fetoprotein (AFP) which is expressed by foetal hepatoblasts (liver buds). In order to determine which (if any) of the available hESC lines had a predilection towards hepatic lineages, embryoid bodies were formed using the hanging drop technique and tested for AFP production.

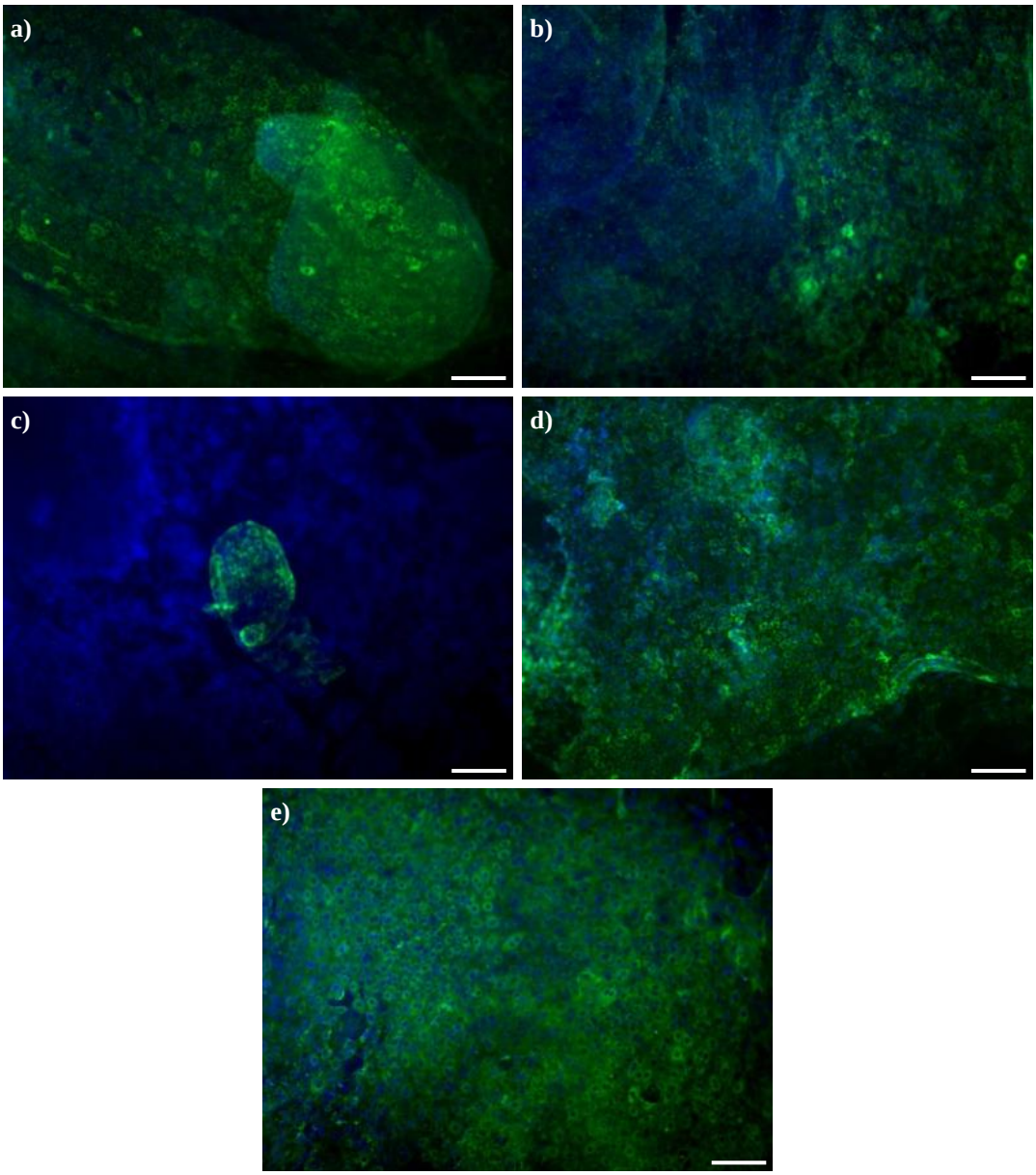

Figure 7.12 *– Fluorescence images of HLCs showing α-fetoprotein (AFP) production in green and DAPI in blue: a) hESC line RC-6; b) hESC line RC-7; c) hESC line RC-8; d) hESC line RC-9; e) hESC line RC-10 (scale bars 100 µm)*

Human ESC lines RC-6 and RC-9 showed good AFP production, line RC-7 had low production, line RC-8 was extremely poor, but line RC-10 showed the highest AFP expression and the cells had better morphology with increased size and bi-nucleation. However, the differentiation was undirected and better results could be achieved if a more controlled approach was adopted.

7.4.3 Directed differentiation of hPSCs into HLCs

A modified version of the three-step protocol devised by Hay et al. [23] was used to direct the differentiation of hESCs into hepatocyte-like cells (HLCs). After the hESCs

had reached a confluence level of 50-70%, StemPro® hESC SFM was replaced with RPMI-B27 medium (Invitrogen) and the hESCs were treated with activin A and Wnt 3a for three days. Following this, the cells were cultured in serum replacement medium (SR/DMSO: knockout-Dulbecco's modified Eagle's medium [KO-DMEM] containing 20% SR, 1 mM glutamine, 1% nonessential amino acids, 0.1 mM ß-mercaptoethanol, and 1% dimethyl sulfoxide [DMSO]) for 5 days. For the final maturation step, cells were cultured in L15 medium supplemented with 8.3% foetal bovine serum (FBS), 8.3% tryptose phosphate broth, 10 μM hydrocortisone 21-hemisuccinate, 1 μM insulin, and treated with 10 ng/mL hepatocyte growth factor (HGF) and 20 ng/mL oncostatin M (OSM) for nine days.

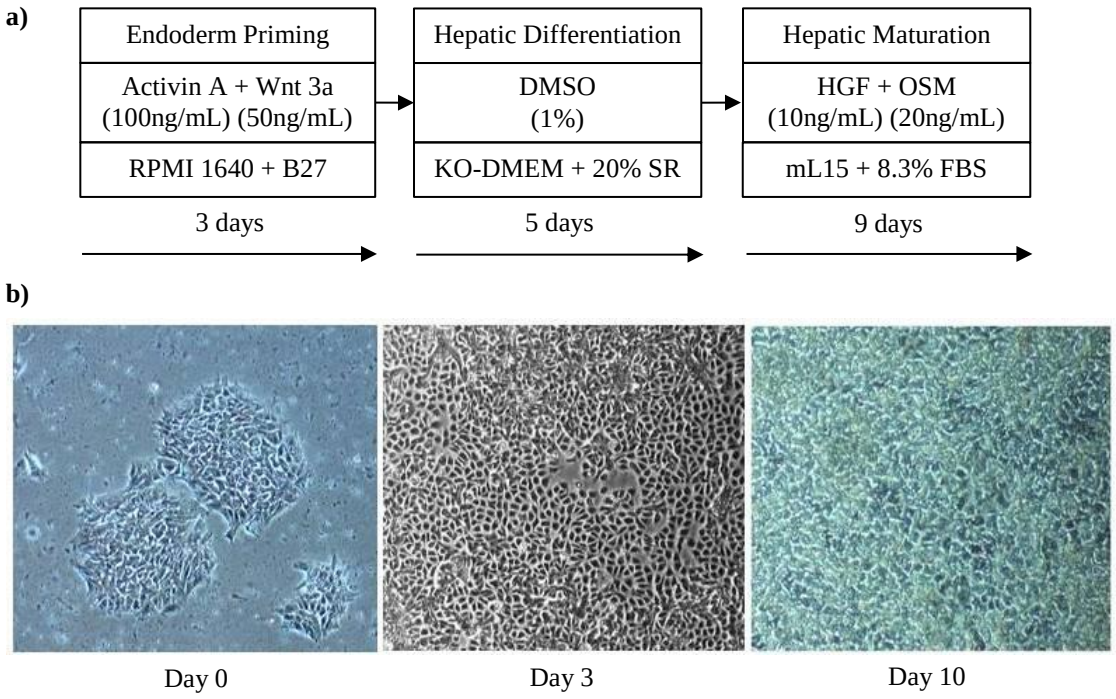

Figure 7.13 *– The three-step protocol used to differentiate hESCs into HLCs: a) Schematic representation of the three-steps; b) Images showing morphological changes from hESCs to HLCs*

Three different hESC lines (RC-6, RC-9 and RC-10) were subjected to the directed differentiation protocol in order to determine which, if any, had a tendency to produce better hepatocyte-like cells than the others. The cells should be positive for hepatocyte nuclear factor 4 alpha (HNF4α) if they have started differentiating into hepatocytes. As the cells mature they should begin to express albumin, which can only be synthesised in large quantities by mature hepatocytes (immature hepatocytes also express albumin but at much lower levels) [23,27].

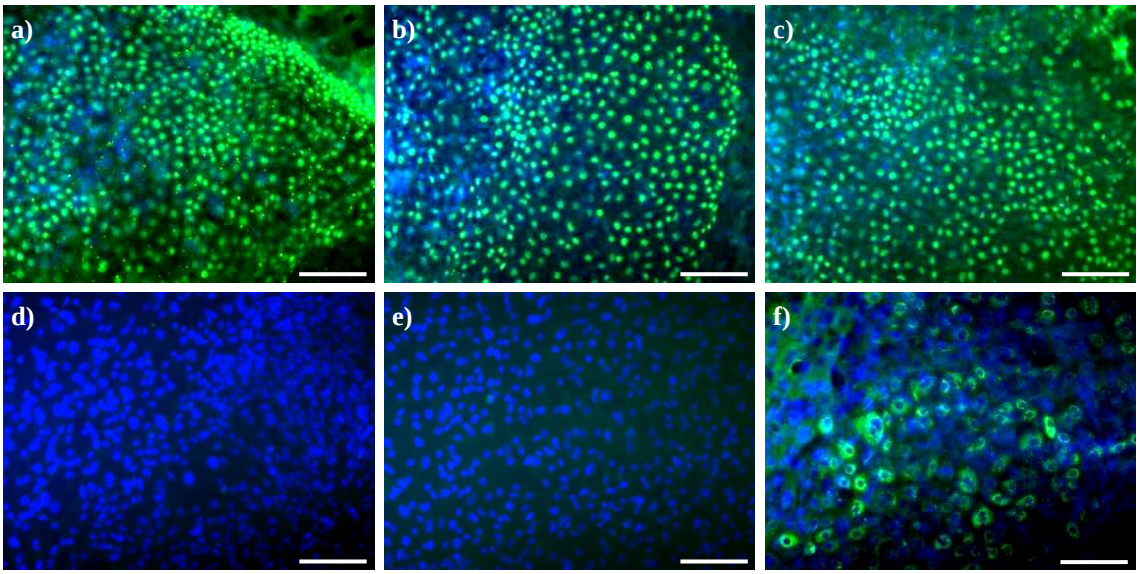

Figure 7.14 *– Fluorescence images of HLCs: (a-c) showing HNF4α expression in green and DAPI in blue: (a) hESC line RC-6; (b) hESC line RC-9; (c) hESC line RC-10; (d-f) showing albumin expression in green and DAPI in blue: (d) hESC line RC-6; (e) hESC line RC-9; (f) hESC line RC-10 (scale bars 100 µm)*

Of the three cell lines tested after being subjected to the directed differentiation protocol, all three were positive for hepatocyte nuclear factor 4 alpha but only line RC-10 also showed high albumin expression, indicating the presence of mature HLCs.

As hESC line RC-10 consistently outperformed all of the other tested lines, it was selected for further testing. A number of modifications were made to the differentiation protocol to improve the expression of the hepatocyte markers and a fresh batch of RC-10s was subjected to the modified protocol. In addition to HNF4α and albumin expression, the cells were also given an antibody for tight junction protein zona occludens 1 (ZO-1), which stains the cell-cell boundaries to check the cell morphology. Undifferentiated RC-10 cells provided the negative control.

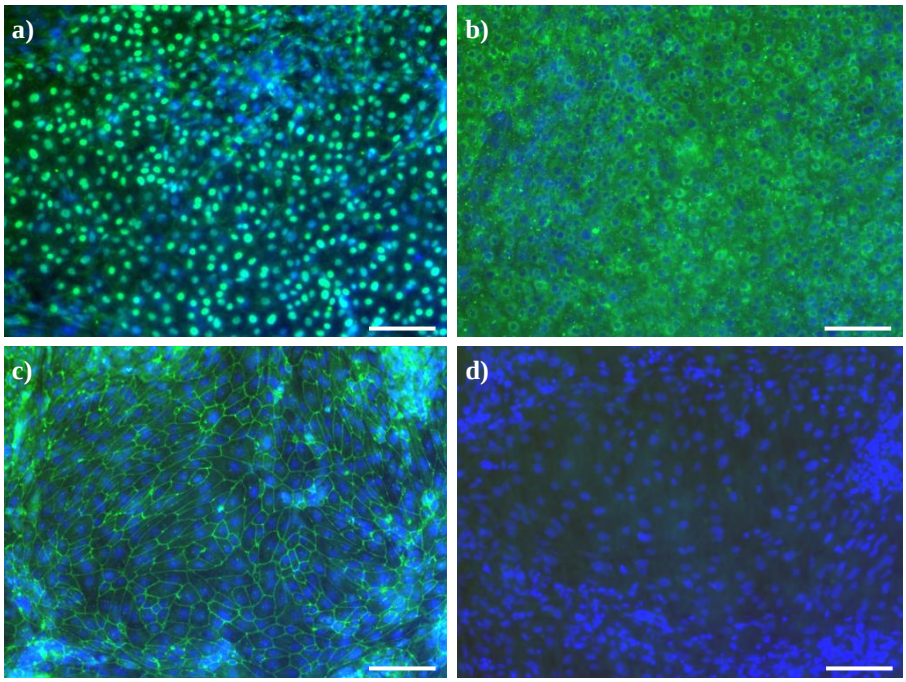

Figure 7.15 *– Fluorescence images of day 17 HLCs showing hepatocyte marker expression in green and DAPI in blue: a) HNF4α; b) Albumin; c) ZO-1; d) Negative Control (scale bars 100 µm)*

The resulting cells remained positive for HNF4α, were highly positive for albumin, and albumin ELISAs have shown that there is good albumin secretion. The ZO-1 antibody shows that the cells have hepatocyte-like morphology.

7.4.4 Bioprinting HLCs

During the course of the experimental work it was discovered that cells were the most stable at day 6 through the differentiation process, so a large quantity of day 6 HLCs were prepared to ascertain whether the bioprinting process affected the differentiation when in progress. Cells were differentiated up to day 6 and frozen until a sufficient population was available for printing. Subsequently, the day 6 HLCs were thawed, dissociated into single cells and printed into the wells of a 12-well plate. Printing was carried out using a pulse time of 8 ms at an inlet pressure of 8 PSI. Non-printed cells were included as a control. Once the cells had adhered to the surface after printing, the differentiation protocol was resumed. On day 17 the cells were fixed and stained for hepatic markers (albumin and HNF4α); ZO-1 was used to check the morphology of the cells.

Both hESC- and hiPSC-derived HLCs were bioprinted, with the latter having some minor modifications to the differentiation protocol regarding culture media.

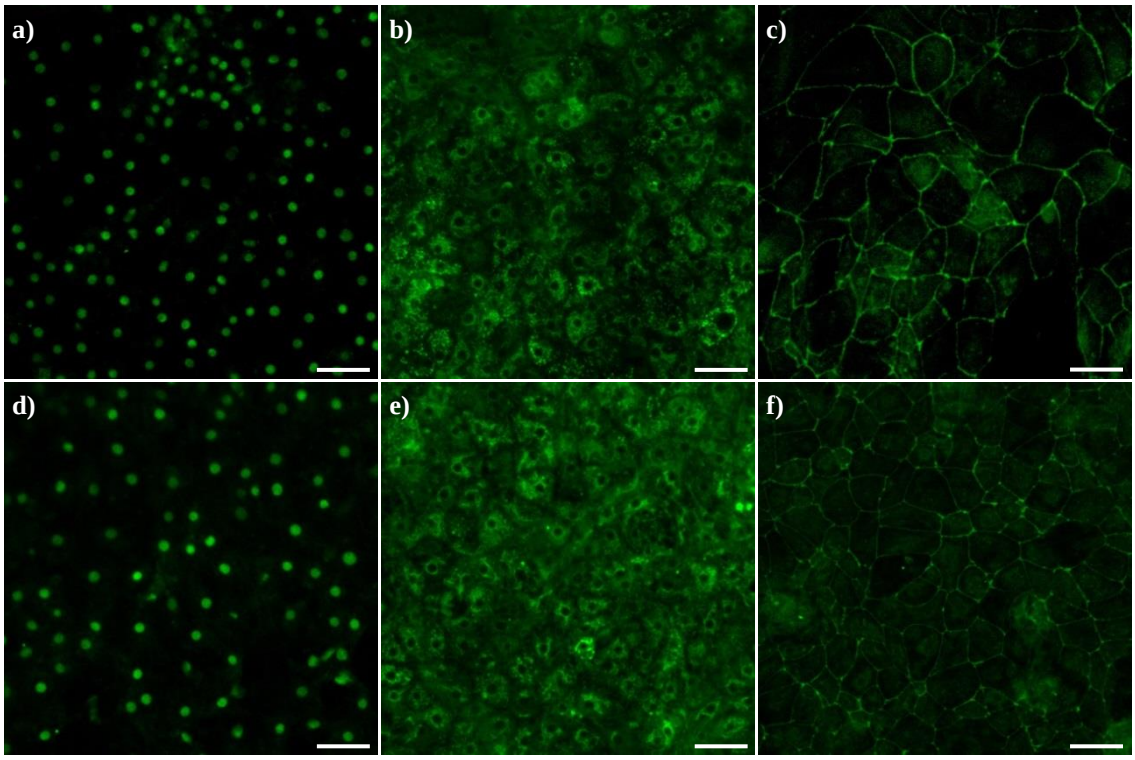

Figure 7.16 *– Fluorescence images of printed hESC-derived hepatocytes showing hepatocyte marker expression in green: a-c) control: a) HNF4α; b) Albumin; c) ZO-1. d-f) printed: d) HNF4α; e) Albumin; f) ZO-1 (scale bars 50 µm)*

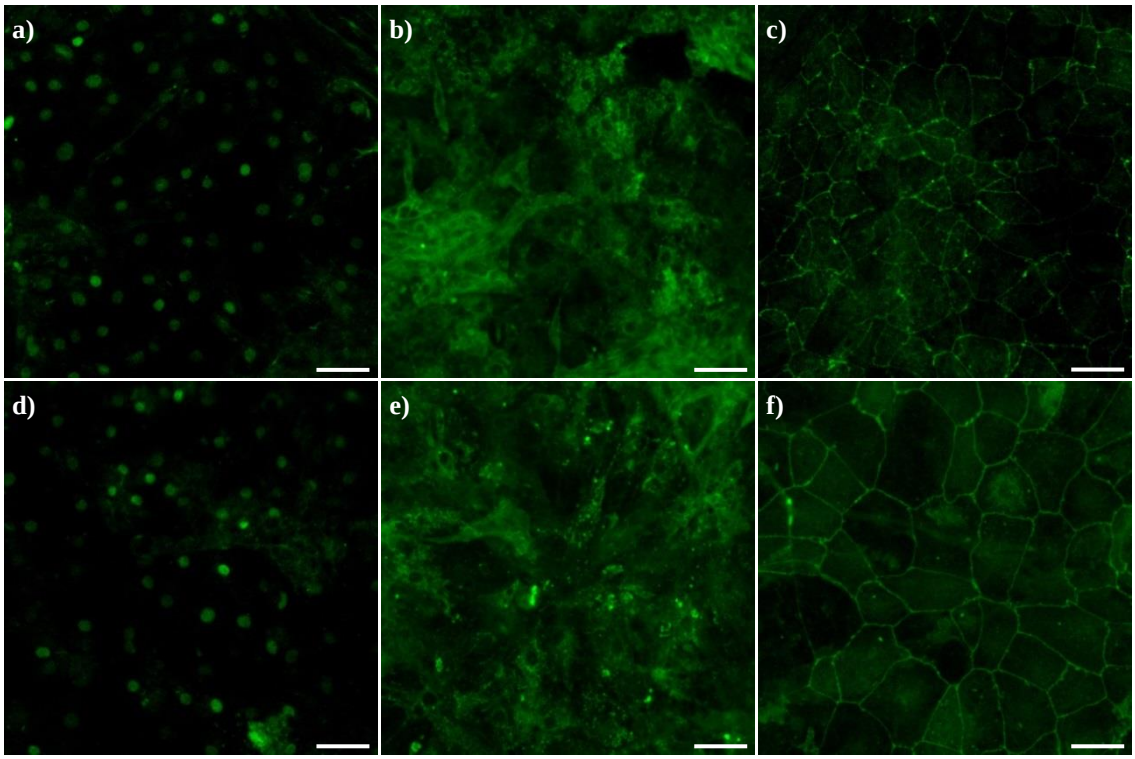

Figure 7.17 *– Fluorescence images of printed hiPSC-derived hepatocytes showing hepatocyte marker expression in green: a-c) control: a) HNF4α; b) Albumin; c) ZO-1. d-f) printed: d) HNF4α; e) Albumin; f) ZO-1 (scale bars 50 µm)*

When the cells were compared to the unprinted control, there was virtually no difference between them. The tight junctions form clearly and are well defined in both cases, demonstrating that the cells have good morphology. The average cell size appears to be slightly smaller in the printed sample but this is to be expected as cells were more confluent. This result indicates that the HLCs can be printed using the valve-based bioprinter during directed differentiation without interrupting the differentiation or changing the lineage of the cells.

7.5 Printing HLC Co-culture with Supporting Cells

The process of *in vivo* liver organogenesis occurs in the developing foregut, when newly specified hepatic cells separate from the endodermal sheet and form a dense hepatoblast (liver bud) which is quickly vascularised [28,29]. The hepatic progenitor cells interact strongly with stromal cells (comprising hepatic sinusoidal endothelial cells, hepatic stellate cells, and Kupffer cells), which help to control various aspects of hepatic development such as the promotion of outgrowth from the initial liver bud [29]. Therefore, in order to create micro-liver tissue *in vitro*, a co-culture of stromal cells, vasculature endothelial cells, and hepatocytes would be required. The ideal ratio of cells required to form a liver-like micro-tissue was then investigated.

7.5.1 Cell Culture

Human embryonic stem cell line RC-10 was supplied by Roslin Cells Ltd for this research. The hES cells were cultured in complete StemPro® hESC SFM (supplement, DMEM/F-12, BSA, FGF basic, and 2-mercaptoethanol) (Life Technologies) supplemented with 8 ng/mL of human basic fibroblast growth factor (hbFGF). Human hepatic stellate cells in hepatic/pancreatic stellate growth medium and human umbilical vein endothelial cells in endothelial growth medium were purchased from ZenBio, Inc. Cells were cultured in a laboratory incubator set at 36.0-37.5°C, 5.0±0.5% CO_2. Under these conditions the cells are maintained in an undifferentiated state.

7.5.2 Manual Co-Culture

As each cell type is pre-cultured in different media, it was important to establish that they could be cultured in a single common medium for this co-culture experiment. Human umbilical vein endothelial cells (HUVECs), hepatic stellate cells and HLCs had their old media aspirated and were re-suspended in the same culture medium (L15) before being manually plated on a 24-well plate. The cells were stained with different

fluorescent markers so that they could be differentiated using a fluorescent microscope; HUVECs were stained with Vybrant and the hepatic stellate cells with DAPI. The cells were monitored under the microscope at 24 hours after printing.

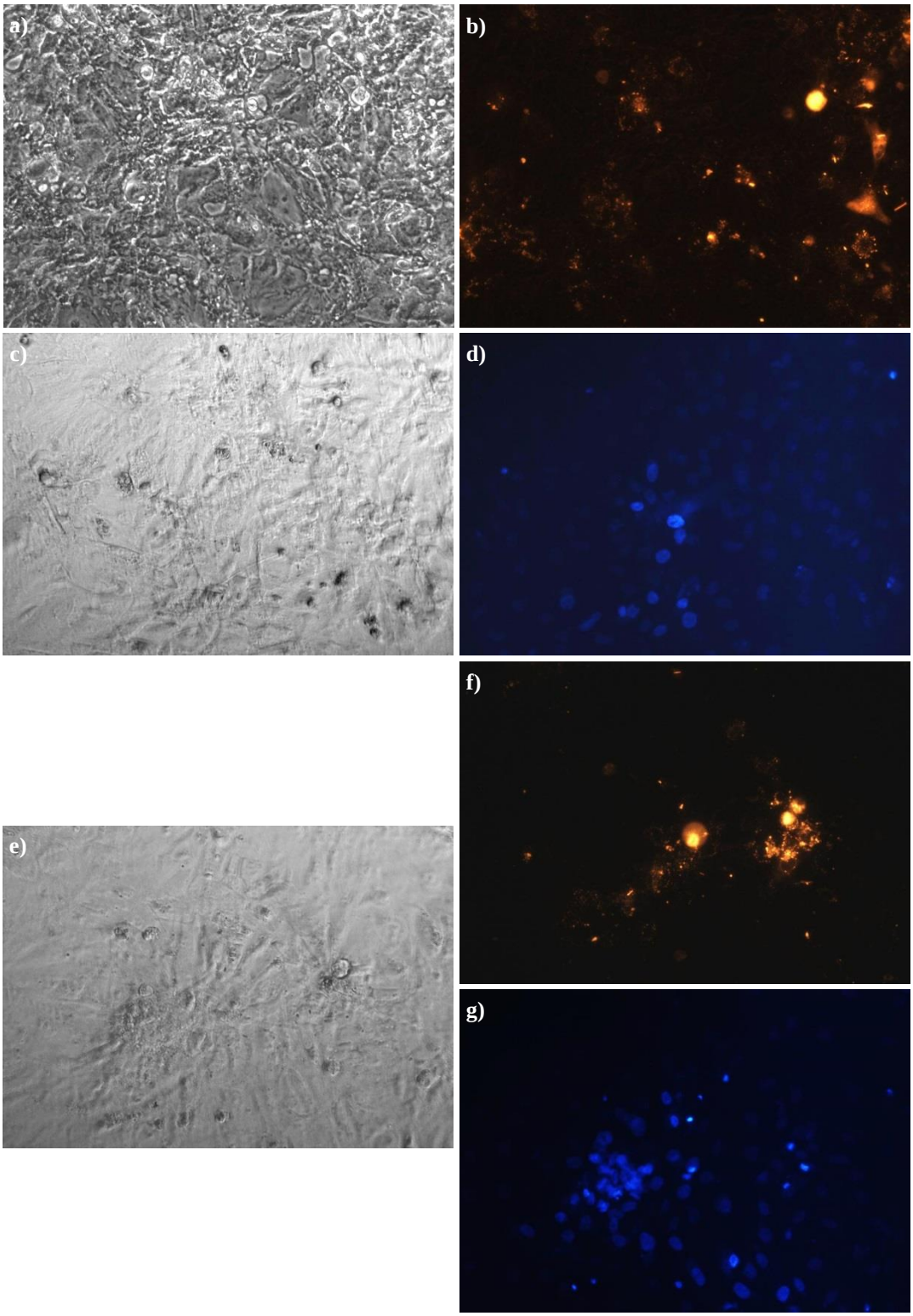

Figure 7.18 *– Co-culture of HUVECs, hepatic stellate cells and HLCs: a-b) HLCs and HUVECs co-culture a) phase contrast, b) vybrant stain showing HUVECs; c-d) HLCs and stellates co-culture c) phase contrast, d) DAPI stain showing stellates; e-g) HLCs, HUVECs and stellates co-culture e) phase contrast, f) vybrant stain showing HUVECs, g) DAPI stain showing stellates*

All three cell types were found to be viable in the co-culture, demonstrating that the cells can be cultured together in a single medium without any detrimental effects.

7.5.3 2D Gradient of Supporting Cells

An experiment was devised to attempt to determine the correct ratio of supporting cells required to form a micro-liver. 96-well plates would be used as the substrate for this experiment. 20 µL of Hepatocytes suspended in media would be added to 36 wells of the 96-well plate. Two programs were written to describe two perpendicular volume gradients from 20 µL to 0 µL, similar to those used in section 6.4.2. One of the bio-ink reservoirs would be loaded with vasculature endothelial cells suspended in medium, while the other would be loaded with stellate cells suspended in medium. The resulting array of 36 wells would have a constant concentration of HLCs, but two perpendicular gradients of supporting cells with every combination of ratios decreasing in 20% intervals.

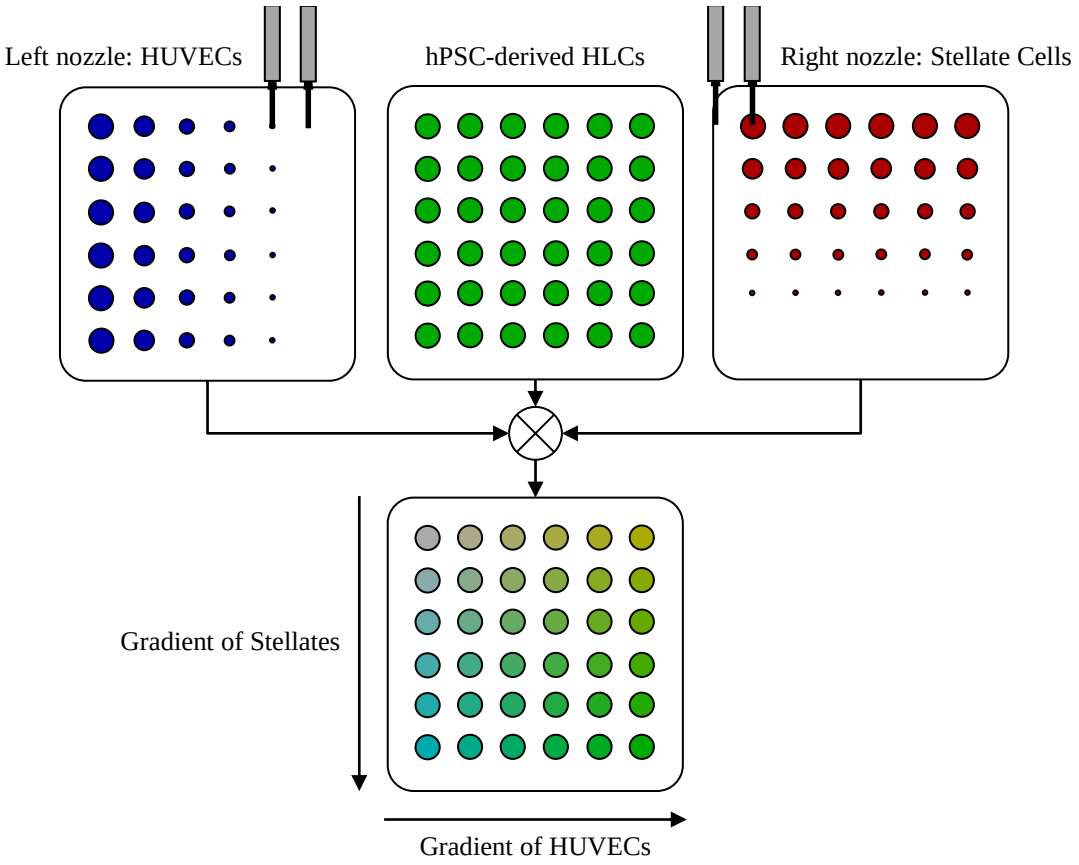

Figure 7.19 *- Schematic of the combinatorial printing process for creating a 2D gradient of supporting cells over an array of hepatocyte-like cells*

RC-10 hESCs at a concentration of 1×10^6 cells/mL were manually seeded into 36 wells of a 96-well plate (20 µL in each well) and differentiated according to the protocol described earlier. In order to dispense the required 20 µL maximum volume, the pressure was set at 3.6 PSI and the pulse time to 720 ms. HUVECs at a concentration of approximately 7.5×10^5 cells/mL loaded into the left reservoir. The other reservoir was loaded with hepatic stellate cells at a concentration of approximately 7.5×10^5 cells/mL. At day 14 of the differentiation process, the perpendicular gradients of HUVECs and stellates were printed over the differentiating cells, resulting in droplets representing multiple variations of ratios between the supporting cells. The cells were cultured for 48 hours in a CO_2 incubator at 36.0-37.5°C, 5.0±0.5% CO_2 to allow the supporting cells to integrate with the existing HLC cell matrix prior to a media change and the resumption of the differentiating protocol. The cells were sacrificed and analysed for cytochrome P450 (CYP) activity using the Promega Glo assay at day 20 and day 22 of HLC differentiation.

Stellate cells and HUVECs were also printed without HLCs on day 14 to act as a negative control for the Promega Glo assay by providing a background CYP level. A manual version of the experiment was also carried out to act as a positive control to identify any possible variation caused by the printing process.

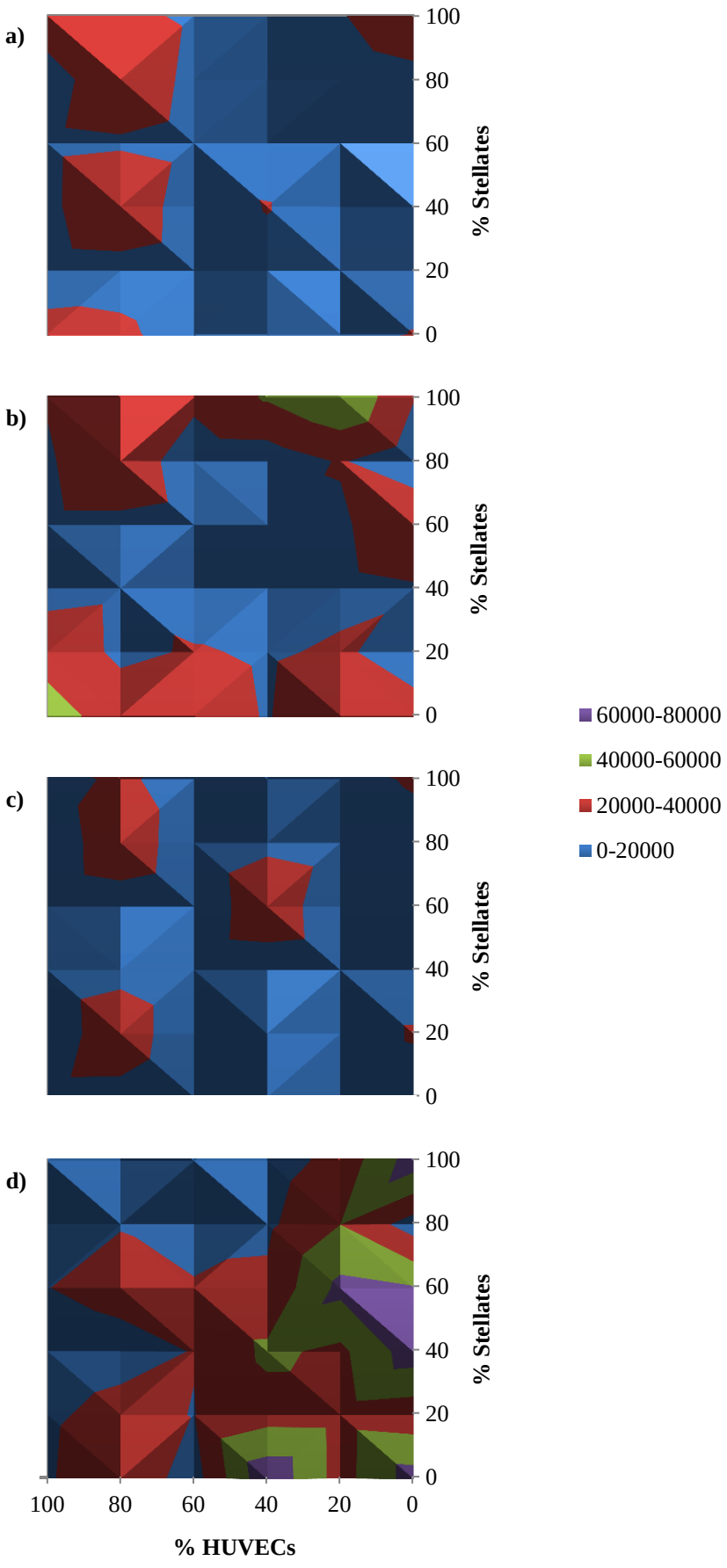

Figure 7.20 *– Average CYP level per sample for each combination of HUVECs, stellates and HLCs: a-b) Day 20 – a) printed; b) manual control; c-d) Day 22 – c) printed; d) manual control*

The results, although visually appealing, did not result in a clear indication of optimal co-culture conditions. There was also very little correlation between the samples or clear patterns on the plates and wells without stellate or endothelial cells sometimes had higher CYP activity than those with both supporting cells. However, a positive result was that there was no contamination present and the cells appeared to be still viable.

7.6 Conclusions

These experiments demonstrate that the valve-based printing process is capable of patterning hydrogels with reasonably high resolution, even for complex and tall structures. Because the volume and component ratios of each droplet in a programmed structure can be specified, the system is able to create specific conditions for specific hydrogel properties and structure resolution, and even create different mechanical properties at different points in the printed structures.

The ability to print cells encapsulated in 3D hydrogel structures will allow the creation of more accurate human tissue models, which would be extremely useful for *in vitro* cell studies including drug development or even drug production.

A number of different hESC lines were directed to differentiate into HLCs and the resulting cells were examined for the expression of a number of hepatic factors. Line RC-10 was found to result in the best HLCs, being positive for nuclear factor 4 alpha while also secreting albumin; the morphology was also found to be similar to that of hepatocytes. It was shown that cells can be printed during directed differentiation without interrupting the differentiation or changing the lineage of the cells. This is important as it means that these cells can be patterned in 3-dimensions using the bioprinter while differentiating, which will greatly speed up the creation of mini-liver tissue structures. The ability to print human pluripotent stem cells (both hESCs and hiPSCs) whilst maintaining their pluripotency or directing their differentiation into specific lineages will allow us to create more accurate human tissue models, which is essential to the *in vitro* drug development and toxicity-testing. Additionally, this may also pave the way for human stem cells to be incorporated into clinical protocols, either for patient implantation of *in vitro* regenerated organ or direct *in vivo* cell printing for tissue regeneration.

Supporting cells were dispensed with HLCs in various ratios in an attempt to improve the function of the HLCs. Unfortunately, there were no clear improvements in CYP levels, and there was little correlation between the printed and control groups. Further optimisation of this experiment is clearly required.

7.7 References

[1] Khalil S, and Sun W, (2009). "Bioprinting Endothelial Cells With Alginate for 3D Tissue Constructs," *Journal of Biomechanical Engineering*, **131**(11), p. 111002.

[2] Wüst S, Müller R, and Hofmann S, (2011). "Controlled Positioning of Cells in Biomaterials—Approaches Towards 3D Tissue Printing," *Journal of Functional Biomaterials*, **2**(4), pp. 119–154.

[3] Huh D, Hamilton GA, and Ingber DE, (2011). "From 3D cell culture to organs-on-chips," *Trends in Cell Biology*, **21**(12), pp. 745–754.

[4] Dunn JC, Yarmush ML, Koebe HG, and Tompkins RG, (1989). "Hepatocyte function and extracellular matrix geometry: long-term culture in a sandwich configuration.," *The FASEB journal*, **3**(2), pp. 174–177.

[5] Tan W, and Desai TA, (2004). "Layer-by-layer microfluidics for biomimetic three-dimensional structures," *Biomaterials*, **25**(7-8), pp. 1355–1364.

[6] Guillotin B, and Guillemot F, (2011). "Cell patterning technologies for organotypic tissue fabrication," *Trends in Biotechnology*, **29**(4), pp. 183–190.

[7] Peppas NA, Hilt JZ, Khademhosseini A, and Langer R, (2006). "Hydrogels in Biology and Medicine: From Molecular Principles to Bionanotechnology," *Advanced Materials*, **18**(11), pp. 1345–1360.

[8] Burdick JA, and Murphy WL, (2012). "Moving from static to dynamic complexity in hydrogel design," *Nat Commun*, **3**, p. 1269.

[9] Slaughter BV, Khurshid SS, Fisher OZ, Khademhosseini A, and Peppas NA, (2009). "Hydrogels in Regenerative Medicine," *Advanced Materials*, **21**(32-33), pp. 3307–3329.

[10] Drury JL, and Mooney DJ, (2003). "Hydrogels for tissue engineering: scaffold design variables and applications," *Biomaterials*, **24**(24), pp. 4337–4351.

[11] Hoffman AS, (2002). "Hydrogels for biomedical applications," *Advanced Drug Delivery Reviews*, **54**(1), pp. 3–12.

[12] Dickson M, and Gagnon JP, (2009). "The Cost of New Drug Discovery and Development," *Discovery Medicine*, **4**(22), pp. 172–179.

[13] Kaitin K, (2010). "Deconstructing the Drug Development Process: The New Face of Innovation," *Clin Pharmacol Ther*, **87**(3), pp. 356–361.

[14] Paul SM, Mytelka DS, Dunwiddie CT, Persinger CC, Munos BH, Lindborg SR, and Schacht AL, (2010). "How to improve R&D productivity: the pharmaceutical industry's grand challenge," *Nature Reviews Drug Discovery*, **9**, pp. 203–214.

[15] Kolaja K, (2014). "Stem Cells and Stem Cell-derived Tissues and Their Use in Safety Assessment," *J. Biol. Chem.*, **289**(8), pp. 4555–4561.

[16] Huh D, Matthews BD, Mammoto A, Montoya-Zavala M, Hsin HY, and Ingber DE, (2010). "Reconstituting Organ-Level Lung Functions on a Chip," *Science*, **328**(5986), pp. 1662–1668.

[17] Murry CE, and Keller G, (2008). "Differentiation of Embryonic Stem Cells to Clinically Relevant Populations: Lessons from Embryonic Development," *Cell*, **132**(4), pp. 661–680.

[18] Fenno LE, Ptaszek LM, and Cowan CA, (2008). "Human embryonic stem cells: emerging technologies and practical applications," *Current Opinion in Genetics & Development*, **18**(4), pp. 324–329.

[19] Itskovitz-Eldor J, Schuldiner M, Karsenti D, Eden A, Yanuka O, Amit M, Soreq H, and Benvenisty N, (2000). "Differentiation of human embryonic stem cells into embryoid bodies compromising the three embryonic germ layers.," *Mol Med*, **6**(2), pp. 88–95.

[20] Xu F, Sridharan B, Wang S, Gurkan UA, Syverud B, and Demirci U, (2011). "Embryonic stem cell bioprinting for uniform and controlled size embryoid body formation," *Biomicrofluidics*, **5**(2), pp. 22207–15.

[21] Gage FH, (2000). "Mammalian Neural Stem Cells," *Science*, **287**(5457), pp. 1433–1438.

[22] Hay DC, Fletcher J, Payne C, Terrace JD, Gallagher RCJ, Snoeys J, Black JR, Wojtacha D, Samuel K, Hannoun Z, Pryde A, Filippi C, Currie IS, Forbes SJ, Ross JA, Newsome PN, and Iredale JP, (2008). "Highly efficient differentiation of hESCs to functional hepatic endoderm requires ActivinA and Wnt3a signaling," *PNAS*, **105**(34), pp. 12301–12306.

[23] Hay DC, Zhao D, Fletcher J, Hewitt ZA, McLean D, Urruticoechea-Uriguen A, Black JR, Elcombe C, Ross JA, Wolf R, and Cui W, (2008). "Efficient Differentiation of Hepatocytes from Human Embryonic Stem Cells Exhibiting

Markers Recapitulating Liver Development In Vivo," *STEM CELLS*, **26**(4), pp. 894–902.

[24] Fedorovich NE, Alblas J, de Wijn JR, Hennink WE, Verbout AJ, and Dhert WJA, (2007). "Hydrogels as Extracellular Matrices for Skeletal Tissue Engineering: State-of-the-Art and Novel Application in Organ Printing," *Tissue Engineering*, **13**(8), pp. 1905–1925.

[25] Kong H-J, Lee KY, and Mooney DJ, (2002). "Decoupling the dependence of rheological/mechanical properties of hydrogels from solids concentration," *Polymer*, **43**(23), pp. 6239–6246.

[26] Shoichet MS, Li RH, White ML, and Winn SR, (1996). "Stability of hydrogels used in cell encapsulation: An in vitro comparison of alginate and agarose," *Biotechnology and Bioengineering*, **50**(4), pp. 374–381.

[27] Yan Y, Wang X, Pan Y, Liu H, Cheng J, Xiong Z, Lin F, Wu R, Zhang R, and Lu Q, (2005). "Fabrication of viable tissue-engineered constructs with 3D cell-assembly technique," *Biomaterials*, **26**(29), pp. 5864–5871.

[28] Takebe T, Sekine K, Enomura M, Koike H, Kimura M, Ogaeri T, Zhang R-R, Ueno Y, Zheng Y-W, Koike N, Aoyama S, Adachi Y, and Taniguchi H, (2013). "Vascularized and functional human liver from an iPSC-derived organ bud transplant," *Nature*, **499**(7459), pp. 481–484.

[29] Si-Tayeb K, Lemaigre FP, and Duncan SA, (2010). "Organogenesis and Development of the Liver," *Developmental Cell*, **18**(2), pp. 175–189.

Chapter 8 – 3D Bioprinting of Smart DNA-based Hydrogels

8.1 Introduction

Polymeric hydrogels, such as those discussed in the previous chapter, can suffer from a number of limitations including poorly defined structure and irreversible bonds [1–3]. Recently, new types of hydrogel have been developed: supramolecular hydrogels, which are composed of low molecular weight organic compounds and water molecules, have self-healing properties and reversible formation due to their transient crosslinks [2–9]; and DNA-based hydrogels, which do not require organic solvents or harsh formation conditions but can be cross-linked by enzymes and self-assemble nano-structures [10–18].

Hybrid hydrogels can be created by combining DNA-based hydrogels with traditional polymeric hydrogels. However, most so-called DNA-hybrid hydrogels use acrylic to form carbon-carbon backbones which seriously limits their applications due to the non-biodegradability of acrylic [17,19,20]. Polypeptide-based hydrogels show great promise due to their biocompatibility, biodegradability, easy incorporation of functional groups and well-defined sub-structures [21–25]. Prior to this research, no hydrogels have been developed that successfully combined the unique properties of DNA and polypeptide materials.

Researchers at Tsinghua University have recently created a novel hybrid hydrogel with a broad range of programmable properties that could be used interactively with living cells. This chapter contains the report of the first investigation into the polypeptide-DNA hybrid supramolecular hydrogel that exhibits the positive attributes of both polypeptide and DNA components. The rapid and gentle *in situ* formation of the hydrogel from two low viscosity components makes it suitable and attractive for use with 3D bioprinting platforms to produce small structures with tissue-like architectures containing embedded viable and functional cells. The biocompatibility of the hydrogel, and its components was verified using 3D cell viability assays, verifies its suitability for use in tissue engineering applications [26–28].

8.2 Project Acknowledgements

The project was performed in collaboration with Juan Jin, Chuang Li and Yijie Wang from Tsinghua University, Beijing, China who provided the DNA-based hydrogels, and Dr. Alison Dun and Prof. Rory Duncan from the Life Science Interface Laboratory at

Heriot-Watt University. The Life Science Interface Laboratory provided the cells and associated medium used in the following experiments, in addition to access to and the use of an incubator and super-resolution microscopes for the analysis of experimental results.

8.3 Polypeptide-DNA Hydrogels

The hydrogel used in this section of the research is a novel two-component polypeptide-DNA hybrid supramolecular hydrogel. This hydrogel can be formed *in situ* in seconds under physiological conditions by the simple mixing of two building materials (polypeptide-DNA conjugate and complimentary DNA linker). The mechanical properties of the hydrogel can be adjusted by altering the relative molar ratio of the two components, the length of the "sticky ends" and the environmental pH. Experiments investigating responses to multiple physical and biological stimuli – such as temperature, salts, pH, enzymes and proteases – can be designed due to the polypeptide-DNA hybrid structures. The hydrogel networks can be broken down in several ways: the dehybridization of DNA upon heating (cooling will rehybridize the hydrogel networks); the digestion of DNA linker by the addition of specific DNA restriction enzymes; or the breakdown of the polypeptide backbone by the addition of protease. Due to the two-component nature of the hydrogel, it is highly applicable for tissue engineering applications using bioprinting techniques.

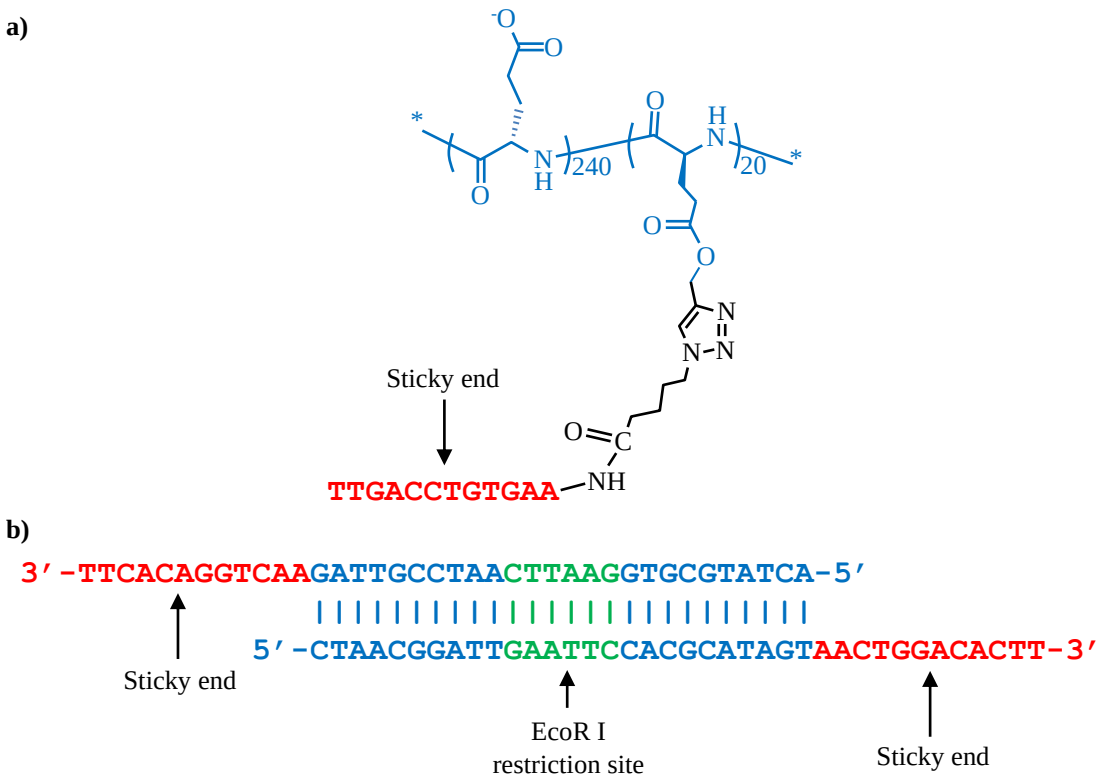

Figure 8.1 *– Molecular structures of the polypeptide-DNA hybrid hydrogel components: a) polypeptide-DNA conjugate and b) DNA linker*

The hybrid hydrogel can be made by mixing two components: the polypeptide-DNA conjugate, which is a polypeptide backbone grafted with multiple single strand DNA nucleotides (ssDNA) that act as "sticky ends"; and the DNA linker which is a double stranded DNA nucleotide (dsDNA) with two "sticky ends", complimentary to those in the polypeptide-DNA conjugate.

DNA sequences were synthesised using a DNA synthesiser (ABI 394) following the standard phosphoramidite DNA synthesis protocol [29,30] and purified by high-performance liquid chromatography (HPLC). The following items were purchased: restriction enzymes BamH I and EcoR I (TaKaRa Biotech Company, Dalian, China); endoproteinase Glu-C (Sigma-Aldrich Co. LLC). Hydrogel structures were bioprinted by dispensing an array of droplets of polypeptide-DNA conjugate solution from the left nozzle and then overprinting droplets of DNA linker solution from the right. After a few seconds, the DNA self-assembles to form a hydrogel matrix. If adjacent droplets overlap they gel together and form a single contiguous layer.

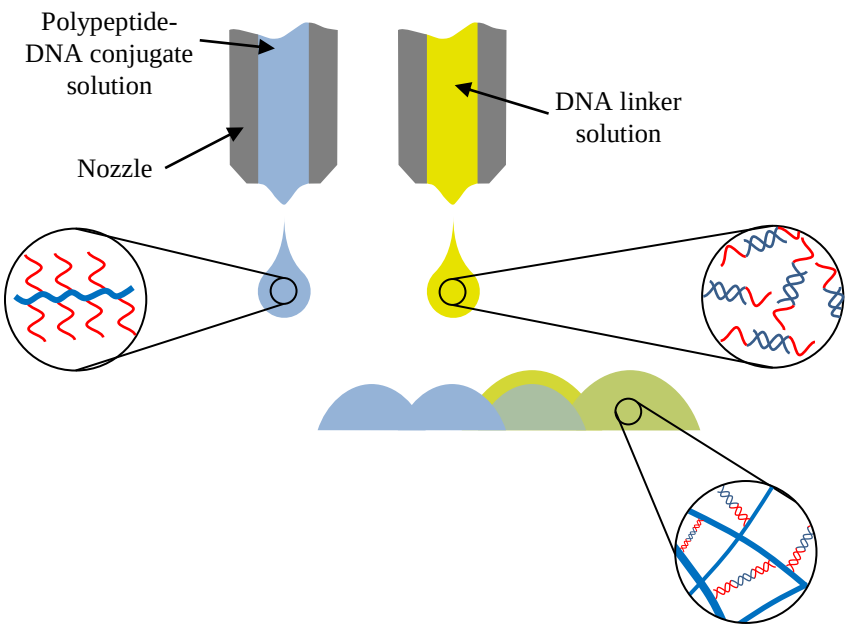

Figure 8.2 *– Schematic of the combinatorial printing process for polypeptide-DNA hydrogel creation.*

The largest challenge encountered during the research described in this chapter was the extremely small quantity of polypeptide-DNA conjugate and DNA linker that was provided by Tsinghua University. This was due to the extremely complex and time-consuming process of preparing the polypeptide-DNA conjugate and DNA linker components. Therefore, more of the preliminary characterisation experiments were carried out with alginate which, at a low concentration, had similar properties to polypeptide-DNA hydrogel. This led to a number of experimental variables that had to be reactively fine-tuned during the experimental process.

When the polypeptide-DNA hydrogel was used, only 100 µL was available of each component for testing purposes; therefore, minimal volumes had to be loaded into the deposition systems for printing. However, there had to be sufficient volume loaded to prime the system while maintaining a meniscus seal around the feeder tube between the valve and the cartridge throughout the entire experiment. If the seal broke, air would enter the feeder tube and disrupt the size of the droplets being generated. The solution to this issue was to use mineral oil as a buffer solution. Mineral oil was loaded on top of the hydrogel components and, as the oil does not mix with the water-based hydrogel components, it remains in a layer on top [31]. This is shown in Figure 8.3 below. Volumes as low as 10 µL were successfully dispensed using this technique.

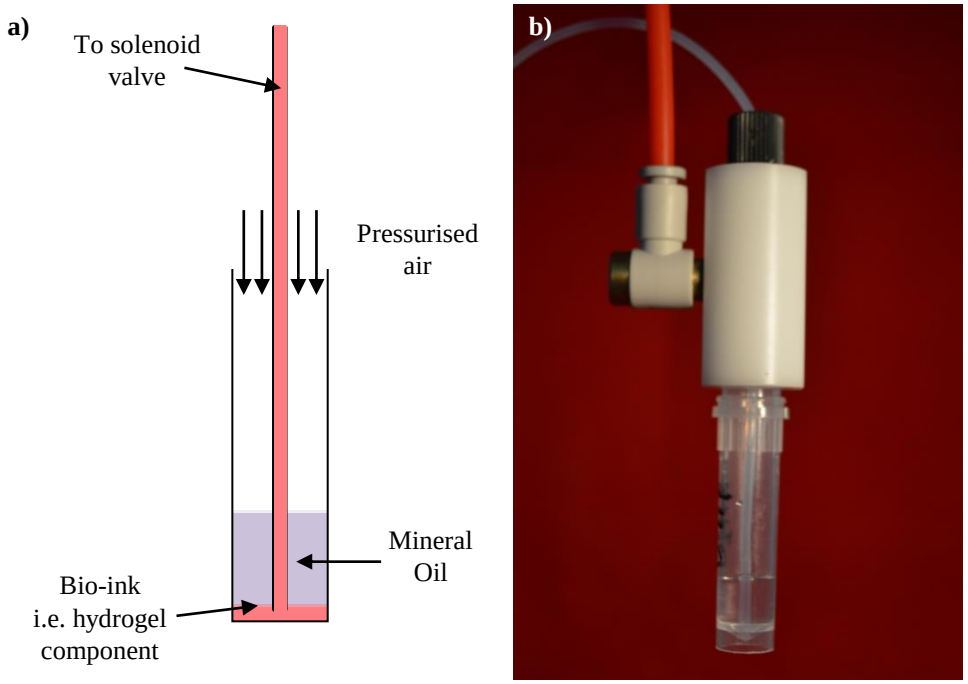

Figure 8.3 *– a) Detailed schematic of the oil buffer setup for small volume dispensing; b) Photograph of the setup*

Chitosan hydrogels were also investigated in parallel with the alginate testing as a precursor to using DNA-based hydrogels. Unfortunately, chitosan hydrogels take much longer to crosslink than alginate and DNA-based hydrogels so they did not serve as analogues for the DNA-based hydrogels.

8.4 Array Printing

In order to characterise the size of printed polypeptide-DNA hydrogel droplets, the inlet pressures were set to nominal values (derived experimentally) to dispense the smallest possible droplets. Droplets of hydrogel are formed *in situ* by alternately printing polypeptide-DNA conjugate and DNA linker at the same point. A simple array of 25 droplets, with 3 mm spacing between each droplet, was designed. The volume gradient was provided by increasing the number of layers in each successive column by one. 100 µL each of polypeptide-DNA conjugate (6 wt.%) and DNA linker (2 mM) were loaded into separate cartridges of the bioprinter and the array was printed.

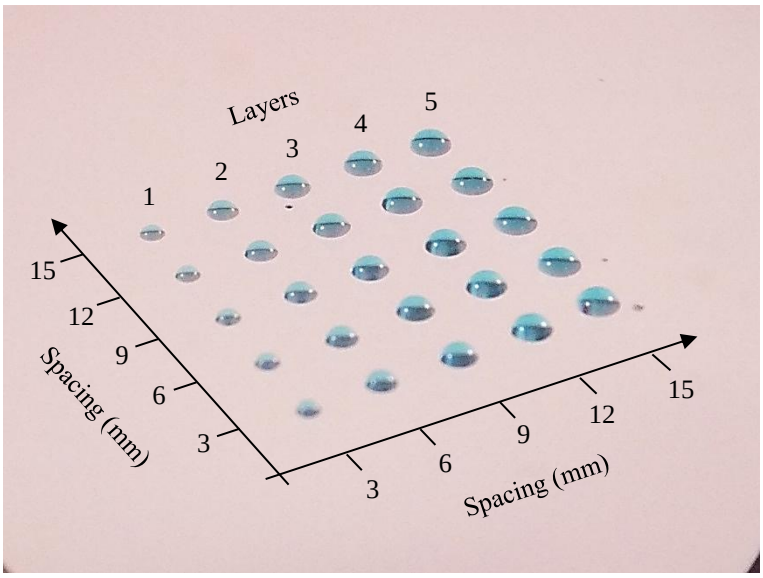

Figure 8.4 *– An array of printed Polypeptide-DNA hydrogel droplets with an increasing volume gradient by overprinting droplets (blue dye added for improved visibility)*

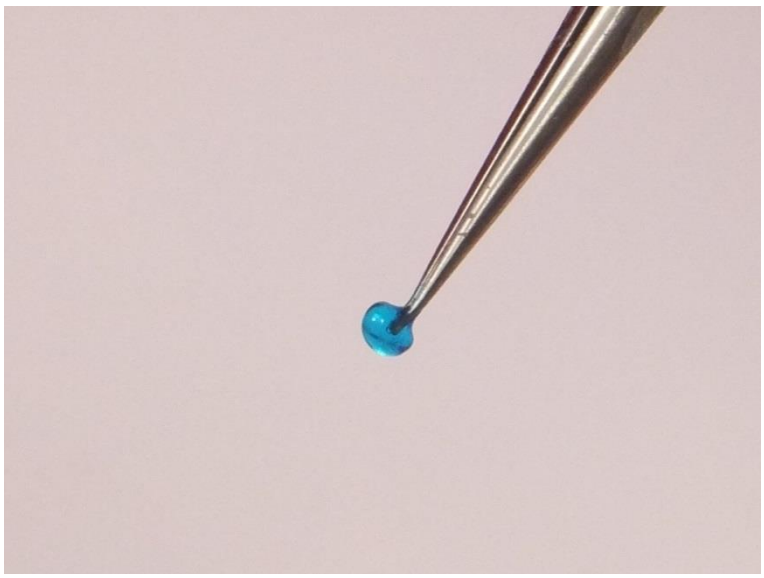

Figure 8.5 *– A single 20 layer droplet structure printed with polypeptide-DNA hydrogel (blue dye added for improved visibility)*

The smallest printed hydrogel droplet measured approximately 500 µm in diameter and 80 µm in height, equalling a volume of approximately 60 nL. Gel formation occurred very rapidly (in only a few seconds), though it should be noted that this could be due to the small volume and lower diffusion distance of the created droplets. Hydrogel droplets were created from up to 20 layered droplets. Each was found to be mechanically strong, sufficient to be physically manipulated with tweezers without fragmenting. It should be noted that crosslinking occurred in all three dimensions and the final printed structures were solid and contiguous. This is most likely due to the way the hydrogel is formed in situ in a layer-by-layer approach.

8.4.1 Complex Structure Printing

More complex multi-layer structures were designed, including simple geometric shapes and alphabetic letters; since the polypeptide-DNA hydrogel came from Tsinghua University, the letters "THU" were designed; "HWU", for Heriot-Watt University, were also designed.

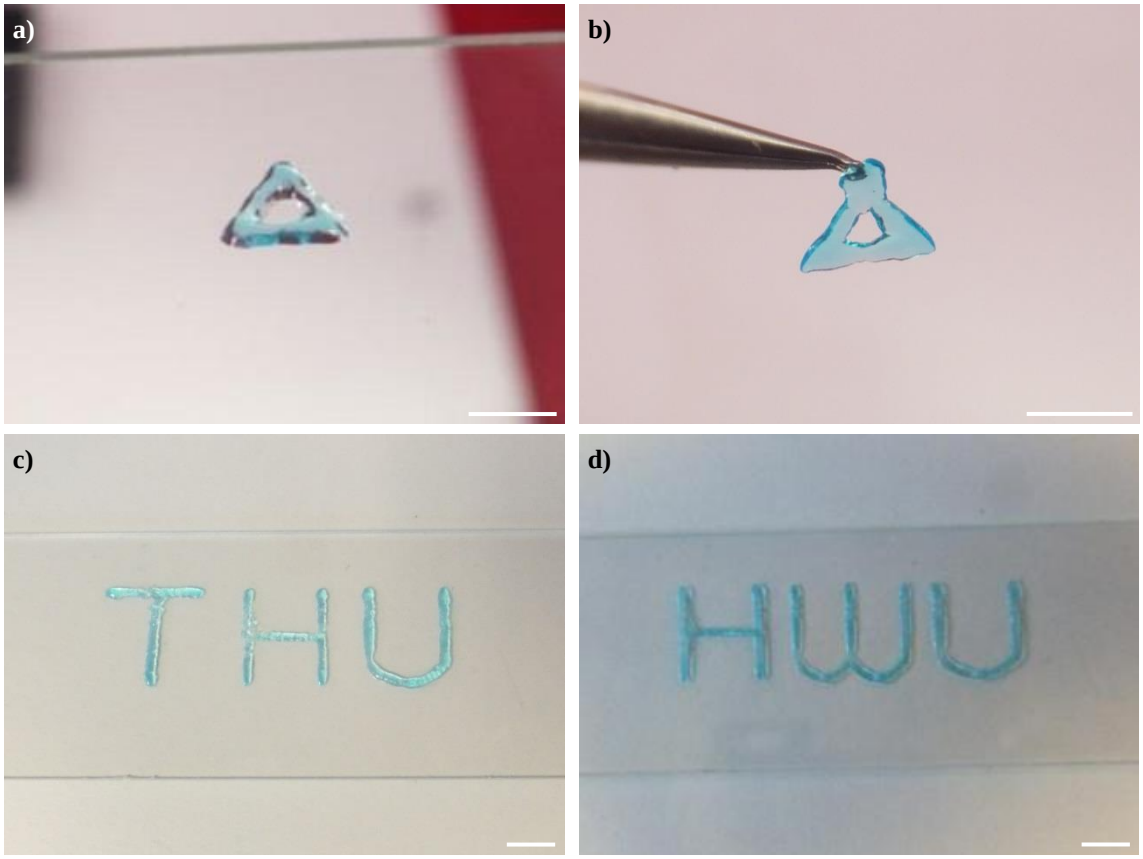

Figure 8.6 *– Complex polypeptide-DNA hydrogel 3D bioprinted structures with blue dye added for improved visibility: a-b) 5 mm equilateral triangle with 10 layers; c-d) letters printed with 5 layers c) "THU" and d) "HWU" (scale bar 5 mm)*

These complex structures were printed out in a matter of minutes. The triangular structure was strong enough to be physically manipulated with tweezers, but the structure deformed slightly under its own weight (as seen in Figure 8.6b), which demonstrates the strength of the hydrogel. This result is in contrast with the alginate results, which did not deform when the structures were manipulated. Additionally, the printed structures are optically transparent and uniform, layer boundaries are not visible and no other defects are in evidence. This is most likely due to the way the hydrogel is formed *in situ* in a layer-by-layer approach. These results demonstrate that the novel polypeptide-DNA hybrid hydrogel is 3D-printable and the resulting structures are contiguous and optically transparent.

8.5 Biocompatibility Testing

Due to the novel nature of this polypeptide-DNA hydrogel, it is important to investigate how, if at all, cells react to it. In order to test the biocompatibility of this supramolecular hydrogel, NIH-3T3 cells (murine fibroblast cell line) were co-cultured with each component separately. Each component was added into the cell culture media in different concentrations and the 3T3 cells were cultured for 24h in an incubator at 36.0-37.5°C, 5.0±0.5% CO_2. The viability of the cells was assessed with a fluorescent live/dead staining assay.

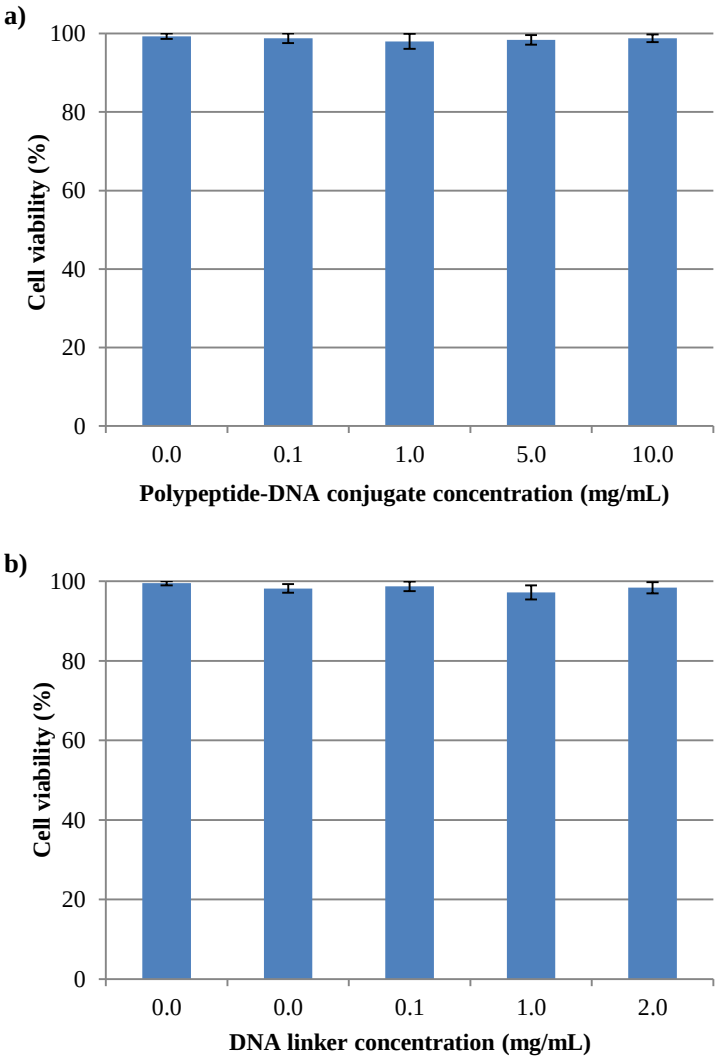

Figure 8.7 *– Cell viability test of the components in the hydrogel: (a) polypeptide; (b) DNA linker*

After 24h, cell viability was measured as 99.0±0.5% over a polypeptide concentration range of 0-10 mg/mL and a DNA linker concentration of 0-2 mM. This proves that the two components of the polypeptide-DNA hydrogel are highly biocompatible.

To investigate the biocompatibility of the novel polypeptide-DNA hydrogel as a whole, three different cell types were chosen to be cultured over a period of a day or more in a manually created 3D hydrogel structure. NIH-3T3, AtT-20 and HEK-293 cell lines were used to analyse the biocompatibility.

The structures were to be cultured in a 12-well tissue culture plate and a special substrate was prepared for this experiment to ensure that the samples could be imaged as easily as possible. Glass coverslips, which fit perfectly within the wells of the culture plate and are optically transparent, were chosen as the base for the substrate. In order to prevent the hydrogel structures from coming off the surface of the coverslip during removal from the culture plate for imaging, Polydimethylsiloxane (PDMS) rings were created measuring 12 mm in external diameter, 4mm in internal diameter and 3 mm in height. These were mounted centrally on 25 mm glass coverslips. These substrates ensured optical transparency in the viewing axis whilst maintaining the structures position in the centre of the coverslip, and were an appropriate size for culturing the structures in the wells of 12-well tissue culture plates.

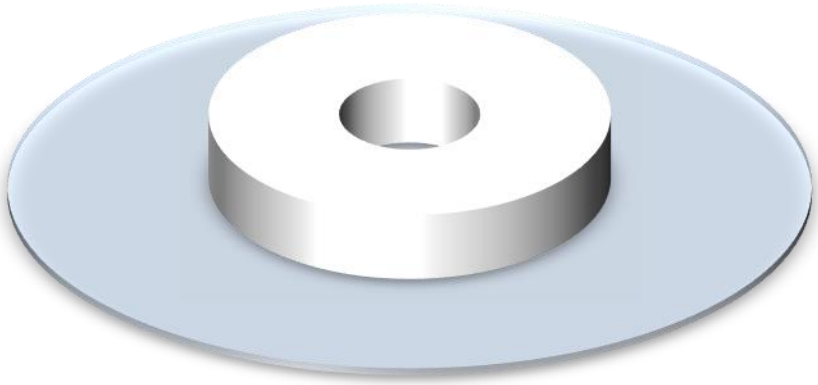

Figure 8.8 *– 3D rendering of the modified coverslip substrates with PDMS boundary rings*

In a typical experiment, cells were mixed with polypeptide-DNA conjugate into which an appropriate amount of DNA linker solution was added. Hydrogel formation was induced by gently stirring the mixture and culture medium was added, covering the hydrogel structure, to provide nutrients for the cells. The hydrogel structures were cultured in an incubator at 36.0-37.5°C, 5.0±0.5% CO_2 for 24 hours, after which the culture media was removed and the encapsulated cells were stained with fluorescein diacetate/propidium iodide (FDA/PI) and cultured for 30 minutes. They were then imaged with a confocal laser-scanning microscope (CLSM) (SP5 SMD gated-STED,

Leica) and the cell viability was measured using a fluorescent live/dead assay. Multiple samples were created for testing over the period of several days.

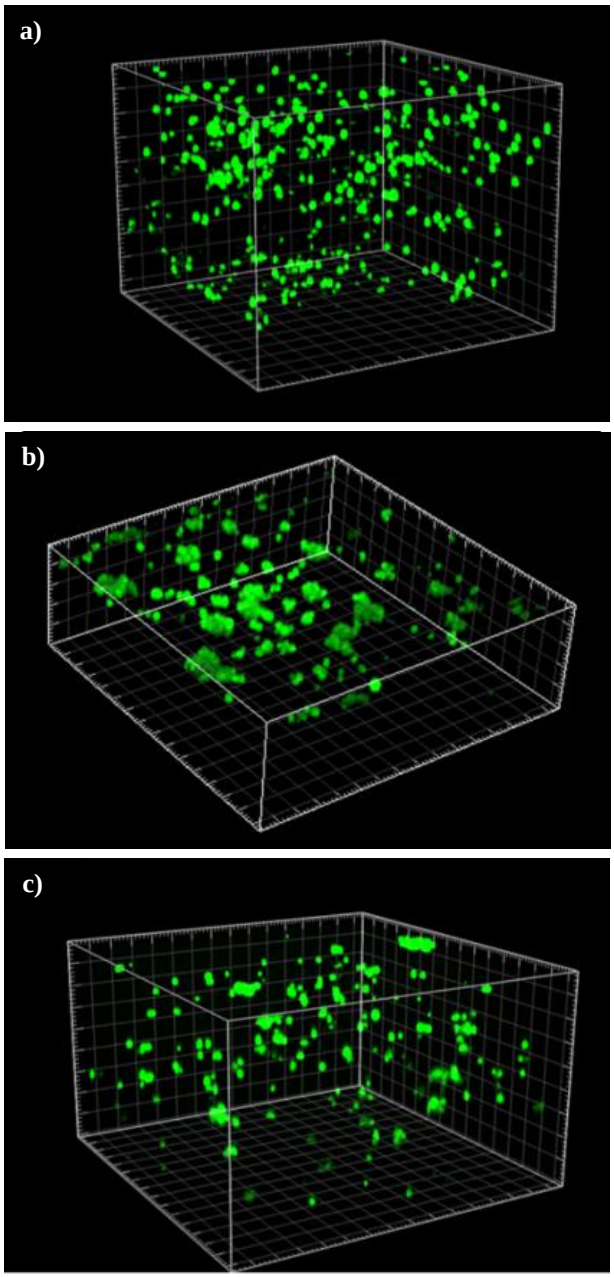

Figure 8.9 *– Fluorescence microscopy images of 3D polypeptide-DNA hydrogel structures with different cell types and time points and FDA staining in green: a) A 3-D stack of NIH-3T3 cells imaged after 24 h; b) AtT-20 cells imaged after 48 h; c) HEK-293 cells imaged after 48h (gridlines are 50 µm)*

As shown in Figure 8.9a, the viability assays detected no dead NIH-3T3 cells after 24 hours. The viabilities of AtT-20 and HEK-293 cells after 48 hours was measured as 99.1 ± 1.7% and 99.3 ± 1.4%, respectively. After 96 hours of 3D culture the viability was still high at 95.8 ± 5.9%; this demonstrates that the polypeptide-DNA hydrogels have good biocompatibility and are permeable to nutrients for long-term culture,

meaning that they would be suitable for use in 3D cell culture and tissue engineering applications.

8.6 3D Printed Cell-laden Hydrogel

Next, the viability of bioprinted cells encapsulated within 3D structures printed from polypeptide-DNA hydrogel was investigated. 20 µL of AtT-20 (a murine pituitary epithelial-like tumour cell line) cells at a concentration of 1×10^7 cells/mL was added to 100 µL of the polypeptide-DNA conjugate component (6 wt.%) which was loaded into one cartridge of the bioprinter. 120 µL of DNA linker (2mM) was loaded into another cartridge.

A simple cylindrical pattern was programmed and hydrogel components with cells were printed into the modified coverslip substrates described previously. Half of the printed samples were stained with 40 µg/mL Fluorescein diacetate (FDA) and 10 µg/mL of propidium iodide (PI) in serum-free DMEM and cultured in an incubator at 36.0-37.5°C, 5.0±0.5% CO_2 for 30 minutes. Images were recorded using a confocal laser-scanning microscope (CLSM) (SP5 SMD gated-STED, Leica) and the cell viability was measured using a fluorescent live/dead assay. 10 nM of Lysotracker-Red was added to the remaining samples which were cultured in the same manner as the previous samples before 3D image stacks were recorded using an inverted total internal reflection fluorescence microscope (TIRF) (IX81, Olympus).

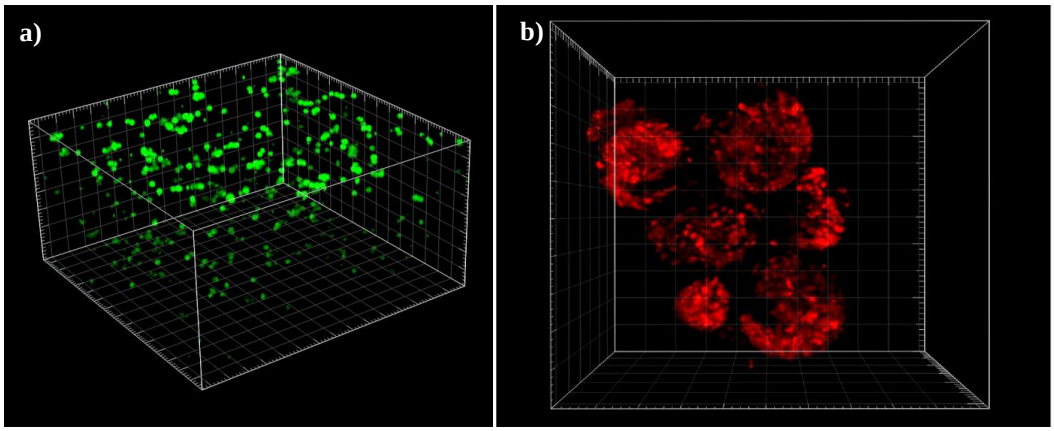

Figure 8.10 *– Fluorescence microscopy images of AtT-20 cells bioprinted in polypeptide-DNA hydrogel: a) A 3D stack of AtT-20 cells printed in hydrogel, with FDA staining in green (gridlines are 50 µm); b) A higher magnification 3D stack of AtT-20 cells printed in hydrogel and stained with Lysotracker-Red (gridlines are 5 µm)*

The live/dead assay reported a 3D bioprinted viability of 98.8±1.4%, which is extremely high. It should be noted that AtT-20 is a tumour cell line, so is far more resilient than more fragile cell lines such as hESCs. By increasing the magnification, single cells could be observed (Figure 8.10b).

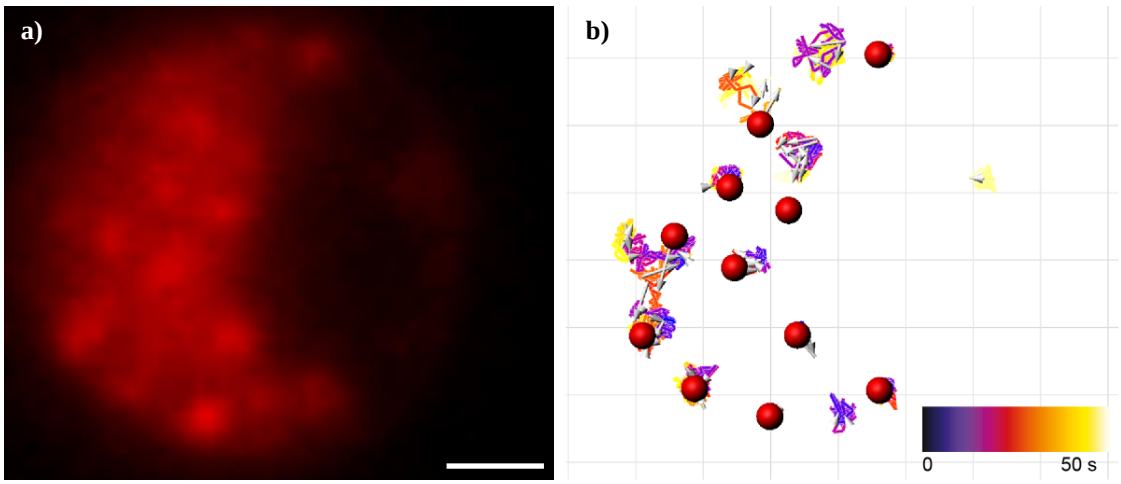

Figure 8.11 *– Vesicles tracked in AtT-20 cells bioprinted in polypeptide-DNA hydrogel: a) Wide-field microscopy images of AtT-20 cells printed in hydrogel and stained with Lysotracker-Red, a cross section of the cells shows intracellular organelles (scale bar 1 µm); b) Organelle trajectory traces from inside the cell in a) – the organelles are shown as red spheres and paths as coloured lines (colour represents time in seconds, gridlines are 1 µm)*

By further increasing the magnification of the microscope, it was possible to observe the intracellular organelles (including lysosomes and large, dense-cored vesicles) within the cytosol of a single AtT-20 cell suspended in 3D within the printed polypeptide-DNA structure (Figure 8.11a). A four-dimensional image stack of this single cell was recorded and the intracellular organelles were tracked over time (Figure 8.11b); by analysing the motion paths, it was determined that the analysed AtT-20 cells suspended in 3D within the printed polypeptide-DNA structure were viable, had normal morphology in 3D, and were capable of performing cellular functions such as proton pump activity, metabolic turnover and membrane trafficking [32].

8.7 Conclusions

This research contains the first study of a novel polypeptide-DNA hybrid supramolecular hydrogel which possesses a wide range of controllable and tuneable mechanical properties, including an analysis of its suitability for use in a 3D cell bioprinting process. Several 3D structures were successfully bioprinted, all of which demonstrated the ability of the hydrogel to maintain its shape after printing. The biocompatibility of the novel supramolecular hydrogel was verified for both

components, separately and in gel form, and the viability of 3D encapsulated cells is very high. 3D cell-encapsulating hydrogel structures were created using the bioprinter and the cells were found to be highly viable, functional and morphologically normal. This novel hydrogel addresses several limitations in current 3D hydrogel cell culturing technology and will undoubtedly have important applications in tissue engineering. However, the synthesis methodologies require some improvement in order to enable larger scale manufacturing of the hydrogel components prior to more in-depth experiments.

8.8 References

[1] Appel EA, del Barrio J, Loh XJ, and Scherman OA, (2012). "Supramolecular polymeric hydrogels," *Chemical Society Reviews*, **41**(18), p. 6195.

[2] Yan X, Wang F, Zheng B, and Huang F, (2012). "Stimuli-responsive supramolecular polymeric materials," *Chemical Society Reviews*, **41**(18), p. 6042.

[3] Dankers PYW, Hermans TM, Baughman TW, Kamikawa Y, Kieltyka RE, Bastings MMC, Janssen HM, Sommerdijk NAJM, Larsen A, van Luyn MJA, Bosman AW, Popa ER, Fytas G, and Meijer EW, (2012). "Hierarchical Formation of Supramolecular Transient Networks in Water: A Modular Injectable Delivery System," *Adv. Mater.*, **24**(20), pp. 2703–2709.

[4] Maity GC, (2008). "Supramolecular Hydrogels," *Journal of Physical Sciences*, **12**, pp. 173–186.

[5] Nakahata M, Takashima Y, Yamaguchi H, and Harada A, (2011). "Redox-responsive self-healing materials formed from host–guest polymers," *Nat Commun*, **2**, p. 511.

[6] Zhang Y, Gu H, Yang Z, and Xu B, (2003). "Supramolecular Hydrogels Respond to Ligand−Receptor Interaction," *J. Am. Chem. Soc.*, **125**(45), pp. 13680–13681.

[7] Yan X, Xu D, Chi X, Chen J, Dong S, Ding X, Yu Y, and Huang F, (2012). "A Multiresponsive, Shape-Persistent, and Elastic Supramolecular Polymer Network Gel Constructed by Orthogonal Self-Assembly," *Adv. Mater.*, **24**(3), pp. 362–369.

[8] Ghoussoub A, and Lehn J-M, (2005). "Dynamic sol–gel interconversion by reversible cation binding and release in G-quartet-based supramolecular polymers," *Chem. Commun.*, (46), pp. 5763–5765.

[9] Appel EA, Biedermann F, Rauwald U, Jones ST, Zayed JM, and Scherman OA, (2010). "Supramolecular Cross-Linked Networks via Host−Guest Complexation with Cucurbit[8]uril," *J. Am. Chem. Soc.*, **132**(40), pp. 14251–14260.

[10] Um SH, Lee JB, Park N, Kwon SY, Umbach CC, and Luo D, (2006). "Enzyme-catalysed assembly of DNA hydrogel," *Nat Mater*, **5**(10), pp. 797–801.

[11] Lee JB, Peng S, Yang D, Roh YH, Funabashi H, Park N, Rice EJ, Chen L, Long R, Wu M, and Luo D, (2012). "A mechanical metamaterial made from a DNA hydrogel," *Nat Nano*, **7**(12), pp. 816–820.

[12] Qi H, Ghodousi M, Du Y, Grun C, Bae H, Yin P, and Khademhosseini A, (2013). "DNA directed self-assembly of shape-controlled hydrogels," *Nat Commun*, **4**, p. 2275.

[13] Wei B, Cheng I, Luo KQ, and Mi Y, (2008). "Capture and Release of Protein by a Reversible DNA-Induced Sol–Gel Transition System," *Angewandte Chemie*, **120**(2), pp. 337–339.

[14] He X, Wei B, and Mi Y, (2010). "Aptamer based reversible DNA induced hydrogel system for molecular recognition and separation," *Chem. Commun.*, **46**(34), pp. 6308–6310.

[15] Cheng E, Xing Y, Chen P, Yang Y, Sun Y, Zhou D, Xu L, Fan Q, and Liu D, (2009). "A pH-Triggered, Fast-Responding DNA Hydrogel," *Angewandte Chemie*, **121**(41), pp. 7796–7799.

[16] Xing Y, Cheng E, Yang Y, Chen P, Zhang T, Sun Y, Yang Z, and Liu D, (2011). "Self-Assembled DNA Hydrogels with Designable Thermal and Enzymatic Responsiveness," *Adv. Mater.*, **23**(9), pp. 1117–1121.

[17] Yang H, Liu H, Kang H, and Tan W, (2008). "Engineering Target-Responsive Hydrogels Based on Aptamer−Target Interactions," *J. Am. Chem. Soc.*, **130**(20), pp. 6320–6321.

[18] Guo W, Orbach R, Mironi-Harpaz I, Seliktar D, and Willner I, (2013). "Fluorescent DNA hydrogels composed of nucleic acid-stabilized silver nanoclusters," *Small*, **9**(22), pp. 3748–3752.

[19] Zhu Z, Wu C, Liu H, Zou Y, Zhang X, Kang H, Yang CJ, and Tan W, (2010). "An Aptamer Cross-Linked Hydrogel as a Colorimetric Platform for Visual Detection," *Angewandte Chemie International Edition*, **49**(6), pp. 1052–1056.

[20] Gao M, Gawel K, and Stokke BT, (2011). "Toehold of dsDNA exchange affects the hydrogel swelling kinetics of a polymer–dsDNA hybrid hydrogel," *Soft Matter*, **7**(5), pp. 1741–1746.

[21] Chen Y, Pang X-H, and Dong C-M, (2010). "Dual Stimuli-Responsive Supramolecular Polypeptide-Based Hydrogel and Reverse Micellar Hydrogel Mediated by Host–Guest Chemistry," *Adv. Funct. Mater.*, **20**(4), pp. 579–586.

[22] Kyle S, Felton SH, McPherson MJ, Aggeli A, and Ingham E, (2012). "Peptide-Based Biomaterials: Rational Molecular Design of Complementary Self-Assembling Peptide Hydrogels (Adv. Healthcare Mater. 5/2012)," *Advanced Healthcare Materials*, **1**(5), pp. 679–679.

[23] Cheng Y, He C, Xiao C, Ding J, Cui H, Zhuang X, and Chen X, (2013). "Versatile Biofunctionalization of Polypeptide-Based Thermosensitive Hydrogels via Click Chemistry," *Biomacromolecules*, **14**(2), pp. 468–475.

[24] Khan W, Muthupandian S, Farah S, Kumar N, and Domb AJ, (2011). "Biodegradable Polymers Derived From Amino Acids," *Macromol. Biosci.*, **11**(12), pp. 1625–1636.

[25] Deming TJ, (2007). "Synthetic polypeptides for biomedical applications," *Progress in Polymer Science*, **32**(8–9), pp. 858–875.

[26] Mironov V, Boland T, Trusk T, Forgacs G, and Markwald RR, (2003). "Organ printing: computer-aided jet-based 3D tissue engineering," *Trends in Biotechnology*, **21**(4), pp. 157–161.

[27] Chang R, Emami K, Wu H, and Sun W, (2010). "Biofabrication of a three-dimensional liver micro-organ as an in vitro drug metabolism model," *Biofabrication*, **2**(4), p. 045004.

[28] Derby B, (2012). "Printing and Prototyping of Tissues and Scaffolds," *Science*, **338**(6109), pp. 921–926.

[29] Caruthers MH, (1991). "Chemical synthesis of DNA and DNA analogs," *Accounts of chemical research*, **24**(9), pp. 278–284.

[30] Beaucage SL, and Iyer RP, (1992). "Advances in the Synthesis of Oligonucleotides by the Phosphoramidite Approach," *Tetrahedron*, **48**(12), pp. 2223–2311.

[31] Chandler D, (2002). "Hydrophobicity: Two faces of water," *Nature*, **417**(6888), pp. 491–491.

[32] Yang L, Dun AR, Martin KJ, Qiu Z, Dunn A, Lord GJ, Lu W, Duncan RR, and Rickman C, (2012). "Secretory Vesicles Are Preferentially Targeted to Areas of Low Molecular SNARE Density," *PLoS ONE*, **7**(11), p. e49514.

Chapter 9 – Summary of the Conclusions and Recommendations for Future Work

9.1 Research Assessment

The initial aim of this research was to develop a novel mechanical device that could quickly and reliably position viable biological cells into pre-determined patterns and locations onto a heterogeneous substrate; regardless of cell type printed, all cells must be viable. As research advanced, it became increasingly apparent that the technology could be applied to a much broader range of applications beyond initial simple 2D patterning. Although the valve-based bioprinting platform was successfully developed, its development could have been greatly sped up if the base machine for the Mark I had been a 3D printer rather than a CNC machine which required the introduction of several complex workarounds to make operational. One of the main goals was to investigate the response of cells to the bioprinting process, with particular emphasis on viability. Primary cell compatibility testing was performed with HEK 293 cells, but because this line is experimentally transformed, they are not a particularly good model for normal cells. The world's first investigation into the responses of both hESCs and hiPSCs to the bioprinting process was successfully undertaken, with validation of pluripotency maintenance post-printing. Other goals involved the continued improvement and development of the bioprinting platform, incorporation of multiple bio-ink printing, and validation and characterisation of the printer's capabilities. To this end, experiments were carried out to explore the possibilities enabled by this technology.

9.2 Conclusions Summary

The overall aim of this thesis was to develop a novel mechanical device that can quickly and reliably position viable biological cells and other liquid materials into pre-determined three-dimensional patterns – a cell printer. This objective has been successfully achieved and the key findings are summarised below with images to illustrate each one:

- A novel multi-nozzle valve-based bioprinting platform was developed and software was written to control it, including a graphical user interface. The bioprinter was able to position droplets of bio-ink (down to single nanolitres in volume) with high spatial accuracy in three-dimensions; furthermore, the system was sterilisable and had high throughput.

Bioprinter

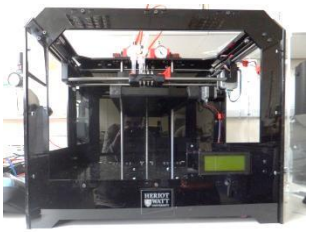

Custom Design

Custom Software

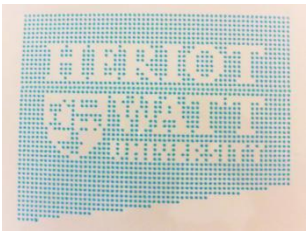

High Spatial Accuracy

Figure 9.1 *– Pictorial summary of the bioprinter development carried out*

- Human pluripotent stem cells (hESCs and hiPSCs) were shown to retain high viability and pluripotency post-printing, confirming that the novel bioprinting platform is compatible with cell transfer and gentle enough to not affect the cells or trigger differentiation. This was the first investigation of this kind and will enable the use of hPSCs in more complex tissue (re)generation applications.

Human Pluripotent Stem Cells

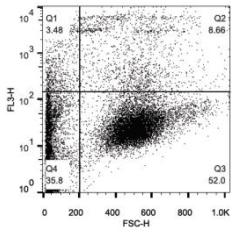

High Viability

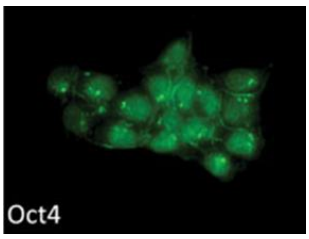

Pluripotency Maintained

Figure 9.2 *– Pictorial summary of the hPSC research carried out*

- Spheroid aggregates of uniform, controllable and reproducible sizes were created from human embryonic stem cells using a bioprinted-hanging droplet hybrid technique. Due to the programmable sizes of the spheroids, this technique could be used to direct the differentiation of hPSCs along specific lineages or to speed up tissue (re)generation, using the spheroids as primary building blocks.

Spheroid Aggregates

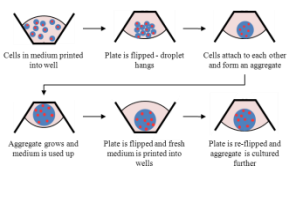

Hanging Drop Formation

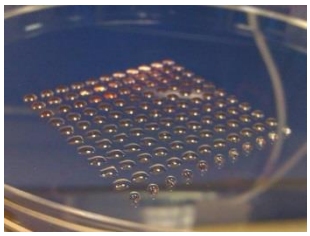

Volume Gradient Printing

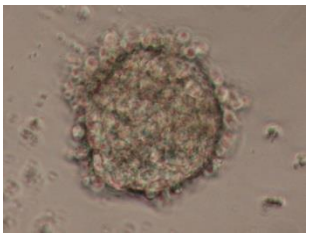

Spheroid Aggregate

Figure 9.3 *– Pictorial summary of the spheroid aggregate research carried out*

- Complex three-dimensional structures were bioprinted using two-component hydrogels with reasonably high resolution, even for complex and tall structures. The properties of the hydrogel can be modified by altering the ratio and concentration of the two components; therefore, structures with programmable heterogeneous properties throughout the structure can be created.

3D Hydrogel Structures

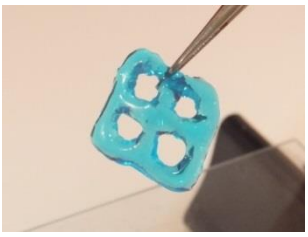

Alginate Grid Structure

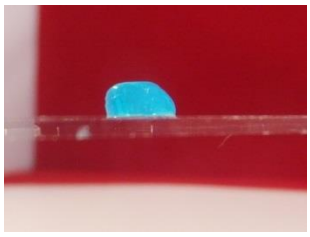

Tall Alginate Structure

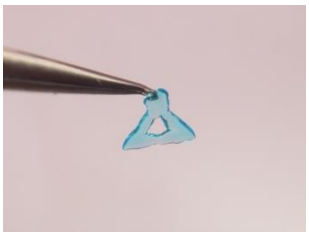

Polypeptide-DNA Triangle Structure

Figure 9.4 *– Pictorial summary of the hydrogel research carried out*

- Cells were suspended within hydrogel components and successfully printed into three-dimensional structures encapsulating cells; the cells were found to be highly viable, functional and morphologically normal.

3D Cell-laden Hydrogel Structures

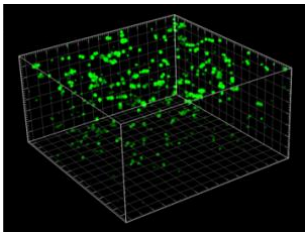

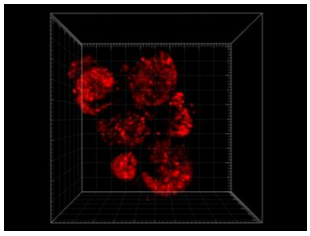

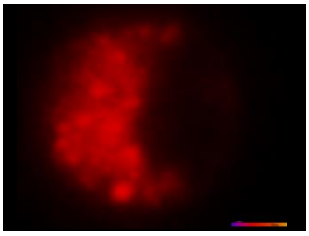

Fluorescence microscopy images with increasing magnification of AtT-20 cells bioprinted in polypeptide-DNA hydrogel

Figure 9.5 *– Pictorial summary of the cell-laden hydrogel research carried out*

- Human pluripotent stem cells (hESCs and hiPSCs) were successfully directed to differentiate into hepatocyte-like cells which were positive for a number of hepatic markers, including HNF4α and Albumin, and had similar morphology to hepatocytes. It was shown that cells can be printed during directed differentiation without interrupting the differentiation or changing the lineage of the cells. This is an important result as it means that these cells can be patterned in 3-dimensions using the bioprinter while differentiating which will greatly speed up the creation of mini-liver tissue structures.

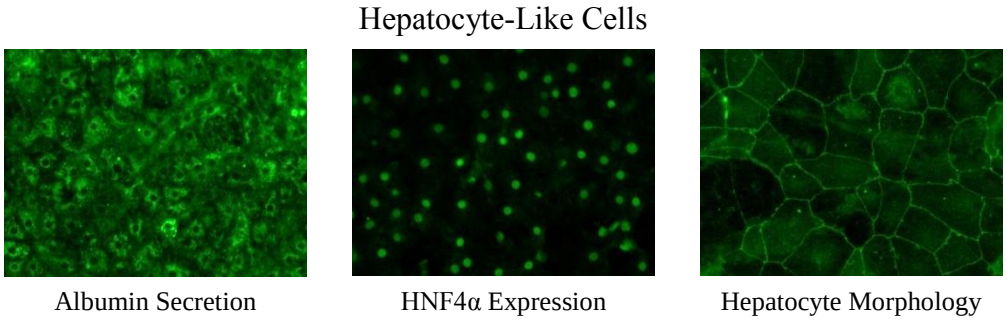

Figure 9.6 *– Pictorial summary of the HLC research carried out*

9.3 Future Work Recommendations

With regard to the possibility of continuing this line of research, the following recommendations are provided:

- Based on the feedback received from the biologists that have used the bioprinters, the main problem with the machine is that it is not very user-friendly; there are a number of possible upgrades to the bioprinting platform itself that could help improve the machine, including a more streamlined interface and self-cleaning abilities. The interface could be improved by re-ordering the menu items to bring more frequent routines to the top and lesser-used functions to sub-menus. Self-cleaning could be achieved by adding machine-interchangeable bio-ink cartridges. Another issue was that although the machine fits within a standard tissue culture hood, it takes up most of the space, leaving little space for bio-ink preparation. This could be solved by decreasing the size of the machine by removing dead space within the machine and scaling down some components.
- The development of the software for creating programs for the bioprinter to run has not kept up with the development of the bioprinting platform. The most

recent software is adequate for generating programs defining simple two-dimensional patterns and populating multi-well plates, but further software development is required for the generation of programs defining complex three-dimensional structures.

- Each time a new material is used in the bioprinter it must be characterised to determine the optimum and boundary settings for its use, which is time consuming and requires a lot of material. By carrying out more in-depth analysis and simulation of the bioprinting system, it might be possible to automatically determine the correct settings for new materials, as opposed to the current trial and error approach.
- By combining together the work on 3D bioprinting of cell-laden hydrogels with the research printing HLCs and supporting cells, it should be possible to bioprint 3D liver micro-tissues that replicate the response and functions of a human liver but on a much smaller scale. Such micro-tissues could be used to improve the efficiency of novel drug testing, or they could alternatively be implanted into a patient with a damaged liver.
- Besides the liver, there are many other types of cells and tissues that could be created and studied using this bioprinting platform. Controllable and repeatable creation of pancreatic islets has obvious applications in the treatment of diabetes. Cardiac patches could be printed for implantation to repair damage or defects in heart tissue. There is no limit to potential applications for this technology.
- The next logical step for the portable bioprinting system would be the development of an *in vivo* bioprinter to create structures or repair damage *in situ*. Such a system should be as small and simple as possible to facilitate mounting to an existing laparoscopic probe.